OPTIONS
méditerranéennes

SERIES B: Studies and Research
2012 – Number 67

The use of remote sensing and geographic information systems for irrigation management in Southwest Europe

Coodinators:
M. Erena, A. López-Francos, S. Montesinos, J.-F. Berthoumieu

The loss of competitiveness and the abandonment of agricultural activities in many rural areas of Southwest Europe are worsened by problems related to water shortage and the rise in natural hazards such as droughts. Remote sensing and geographic information systems offer a huge potential to improve water management in agriculture, as they are able to provide a great amount of relatively cheap information, which can be automated, and processed and analysed for a wide range of agronomic, hydraulic and hydrological purposes. New developments in ICTs allow the products of those technologies to be easily available for end-users for practical applications.

This publication is a result of the TELERIEG project (Use of remote sensing for irrigation practice recommendation and monitoring in the SUDOE space, SOE1/P2/E082, 2009-2011), co-financed by the Programme Interreg IVB-Sudoe of the EU-ERDF, with the participation of 9 beneficiary institutions from France, Portugal and Spain. The final target was to achieve a better environmental protection through more efficient and rational management of water resources in agriculture and a more effective prevention and response against natural risks. The project has generated a vigilance and recommendations system for vast areas. Specifically, data collection, information analysis and decision-making services were developed, based on geographical information systems (GIS) and remote sensing, allowing water users and managers to have timely information and a useful decision-making tool for irrigation water management.

The chapters of this book were part of the learning and support materials prepared by the lecturers of the international course on “The use of remote sensing for irrigation management”, organised by the Mediterranean Agronomic Institute of Zaragoza in November 2011, with the aim of disseminating the knowledge and tools created by TELERIEG and by other initiatives in the field of the application of remote sensing to agricultural water management. The chapters collect information at different levels: generalities on remote sensing and the theoretical basis of its application to agriculture, methodologies for specific measurements and applications, and field experiences and case studies. The book is accompanied by a DVD containing additional materials which were used for the course, such as presentations, teaching practical materials (images and data), software practicals and the pdf version of the book chapters.

Instituto Murciano de Investigación y Desarrollo Agrario y Alimentario

CIHEAM
MAI ZARAGOZA

UE/EU • FEDER/ERDF

ISBN: 2-85352-482-5
ISSN: 1016-1228

OPTIONS méditerranéennes
CIHEAM
OPTIONS méditerranéennes
The use of remote sensing and geographic information systems for irrigation management in Southwest Europe
OPTIONS méditerranéennes
2012
B 67

The use of remote sensing and geographic information systems for irrigation management in Southwest Europe

Coodinators:
M. Erena, A. López-Francos, S. Montesinos, J.-F. Berthoumieu

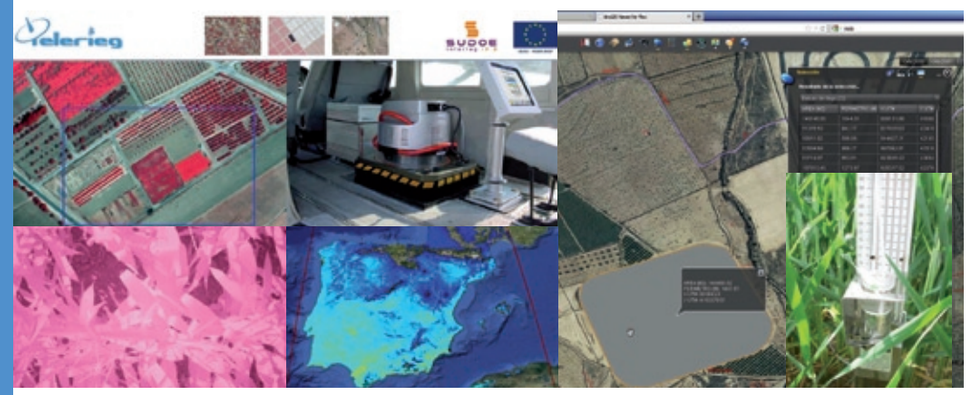

OPTIONS
méditerranéennes

SERIE B: Studies and Research
2012 - Number 67

CIHEAM

The use of remote sensing and geographic information systems for irrigation management in Southwest Europe

Coordinators: M. Erena, A. López-Francos, S. Montesinos, J.-F. Berthoumieu

This publication has been financed by the TELERIEG project (The use of remote sensing for irrigation practice, recommendation and monitoring in the SUDOE space), contract no. SOE1/P2/E082, co-financed by the Interreg IV B SUDOE Programme (Southwest European Space Territorial Cooperation Programme) through the European Regional Development Fund (EU-ERDF), within the framework of the European Territorial Cooperation Objective for 2007-2013.

OPTIONS
méditerranéennes

Head of publication: Francisco Mombiela

2012 | Series B: Studies and Research | Number 67

L'édition technique, la maquette et la mise en page de ce numéro d'Options Méditerranéennes ont été réalisées par l'Atelier d'Édition de l'IAM de Zaragoza (CIHEAM)

Technical editing, layout and formatting of this edition of Options Méditerranéennes was carried out by the Editorial Board of MAI Zaragoza (CIHEAM)

Crédits des photos de couverture / *Cover photo credits* :
Telerieg Project, IMIDA, Irstea

Tirage / *Copy number* : 400 ex.
Printer: INO Reproducciones, S.A.
Pol. Malpica, calle E, 32-39
(INBISA II, Nave 35)
50016 Zaragoza-Spain
Dep. Legal: Z-2893-91

Fiche bibliographique / *Cataloguing data* :

The use of remote sensing and geographic information systems for irrigation management in Southwest Europe. M. Erena, A. López-Francos, S. Montesinos, J.-F. Berthoumieu (cords). Zaragoza: CIHEAM / IMIDA / SUDOE Interreg IVB (EU-ERDF). 2012, 239 p. + DVD (*Options Méditerranéennes*, Series B: Studies and Research, no. 67)

Catalogue des numéros d'Options Méditerranéennes sur / *Catalogue of Options Méditerranéennes issues on* :
www.ciheam.org/publications

ISSN : 1016-1228 – ISBN : 2-85352-482-5

List of contents

Applications of remote sensing of high resolution

Case studies

Foreword

Rural areas in South-western Europe are living in a context of uncertainty and decay, especially in the agricultural sector. This situation is caused by the loss of competitiveness and abandonment of agricultural activity in many areas, processes that are worsened by problems related to water shortage and the rise in natural hazards (such as droughts), whose negative effects exceed the scope of the agricultural sector and extend to drinking water availability, rural population maintenance, environmental damages and social conflicts between water resource users. On the other hand, the presence of research and development in the agricultural sector is still scarce and very fragmented, and this represents a threat to the survival of the sector. All these problems may be tackled overall through actions in which all the stakeholders involved take part, from the Administration to producers and the research sector.

This publication is a result of the TELERIEG project (Use of remote sensing for irrigation practice recommendation and monitoring in the SUDOE space), co-financed during 2009-2011 by the Programme Interreg IVB-Sudoe of the European Union, and coordinated by the IMIDA (Instituto Murciano de Investigación y Desarrollo Agrario y Alimentario, Spain) with the participation of 9 beneficiary institutions and 19 collaborator stakeholder institutions from France, Portugal and Spain. The final target of the project was a better environmental protection through more efficient and rational management of water resources in agriculture and a more effective prevention and response capacity against natural risks. For achieving this objective, the project has generated a vigilance and recommendations system in vast areas. Specifically, collection, information analysis and decision-making services were developed, based on geographical information systems (GIS) and remote sensing, allowing water users and managers to have timely information and a useful decision-making tool for irrigation water management.

The last activity of the project was an international advanced course organised by the Mediterranean Agronomic Institute of Zaragoza (IAMZ-CIHEAM) in Zaragoza (Spain) on November 2011, with the aim of disseminating the knowledge and tools created by TELERIEG and by other initiatives in the field of the application of remote sensing to agricultural water management. Almost all chapters of this book were part of the learning and support materials prepared by the lecturers of this course, and they collect information at different levels: generalities on remote sensing and the theoretical basis of its application to agriculture, methodologies for specific measurements and applications, and field experiences and case studies. The book is accompanied by a DVD containing additional materials which were used for the course, as presentations, teaching practical materials (images and data), software practicals and the pdf version of the book chapters.

We acknowledge all the partners of the TELERIEG project and all authors of this publication for the efforts carried out during the three years of the project, one of whose products is the present publication.

The editors

Introduction

The TELERIEG Project

M. Erena* and A. López-Francos**

* Instituto Murciano de Investigación y Desarrollo Agrario y Alimentario (IMIDA),
C/ Mayor, s/n, 30150 La Alberca, Murcia (Spain)
**Mediterranean Agronomic Institute of Zaragoza (IAMZ-CIHEAM),
Av. Montañana, 1005, 50059 Zaragoza (Spain)

Abstract. The TELERIEG (The use of remote sensing for irrigation practice, recommendation and monitoring in the SUDOE space, www.telerieg.net), co-financed by the Interreg IVB SUDOE Programme of the European Union, has spent three years of activity with the objective of developing knowledge and tools on the application of remote sensing and geographic information systems for the improvement of irrigation water management and the response to natural risks affecting agriculture in the Southwest of Europe. The main results include an automated image processing that generates daily maps with useful parameters for irrigation management, and a geoportal adapted to the INSPIRE Directive, made up of large databases of agroclimatic and cartographic information, as well as utilities and tools based on geographic information systems and remote sensing allowing users to calculate irrigation requirements at plot scale. A collaboration network has been created of institutions working in the field of remote sensing and irrigation water management, using the most advanced techniques of high resolution images processing for estimation of agronomic parameters at field scales. All these results have been disseminated at local and international scale, covering mainly the project areas of Southwestern Europe but also other Mediterranean countries. The technologies developed by TELERIEG can contribute to improvements in optimization of the agricultural production factors mainly water.

Keywords. Irrigation – Remote sensing – Decisión support system – Southwest Europe – Interreg.

Le projet TELERIEG

Résumé. *Le projet TELERIEG (Utilisation de la télédétection pour la recommandation et le suivi des pratiques d'irrigation dans l'espace SUDOE), cofinancé par le Programme SUDOE-Interreg IV-B de l'Union européenne, compte déjà trois années d'activité dans l'objectif de développer les connaissances et les outils pour l'application de la télédétection et des systèmes d'information géographique à l'amélioration de la gestion de l'eau d'irrigation et à la réponse aux risques naturels que subit l'agriculture dans le Sud-Ouest de l'Europe. Les principaux résultats comprennent le traitement automatisé des images, permettant la création de cartes journalières où figurent des paramètres utiles pour la gestion de l'irrigation, et un géoportail adapté à la Directive INSPIRE qui héberge de vastes bases de données d'information agroclimatique et cartographique, ainsi que des utilités et outils basés sur les systèmes d'information géographique et la télédétection, permettant aux usagers de calculer les besoins en irrigation à l'échelle de la parcelle. Un réseau de collaboration a été créé pour les institutions travaillant dans le domaine de la télédétection et de la gestion de l'eau d'irrigation, utilisant les techniques les plus avancées de traitement d'images à haute performance pour l'estimation de paramètres agronomiques à l'échelle du terrain. Tous ces résultats ont été diffusés au niveau local et international, couvrant les zones du projet dans le Sud-Ouest de l'Europe et d'autres zones de pays méditerranéens. Les technologies développées par TELERIEG peuvent contribuer à l'optimisation des facteurs de production agricole, l'eau notamment.*

Mots-clés. *Irrigation – Télédétection – Système d'aide à la décision –Sud-ouest de l'Europe – Interreg.*

I – Background

TELERIEG (The use of remote sensing for irrigation practice, recommendation and monitoring in the SUDOE space, contract no. SOE1/P2/E082) was a 33 months (2009-2011) transnational project cofinanced by the beneficiary institutions and the Interreg IV B SUDOE Programme

(Southwest European Space Territorial Cooperation Programme) through the European Regional Development Fund (ERDF), within the framework of the European Territorial Cooperation Objective for 2007-2013).

The objective of the SUDOE Cooperation Programme is to consolidate the territorial cooperation of the Southwest European regions in the fields of competitiveness, innovation, environmental protection, and the sustainable planning and development of the area, contributing to the harmonious and balanced integration of the SUDOE regions and their social and economic cohesion within the European Union. The Southwest European Space (SUDOE), consists of 30 regions and autonomous cities (Fig. 1), covering 770,120 km^2 and populated by 61.3 millions inhabitants.

Fig. 1. The SUDOE Space.

TELERIEG (www.telerieg.net) was one of the Programme projects included in its Priority number 2, which addressed the "Improvement of sustainability for the protection and conservation of the environment and natural surroundings ofd the SUDOE Space", involving activities of risk prevention and conservation of natural resources.

This project is framed in a context of uncertainty in the rural areas of the SUDOE Space (Fig. 1), especially in the agricultural sector specially. This uncertainty is caused by the loss of competitiveness loss and abandonment of the agricultural activity in many areas because of problems related with the water shortage and the rise in natural risks (as droughts), whose negative effects exceed the scope of the agricultural sector and extend to drinking water availability, rural population maintenance, environmental damages and social conflicts between water resource users. On the other sidehand, the presence of research and development in the agricultural sector is still scarce and very fragmented, and this represents a threat to the survival of the sector survival.

All these problems may be tackled overall through actions in which all the involved stakeholders involved take part, from the Administration to producers and the research sector.

TELERIEG partners have been cooperating in projects related with this issue since for a long time, being the PRECIRIEG Project (SUDOE) being a recent example. The TELERIEG project emanated from this last project activities and results, and has intended to face up the necessity of improving the efficiency of the natural resources management, adapting the economical activities to a more rational resources management (thus improving the competitiveness) and also improving the management capacity of the economical and social agents and the Administration for data collection and analysis and decision-making.

II – Project objectives

The final objective of the project has been a better environmental protection through a more efficient and rational management of water resources in agriculture and a more effective capacity of prevention and response to natural risks.

For achieving this objective the project is targeted to generating a surveillance and recommendations system for vast areas. More specifically, collection of information, analysis and decision-making services have been developed, allowing a more efficient management of the resource and optimization of the response capacity ahead of the natural risk, such as drought. These services are based on Geographical Information Systems (GIS) and on Remote Sensing, and include adaptionsadaptations to the management of drought and the reduction of climate change impacts. They make on-time information and decision-making utilities available to water users and managers.. Besides, the system is an opportunity for a regional development based on the creation of new services for the irrigation water user's communities and companies, optimizing the productions and the resource uses, besides contributing to develop the information society. Finally, the availability of information about the SUDOE area has the potential to create an important opportunity for the transmission of results and their application throughout the whole SUDOE area. It is to be highlighted that the project has been working with the standards set up by the INSPIRE Directive (Infrastructure for Spatial Information in the European Community), which had not yet been put into practice by any initiative in the SUDOE space. This fact supposes an important innovation and an element of territorial cohesion, because it will allow the SUDOE area to work with the same data set, which will generate important benefits for working together in the future.

III – Project partenariat partnership and involved territories involved

The Telerieg project involved nine partners from 8 regions of the SUDOE Space (Fig. 2):

1. IMIDA: Instituto Murciano de Investigación y Desarrollo Agrario y Alimentario de la Consejería de Agricultura y Agua - Región de Murcia (Spain). Project leader beneficiary.
2. ACMG: Association climatologique de la moyenne Garonne (France).
3. IVIA: Instituto Valenciano de Investigaciónes Investigaciones Agrariasde la Consejería de Agricultura - Generalitat Valenciana (Spain).
4. ISA: Instituto Superior de Agronomia de la Universidade Técnica de Lisboa (Portugal).
5. ANPN: Association nationale des producteurs de noisettes (France).
6. IRTA: Institut de Recerca i Tecnologia Agroalimentàries - Generalitat de Catalunya (Spain).
7. CEMAGREF: Centre national du machinisme agricole, du génie rural, des eaux et des forêts de Montpellier, actually currently IRSTEA (France).

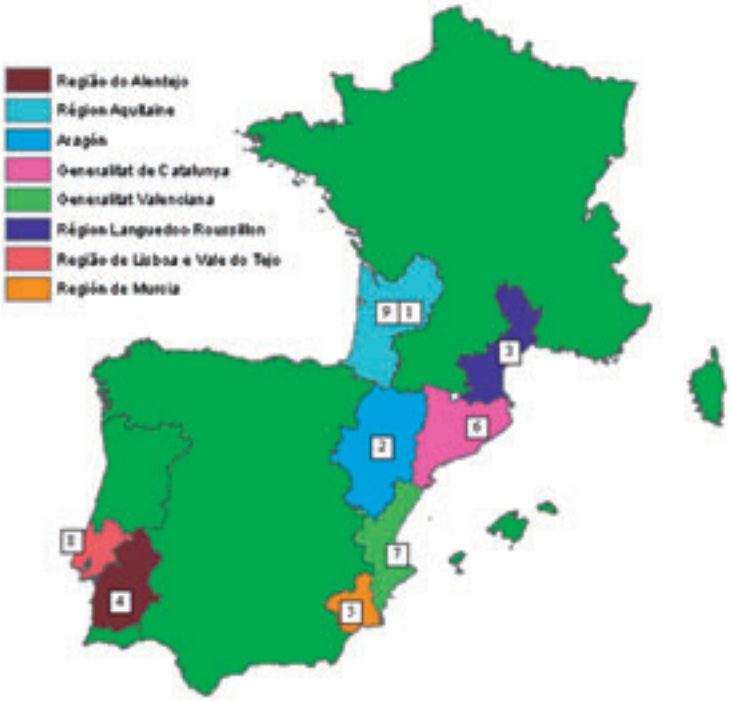

Fig. 2. Regions participating in the Telerieg Project. In each region, partners are identified by their number in the list above.

8. COTR: Centro Operativo e de Tecnologia de Regadio (Portugal).
9. IAMZ-CCIHEHAM: Mediterranean Agronomic Institute of Zaragoza (Spain).

Telerieg also involved a number of collaborators that have contributed to the project activities through different inputs: technical and sicientificscientific expertise, field experiments, practical applications, data and information, etc. These collaborators were the following:

1. A.S.A de la Baysole: Association Syndicale Autorisée pour l'irrigation des coteaux de la Baysole (France).
2. AEMET Murcia: Agencia Estatal de Meteorología (Spain).
3. IGN: Instituto Geográfico Nacional. Plan Nacional de Teledetección (Spain).
4. DARTCOM: Weather Satellite and Remote Sensing Ground Stations (UK).
5. AQUITANE: Fruits et légumes d'Aquitaine (France).
6. AREFLH: Assemblée des Régions Européennes Fruitières, Légumières et Horticoles (France).
7. C.R.D.O. Jumilla: Consejo Regulador de la Denominación de Origen Jumilla (Spain).
8. CEBAS-CSIC: Centro de Edafología y Biología Aplicada del Segura (Spain).
9. CGAT: Grupo de Investigación de Cartografía GeoAmbiental Geoambiental y Teledetección, Universidad Politécnica de Valencia (Spain).

10. CRCC: Comunidad de Regantes del Campo de Cartagena (Spain).
11. GEOSYS, S.L.: Sistemas Sistemas de Información de la Tierra (Spain).
12. IDR: Instituto de Desarrollo Regional. Universidad de Castilla la Mancha (Spain).
13. INDRA S.A.: Indra Espacio (Spain).
14. DEIMOS S.A.: Deimos Space (Spain).
15. SCRATS: Sindicato Central de Regantes del Acueducto Tajo-Segura (Spain).
16. SYNGENTA: Syngenta seeds.
17. UNICOQUE: Coopérative Unicoque (France).
18. UPCT: Universidad Politécnica de Cartagena (Spain).
19. ADOUR-GARONE: L'Agence de l'eau Adour-Garonne (France).

IV – Project actions and main results

To achieve the aims of the project, a net of transnational cooperation has been created to develop assessment services based on remote sensing and geographic information systems. The net permitted the knowledge transfer and technical innovation in water resources management issues and the fight against drought.

The Project activities were articulated into several groups of tasks:

- GT.1 Coordination and management of the project.
- GT.2 Development of the automatic processing of the remote sensing data.
- GT.3 Vegetation monitoring system.
- GT.4 Network of demonstrative pilot plots.
- GT.5 Extensive areas irrigation assessment system.
- GT.6 Monitoring and evaluation of the project.
- GT.7 Publicity, information and capitalization of the project.

The TELERIEG tools in the pilot zone permit the integration and management of georeferenced agroclimatic data, soil maps, quantity and quality of waters, crop information and other technical parameters of a farm or an irrigated area. The final product is a decision support system to facilitate decision-taking processes in a comfortable and generic access through internet, incorporating different techniques and access into GIS and remote sensing data.

The information technologies and in a more precisely way, the new technologies, applied in different agriculture environments, can introduce important improvements in optimization of the agricultural production factors. The main beneficiaries of the information and decision taking systems are, in one sideon the one hand, the irrigators communities, which would improve the efficiency and the productivity of the available water, fulfilling environmental guidelines and including the water management in deficitary irrigation conditions; in on the other sidehand, the authorities in water and in natural risks management, which can relay on an information system for water management, drought prevention and improving the adaptation to climate change.

Amongst the different outcomes of the Project the following can be highlighted: in the first phase an automated image processing system has been developed using NOAA's images, which are

of low resolution but are taken at high frequency and cover the SUDOE area. This tool generates daily soil temperature, vegetation and irrigated surface area maps for the different zones of the SUDOE area, mainly for the Segura Basin (Spain), where additional parameters have been estimated, such as air temperature and crop evaporative demand.

In the second phase, and with the objective of calibrating the results obtained from remote sensing, partnerships have been established among institutions that have experimental plots such as IRTA, ACMG, ANPN, IRSTEA, ISA, COTR, CEBAS, UPCT, UPV and IVIA, among others, with the idea of implementing a collaboration network in the field of remote sensing and irrigation water management. On the other hand, a geoportal has been developed and adapted to the European directive on Spatial Data Infrastructures –INSPIRE–, made up of large databases of agroclimatic and cartographic information, as well as utilities and tools based on geographic information systems and remote sensing "allowing users to calculate and customize irrigation requirements for a given plot and taking into account maximal environmentally and technically efficient parameters". Finally, this portal also offers a monitoring and advisory service for farmers, who can have access to a large amount of agriculture- and environment-related information about large areas so that they can be more efficient and effective in managing irrigation water.

It should also be pointed out that the most advanced technologies have been used for estimating agronomic data on the crops at the pilot zones, since very high resolution imagery has been used, 25 cm pixels, obtained through satellite- or airplane-borne cameras or with unmanned vehicles.

In closing, we could not ignore the big contribution of cartographic information, as well as satellite images provided by the Plan Nacional de Teledetección de España [Spain's Remote Sensing National Plan] developed by the Instituto Geográfico Nacional [National Geographic Institute], which have endowed the project geoportal with many contents.

The involvement of final users, such as farmers unions and irrigators associations, in the project development and dissemination activities has meant that the products developed within the project can be used by water users when managing their farms or irrigation districts. Moreover, the latest TELERIEG activity was an advanced international course on "The use of remote sensing for irrigation management ", organized by the IAMZ in Zaragoza (Spain), from 21 to 26 November 2011. The course included the participation of 30 attendees from 11 Mediterranean countries and 16 lecturers from TELERIEG partner institutions and other organizations, guaranteeing the dissemination of the project among professionals involved in irrigation in the above-mentioned countries. This course combined new image-processing techniques used in remote sensing with field-sensor approaches, and offered an overview of the state-of-the-art and future possibilities to improve irrigation management; the project results were also presented and discussed, both at the level of plot experimentation as well as concerning management and decision-support products. The contents of the present book, which is a last dissemination product of TELERIEG, were used as supporting material in the course.

De los diversos resultados del proyecto se pueden resaltar, que en una primera fase se conseguido desarrollar un sistema de procesado automático de imágenes del satélite meteorológico NOAAA, de baja resolución pero de alta frecuencia que cubre el área SUDOE, esta herramienta permite generar mapas diarios de la temperatura del suelo, del estado de la vegetación y de la superficie regada en las diferentes zonas del área SUDOE, y especialmente en la Cuenca del Segura, donde han estimado además de los anteriores parámetros, la temperatura del aire y la demanda evaporativa de los cultivos.

En una segunda fase, y con el propósito de calibrar los resultados obtenidos por teledetección, se ha colaborado con otras instituciones que tienen parcelas de experimentación como son el IRTA, ACMG, ANPN, IRSTEA, ISA, COTR, CEBAS, UPCT, UPV y IVIA, entre otras, con la idea de crear una red de colaboración en el ámbito de la teledetección y la gestión del agua para riego. Por otro

lado, se ha desarrollado un geoportal adaptado a la directiva europea sobre Infraestructuras de Datos Espaciales -INSPIRE constituido por amplias bases de datos agroclimáticas y cartográficas, así como utilidades y herramientas basadas en los sistemas de información geográfica y la teledetección "que permiten a los usuarios calcular las necesidades de riego de una parcela de forma personalizada y bajo los parámetros de máxima eficiencia técnica y medioambiental". Por último, mediante este portal se ha desarrollado un sistema de vigilancia y recomendaciones en áreas extensas que permite a los agricultores acceder a gran cantidad información agraria y medio ambiental para que realicen una gestión más eficaz y eficiente del agua de riego.

También se puede resaltar que se han utilizado las metodologías mas avanzadas para la estimación de los datos agronómicos de los cultivos en las zonas piloto, ya que se han utilizado imágenes de muy alta resolución, 25 cm de pixel, que se han obtenido mediante el uso de cámaras aerotransportadas en satélites, aviones ó mediante vehículos no tripulados.

Para terminar no podíamos olvidar la gran aportación de información cartográfica, así como las imágenes procedentes de satélite facilitadas por el Plan Nacional de Teledetección de España desarrollado por el Instituto Geográfico Nacional y que han servido para dotar de gran cantidad de contenidos al geoportal del proyecto.

IV – Conclusions

The TELERIEG tools in the pilot zone permit the integration and management of georeferenced agroclimatic data, soil maps, quantity and quality of waters, crop information and other technical parameters of a farm or an irrigated area. The final product is a decision support system to facilitate decision-taking processes in a comfortable and generic access through internet, incorporating different techniques and access into GIS and remote sensing data.

The information technologies and more precisely, the new technologies, applied in different agriculture environments, can introduce important improvements in optimization of the agricultural production factors. The main beneficiaries of the information and decision taking systems are, on the one hand, the irrigators communities, which would improve the efficiency and the productivity of the available water, fulfilling environmental guidelines and including water management in deficitary irrigation conditions; on the other hand, the authorities in water and in natural risk management, which can rely on an information system for water management, drought prevention and improving adaptation to climate change.

Background of TELERIEG project

J.-F. Berthoumieu

ACMG, 47520 Le Passage d'Agen (France)

Abstract. Irrigation management is now possible by monitoring plant and soil water status in a special location in a field that is supposed to well represent a larger surface. This place, used as a reference, is often equipped with point sensors (as EnviroScan and others) to measure the precise variation of the available water into the root zone. Completed with weather forecast it enables a decision taking about the best moment and best amount of irrigation, preventing any risk of stress by lack of water or lack of air (brief saturation with anoxia) and reducing diffuse pollution by drainage (see PRECIRIEG project, www.precirieg.net). As it is quite expensive and time consuming to install probes in many locations the TELERIEG (www.telerieg.net) project is trying to reveal the potential of remote sensing tools in order to extend the principles of precise irrigation advice over larger irrigated areas. In this article we describe the different objectives and principal findings that are presented in other papers in this book.

Keywords. Irrigation management – Capacitance probe – Remote sensing – Precise irrigation – Water management.

Le contexte du projet TELERIEG

Résumé. *La gestion de l'irrigation à échelle fine s'appuie de plus en plus sur le suivi de parcelles de référence équipées pour observer le fonctionnement des plantes et l'évolution de l'humidité du sol. Ce lieu référentiel est généralement équipé d'outils de mesures précis de l'humidité du sol au sein du système racinaire (sondes EnviroScan et autres). En complément avec une prévision du temps il est possible de décider quand il faut irriguer la quantité optimale, de manière à : (i) éviter tout risque de stress par déficit hydrique ou par manque d'air (état de saturation avec anoxie) ; et (ii) réduire les phénomènes de pollution diffuse par drainage (voir projet PRECIRIEG, www.precirieg.net). Cependant comme il est difficile d'installer des sondes dans tous les champs irrigués (coûts d'investissement et de fonctionnement) le projet TELERIEG (www.telerieg.net) vérifie le potentiel des outils de télédétection pour étendre sur de plus grandes surfaces les conseils basés très localement sur les principes de l'irrigation de précision. Nous présentons ci-après notre démarche et nos objectifs et les principales conclusions de ce travail de 3 ans qui est décrit plus précisément dans ce livre.*

Mots-clés. *Pilotage de l'irrigation – Sondes capacitives – Télédétection – Irrigation de précision – Gestion de l'eau.*

I – Short history

Precise irrigation management is necessary for preserving a sustainable water resource allowing at the same time a better efficiency and quality of food production. Antique knowledge preserved by Arabic and Asiatic civilisations allowed until now sustainable gravity irrigation in many Mediterranean and Asiatic countries. New technologies based on available energy at quite low cost have permitted during the last decades the development of pressured-based irrigation through sprinkling and dripping systems. We present here what it has been used and experimented by ACMG (Association Climatologique de la Moyenne-Garonne, see at www.acmg.asso.fr) in the South-West of France since 1960. Other presentations in this book will explain what it has been accomplished by the other partners in other places of South-West of Europe. This short history allows understanding why we have been working all together for developing remote sensing tools and the directions of work that we have been taking during the 3 years of the TELERIEG project.

One of the first tools for better monitoring irrigation has been water balance models resting on the estimation of the so-called ETo or Potential EvapoTranspiration (PET) obtained directly from the daily observed evaporation of water in a Sunken Colorado pan or from Piche evaporimeter or through a micrometeorological equation (Penman-Monteith) including several parameters as solar energy, wind velocity, temperature and moisture of the air (Allen *et al*., 1998). The objective is to determine the water needs of the plants from atmospheric parameters. This method was mainly developed in the years 1950 to 1970, while not many tools were available or it was too expensive to monitor the real water consumption in the soil. The Water Balance is still used in many zones but the precision is low and, for example, it does not take correctly into account the vertical transfer of water from or to the water table. Our experience here in the South-West of France in the mid 80^{ties} showed that we were over irrigating more than 1/3 of the fields and it forced us to abandon that theoretical tool.

The development of new technologies and cost reduction of electronics allowed measuring indicators and parameters directly from the plant and from the soil, in situ in the root system where the exchange of water and minerals with the plant takes place. The first tool available and that we used since 1963 at ACMG is the neutron probe, then we used the Pressure Chamber or Scholander bomb completed by the gravity method, the tensiometer and the dendrometer or Pepista in France.

The pressure chamber or Scholander bomb (Scholander *et al*., 1995) remains today the reference for giving the water potential of plant tissues. It gives directly at which pressure the transpiration, activated by solar energy, "pumps" the water through the roots in the soil toward the stomata where most of that water is transpired. The higher that pressure is, the more difficult the water is taken from the soil, and the more the plant is stressed. Once measured only just at down, stem base potential is now used during day time to follow the maximum of stress and it can be used for interpreting other indicators of water stress. Within the TELERIEG program this tool has been used by most of us to complete other methods. The difficulty of its use prevented from developing the service or irrigation scheduling assessing based on this method.

The neutron probe (Musy and Higy, 2004; AIEA, 2003) was quite largely used and it is still used to measure soil water content at different depths. It uses a vertical tube installed in and below the root system and a radioactive source equipped with a receptor that is slid into the tube. The interaction of fast neutrons produced by the source and hydrogen nuclei present in the soil produces slow neutrons that are measured by the detector. Since most of the hydrogen nuclei are supposed to be contained by the water, it gives a measure of soil moisture. The problems with safety are making quite difficult to employ routinely this device that has been used in the 80^{ties} and early 90^{ties} by consultants in different countries. We stopped using it after early 90^{ties} when we had to pay more to store the old radioactive source than to buy a new one. We used instead the classic gravimetric method, taking samples of soil within the root system every 10 cm, weighing it, drying it at 110°C during 24 h and weighing again to obtain through the difference of weight the exact quantity of water relative to the mass of dry soil. With that method we monitored from 1987 till 2003 up to 550 fields every week from May till September with 4 to 5 technicians. We knew we were making errors by sampling every time a different soil even though it was at only a distance of 50 cm but we were obtaining a relative good profile of moisture and we were often doing root profiles, therefore learning much from them.

Meanwhile we tested other tools as tensiometers with water, Watermark and gypsum blocks, TDR probes (Robinson *et al*., 2003) (*Time Domain Reflectivity – it measures the travel time of an electromagnetic wave on a transmission line. The velocity depends of the water content along the line*), dendrometer (PEPISTA) (Crété *et al*., 2008), eddy covariance and some others means without much success as it was either expensive, difficult to handle for all a season, or too much perturbing the soil and the root system. For example with the TDR we have had to make a big hole to put

the probes horizontally at different depths to obtain a profile and this produced bias as the root system was damaged and the structure of the soil seriously modified. With the tensiometers with water and the Watermark it is possible to use them in loam soils but more difficult in clay and sandy soils and the technicians used to the gravimetric method did not feel as confident with these measurements. The dendrometer is a device used mainly in forestry to measure the diameter of branches or trunks. When associated with an electronic device able to measure microns it can show the reduction of size of this diameter or contour as the sap flow is drained by transpiration. If we put that sensor around young branches it allows observing the growing during the season with natural daily variation, minimum during the hottest hours, maximum at night. If the minimum stops progressing during the growing season, it shows an ongoing stress. The main difficulty is to be able to follow the same tree for more than a year and pruning may harm the equipment.

In early 2000 with the University of Paris Jussieu we tested a system aimed to measure the soil conductivity based on a technology developed earlier to look for water or oil into deep layers of the soil and called multielectrode earth resistivity testing (Samouelian *et al*., 2005). It is precise but difficult to use in a routine way by technicians. It helped us to confirm that electrical parameters of the soil are there to be measured. We found out that in Australia the Sentek Company (http://www.sentek.com.au/products/sensors.asp#soil) had developed an equivalent tool based on the measure of the dielectric of the soil through a sensor that uses capacitance based technology (Sentek, 2001) (Fig. 1).

Fig. 1. Sentek probe in a field of corn.

We have tested this product during two seasons in 2003 and 2004, and we are now using it for assessing directly or through trained persons more than 1000 farmers in France and abroad. This number of persons has been increasing every year since 2007 and in France most of the neutron probe operators are now using or planning to use the portable soil water monitoring device, Diviner 2000. It allows to follow 99 sites making profiles in preinstalled tubes of 56 mm diameter down to 1.60 m if necessary and generally with a 1 m probe. In some of the locations for reducing manpower and trip costs we leave fixed probes as EnviroScan (same size of the tube for the Diviner) or EasyAg connected to the web via a GPRS modem. See for example http://agralis.fr/sentek/carte_ref_2.php

II – Remote sensing option and directions of work

We know that we cannot equip all the fields with EnviroScan probes or tubes for Diviner, therefore it is important to better assess the spatial representativeness of the measurements with the aim to advice objectively the farmers over larger surfaces. That is why since the end of the 80^{ties} we are working with remote sensing technologies provided mainly through airborne and satellite platforms.

First we used a thermal infrared thermometer to verify remotely the canopy temperature but the precision of our tool did not give us a good signal and we abandoned it in 1990. Then we started making our own near infrared vertical pictures using a small aircraft. It allowed us to make thousands of observation of NDVI (Normalized Differential Vegetation Index) (Fig. 2) and Brilliance Index over the fields of South-West of France. We were able to diagnose the problems in the fields related to lack of water but also lack of nutrients or presence of diseases (Colette and Colette, 1999). We favoured using a small aircraft as we were able to get a higher spatial resolution when needed (vineyards) and to contour the cumulus clouds, taking data of sunny fields whereas with the satellite the picture is often not available. Also we were ready to make flights any time when the best conditions were supposed to happen in the fields (no rain during the last 8/10 days, high temperature, light wind and low cloudiness). We stopped making NDVI pictures when the technology with special Kodak infrared film stopped in 2004/2005 and we did not invest into a new digital near infra red camera while we were testing the new Sentek probes.

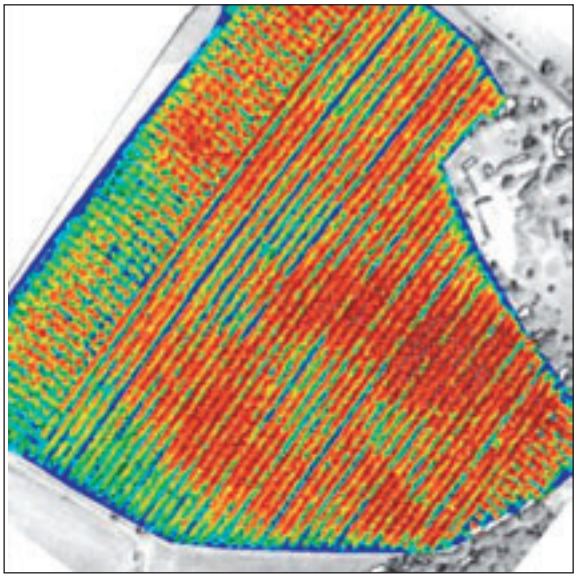

Fig. 2. NDVI map of a nuts field made with an aircraft.

At the end of the PRECIRIEG project in 2008, when we developed a methodology of consulting resting on Sentek capacitance probes and ETo forecast, we proposed our partners to start a new project where we would focus on the possibility to use remote sensing technologies for assessing the water status and comfort of the plants based on both the local field measurements (profiles of moisture, etc.) and maps obtained through remote sensing.

Three scales have been explored and are presented in this book by the different partners:

(i) The finer scale with a pixel of less than 10 cm with for example the observation of a tree from a short distance or from above canopy with a near infrared and visible camera coupled with a thermal camera *(CEMAGREF and IVIA).*

(ii) A pixel of 10 cm to few meters using cameras installed on light aircrafts *(Avion Jaune, IRTA, IVIA, UNICOQUE, ACMG)* or model aircraft *(IRTA, IVIA)* and satellites with high resolution as SPOT, DMC *(CEMAGREF, ACMG).*

(iii) a spatial resolution higher than 50 m to more than a km including thermal, visual and near infrared waves length as Landsat 5 (120 m) and 7 (60 m), HJ (China), NOAA, MODIS (240 m for visible and 960 m for thermal), *(IMIDA, COTR, ACMG, IVIA).*

When we wrote down our proposal we thought that we could use only SPOT type pictures but we have been quite disappointed to reveal that when a visual or near infra red wave signature gives a warning, it is already too late for the farmer to react for helping the plant to recover. The harm is already done when it is visible through remote sensing using waves length from visible to near infra red and resilience is not possible. We confirmed that in 2009 by comparing the NDVI of different trees having different moisture availability. At the same time we confirmed that pictures taken at noon (local time) were already well representative of the gradients shown later during the day when the maximum stress is reached between 14 and 17 h (local time).

We were quite disappointed by these results as from our past experience we had seen many local signatures of reduced NDVI related to reduced irrigation. We thought it was possible to look at the gradient and to diagnose early enough the stage where still it was possible to irrigate and to help the plant to recover. But no, the NDVI or later the NDWI (Gao, 1996) for Normalized Difference of Water Index ((NIR-SWIR) / (NIR+SWIR) where SWIR is the Short Wave Infrared waves length, were not able to give an enough early alert of water stress in the plants. The SWIR reflectance varies in both the vegetation water content and the structure in vegetation canopy but it is a reflectance form the sun light that is measured. An example of a daily NDWI can be found from http://edo.jrc.ec.europa.eu/php/index.php?action=view&id=34 and below in Fig. 3 we show two pictures of NDVI and NDWI computed over the Middle Garonne form a Landsat picture taken on April 9th 2011. Legend is the same for both.

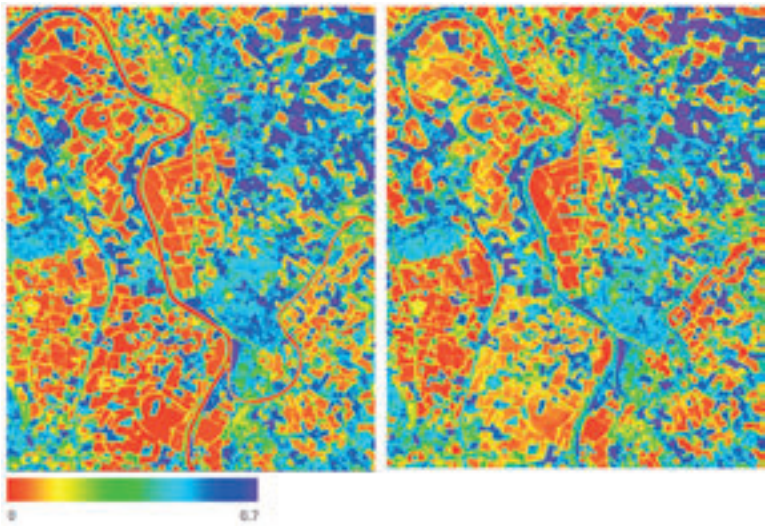

Fig. 3. Map of NDVI (left) and NDWI (right) computed over Middle Garonne from a Landsat picture taken on 2011 April 9th.

We concluded that the NDVI and NDWI are good indicators of the maximum water need at one location but it does not give any early information on the level of moisture still available in the soil. When the NDVI drops it is too late for an advice in real time.

Luckily our partner from CEMAGREF had conducted on one of our experimental fields some other measurements with thermal camera at two scales, 5 cm pixel with a camera from an elevated work platform over the canopy and 0.5 m pixel from an ultra light aircraft (http://www.lavion-jaune.fr). From that last scale we were able to look at differences in temperature in two orchards with walnuts and nuts that were explained by differences in amount of water available through irrigation while the NDVI was quite similar. The principle is simple, when there is transpiration, the latent heat of evaporation of the transpired water is taken from the leaves and the air cools against it and by convection drops to the soil with more moisture where it makes a sort of buffer zone (cool air is heavier) preventing evaporation of the soil moisture when the wind is not strong enough to take it away and to replace it with hotter and drier air. When there is not enough water available in the soil (for example below the easy to use water level), the transpiration rate is reduced, some plants are closing their stomata, other not as the kiwi, and the temperature of the leaves is getting hotter than the air. The thermal signature allows comparing zones where the leaves are cooler than the air (enough water available in the soil profile) with other warmer zones where we can suppose that a hydraulic stress is already ongoing as the total available moisture gets just above the permanent wilting point. *We know that the surface temperature of a plant canopy gets warmer than the air when the rate of moisture that the roots can uptake is less than what the plant should transpire through the stomata.*

Confronted to our past bad experience with the thermal signature obtained with a single thermo point, we contacted Richard G. Allen (Tasumi and Allen, 2007) who developed an algorithm called METRIC that computes ET (daily evapotranspiration) using remote sensing measurement and mainly resting on the energy balance at land surface: incoming energy as solar radiation and atmospheric emissions equals outgoing energy fluxes as reflected solar energy, surface emission (thermal signature), sensible heat flux, soil flux and latent heat flux (ET). We can measure the ongoing fluxes with a pyranometer or by knowing the transmittance of the atmosphere; the albedo (reflection coefficient) allows to compute the reflected solar energy, the thermal camera airborne or on the satellite is giving us the energy emission at large wave length, the sensible heat flux (H) and soil heat flux (G) can be measured by weather stations or derived from observations, remains the ET or latent heat flux (W/m^2) with ET = Rn – G – H where Rn is the net radiation flux at surface = incident flux – (reflected flux + emitted flux).

Dr. Allen is using a derived model from the Surface Energy Balance Algorithm for Land (SEBAL) developed by Bastiaanssen *et al*. (2005) from WaterWatch Company in Netherlands who is running this model and with who we are working since. See at http://www.waterwatch.nl

In this introduction we are not presenting all the details and explanation on how SEBAL works as it is done directly in one paper by Dr Wim Bastiaanssen, but we are just bringing up our first results and comments on this very impressive way of looking at the future of water management.

III – First conclusions and perspectives

In 2010 and 2011 we received, during the summer season, pictures taken through different satellites over our zone of work in the middle Garonne, between Toulouse and Bordeaux in the South-West of France. These pictures were selected by WaterWatch and included the wavelength needed to run the SEBAL model with visible, near infrared and thermal infrared. WaterWatch made the computing of NDVI, temperature and ET (Fig. 4) for the fields where we had positioned our probes for a ground truth comparison.

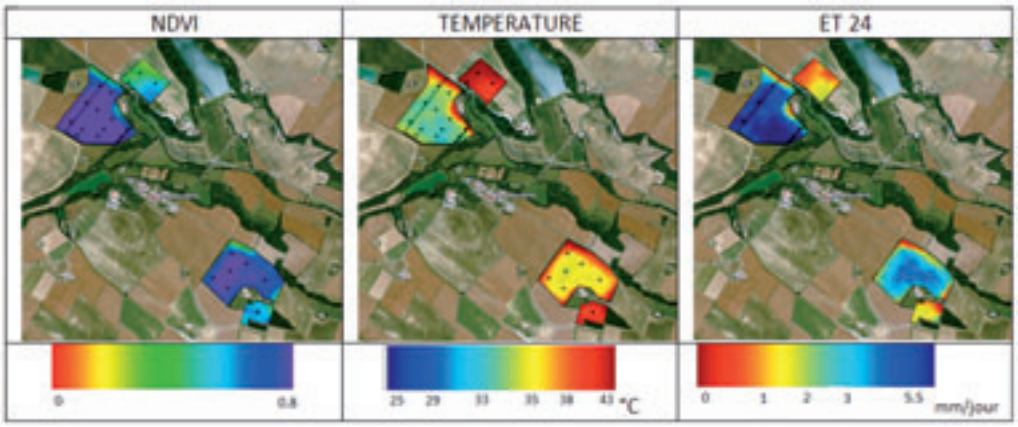

Fig. 4. Example of pictures sent to the farmer 3 days after taken by the satellite and showing on the left NDVI, center the temperature and right the ET computed with SEBAL.

During the two years we have been running a network of weather stations and Sentek probes over about 50 farms with continuous logging and over more than 250 fields with the portable device Diviner. From the first selection of 50 farms over the 250 we are already servicing on irrigation monitoring and consulting, we selected 5 farmers who were very interested by the project and who really wanted to improve their way of managing their irrigation. In each farm about 10 to 20 tubes were installed to record the moisture variation in the profiles of soil where the plants are feeding. From these local measurements we provided the farmer a once a week consultancy, either directly on the web or sent by e-mail. An example is given in Fig. 5 of a graph sent to the farmer or available on the net.

In our region the clouds are the main obstacle for providing a service for irrigation management on an entire farm based upon only remote sensing using satellites! The actual low number of satellites providing thermal pictures is the second problem. Europe has not such a satellite and we have to rest on old generation of satellites from the USA, Landsat 5 and 7; in 2011 none of these 2 platforms were able to take a good picture over our zone during the summer season! We tried using Chinese HJ new generation of satellite that are like MODIS with a bigger thermal pixel but associated simultaneously with visual and near infra red pictures taken with high good precision at 30 m over a very large zone.

Using a sharpening method, WaterWatch produced a thermal map with a 30 m pixel (Jeganathan *et al*., 2011). The physical justification is that high NDVI pixels are related to cooler vegetation and poor NDVI with high albedo to warmer fields driven by sensible heat flux rather than latent. While there is no other option for the moment we used these sharpened pictures of temperature and ET. It looks like a fair representation of the reality but we found that biases are increasing the errors and therefore we have decided not to use for the moment these sharpened thermal pictures for our diagnostic. More research is needed to improve the precision of that solution and to secure the consultancy based on that observation.

But the cloud problem remains and the perfect timing for observing the fields is also central as we got for example a picture just a day after a good rain that erased all the differences.

To contour this main problem of satellite application in our zones where clouds happen often (in dryer countries it is more the dust and bad transmittance that will make troubles) we believe there are more than one solution:

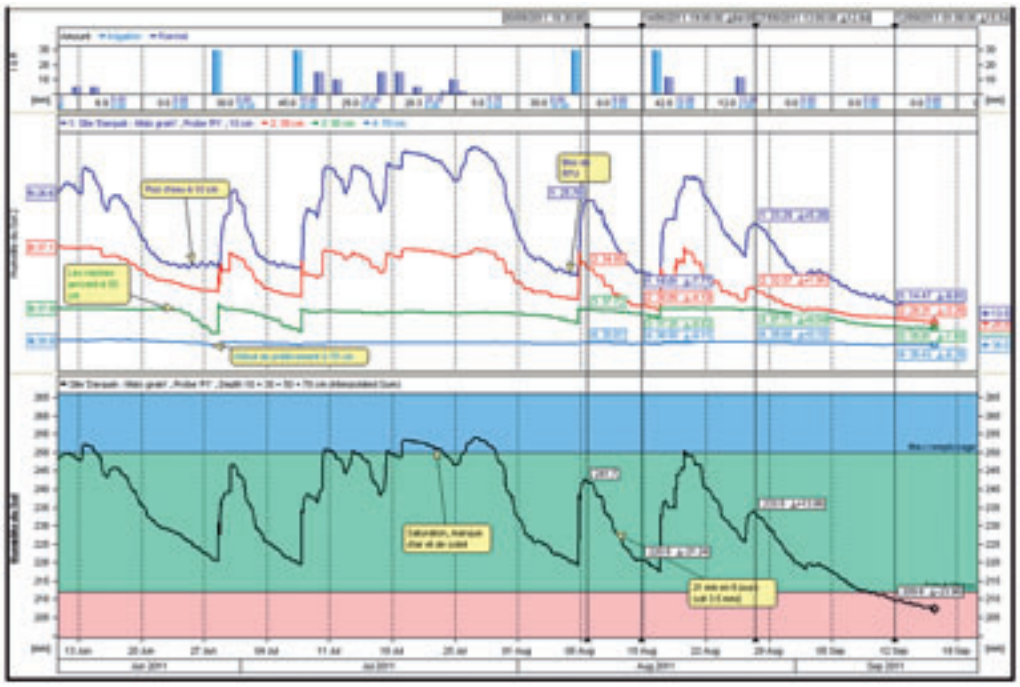

Fig. 5. Soil humidity measured by Sentek probe from June till September in a field of corn. Top graph is giving quantity of rain and irrigation; middle graph shows the variation of humidity in mm/10 cm at 10 cm (blue), 30 cm (red), 50 cm(green) and 70 cm (clear blue); bottom graph presents the interpolated sum of humidity in mm for 70 cm of soil profile (blue zone where there is lack of air, green zone the better available water and rose zone where water stress happens).

(i) To use an airborne platform as a small aircraft to be able to fly around the shades made by the convective cumuli clouds. Generally when cumuli clouds form, their life time is from 10 to 20 min and light wind pushes them at 10 to 30 km/h. therefore our experience is that it is possible to wait just few minutes to get an entire field in the picture. But this system has a cost of about 150/200 000€ for the equipment to put on the aircraft plus about 250 €/h for the flight if it is a light aircraft, a little less if it is an Ultra light aircraft but with lower cruise speed and therefore smaller surface covered during one flight from 1 to 4 pm.

(ii) To have more satellites available in order to get more chances to have a picture the needed day. Unfortunately for the moment only one new Landsat is ready to be launched in December 2012. ESA has no project and China is not yet organized to sell us with a short delay their pictures, their main tasks being over their country. CESBIO with Gérard Dedieu has a project of one research satellite at 120.000.000 € able to provide a thermal picture every day and night but it needs funding and ESA just declined to invest in it.

(iii) To base the consulting not on remote sensing as the main tool but as a complementary tool that will provide, when pictures with good resolution (less than 60 m) are available, a map of water evapotranspiration (ET), temperature and NDVI. From these maps the farmer or the consultant should be able to extrapolate over large areas the consulting done in one single place by the Sentek probes or any other type of probe providing with a good precision the humidity profile in the soil and the humidity consumption. It is possible to associate these direct meas-

urements with models providing a water balance of the moisture of the soil. However our experience with such models shows that they need to be recalibrated based on direct measurements minimum once every 7/9 days in clay soils and every 4/5 days in sandy soils.

For countries where the clouds are not a problem, there is a huge potential and the technology is ready associating remote sensing with a network of moisture probes completed with temperatures of soil and air, amount of rain and irrigation and weather forecast.

Acknowledegments

This work has been enabled by the INTEREG IV B SUDOE programme through the TELERIEG porject (SOE1/P2/E082), Agence de l'Eau Adour Garonne, the farmers participating in the program of Appui technique aux irrigants and ACMG financing.

We thank the 50 farmers and particularly Pascal Gouget, Mathieu Drapé, MM. Delmotte, Colombano and Couturié for their time and for allowing us to test these technologies in their fields. This applied research work has been made possible altogether by the team of ACMG and his commercial company Agralis with the help of other researchers as Marc Graven (scientific visitor from New Zealand Institute for Plant & Food Research Limited), Wouter Meijninger and Wim Bastiaanssen from WaterWatch (Netherlands) and the team of CEMAGREF CIRAD of Montpellier with the company L'Avion Jaune.

We thank Manuel Erena Arrabal for his work as leader of TELERIEG with his colleagues from EuroVértice.

References

AIEA, 2003. *Les sondes à neutrons et à rayons gamma: leurs applications en agronomie*. Collection Cours de Formation Nº 16/F. Vienna : AIEA. Available at : http://www-pub.iaea.org/MTCD/Publications/PDF/TCS-16F-2_web.pdf

Allen R.G., Pereira L.S., Raes D. and Smith M., 1998. Crop Evapotranspiration – Guidelines for Computing Crop Water Requirements. FAO Irrigation and Drainage Paper, 56. Rome, Italy: Food and Agriculture Organization of the United Nations. ISBN 92-5-104219-4. http://www.fao.org/docrep/X0490E/x0490e00.htm. Retrieved 2011-06-08 or see at other papers at http://www.fao.org/landandwater/aglw/cropwater/publicat.stm

Bastiaanssen W.G.M., Noordman E.J.M., Pelgrum H., Davids G., Thoreson B.P. and Allen R.G., 2005. SEBAL Model with Remotely Sensed Data to Improve Water-Resources Management under Actual Field Conditions. In: *Journal Of Irrigation And Drainage Engineering © ASCE*, January/February 2005, p. 85-93. Availabe at: http://www.kimberly.uidaho.edu/water/papers/remote/

Crété X., Faure K., Ferré G. and Tronel C., 2008. CEHM. Pomme 2008, pilotage comparé de deux systèmes d'irrigation en vue d'une optimisation des apports. Comparaison d'outils de pilotage des irrigations. Action n° 3.01.02.35.

Gao B.-C., 1996. NDWI - A normalized difference water index for remote sensing of vegetation liquid water from space. In: *Remote Sensing of Environment*, 58, p. 257-266.

Girard M.-C. and Girard C.-M., 1999. *Traitement des données de télédétection*. Paris : Dunod, 529 p.

Jeganathan C., *et al*. 2011. Evaluating a thermal image sharpening model over a mixed agricultural landscape in India. In: *International Journal of Applied Earth Observation and Geoinformation*, 13 (2011), p. 178-191.

Musy A. and Higy C., 2004. *Hydrologie: Une science de la nature*. Lausanne : Presses Polytechniques et Universitaires Romandes. 326 pp.

Robinson D.A., Jones S.B., Wraith J.M., Or D. and Friedman S.P., 2003. A review of advances in dielectric and electrical conductivity measurements in soils using time domain reflectometry. In: *Vadose Zone Journal*, 2, p. 444-475.

Samouelian A., Cousin I., Tabbagh A.,Bruand A. and Richard G., 2005. Electrical resistivity survey in soil science: a review. In: *Soil and Tillage Research,* Volume 83, Issue 2, p. 173-193. http://hal.archives-ouvertes.fr/docs/00/06/69/82/PDF/Ary.Bruan-2006-Soil_Tillage_Research.pdf 23/09/2011.

Scholander P., Bradstreet E., Hemmingsen E. and Hammel H., 1965. Sap Pressure in Vascular Plants: Negative hydrostatic pressure can be measured in plants. In: *Science,* 148 (3668), p. 339-346.

Sentek, 2001. *EnviroScan reference list*. Available at: http://www.sentek.com.au/applications/enviroscanreference.pdf and http://www.sentek.com.au/products/sensors.asp#soil

Tasumi M. and Allen R.G., 2007. Satellite-based ET mapping to assess variation in ET with timing of crop development. In: *Agricultural Water Management*, 88 (2007), p. 54-56.

Geographic Information Systems: data *versus* information. Introduction to Remote Sensing

S. Montesinos and L. Fernández

GEOSYS S.L., Sector Foresta 23, locales 7 y 8, 28760 Tres Cantos, Madrid (Spain)

Abstract. In a modern society, decision-making process realised by managers or planners must be based on true information which has been obtained from reliable and consistent data. Geographic Information Systems are tools that allows us to convert pre-existing "data" into "information" Remote sensing is defined as the ability to obtain information from an object without physical contact with it. Remote sensing term is restricted to all methods that use the reflected or irradiated electromagnetic energy of objects.

Keywords. GIS – Data – Information – Remote sensing.

Systèmes d'information géographique : donnés* vs *information. Introduction á la télédétection

Résumé. *Dans une société moderne, le processus de prise de décisions qui font les gestionnaires et les planificateurs doit être fondé sur une information véritable, qui au même temp a été obtenu des données fiables et cohérentes. Les Systèmes d'information géographique sont des outils qui nous permettent de convertir les données existantes en information. La télédétection est définie comme la capacité d'obtenir des informations provenant d'un objet sans contact physique avec lui. Le terme Télédétection se limite à toutes les méthodes qui utilisent la réflexion ou l'irradiation d'énergie électromagnétique des objets.*

Mots-clés. *SIG – Donnés – Information – Télédétection.*

I – GIS: data *vs* information

In a modern society, the "decision-making" process to be carried out by managers or planners must be based on "true information", which has been obtained from "reliable and consistent data".

In organizations that performs a constant process of decision making, the "information" plays a decisive role, because without it would not be possible the evaluation of different alternatives.

Geographic Information Systems are tools that allow us to convert "data" into interpretable "information" (Fig. 1).

BURROUGH (1986) defines a Geographic Information System: *is a powerful set of tools for collecting, storing, retrieving at will, transforming and displaying spatial data from the real world for a particular set of purposes.*

Geographic data describe the elements of real World in terms of: their position in space with respect to a coordinate system, their attributes (colour, cost, pH...) and their spatial relationships which shows us how they are related or how we can move between them.

Take as example a network of meteorological stations distributed by a territory that send us precipitation data each 5 minutes. This observation network provides us a huge number of measures, definitive data, which often are transformed into a list of difficult interpretation.

A GIS tool will allow to store in a structured way the data in table forms, positioning it into the territory, accumulating it to make data more representative, interpolating it to get data from those

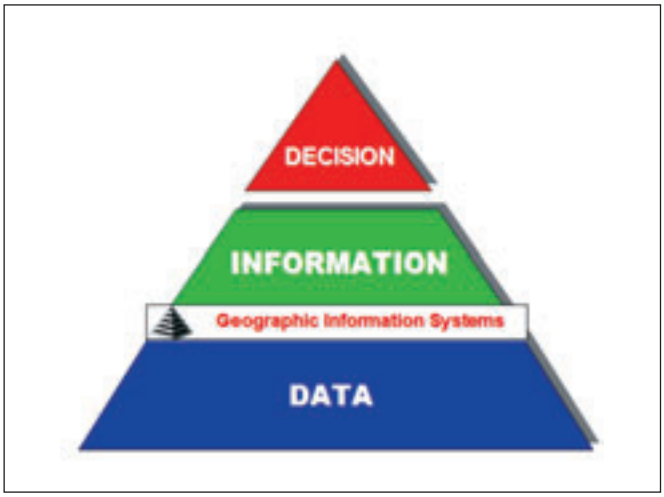

Fig. 1. Conceptual model of pyramidal decision.

areas where is not possible the observation, definitively, to convert "data" into useful "information" to the managers of the territory (Fig. 2).

Conceptually, a GIS is a relational database consisting on a graphic database linked to an alphanumeric database.

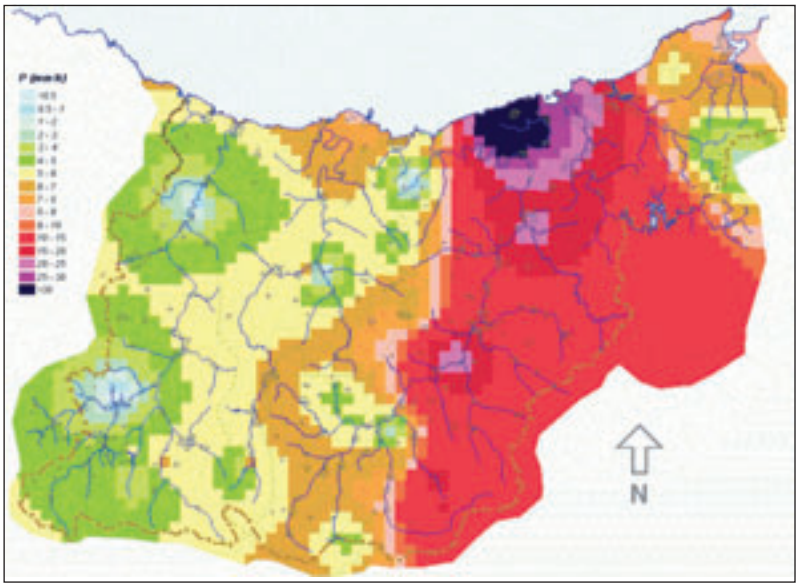

Fig. 2. Rainfall map (mm/h) obtained with punctual data from rainfall stations distributed along territory (Gipuzkoa, Spain).

When incorporating geographical entities into GIS, the digital representation is done into two different ways: Raster mode (cells) or Vectorial mode (Fig. 3).

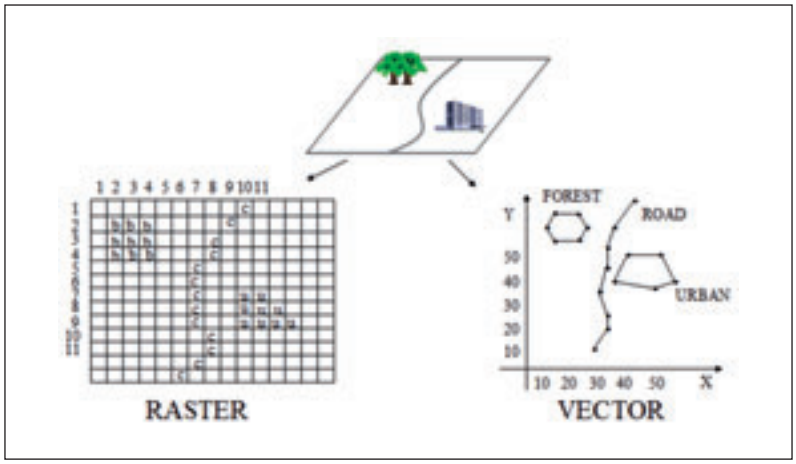

Fig. 3. Data structure into GIS.

A raster structure consists on a matrix of cells with uniform size, each of them referenced by a positional unique index (number of line and column). It contains a number or a code that represents an attribute value that has been mapped. Digital photography has a typical raster structure.

On the other hand, a vector structure represent the points thanks to a pair of coordinates; the lines by a string of coordinates, uniform or random spaced; and the areas or polygons by their edges or boundaries. Conventional mapping (geological, topographical, land use maps…) are digitally stored in vectorial mode.

Data are stored as georeferenced layers from any available source data (Fig. 4).

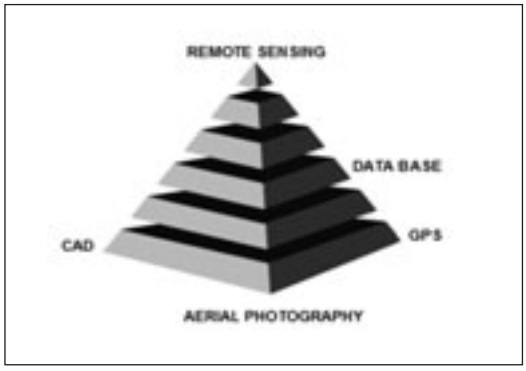

Fig. 4. Conceptual model of a GIS.

As a result of the analysis of these layers, new layers of information can be created that feed back the system. The results of the analysis are represented in alphanumerical (informs and tables) and graphical (images and maps) forms.

II – Introduction to Remote Sensing

Remote sensing is defined as the ability to obtain information about an object without physical contact with him. The term Remote sensing is restricted to those methods that use reflected or irradiated electromagnetic energy by the objects, which excludes electrical, magnetic or gravimetric parameters that measure force fields (Sabins, 1978).

This technique, which allows acquiring information of an object in distance, is based on that terrestrial surface materials have a spectral response of its own, that allows identifying them. For this, it is necessary to have instruments capable of recording the radiation from the Earth and then transform it into a signal capable of being operated in analogue (photographic products) or digital (CCTs, exabytes tapes or CDs) forms.

The laser, the radar, the multispectral scanners and the cameras are the sensors most used in Remote sensing; and the aircraft and the satellites are the platform on which to install these sensors for data acquisition.

Artifical satellites are the best viewing platform on which to install these sensors. Depending on their orbital characteristics, these satellites can be classified into three groups (Fig. 5):

(i) Geostationary satellites.

(ii) Polar orbiting satellites.

(iii) General orbit satellites.

Geostationary satellites, also called geosynchronous, are those that appear as if they were still on a fixed point on the surface. This is because the satellite is orbiting at a height such that his orbital period i(time that a satellite takes to complete an orbit around a planet) s equal to the speed of the Earth rotation.

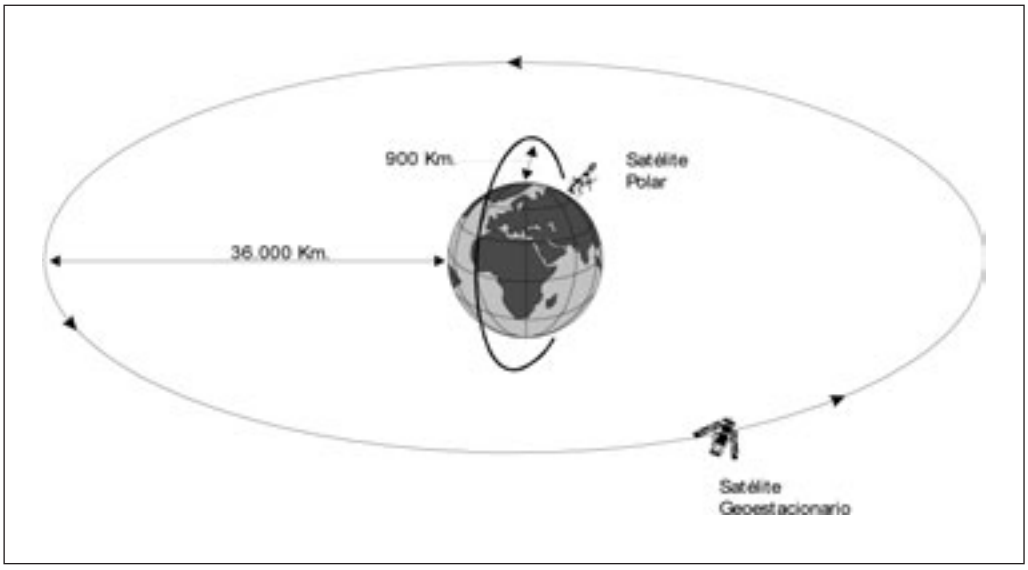

Fig. 5. Polar orbiting and geostationary Satellites (Montesinos, 1990).

This orbital altitude is about 35,800 km, that is, 5.6 times the Earth's radius (about 6,370 km). For this reason, geosynchronous orbits are equatorial or quasi-equatorial. Examples of geostationary American meteorological satellites are ATS (*Applications Technology Satellites*) and GOES (*Geostationary Operational Environmental Satellites*), or the European METEOSAT. They are characterized by low spatial resolution and the high frequency of their observations (several times a day).

Polar-orbiting satellites are also called sun-synchronous, because the angular relationship between Sun and the satellite is constant (WIDGER, 1966; PETRIE, 1970). This means that the satellite passes by the same point of the ground surface at the same time.

The three principal elements in any system of remote sensing are the sensor, the observed object and the energy flow that occurs between them. Of the types of energy flow that can occur, remote sensing uses the reflected and emitted energy (Fig. 6).

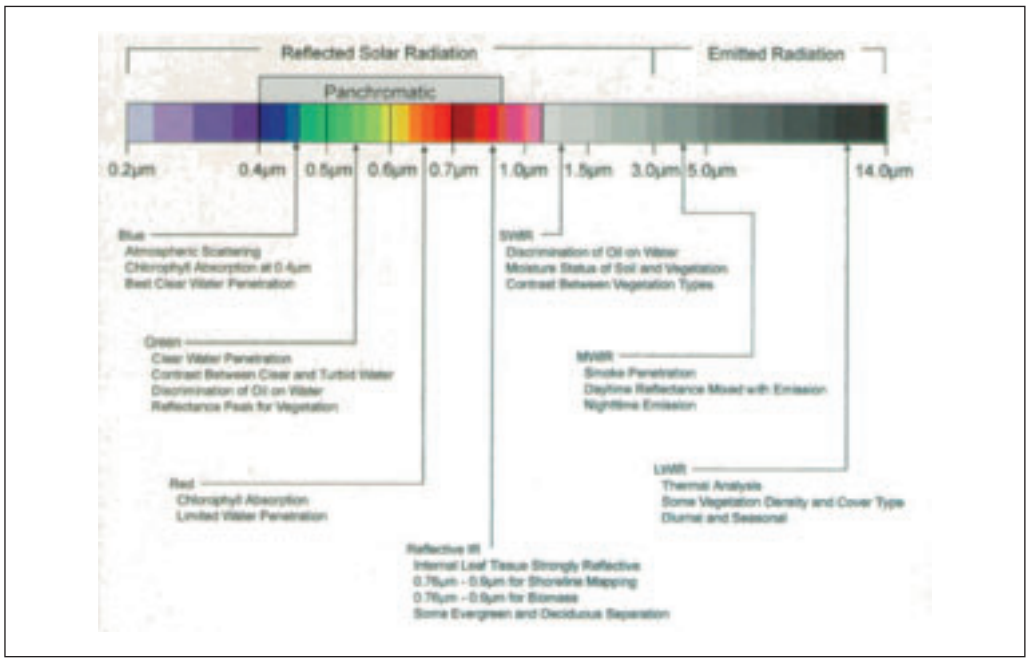

Fig. 6. The regions of the electromagnetic spectrum and their principal applications.

In remote sensing, the most widely used type of energy is the reflected by the Earth due to the solar illumination. When sun ray's strike in the Earth surface, some of this energy is absorbed and the rest is reflected back into the atmosphere by an amount dependent of the characteristics of the terrain at this point. This reflected energy flow is detected by the sensors aboard satellites and from them it is encrypted and sent to receiving stations on Earth. Passing through the atmosphere, the flow undergoes a series of interactions with the particles in it, producing modifications like absorption, dispersion… in the original reflected energy by the Earth surface.

Similarly, the observation can be based on the emitted energy by the own coverts or by the energy capable to generate their own energy flow and to collect their reflection late on the surface.

Remote sensing from satellites provides a big amount of information with particular interest in planning and management of the natural resources, whether agricultural, forestry, hydrological or mining. The information that this technique is available to us (Montesinos, 1995):

(i) *Temporal Information:* Due to their orbital characteristics, these types of satellites fly over the same area every short periods (16 days for Landsat and 25 days SPOT). This means, for example, that Landsat satellite obtained more than 20 images each year from any part of the Earth surface. To this we add that the first Landsat satellite was launched in 1972, so we have more than 800 observations available of the same point along the past 40 years.

Currently, these satellites are sending images continuously to a graphical database, thanks to this its possible not only to know past situations, but also plan future observations.

(ii) *Spatial Information:* Satellite images cover large areas of land. A Landsat scene covers about 35,000 km^2 (185 x 179 km) and SPOT, around 3,600 km^2 (60 x 60 km), allowing the integration of the study area within the physical frame to which it belongs. Spain is covered by around 50 Landsat images and 250 SPOT.

(iii) *Spectra Information:* Sensors used onboard satellites capture information not only in the visible region (which is accessible to the human eye) but also in the infrared region. This feature is especially important in the discrimination of vegetal crops, soils and lithology types.

(iv) *Radiometric Information:* Encoding electromagnetic radiation is done digitally, usually in a byte (2^8) or, which is, in a range of values ranging from 0 to 255. This digital encoding allows us to analyze the collected data by the sensors.

References

Burrough P.A., 1986. *Principles of Geographical Information Systens for Land Resources Assessment.* Oxford University Press, Oxford, 194 pp.

Hunt G.R., 1980. Electromagnetic radiation: the communication cinta in Remote Sensing. In: Siegal B.S. and Gillespie A.R. (eds), *Remote Sensing in Geology.* John Wiley. New York, p. 5-45.

Montesinos S., 1995. Desarrollo metodológico para la evaluación del riesgo de erosión hídrica en el área mediterránea utilizando técnicas de Teledetección y S.I.G. PhD Thesis, Faculty of Geological Sciences, Madrid.

Montesinos S., 1990. Teledetección: su utilización en la cuantificación y seguimiento de recursos hidráulicos aplicados al regadío. *In: Informaciones y Estudios n. 51. SGOP.* Madrid. 108 p.

Petrie G., 1970. Some considerations regarding mapping from earth satellites. In: *Photogrammetric Record,* 6, p. 590-624.

Sabins F.F., 1978. *Remote Sensing. Principles and Interpretation.* San Francisco: Freeman.

Widger W.K., 1966. Orbits, altitude, viewing geometry, coverage and resolution pertinent to satellite observations of the Earth and its atmosphere. In: *Proceedings of the 4th Symposium on R.S. of Environment*, p: 484-537.

Generation and interpretation of images

S. Montesinos and L. Fernández

GEOSYS S.L., Sector Foresta 23, locales 7 y 8, 28760 Tres Cantos, Madrid (Spain)

Abstract. A digital image is a representation of a real object using a numerical two-dimensional matrix where each element is called pixel. The digital process is the set of numerical transformations performed on the original matrix to obtain more appropriate representations of the image, depending on applications. Restoration processes are aimed to eliminate the radiometric errors sounds and geometric distortions generated during the compilation and transmission of data. The highlight consists on a set of techniques to improve the visual interpretation of the image. The multitemporal and multiespectral character of remote sensing data allows transformations that produce new components or bands of the image.

Keywords. Digital image processing – Restoration – Highlight – Information extraction.

La génération et l'interprétation des images

Résumé. *Une image numérique est une représentation d'un object réel en utilisant un tableau numérique à deux dimensions où chaque élément du tableau est appelé pixel. Des processus numériques sur la matrice d'origine sont utilisés pour obtenir des représentations appropriées de l'image, en fonction des applications. Les processus de restauration visent à éliminer les erreurs radiométrique et géometrique et de bruit générées lors de la compilation et la transmission de données. Le point culminant est un ensemble de techniques visant à améliorer l'interprétation des images visuelles. Le caractère multi-temporelle et multispectrale des données de télédétection permet des transformations qui produisent de nouveaux composants ou des bandes de'image.*

Mots-clés. *Traitement d'image numérique – Restauration – Amélioration –Extraction de l'information.*

I – Introduction

It is possible to carry out different types of analysis of images depending on data media. If the available data are of analogue nature, in black or white or in colour, a photo-interpretation is performed according to similar criteria used for aerial photography, its means depending on colour function, tone, texture, etc. If data are available in digital media, we can perform a spatial analysis based on digital image processing, which consist on a set of numerical transformations performed over the original data to obtain representations more appropriate of the image depending on future applications.

II – Overview of digital image processing

A *digital image* is a representation of a real object using a numerical bi-dimensional matrix where each element of matrix is called pixel. Each pixel has assigned a digital value that represents the associated energy with the range of wavelengths within sensibility of the detector. Thus, the measured proprieties are converted from a continuous range of values to a range expressed by a finite integer numbers that are recorded in a byte or binary code (2^8 values, from 0 to 255). The position of the pixels in an image is determinate by a coordinate system in (x,y) with the origin in the upper left corner (Fig. 1).

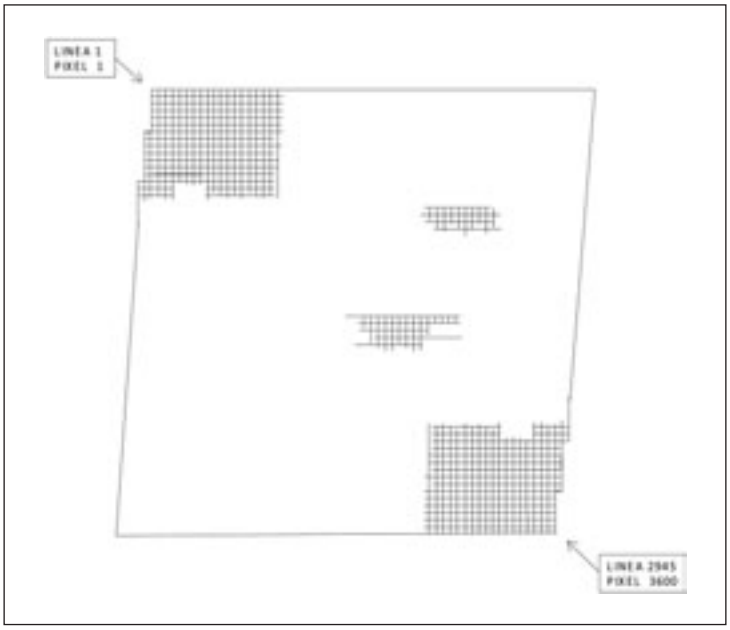

Fig. 1. Arrangement of pixels in a quarter of Landsat TM scene.

The *digital process* is the set of numerical transformations performed on the original matrix to obtain more appropriate representations of the image, depending on the applications.

In general, digital image processing can be divided into three parts:

(i) Image Restoring: Radiometric correction; Geometric correction.

(ii) Image Enhancement: Radiometric enhancement; Geometric enhancement.

(iii) Information Extraction: Main components, Arithmetic; Multispectral classifications.

The mathematical basis of the image process can be found in Dainty and Shaw (1976), Rosenfeld and Kak (1976), Andrews and Hunt (1977), Pratt (1978) and Gaskill (1978).

III – Image restoring

When sensors aboard satellites capture an image, errors can be caused in the geometry and radiometric values assigned to pixels. Restoration process are aimed to eliminate radiometric errors, as well as noise and geometrical distortions generated during the capture and transmission of the data.

The origins of radiometric errors are:

(i) The atmosphere effect on the electromagnetic radiation: the atmosphere disperses selectively the electromagnetic radiations according to their wavelength. In general, the visible bands used to be affected much more infrared bands. This leads to a loss in the calibration of the radiometric values associated with a specific pixel.

(ii) Errors of instrumentation: mainly due to the design and operating mode of the sensor. The most widespread of these errors is due to detectors.

Radiometric correction is performed by mathematical algorithms that relate the digital values of pixels in each band, providing the real reflectance of field (RICHARDS, 1986). Developments of these algorithms can be found in Turner and Spencer (1972), Slater (1980) and Foster (1984).

The origin of geometrical distortions is due to several factors (Fig. 2):

(i) The Earth's rotation during image acquisition.

(ii) Panoramic distortion due to scanner.

(iii) Skewness in the sweep.

(iv) Variations in the mirror speed.

(v) Variations in the altitude, attitude and speed of the spectral platform.

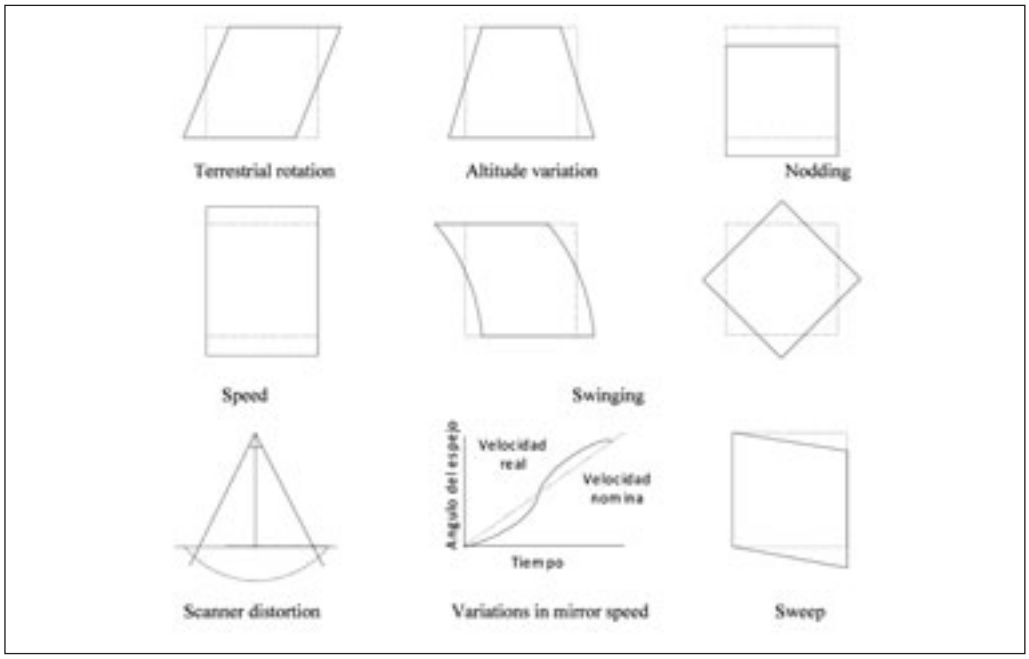

Fig. 2. Geometrical distortions of satellite images.

IV – Enhancement of the image

The enhancement is a set of techniques to improve the interpretation of the image. It can be radiometric or geometric. Radiometric enhancement modifies the pixel individually, increasing the contrast of the image. Geometric enhancement involves a spatial improvement, because digital pixel values are changed using the value of the surrounding pixels.

Colour composition, as an example, is one of the methods able to enhance digital images, because human eye only is capable to distinguish 30 levels of grey, spite is very sensible to colour (Fink, 1976; Shepard, 1969; Drury,1987).

A satellite scene is defined by the histogram. If each image pixel is examinated, it is possible to construct a graphic which represent the number of pixels with a specified value over a range of

values. The histogram of an image can also be seen as a discrete distribution of probability, because the relative height of each bar represents the statistical probability of finding a particular digital image value (Fig. 3).

Tonal or radiometric quality o fan image can be determinate from its histogram, because an image that cover the full range of digital values Hill not present accumulation of frequencies in at the ends.

An image has only one histogram, although exist the possibility that the same histogram represent several images. The histogram indicates the contrast and homogeneity of the scene.

Associated with this idea is the concept of cumulative histogram (Fig. 3) representing the threshold value of the image in relation to the total number of pixel. It is a continuous function of the value change within the image.

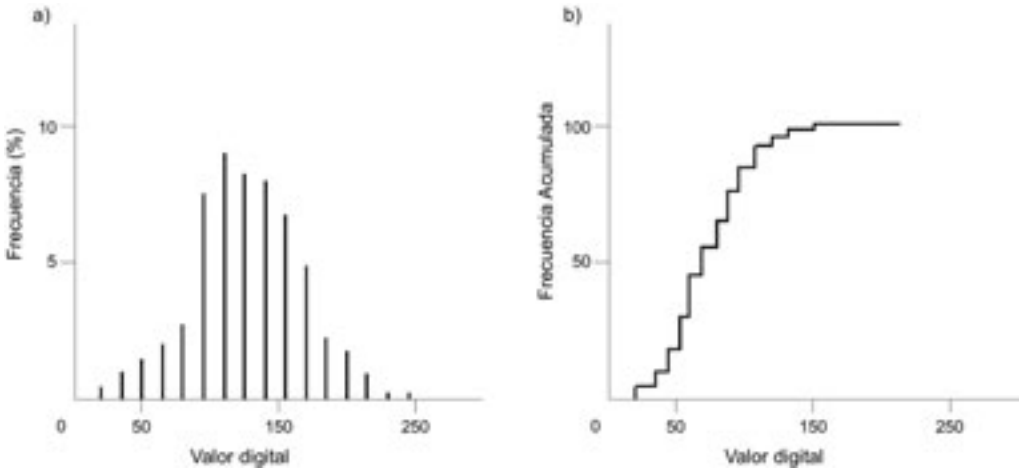

Fig. 3. (a) Original histogram; (b) Cumulative histogram.

Radiometric enhancement techniques more commonly used are:

(i) Amendment of contrast.

(ii) Histogram equalization.

(iii) Density slicing.

Geometric enhancement techniques consist in the implementation of filters, where the pixel value will be recalculated based on pixels around it. These filters are used to soften the noise of the image and to detect edges and lines.

We must keep in mind that enhancements can not be used until the other treatments are completed, as they distort the original values of pixels (Soha *et al.*, 1976).

V – Information extraction

Multitemporal and multispectral character of remote sensing data allows transformations that produce new components or bands in the image. These components are an alternative and different representation of collected data in the image. The relationship between new and old values

is done by means of linear operations. Among the most important and widespread techniques to extract information, the following are included:

(i) The *principal component analysis*: The information provided by various bands of a sensor use to be redundant within a range of wavelengths of the visible or infrared, so sometimes it is possible to omit some of them. An initial statistical analysis of the bands allows us to know:

– The mean and standard deviation of grey values for each band (frequency histograms)

– The correlation coefficients of bands.

– The variance-covariance matrix.

These variables indicate the additional information that each band bring to the image and the redundancy of data, allowing to eliminate all those that represent a high correlation, without involving a loss of information.

The principal component analysis consist then in the generation of a new set of spectral bands whose correlation is zero and the variance is maximum, meaning that previously information that was contained in "m" bands correlated each others (this implies redundancy in the contend information) now is expressed in "p" principal components, being "p<m".

(ii) *Arithmetic* between bands (addition, subtraction, multiplication and division): are performed on two or more images of the same area. These images may contain multispectral multiespectral (different bands) or multitemporal (various dates) information.

The addition is used to check if the dynamic range of an image is the same as the original ones or on the contrary is necessary to be rescaling. It is used to dampen noise.

Subtraction is used to highlight the different between images and is mainly used to detect changes between images of different dates.

Multiplication is performed between a spectral band and a matrix (mask) consisting on ones and zeros. Thus, pixel value multiplied by 0 becomes 0, and yet values multiplies by 1 keep its value. It is used when an image is form by several different areas as an example, a coastal zone where interest must be focus on sea or land. The mask will isolate this area doing zero the rest of the image.

Division or ratio between bands is one of the transformations more used in remote sensing. The reason why ratios bands are used can be summarized in two: correlation between ratio values and the shape of spectral reflectance curves between two wavelengths and the reduction of the topography effect.

iii) *Techniques of classification* are defined as the process of assignation of individual pixels of multispectral images to discrete categories of thematic category or information about radiometric values that best fit (Fig. 4).

There are two different techniques that often used to be complementary:

– Unsupervised classification: is the measure that image pixels are assigned to spectral classes without operator knows the nature of these classes. Algorithms used are clusters or groupins. These procedures are used to determinate the number and localization of spectral classes in which digital data can be divided. Operator can identify late the nature of these classes, with help of maps and field information.

– Supervised classification: In this case, operator specifies number of classes to be distinguished and statistical characteristics of each class. It is certain that the procedure more used is the quantitative analysis of remote sensing data. The different algorithms used are based on each spectral class can be described by a probabilistic distribution model in the multispectral space.

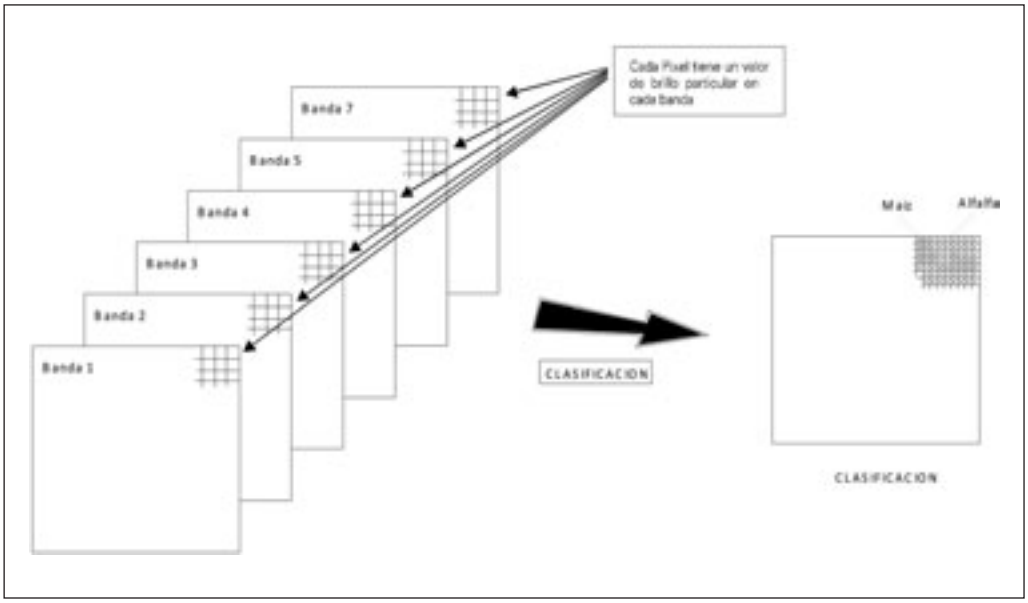

Fig. 4. Concept of automatic classification. Data correspond to 6 bands of reflexion bands of Thematic mapper sensor.

References

Andrews H.C. and Hunt B.R., 1977. *Digital image restoration*. Englewood Cliffs, N.J.: Prentice-Hall

Dainty J.C. and Shaw R., 1976. *Image Science*. Academic Press. New York.

Drury S.A., 1987. *Image Interpretation in Geology.* Allen & Unwin. London.

Fink W., 1976. Image coloration as an interpretation aid. *In: Proc. SPIE/OSA Conf. Image Process,* 74, p.209-215.

Foster B.C., 1984. Derivation of Atmospheric Correction Procedures for Landsat MSS with particular reference to urban data. In: *Int. Journal Remote Sensing*, 5, p. 799-817.

Gaskill J., 1978. *Linear systems, Fourier transforms and optics*. John Wiley and Sons. New York.

Pratt W.K., 1978. *Digital image processing*. John Wiley and Sons. New York.

Richards J.A., 1986. *Remote Sensing Digital Image Analysis. An Introduction*. Springer-Verlag. Berlin.

Rosenferd A. and Kak A.C., 1976. *Picture processing by computer*. Academic Press. New York.

Sheppard J.J., 1969. Pseudocolor as a means of image enhancement. In: *Am. J. Ophtalmo. Arch. Am. Acad. Optom.*, 46, p. 737-754.

Slater P.N., 1980. *Remote Sensing – Optics and Optical Systems*. Addison-Wesley. London.

Turner R.E. and Spencer M.H., 1972. Atmospheric Model for Correction of Spacecraft Data. In: *Proceedings 8th International Symposium on Remote Sensing of the Environment. Ann Arbor. Michigan*; p. 895-934.

Spanish National Remote Sensing Program, a way to achieve massive use of remote sensing data

J.J. Peces, G. Villa, A. Arozarena, N. Plaza, J.A.Tejeiro and E. Domenech

Instituto Geográfico Nacional (IGN), C/ General Ibáñez Íbero, 3, 28003 Madrid (Spain)
gmvilla@fomento.es – jjpeces@fomento.es

Abstract. Spanish National Remote Sensing Program (PNT) provides regular coverage of the Spanish territory with current and historical satellite imagery. This imagery is acquired with multi-user licenses for all Spanish Public Institutions, and processed once with geometric and radiometric processing agreed by experts of Spanish scientific community, and it is distributed to all users from Spanish Public Institutions. This way, we promote the massive use of remote sensing data. Spanish imagery is structured in three levels of spatial and temporal resolution: (i) High resolution: Images from 2 to 10 m of spatial resolution in panchromatic mode and from 10 to 30 m in multispectral mode. It is acquired a complete coverage every year with summer images. From 2005 to nowadays SPOT5 satellite is selected to provide that type of resolution. In future, with Spanish high resolution satellite called Ingenio, we will have several annual coverages. (ii) Medium resolution: Images from 10 to 15 m of spatial resolution in panchromatic mode and from 20 to 50 m in multispectral mode. It was planned to acquire at least four coverage every year, but since January 2008 all Landsat5 (TM) imagery captured over Spain is acquired. During 201, as well, Spot4 and Deimos1 images are being acquired. (iii) Low resolution: Multispectral images from 50 to 1000 m of spatial resolution, with a periodicity of 1 or 2 days. MODIS and MERIS sensors are the main source of this type of resolution. Nowadays, in PNT, more than 2000 images are processed every year to obtain derivate products such us georeferenced images, mosaics of images, etc. To reduce the time between the collection of data and the moment the information is available, PNT has designed a storage infrastructure suitable to the volume of information, an appropriate workflow, distribution control and an efficient spreading.

Keywords. Spanish National Remote Sensing Program – PNT – Satellite imagery – Image proccesing.

Le Plan National de Télédétection, un moyen de parvenir à une utilisation généralisée de l'information de télédétection

Résumé. *Le Plan National de Télédétection (PNT) offre une couverture régulière du territoire espagnol avec des images satellites actuelles et historiques. Cette imagerie est acquis avec licences multi-utilisateurs pour toutes les institutions publiques espagnoles, et traitée avec un traitement à la fois géométrique et radiométrique accepté par les experts de la communauté scientifique espagnole, et finallement elle est distribuée à tous les utilisateurs des institutions publiques espagnoles. De cette façon, nous favorisons l'utilisation massive de données de télédétection. L'imagerie espagnole est structuré en trois niveaux de résolution spatiale et temporelle: (i) Haute résolution: Images de 2 à 10 m de résolution spatiale en mode panchromatique et de 10 à 30 m en mode multispectral. Il est acquis une couverture complète chaque année avec des images d'été. De 2005 à nos jours, le satellite SPOT5 est sélectionné pour fournir ce type de résolution. À l'avenir, avec le satellite de haute résolution espagnole appelé Ingenio, nous aurons plusieurs couvertures annuelles. (ii) Moyenne résolution: Images de 10 à 15 m de résolution spatiale en mode panchromatique et de 20 à 50 m en mode multispectral. Il était prévu d'acquérir au moins quatre couvertures chaque année, mais depuis Janvier 2008, tous les images Landsat5 (TM) capturées sur l'Espagne ont été acquises. En 2011, les images Spot4 et Deimos1 sont aussi en cours d'acquisition. (iii) Basse résolution: les images multispectrales de 50 à 1000 m de résolution spatiale, avec une périodicité de 1 ou 2 jours. Les capteurs MODIS et MERIS sont la principale source de ce type de résolution. Aujourd'hui, dans le PNT, plus de 2000 images sont traitées chaque année pour obtenir des produits dérivés tels que des images georreferencées, des mosaïques d'images, etc. Afin de réduire le temps entre la collecte de données et le moment où l'information est disponible, le PNT a conçu une infrastructure de stockage adaptée au volume de l'information, un workflow échéant, un contrôle de la distribution et une efficacité de propagation.*

Mots-clés. *Plan National de Télédétection – PNT – Imagerie satellitale – Traitement des images.*

I – Introduction

In this century, XXI, Spain has posed two challenges, both of them very important for its sustainable development, besides the intention of modernization, the impulse of the infrastructure and the concern about the environment. The recently dynamism of the Spanish society as well as the development of the whole country causes a great impact over our territory.

All of these aspects demand the availability of accurate information about the territory constantly updated and adapted to the geographical data standards (ISO, INSPIRE, IDEE...). The satellite images give the possibility to answer about the dynamic changes that are taking place in our territory. These images are also an important part of the geographical and environmental information. Therefore, the applications and the uses are increasing.

The Remote Sensing is a mature technique with even more applications than it used to have, some of them have reached such a development that makes them being in "operational phase". However, most of the techniques and their required processing are complex, so a great specialization and hard work is needed to apply them in the correct and efficient way. This drives us to the necessity to implement systematic production lines, properly designed and constantly improved.

II – Description of Spanish National Remote Sensing Program

1. Legal and administrative framework

The "Consejo Superior Geográfico" (CSG) is the advisory and planning agency of the Spanish State dealing with the geographical information. It depends on the Ministry of Public Works, being regulated by the Royal Decree 1792/1999, November, 26th. Its aim is the coordination of geographic information of Spain. Specifically, the CEOT (special commission of land monitoring) coordinates the photogrammetric flights and territory mapping from satellite.

Under the CEOT, it is created the group of general coordination of the project, formed by the Ministry of Public Works (through the IGN, CNIG), the Ministry of Environment and Rural and Marine Affairs, and the Defence Ministry (through INTA). Likewise, it has been named a Coordinator in every Ministry involved and in every Autonomic Community, to deal with the agreement and negotiate economic transfers needed to the development of the project.

2. Organization

Inside the PNT, different work groups by experts and users have been created in order to consolidate the requirements and identify solutions. The groups created until now are:

(i) Technology Groups: High resolution, medium resolution, low resolution, radar, biophysical parameters and spectro-radiometry and architecture computing, data and metadata.

(ii) Application Groups: Agriculture, forest and fires, agrienvironment index and other applications.

The technology groups have as the mission to define technical specifications of the products to be generated from the original images and productive processes to be implemented in the PNT.

The mission of the application groups is to write technical recommendations about complete processes to facilitate the hiring by the Public Administration of products and services of an added value from the images and basic data generated.

3. Imagery acquisition

The coverage considered on the Spanish National Remote Sensing Program are structured in three levels of spatial and temporal resolution: high, medium and low.

A. High resolution

PNT considers that high resolution is an image from 0.5 m pixel size to 10 m in panchromatic and from 2 m to 30 m in a multispectral. The acquisition forecast of this type of images is a complete coverage a year at least, preferably between June, 15th and September, 15th.

The main applications of these images are: to obtain land cover cartography (project SIOSE and project CORINE land cover of the European Union), updating cartographic database of medium and small scales, to obtain environmental and agricultural information, etc. It also may be obtained "Image Cartography" (Orthoimagery and Carthoimagery).

From 2005 to 2009, the high resolution sensor chosen has been the HRG on board of the satellite SPOT5. Images that this sensor captures are from 2.5 m pixel size in the panchromatic (1 band) and 10 m in the multispectral (4 bands). Other alternatives are Formosat or the Spanish satellite INGENIO (in a near future).

B. Medium resolution

PNT considers that medium resolution is an image from 10 m to 15 m pixel size in the panchromatic and from 20 m to 50 m in multispectral. The regular recurrence initially planned were at least of 4 coverage a year, but all the images taken from Spain by the satellite Landsat5 sensor have been acquired since May 2008.

The repetitive captured of information of the same zone is carried out with the aim to allow the multitemporal monitoring (intra and inter-annual) of environment and territory evolution. It is also useful for environmental management, design of plans and policies of prevention and emergency according to natural catastrophes, risky places, control of environmental quality, etc., in which remote sensing is combined with tools like Geographical Information Systems. Other applications are land cover automatic classification, crop identification, irrigated land detection, forest information, biophysical parameters, etc.

During current year, as well, Spot4 and Deimos1 images are being acquired over all Spanish territory. In the future Sentinel2 will also be available.

C. Low resolution

PNT considers as low resolution coverage with multispectral images from 100 m to 1000 m, of spatial resolution and periodicity from 1 to 30 days.

Low resolution data are used mainly to analyze the evolution of phenomena which change quickly along time, through the creation of biophysical parameters. The daily availability of the images of these sensors and of derivate parameters of them, facilitate the monitoring in nearly real Earth time, directed to the analysis of environmental variables.

So, main applications of the low resolution images are the extraction of the biophysical and environmental parameters (indexes of vegetation, temperatures, quantity of combustible materials, and risk of fire...) these parameters can facilitate the obtaining of standard environmental index by different world organizations.

The suggested sensors are AQUA/TERRA Modis and ENVISAT Meris (with 250 m and 300 m of maximum resolution respectively) Other complementary alternatives of very low resolution are: NOAA, AVHRR, SPOT Vegetation. In the future it will also be available Sentinel 3.

4. Image processing and derivate products

Each type of territory coverage: high, medium and low resolution, counts with its own set of data, work flow and products.

A. High resolution

Spot5 images are received with a processing level 1A. All the subsequent geometric processing, such as the radiometric treatments, is carried out at the National Geographic Institute.

a] Ground control points measurement and block adjustment

The unit LPS from software ERDAS is required. Blocks are formed with the pancrhomatic images and with the multispectral images: one for the whole peninsula and one for each island.

– Block preparation: definition of the geodetic reference system, type of images to be corrected, mathematical model which is going to be used and charge images in the block.

– Ground control points measuring: Around 13 control points are taken per image measuring their terrain coordinates from aerial orthophotographies with 0.5m of pixel size.

– Block adjustment and mathematical model parameters calculation: One only adjustment is required on the block getting a unique set of parameters of the model for each image.

– Block images orthorectification. Finally, the calculated parameters are applied to every image to be transformed into the desired geodetic reference system.

b] Geometric correction

Including ground control points coordinates and tie points coordinates in one only block adjustment, images are georeferenced. The geodetic reference system used is ETRS89, projection UTM.

An exhaustive visual quality control is carried out to make sure there are no geometric deformations in the generation process of corrected images. Besides, a geometric control of the mentioned images is made through the measurement of 10 check points in each image. Check points are measured over panchromatic image and distributed regularly over a mesh defined by technical direction; they are different from ground control points. The check point medium error obtained should be smaller than 1,5 pixels and maximum error in any point, smaller than 2 pixels.

The panchromatic and multispectral images are resampling by bicubic interpolation method, and also by nearest neighbour with multispectral images.

c] Pansharpen

Trough pansharpening it is obtained an image with the same spatial resolution as panchromatic image and same spectral resolution as multiespectral image.

To make pansharpening is used "Fast SRF" method created by María González de Audicana, from Navarra University. This method has the best relation quality-processing time.

d] Radiometric balance

Radiometric balance is used to homogenize the radiometry of images to obtain a continuous mosaic. All radiometric values of all Spot5 images are transformed into radiometric values of a reference image trough a lineal mathematical transformation: $y = a*x + b$. This equation is applied band to band. Formulas to obtain "a" and "b" parameters are:

$$a = s1 / s2$$
$$b = \mu 1 - \mu 2\ (s1/s2)$$

s1: Standard deviation of reference image.

s2: Standard deviation of image to balance.

μ1: Average of reference image.

μ2: Average of image to balance.

A MODIS image has been used as reference image to make balance in 2005. Later date, mosaic generated in 2005 with all spot5 images has been used as referenced image to make new balance.

e] Band combination

Four band combinations are generated: classic false color, assigning bands 321 to RGB colour mode, Corine false colour, assigning bands 342 to RGB colour mode, natural pseudocolor, assigning bands 432 to RGB colour mode and SIOSE natural pseudocolor which is a mixture of 50% from SIOSE natural pseudocolor and a natural color that is derived from a synthetic blue.

f] Enhancement

It is used to obtain an easy image to interpret and consist of a contrast lineal expansion for red, green and blue bands. After that, a gamma function is applied for getting brightness. Enhancement is determinated for each separate portion of land. Only one enhancement is calculated for the penninsula mosaic and it is applied to all mosaic images. As well, different enhancements are calculated for each Spanish island and they are applied to all images of each island. These enhancements were determinated in 2005. From 2006, balance and enhancement are applied to images at the same time because the reference image which is used is mosaic generated in 2005 (which is already enhanced).

g] Mosaics

One mosaic is obtained for Spanish peninsula and Balearic Island and another one for Canary Island. Mosaics are made in different band combinations: natural pseudo-colour and false colour (Fig. 1). Break lines are calculated for repairing big radiometric differences that balance could not save. In 2005 and 2008, Spanish territory was completely covered with high spatial resolution images, so there are two hold mosaics for these years. There is another Spanish coverage within 2006 and 2007, so one mosaic was made for these two years. From 2009 to future an "incremental mosaic" is generated adding new images to most current mosaic for the moment, so users could see the most recent data for each surface point.

B. Medium resolution

Landsat images are received with a level processing called 1G (only sensor deformations). All geometric and radiometric processing subsequent is carried out within Spanish National Remote Sensing Program. The main steps of processing are:

a] Geometric processing

– Ground control points measurement and block adjustment: it is a process similar to that made with to high-resolution images but measuring 33 control points per image.

– Geometric correction: project image to ETRS89 geodetic reference system.

Fig. 1. Pseudo natural color Mosaic with Spot5 images.

b] Radiometric processing for optical wavelength

– Radiance calculation: Radiances are calculated from sensor calibrations coefficients trough next mathematical equation:

$$L_\lambda = G \cdot ND + B$$

L_λ: radiance obtained by sensor (W·m-2·sr-1·μm-1), ND: image digital levels,

G: gain,

B: bias.

– TOA Reflectivity calculation: next mathematical formula it is used:

$$\rho TOA = \frac{\pi \cdot L_\lambda \cdot d^2}{E_{0,\lambda} cos\theta_s}$$

d: land-sun distance at the moment of image capture, expressed in astronomical units (ua).

L_λ: spectral radiance, calculated as in the previous case.

$E_{0,\lambda}$: spectral solar exoatmospheric irradiance.

θ_s: solar zenith angle.

– Atmospheric correction. It is used "dark object model", developing by Chavez (1988; 1996).

$$\rho = \frac{\pi * \left[L - L_a \right] * d^2}{cos\theta * E_0 * \tau_1 * \tau_2}$$

ρ: reflectivity, E_0: spectral solar exoatmospheric irradiance (W·m^{-2}·μm^{-1}), τ_1: atmospherically transmission coefficient on the road Sun-Land, τ_2 : atmospherically transmission coefficient on

the road Land-Sensor, L_a: radiance witch is received by the sensor in an area where there is only atmospheric contribution (area of shadow or water according to the spectral region), L: radiance of the pixel to correct, θ: solar zenith angle and d: land-sun distance, in astronomical units.

– Topographical correction. The empirical-statistical method is used. This is the mathematical algorithm:

$$\rho_{\lambda,h,i} = \rho_{\lambda,i}\, cos\, \gamma_i\, m_\lambda - b_\lambda + \bar{\rho}_{\lambda,i}$$

ρλ,h,i: pixel reflectivity in horizontal land.

ρλ,i: pixel reflectivity in steep land.

$\bar{\rho}_{\lambda,i}$: Reflectivity average of all ρλ,i.

γ_i: incidence angle in a pixel i.

bλ: origin ordinate of the linear regression among γ_i and $\rho_{\lambda,i}$.

m_λ: slope of the linear regresion among γ_i and $\rho_{\lambda,i}$.

C. Low resolution

Images will be acquired in real time using Spanish receiving antennas. Raw data (.pds format) will be transforming into level 1b which are radiance and reflectance at sensor, TOA radiance, TOA reflectivity and observation and illumination angle and georreferenced data. So next values will be calculated:

– TOA radiances and TOA reflectance, RAD-TOA and REF- TOA.

– Latitude and longitude, observation and illumination angles.

– TOA radiances and TOA reflectance for georeferenced images.

TOA radiance will be transform into radiometric temperature (Trad-TOA) for infrared channels according to Planck law. Finally, georeferenced images will be projected to geographic coordinates.

Derivate products will be:

– Radiative products: radiance at sensor, temperature at earth's surface and normalized reflectance at earth's surface.

– Biophysical products: Normalized Difference Vegetation Index (NDVI), Fraction of Vegetation Cover (FVC), Leaf Area Index (LAI) and Fraction of Absorbed Photosynthetically Active Radiation (FAPAR).

5. Dissemination of images and derivate products

There is a working Group in PNT called "Architecture and data" aimed at defining and establishing all items in storage and distribution in PNT project. Storage and distribution must satisfy the following requirements:

(i) *Organized and accessible storage for all generated information*. Needs of hard drive for all generated information in PNT Project reach the amount of 9 Terabytes each year for more than 17.000 images. This disk volume will be increase with the images of "Historic PNT Project" (to acquire all the images captured by different sensors of Landsat constellation from their launch), whose estimated needs of hard drive are about 40 Terabytes. Moreover, it must be remembered the possibility to incorporate coverage from other satellites to PNT project.

To meet the first requirement, it has an EVA array formed by a disk array with enough capacity for storing all current information and possible to expand the storage volume in future. By

implementing a document manager for the Project provides a tool for managing information: definition of metadata-based searches and data organization, allowing the possibility of incorporating a process Management system.

(ii) *Efficient distribution according to the priorities of access*. We must have a bandwidth appropriate to the size of the files and the Lumber of users connected so that the response time is acceptable. Currently, data and derived products are distributed via FTP.

(iii) *Control of the information distribution as data policy says*.The medium and high spatial resolution images are acquired with a multi-user license restricted for Spanish Public Administration, Universities, Public Investigation Agencies and Companies working for Public Administration.

(iv) *Normalization.* To meet the last requirement of the PNT Project in storage and information distribution are considered, among other regulatory issues, the implementation rules of the INPIRE Directive, International Standard ISO and OGC specifications. Derived products in PNT project have their ISO metadata in order to comply with INSPIRE Directive.

III – Current problems, solutions and future work

1. Description of the problem

The big drawback that satellite images users can find when working with them is the subject of the clouds. According to the International Satellite Cloud Climatology Project (ISCCP) estimates that our planet is permanently covered by clouds more than 60%.

From an operational standpoint, clouds are the most significant source of error to calculate the land surface reflectivity and have an adverse effect on most remote sensing applications, making useless many of the images acquired by different satellites.Therefore, the ideal thing to do it would be to eliminate the clouds of any image while preserving the land information.

Until now, the research has been focused on automatic clouds detection. Some detection algorithms have been developed for different sensors but what they get is a mask of clouds, leaving useless that part of the image.

2. Solutions and future works

The National Geographical Institute (PNT coordinator agency), Regional Development Institute of Albacete (IDR), Image Procesing Laboratoty U. Valencia (IPL), and Center for Ecological Research and Forestry Applications in Barcelona (CREAF), are working on a research project to obtain cloudless images from temporal series of images from different sensors with different spatial and temporal resolutions which are available for the same point on earth.

The idea is: using images from multiple sensors to determine the spectro-temporal reflectance surface (STRS) for each point of Earth surface and to make a surface model (Fig. 2). After creating the model of this surface, the reflectivity of any point of surface can be obtained, for any date and wavelength, where there is no baseline data (image).

Therefore, the cloud o fan image may be removed by replacing the radiometric values of affected pixels with the reflectance values corresponding to each pixel. To achieve this purpose it is necessary to deal with two concepts:

– Downscaling or upscaling. This is to transform an image pixel size to another to compare images with different spatial resolution. It allows homogenizing radiometric information from images with different pixel size.

– Temporal interpolation is to obtain information from the earth's surface of a date which there is no image captured, interpolating between the images captured before and after dates.

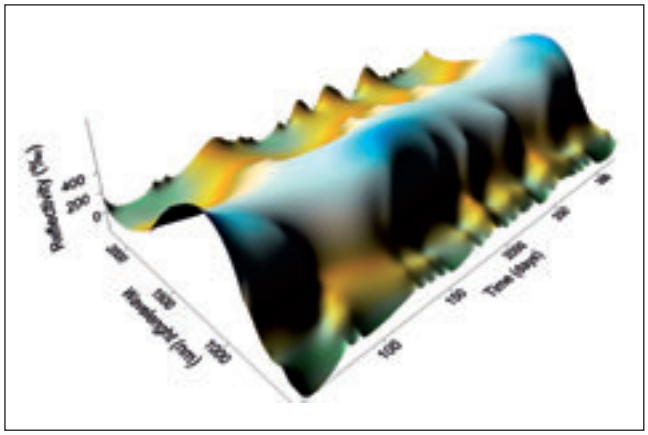

Fig. 2. Spectro-temporal reflectance surface example.

It is also necessary to introduce a new concept: the spectro-temporal reflectance surface (STRS) for each point of an image. From the beginning, in remote sensing each point of image (or Earth surface point) was characterized by its spectral signature (Fig. 3), i.e. by the reflectance value for each wavelength.

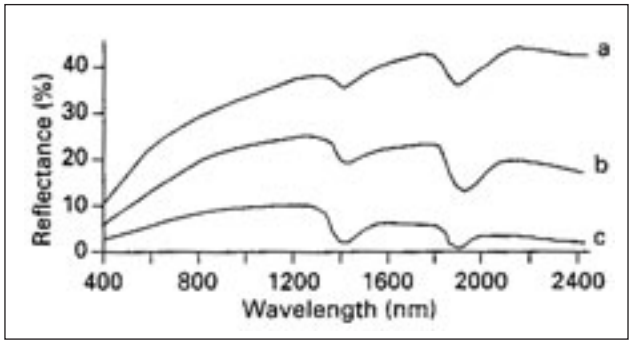

Fig. 3. Spectral signature example.

If time is added, this figure becomes a surface where reflectivity values are represented according to the corresponding wavelength and date.

Once known the STRS for each point on Earth, it would be possible to calculate reflectance values for this pixel of every date, including date where there is no images taken.

This way it is possible to replace radiometric values of pixels with clouds o fan image with reflectance values which represent the existing land bellow the cloud. As well, it is possible to generate synthetic images free of clouds of a desired date where there is any image capture by a satellite.

Future work will include improved methods of merging images of different resolutions (downsacaling and upscaling) and methods of interpolation to achieve better spectro-temporal reflectance surfaces, i.e, surfaces which represent much better the real values.

IV – Conclusions

Thanks to Spanish Remote Sensing National Program (PNT), it has been promoted the massive use of satellite images on multiple projects and jobs. PNT Project is responsible for coordinating the acquisition of satellite imagery, performing basic geometric and radiometric treatments on the images and distributing them to all the Spanish Public Administration, Universities and Public Investigation Agencies.

Now, one more step is intended by solving the major problem that all users of satellite images have for most applications in remote sensing: the clouds. Several Spanish public agencies are collaborating on a research project, where cloudless images of a desired date are obtained by removing radiometric values of pixels with clouds and replacing with reflectance values that represent the existing land below the cloud. As well, it is possible to generate synthetic cloudless images of a desired date where there is any image capture by a satellite.

References

Arozarena A., García Asensio L., Villa G. and Domenech E., 2008. Plan Nacional de Observación del Territorio en España. Conama 2008.

Instituto Geográfico Nacional, 2009. Documento PNT version 2.4. Madrid.

Equipo Técnico Nacional, 2005. Especificaciones Técnicas para el Plan Nacional de Teledetección (PNT). Madrid.

Calera A., Amorós J., Garrido J., Gómez L., Saiz J., Camps G., Villa G. and Peces J.J., 2009. Interpolación Normalizada de Imágenes procedentes de múltiples sensores.

Camacho F., Sobrino J.A., Romaguera M. and Jiménez-Muñoz J.C., 2009. Estudio de los tratamientos a realizar sobre las imágenes de satélite de baja resolución adquiridas para el PNT. Valencia.

Chuvieco E., Hantson S., Moré G., Cea C. *et al.*, 2008. Propuesta de procesado de imágenes Landsat y evaluación de algunos aspectos en zonas piloto para el PNT. Barcelona.

Amorós-López J., Gómez-Chova L., Guanter L., Alonso L., Moreno J. and Camps-Valls G., 2010. Multiresolution Spatial. Unmixing for MERIS and Landsat Image Fusion. In: IEEE Geoscience and Remote Sensing Symposium (IGARSS´10) Hawaii, USA, July 2010.

Tejeiro J.A., 2010. Procedimiento operativo estándar. Plan Nacional de Teledetección. Procesado básico alta resolución. IGN. Madrid.

Introduction to ILWIS GIS tool

S. Montesinos and L. Fernández

GEOSYS, S.L. Sector Foresta 23, locales 7 y 8. 28760 Tres Cantos – Madrid (España)

Abstract. ILWIS for Windows is a Windows-based, integrated GIS and Remote Sensing application consisting of: (i) Display of raster and multiple vector maps in map windows; (ii) Display of tables in table windows; (iii) Interactive retrieval of attribute information, (iv) Image processing facilities, (v) Manipulation of maps in a Map Calculator; (vi) Manipulation of tables in a Table Calculator; (vii) GIS analysis tools and (viii) Script language to perform 'batch' jobs. With Windows, you can start one operation and keep it running while you start one or more additional applications. This is a sort of multitasking. You may work with both Windows and DOS application programs, you can perform one or more ILWIS calculations in the background and at the same time display maps, run other ILWIS operations, print, etc. http://52north.org/communities/ilwis/

Keywords. ILWIS – GIS – Remote Sensing – Land and Water Management.

Introduction à l'outil SIG: ILWIS

Résumé. *ILWIS pour Windows est une application basée sur Windows, intégrant SIG et télédétection, composée de: (i) affichage d'images pixellisées et vectorielles multiples sous Map Windows, (ii) affichage de tableaux sous Table Windows, (iii) extraction interactive d'information sur les attributs, (iv) équipement de traitement d'image, (v) manipulation de cartes dans Map Calculator, (vi) manipulation des tables dans Table Calculator, (vii) outils d'analyse SIG, et (viii) langage de script pour effectuer des travaux groupés. Avec Windows, vous pouvez commencer une opération et la faire fonctionner pendant que vous démarrez une ou plusieurs applications supplémentaires. C'est une sorte de traitement multitâche. Vous pouvez travailler avec Windows et avec des applications DOS, vous pouvez effectuer un ou plusieurs calculs ILWIS en arrière-plan et en même temps afficher des cartes, exécuter d'autres opérations ILWIS, imprimer, etc. http://52north.org/communities/ilwis/*

Mots-clés. *ILWIS – SIG – Télédétection – Gestion de terres et des eaux.*

I – Introduction to ILWIS system

In late 1985, ITC obtained the Dutch government funds to expand its research activities in developing countries. Instead of spreading it into several small projects, ITC decided to concentrate these funds in a single research project that provided a multidisciplinary study and, thus, emphasized the applicability of the results. Allard Meijerink led this new research from ITC obtaining a Geographical Information System to identify land use and water management (Meijerink *et al.,* 1994).

For several months the project became known as *Project Sumatra*. Over time, the system under development became a more appropriate name: *Integrated Land and Water Information System (ILWIS).*

ILWIS is a geographic information system and integrated digital image processing working under Windows environment. Their tools allows to:

– Display a raster map and several vector maps in the same window.

– Display attribute tables, obtaining, interactively, attribute information.

– Digital Images process.

– Perform arithmetic operations with several raster maps.

– Perform arithmetic operations with tables.

– Perform spatial analysis.

– Generate script files to perform automatic calculations.

ILWIS tools for vector files include: scanning over screen or digitizing table, interpolation of lines or dots, calculation of density maps, analysis of patterns and poly.

The tools for raster files include: calculating distance maps, creation of digital elevation models, calculation of slope and aspect maps of slopes, calculating attribute maps, classification of maps from tables, spatial analysis with Boolean functions, –conditional and maths–, cross maps and so on. For satellite images, also has several tools to generate statistics, perform color compositions, classifications, filters and radiometric enhancements.

In addition, ILWIS contains routines to convert data to various formats, edit any kind of files, project transformations, and generation of annotations to print and/or plotter maps, charts and graphics.

II – Data Structure

The first consideration must be taken into account is that ILWIS format stores data of the same object in different files associated with each other, and whose coexistence is necessary. To protect against data loss or corruption of the maps, ILWIS has a tool that copies data from one directory to another without damaging the objects. This *copy* tool is responsible for moving all the files associated with the object or objects to copy (ILWIS, 1997).

There are three basic types of data: raster, vector (segments, polygons and points) and tabular data. Following it describes in more detail, the structure of these types.

1. Raster Maps

A raster map is a two-dimensional matrix consists of square cells. The size of this matrix is given by the number of rows and columns. Each cell, called *pixel*, has a certain value.

The format of the ILWIS raster map is an ASCII file with a .MPR extension, which includes the full description of the object, and a binary file, .MP# extension, which contains the data. Description file (.MPR) refers to the domain and the georeference used by the map, it means their properties.

The maximum size of a raster map is 2 billion lines. The maximum number of columns is: 32000 if is 1 bit map, 1 byte map or 2 bytes map; 16000 if it is 4 bytes map, and 8000 if it is 8 bytes map. The byte indicates the maximum number of different values that can have a pixel, so 1-bit = 2 values (2^1); 1-byte = 8-bit = 256 values (2^8); 2-bytes = 16-bit = 65536 different values (2^{16}), and so on.

2. Vector Maps

Here we must distinguish three types of vector maps based on the included elements. There are segments, polygons and points maps.

The *segment maps* are composed of lines (arcs) whose absolute geographic position is given by coordinate system and georeferene associated to each map. Each line has a certain value (code), which may be unique (ID) or shared with other segments (value, class, etc.). The segment map format is an ASCII file that describes the object and has a .MPS extension and three binary files containing the data, their extensions are:. CD#,. SC# and. SG#. As in the case of raster maps, the description ASCII file includes all the information about the map (domain, georefer-

ence, etc.). The maximum number of segments in the map is 32000, and the maximum number of coordinate pairs per segment is 1000.

The *polygons maps* are composed of lines (segments) that enclose areas, ie polygons. Absolute geographic position of the polygons is determined by the coordinate system and the georeference associated with to each map. Each polygon has a code that can be unique (ID) or shared with other polygons in the map (value, class, etc.). The format of a polygon map consists of a description ASCII file with a .MPA extension and five binary files containing data and with the extensions are: .PC#, .PD#, .PL#, .PS# and .TP#. The maximum number of polygons on a map is 32000 and the maximum number of pairs of coordinates on the edge of a polygon is 1000. This limitation derives from that which exists for the segments, as the edge of the polygon is made up of segments, joined together, form an enclosed area.

The *dot maps* are composed of points whose absolute geographical position is given by the coordinate system and georeference each map associated with it. Each point has a code that can be unique (ID) or shared with other parts of the map (value, class, etc.). The format of a point map is a description ASCII file with an .MPP extension, and a binary data with .MP#. Extension. Each point, therefore, has an associated set of coordinates that place it in space, and a value that depends on the domain of the map. The maximum number of points on a map is 2 billions.

3. Tables

A table is an object that stores columns with alphanumeric information. Such information usually is associated with one or more maps. The format of an attribute table in ILWIS is a description ASCII file with an .TBT extension, and a binary data file with .TB# extension.

The description file of a table stores their properties, this is the table name, their description, their dependence with another object, the number of containing columns and their description, as well as table and each columns domain. In principle, the maximum number of columns that can contain a table is 32000, and up to 2 billion records.

III – ILWIS Operations

Here are the most important operations that can be done in ILWIS, once the data has been entered into the system in the form of maps and / or tables.

They are grouped into 9 groups:

Visualization:

Show map or other object	Display an object in its corresponding window.
Color composite	Make a color composite from several raster maps.
Display 3D	Show a view in 3D perspective.
Apply 3D	Generates a 3D view.
Slide Show	From a list maps, a window is open showing, sequentially, the contained maps in the list.

Raster Operations:

Map Calculation	It is the calculation and spatial analysis module of ILWIS for raster maps. You can perform many mathematical calculations, Boolean algebra operations, conditional, etc.

Atribute map of raster map	Generate new maps from a raster map and an attribute table linked with it.
Cross	Crosses two raster maps and generate a table and/or a new raster map.
Aggregate map	Performs several operations with blocks of pixels: sum, mean, median, standard deviation, count...
Distance calculation	Assign to each pixel the less distance to a group of pixels specified by the user.
Digital Image Processing:	
Filter	Apply filters to a raster maps. The filter can be created by users, but ILWIS includes standards filters too.
Stretch	Apply a process to enhance the contrast of a raster map (usually a satellite image or aerial photo).
Slicing	Clumps pixels with values in a number of intervals.
Cluster	It is a type of unsupervised classification. Pixels are grouped according to their spectral characteristics. The maximum number of bands that can be used is 4.
Classify	Make a multispectral image classification. This is based on the samples set created with the sample operation. The ranking is based on statistical criteria, and the four possible approaches include: parallelepiped, minimum distance, Mahalanobis minimum distance and maximum likelihood.
Resample	Resamples the pixels in a raster map to transform a georeference different. There are three methods for resampling: nearest neighbor, bilinear and cubic convolution.
Statistics:	
Histogram	Calculate the histogram of a raster, polygons, segments or points maps, presenting the result table.
Autocorrelation-Semivariance	Calculate the correlation for a raster map between the values of the pixels map with the values of the pixels of the same map to different jumps in horizontal or vertical.
Principal component analysis	Calculate the relationships between different variables and reduces the amount of data needed to define the image.
Factor analysis	This operation is very similar to principal component analysis.
Variance-Covariance matrix	Calculate the variance-covariance of several raster maps. The variance is a way to express the diversity of values in a raster map. The covariance is a way of expressing the variability of values in two raster maps.
Correlation matrix	Calculated the correlation coefficients between several raster maps. These coefficients define the distribution of pixel values in the maps. Also calculates the mean and standard deviation of each map.
Neighbour polygons	Look adjacent polygons in a polygon map and calculates the length of the boundaries of these polygons. The result is a table.

Interpolation:

Densify	Reduce the size of pixel in a raster map, keeping the same projection.
Contour interpolation	This function first rasterized the contour lines, which are segments, and then calculate the values of all pixels that are not covered by segments.
Point interpolation	Realize interpolations between points randomly distributed and as a result provide a map of points on which they are located on a regular basis (gridding).

Vector Operations:

Unique ID	Assign all the elements of a vector map (segments, polygons or points) the same value. The result is a map and a table that displays a column with the original ID of the elements.
Attribute polygon map	Creates a new polygon map in which the original values are replaced by a table.
Mask polygons	Create a new polygon map in which only show those polygons whose values match those selected as a mask.
Assign labels to polygons	Allows recoding polygons from a points map that act as labels. Each polygon is identified with a point and takes its.
Transform polygons	Transform a polygon map to another projection and/or coordinate system.
Attribute segment map	Generates a new segments map in which the original values are replaced by a table.
Mask segments	Create a new segments map of in which only show those segments whose values match those selected as a mask.
Assign labels to segments	Allows recoding segments from a points map that act as labels. Each segment is identified with the closest point and takes its value.
Attribute point map	Generates a new map of points on which the original values are replaced by a table.

Rasterization:

Polygon to raster	Rasterize a polygon map that is transforming it into a raster map, using the same domain.
Segments to raster	Transforms a segments map into a raster map, using the same domain.
Points to raster	Transforms a point map in a raster map. The resulting map always uses the same domain as the point map.

Vectorization:

Raster to polygon	Generates a polygon map from a raster map. The resulting map use the same domain as the original raster map.
Raster to segment	Generate a segment map from a raster map.

Raster to point	Generates a map of points from a raster map. Each point of resulting map has the same value as the pixel from which comes.
Polygons to segments	Generates a segment map from a polygon map.
Polygon to points	Generates a map of points from a polygon map. Each point will have the same value as the polygon from which.
Segments to polygons	Generates a polygon map from a segment map. To perform this operation, all segments must be connected, forming enclosed areas.
Segments to points	Generates a point map from a segment map.

References

www.itc.nl/Pub/Home/Research/Research_output/ILWIS_-_Remote_Sensing_and_GIS_software.html

ILWIS Department, 1997. Application Guide .*International Institute for Aerospace Survey & Earth Sciences, Enschede, The Netherlands, 139 pp. http://www.itc.nl/ilwis/documentation/version_2/aguide.asp*

Meijerink A.M.J., de Brouwer H.A.M., Mannaerts C.M and Valenzuela, C., 1994. *Introduction to the use of geographic information systems for practical hydrology*. UNESCO, Div. of Water Sciences. ITC Publ. no. 23, 243 pp.

Applications of remote sensing of low resolution

Use of remote sensing for the calculation of biophysical indicators

Z. Hernández*, D. Sánchez*, J. Pecci, D.S. Intrigiolo*** and M. Erena***

*Instituto Murciano de Investigación y Desarrollo Agrario y Alimentario – IMIDA,
30150 La Alberca, Murcia (Spain)
**INDRA ESPACIO, Mar Egeo, 4, Polígono Industrial nº1
28830 San Fernando de Henares, Madrid (Spain)
***Instituto Valenciano de Investigaciones Agrarias – IVIA,
Carretera Moncada-Náquera, km. 4,5, Apdo. Apartado Oficial 46113 Moncada, Valencia (Spain)

Abstract. In recent years, remote sensing has emerged as one of the most useful tools in agronomy. A series of biophysical indicators can be derived from satellite images and become inputs for decision support systems in irrigation management, crop planning or determination of crop yields, thus achieving a better management of resources. An automated system implemented under the Telerieg project provides these indicators on a daily rate to aid in decision-making.

Keywords. NDVI – LST – Remote sensing – NOAA-AVHRR – Telerieg – SUDOE – Evapotranspiration – Temperature – Albedo.

Utilisation de la télédétection pour le calcul d'indices biophysiques

Résumé. *Ces dernières années, la télédétection a émergé comme l'un des outils les plus puissants dans le domaine agronomique. La réception d'images satellite permet de calculer une série d'indices biophysiques qui, à leur tour, peuvent alimenter des systèmes d'aide à la décision dans la gestion de l'irrigation, la planification des récoltes ou la détermination des rendements des cultures, conduisant ainsi à une meilleure gestion des ressources. Un système automatisé mis en œuvre par le projet Telerieg fournit quotidiennement ces indices pour aider à la prise de décisions.*

Mots-clés. *NDVI – LST – Télédétection – NOAA-AVHRR – Telerieg – SUDOE – Évapotranspiration – Température – Albédo.*

I – Introduction

Remote sensing science and technology, and its applications in various fields, have experienced a successful development in recent decades. The Earth observation from space has become an irreplaceable tool for monitoring various environmental processes of great importance. Desertification processes, formation and development of hurricanes, reduction of ice areas at the poles, deforestation and forest loss or damage assessment after flooding or after a tsunami are some aspects that can be studied by remote sensing.

Until recently, applications and surveys using remote sensing were restricted to very large areas, but technological development has increased its spatial, temporal and spectral resolution, allowing for the development of applications and tools with accuracies of less than one meter.

This is why remote sensing starts to spread like a very useful tool in various disciplines, including agriculture, where it helps to define irrigation schemes, monitor crop development or perform remote identification, among others.

One of the most important features of remote sensing is its ability to extract thematic information from certain measurements of the sensor. That is, other factors that help us better understand our environment can be derived from sensor data. For example, the chlorophyll content is a variable not directly measured by the sensor, but which changes the reflectance this latter receives, so it can be estimated indirectly by observing on which spectral bands its effect is more evident and isolating this component from other factors that may also influence such bands (Chuvieco Salinero, 2002).

The Telerieg project (www.telerieg.net), which full name is "Remote sensing use for irrigation practice recommendation and monitoring in the SUDOE space", aims to better protect the environment through a more efficient and rational management of water resources in agriculture and a more effective prevention and better response capacity to natural hazards. One of its objectives is to improve the recommendations and monitoring of irrigation practices in major crops of the area of the Tajo-Segura Aqueduct in Southeastern Spain.

To achieve it, we have designed an automatic processing system to generate remote sensing products combining data from NOAA-AVHRR satellite with data from a network of agro-meteorological stations. This system sets in motion a chain of data-driven processes (i.e., triggered by the availability of data) that produce a first set of six basic remote sensing products that will be analysed later.

II – Automatic processing system

So far, one of the problems for automatic generation of remote sensing products was the need of *in situ* sensor data for some of the development stages: generation, calibration, validation, complementation, etc. In many cases these data were not available for several reasons: compulsory application forms, limited accessibility to data that could also be not compatible with computer applications, lack of security of supply or geographical distribution, etc. This entailed waiting times and lack of regular availability of data, which resulted in increased production costs.

To overcome these drawbacks, there is a current trend that tends to make data more easily accessible and open. The idea is to convert what is initially an *in situ* resource providing details of the near physical environment into a web resource compatible with commonly used software tools. The OGC (Open Geospatial Consortium) has created a series of standards for search, access and distribution, applicable to station data, among others. This standard has been called SOS-SWE (Sensor Observation System – Sensor Web Enablement). This method would solve almost all the above-mentioned issues associated with *in situ* data.

In this scenario, a methodological proposal arises for automatically obtaining products derived from NOAA-AVHRR images through "web sensors", according to OGC-SWE standards. Automation has several advantages: decreased generation time, dedicated technical staff not required, regular supply of data and, ultimately, lower costs per product.

The following Fig. 1 shows a context diagram of the proposed and finally developed system.

The NOAA Station (Dartcom), installed in IMIDA facilities, receives the AVHRR images daily and process them up to level 1b (L1B). These images are automatically detected and become part of the database of products. At the same time, the sensors of the network of agro-meteorological stations record hourly weather observations that are stored in a central database.

When a new NOAA-AVHRR L1B image reaches the data archive, the process chain starts: meteorological observations needed to generate the products are queried from the central database. Then, the available data and images are processed to output the following products:

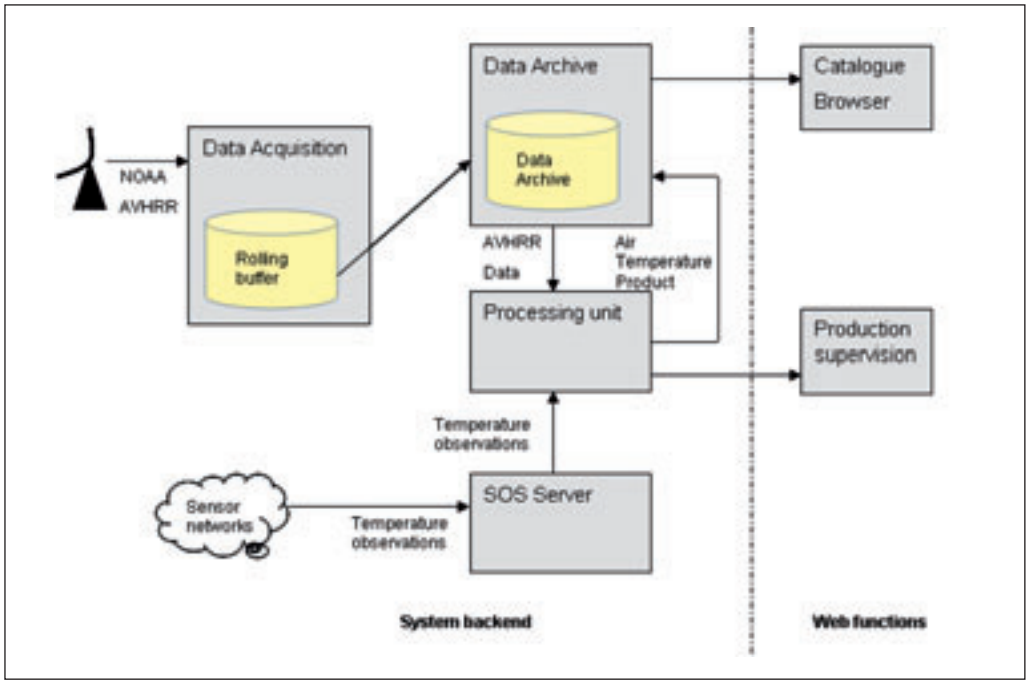

Fig. 1. System description.

1. Level 1C NOAA-AVHRR image (L1C, georeferenced product).
2. NDVI.
3. Land surface temperature (LST).
4. Potential evapotranspiration (ET_0).
5. Air temperature (AT).
6. Albedo (ALB).

Finally, we have developed a web viewer for querying, browsing and downloading products. This catalogue can be searched by acquisition date and product type, and displays the results alongside their legends in an embedded Google Earth viewer. The viewer also offers a smaller version of the metadata for each product and their respective download links.

It should be noted that the design of this system has been driven by expandability and interoperability criteria:

– Receiving data from additional sensors: The system is not limited to the reception of NOAA-AVHRR data, as it can be potentially configured to download Earth Observation (EO) data from any other repository in the world. For example, it could be configured to download and process MODIS data located on an FTP, Landsat or SPOT site.
– It can include additional processors for new products, beyond those initially planned and developed.
– It can process data from other geographical areas where *in situ* images and data are already available.
– It makes use of OGC standards for web services, following the SOS-SWE standard to store and make available data from the sensor observations to any user, ensuring interoperability.

III – Products generated

1. Normalized Difference Vegetation Index (NDVI)

NDVI, proposed by Rouse *et al.* in 1974, is one of the most widely used vegetation indices. This index reveals the presence of vegetation and monitors its development, so we may determine the metabolic efficiency of vegetation in a given area or locate areas where the vegetation growth is less than in the surrounding areas.

This index is based on the distinctive radiometric behaviour of vegetation throughout certain spectral windows. Healthy vegetation shows a characteristic spectral signature with a clear contrast between the visible bands, especially the red band (0.6 to 0.7 µm) and near-infrared (0.7 to 1.1 µm) (Chuvieco Salinero, 2002). The chlorophyll pigments of a leaf absorb most of the energy of the visible light area in contrast to the low absorption of the near-infrared. This marked difference between the absorption spectrum in the visible and near-infrared (NIR) of healthy vegetation allows for distinguishing it from those suffering some kind of stress (water stress, for example, caused by drought), in which there is less reflectance in the NIR and greater absorption in the visible. Thus we can conclude that the greater the contrast between the reflectances of both bands, the greater the vigour of the vegetation cover, a lower difference indicating unhealthy or sparse vegetation. On the other hand, the radiometric spectrum of soil usually does not show this clear difference between the above mentioned spectral bands and, therefore, NDVI makes difficult to distinguish between vegetation and bare soil (Karnieli *et al.,* 2010). To overcome this drawback, indices such as SAVI and MSAVI were created, in order to highlight the vegetation response and reduce that of the soil. The NDVI is calculated using the expression proposed by Rouse *et al.* in 1974:

$$NDVI = \frac{\rho_{NIR} - \rho_{red}}{\rho_{NIR} + \rho_{red}}$$

Where ρ = reflectance in the corresponding band.

NDVI applications are very diverse (Fig. 2). In agriculture, it is used to evaluate the status and evolution of crops, to estimate crop yields (Moges *et al.*, 2004), to identify crops and develop agricultural inventories and to study crop forecasting, as done by Martínez-Casanova, J. *et al.* (2005) for vines.

2. Land Surface Temperature (LST)

Land surface temperature as derived from satellite data can be defined as the temperature radiated by the Earth's surface and observed by the satellite sensor.

The calculation of LST from satellite images is being regularly and widely used in climate and global change studies, in different disciplines such as geology, hydrology, agronomy, ecology or meteorology.

To obtain LST, data from the thermal infrared band is used, since most of the energy detected by the sensor in this spectral region is emitted by the Earth's surface (Jiménez-Muñoz and Sobrino, 2008). In order to know the temperature of the Earth's surface by using pixel radiance of a satellite image as main input data, basically two quantities of radiation must be related: that which reaches the satellite and that coming from the ground, as the latter depends on the temperature we want to estimate *(*Pérez *et al.*, 2003).

The most common methodology for obtaining LST is known as split-window algorithm. Over the past 25 years there have been numerous publications on split-window algorithms. Qin *et al.* (2004)*,* for example, considers up to 17 of them in his comparative study of LST products derived from NOAA-AVHRR images.

Fig. 2. NDVI products in the catalogue browser.

Retrieval of surface kinetic temperature from AVHRR data by this technique was firstly proposed for sea temperature estimation (Quin *et al.,* 2004). Application of the split-window methodology to estimate LST did not begin until the mid-eighties with Price (1984) (Quin *et al.*, 2004).

The study of Quin (2004) compared each of the algorithms in terms of calculation and accuracy, using measures on the ground and simulations obtained from programs such as LOWTRAN, MODTRAN or 6S. Based on these facts, Quin concluded that one of the best algorithms for LST retrieval from AVHRR was proposed by Sobrino *et al.* (1991), published in the journal *Remote Sensing of Environment.* For this reason, Telerieg has used the algorithm proposed by Sobrino *et al.* (1991), later modified by Sobrino and Raissouni (2000) to produce maps of LST. The coefficients used were obtained from Jiménez-Muñoz and Sobrino (2008), which provide those that can be used with different low-resolution sensors.

The algorithm is given by:

$$T_s = T_i + c_i (T_i + T_j) + c_2 (T_i + T_j)^2 + c_0 + (c_3 + c_4 W) (1 - \varepsilon) + (c_5 + c_6 W)\Delta\varepsilon$$

where T_i and T_j are the at-sensor brightness temperatures (in ºkelvin) at the split-window bands i and j, ε is the mean emissivity, $\varepsilon = 0.5(\varepsilon_i + \varepsilon_j)$, $\Delta\varepsilon$ is the emissivity difference of the bands i and j, $\Delta\varepsilon = (\varepsilon_i + \varepsilon_j)$, W is the total atmospheric water vapour content (in grams per square centimetre), and $c_0 - c_6$ are the split-window coefficients determined from simulated data.

3. Evapotranspiration (ET_0)

In agriculture, the estimation of evapotranspiration is especially useful to help determine water demand and thus, irrigation management (definition of irrigation schedules). This in turn improves the management of water resources in the area and thus helps to protect the environment.

Until relatively recently most evapotranspiration estimation models were applied only locally, since they required *in situ* measures from nearby weather stations (e.g. soil water balance, Bowen ratio or Penman-Monteith equation). But with the development of remote sensing, calculation models of evapotranspiration have been applied and extended to larger areas, even where mete-

orological data are unavailable. Remote sensing has thus become a major tool for monitoring the evolution of evapotranspiration at different scales, from whole regions to individual plots, through high-resolution images.

The Telerieg project team has calculated the reference evapotranspiration through the adaptation of the Penman-Monteith equation to remote sensing proposed by Rivas (2004) in his thesis work. This adaptation produces a linear relationship that simply requires calculating two parameters, which represent the radiative and meteorological effects on a hypothetical reference surface, for a given set of local conditions described in Rivas *et al.* (2003). This combination of the Penman-Monteith equation with satellite data is a simple way to estimate evapotranspiration at a regional scale and is expressed as follows:

$$ET_0 = a \cdot T_s + b$$

La temperatura de superficie (T_s) se extrae de las imágenes de satélite NOAA-AVHRR y es uno de los productos ya derivados en el contexto del proyecto Telerieg (ver *apartado 2* de este capítulo). The coefficients a and b are defined on the basis of meteorological data and the features of each region. Meteorological stations must provide data on air temperature, relative humidity, wind speed and solar radiation to estimate analytically the parameters a and b (Rivas *et al.*, 2003). In the present case, we have chosen to use coefficients obtained for a zone similar to that described in the above-mentioned thesis work (Fig. 3). This is the region of Larissa (Greece), whose coefficients are a = 0.14 mm/(day·°C) and b = -0.40 mm/day.

	ET0 NOAA / ET0 in situ	
	R	Nº Valores
14/10/2010	± 0.42	33
15/10/2010	± 0.65	25
17/10/2010	± 0.55	38
18/10/2010	± 0.63	43
19/10/2010	± 0.51	42
20/10/2010	± 0.63	42
TOTAL	**± 0.57**	**223**

Fig. 3. Results of the partial validation of the ET0 algorithm on the region of Murcia.

4. Air Temperature (AT)

The air temperature near the surface is a key variable to describe the energy and water cycles in the Earth-Atmosphere system (Colombi *et al*., 2007). It is also a required parameter in environmental and hydrological calculation models.

The air temperature is usually measured by weather stations, which provide only very specific values. This means that it is very difficult to get data from remote or isolated areas where these stations are less frequent. In the last few years, the improvement of remote sensing techniques has allowed for the implementation of an algorithm to calculate the spatial distribution of air temperature by using data derived from remote sensors.

Telerieg proposes to determine AT from land surface temperature as the two variables are related, although this relationship varies depending on the terrain features and on the daily and seasonal atmospheric conditions. The proposed procedure solves, by empirical methods, the problem of establishing this relationship. Through a linear correlation analysis of LST derived from NOAA-AVHRR and air temperature measured *in situ* by the network of agro-meteorological stations of the

SIAM (Agro-meteorological Information System of the Murcia Region), we obtain coefficients which determine the equation that will generate the values of air temperature for the entire study area.

Since the relationship between the two variables depends on soil types and topography, we defined several linear equations for the different types of terrain found in the studied basin (Fig. 4). After determining the coefficients that define the linear equations, these equations were applied to each pixel of the LST maps derived from NOAA-AVHRR, producing an estimate of air temperature at 1 km resolution.

This method is well documented in the literature. For example, Jones *et al.* (2004) estimate the minimum air temperature at night through MODIS LST products in Alabama. Gang Fu *et al*. (2011) estimate the air temperature in an alpine meadow in northern Tibetan Plateau from MODIS LST products. We can find many more examples in various scientific publications.

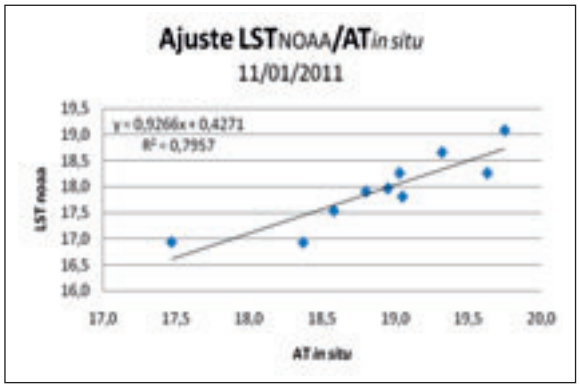

Fig. 4. Least squares fitting for LST-AT values.

5. Albedo (ALB)

Albedo is a quantity that expresses the relationship between incident and reflected energy on the Earth's surface. That is, albedo defines how much solar radiation is reflected (short-wave energy) or absorbed and reemitted (in the thermal infrared) (Dickinson *et al.,* 1990, in Sellers*, et al.,* 1995). Albedo ranges from 0 (totally absorbing surfaces) to 1 (perfectly reflective surfaces).

The albedo calculated in Telerieg has been the TOA (Top-of-Atmosphere). This is a broadband albedo, which measures reflected radiation in the visible range and part of the near-infrared. It is obtained through a linear combination of bands 1 and 2 of NOAA.

The wavelengths of the AVHRR/3 sensor, carried on NOAA-15 and later satellites in the same series, are indicated in Table 1.

Table 1. AVHRR-3 channels. Based on: http://noaasis.noaa.gov/NOAASIS/ml/avhrr.html

Channel	Wavelength (μm)	Spectral region
1	0.58 – 0.68	Visible
2	0.725 – 1.10	Near-infrared
3	3.55 – 3.93	Mid-infrared
4	10.30 – 11.30	Thermal infrared
5	11.50 – 12.50	Thermal infrared

We used the algorithm proposed by Gimeno-Ferrer *et al.* (2001). It is a linear combination of the radiances of bands 1 and 2 (short-wave):

$$L_{0L} = a_0 + a_1 L_1 + a_2 L_2$$

Where L_{0L} = long-wave radiance, L_1 and L_2 = short-wave radiances of band 1 and 2, respectively, and a_0, a_1 and a_2 = previously calculated coefficients depending on the type of surface. In Telerieg, we have used the coefficients defined for the AVHRR sensor in the same publication.

After this calculation and in order to transform the albedo in a percentage, the latter is divided by the incident solar radiation (TOA) estimated for the corresponding day and latitude.

Acknowledgments

This work has been done through the project "Telerieg – Remote sensing use for irrigation practice recommendation and monitoring in the SUDOE space" financed by the South West Europe Territorial Cooperation Programme (Interreg IVB-SUDOE), which supports regional development through European Regional Development Fund (ERDF) co-financing of transnational projects.

References

Chuvieco Salinero E., 2002. *Teledetección Ambiental*. Ed. Ariel Ciencia.

Colombi A., De Michele C., Pepe M. and Rampini A., 2007. Estimation of daily mean air temperature from MODIS LST in alpine areas. In: *EARSeLeProceedings* 6. 1/2007.

Fu G., Shen Z., Zhang X., Shi P., Zhang Y. and Wu J., 2011. Estimating air temperature of an alpine meadow on the Northern Tibetan Plateau using MODIS land surface temperature In: *Acta Ecologica Sinica*, 31 (1), p. 8-13.

Gimeno-Ferrer J.F., Bodas A. and López-Baeza E., 2001. Corrección spectral de medidas de satélite. Transformación de banda estrecha a banda ancha. Aplicación a Meteosat y AVHRR In: *Revista de Teledetección*, 2001. 16, p. 89-93. http://www.aet.org.es/revistas/revista16/AET16-16.pdf

Jiménez-Muñoz J.C. and Sobrino J.A., 2008. Split-Window Coefficients for Land Surface Temperature Retrieval From Low-Resolution Thermal Infrared Sensors. In: *IEEE Geosciencie and Remote Sensing Letters*, Vol. 5. Nº 5.

Jones P., Jedlovec G., Suggs R. and Haines S., 2004. Using MODIS LST to Estimate Minimum Air Temperatures at Night. In: *13th Conference on Satellite Meteorology and Oceanography.* Norfolk, VA.

Karnieli A., Agam N., Pinker R.T., Anderson M.C., Imhoff M.L., Gutman G.G., Panov N. and Goldberg A. 2010. Use of NDVI and land surface temperature for assessing vegetation health: merits and limitations. In: *Journal of Climate*, 23, p. 618-633.

Martínez-Casasnovas J. and Xavier Bordes A., 2005. Viticultura de precisión: Predicción de cosecha a partir de variables del cultivo e índices de vegetación. In: *Teledetección. Avances en la observación de la Tierra.* Editores Arbelo M., Gonzalez A., Perez J., p. 33-36.

Moges M., Raun W., Mullen, R. Freeman K., Johnson G. and Solie J., 2004. Evaluation of Green, Red, and Near Infrared Bands for Predicting Winter Wheat Biomass, Nitrogen Uptake, and Final Grain Yielg. In: *Journal of Plant Nutrition*, 27 (8), p. 1431-1441.

NOAA Satellite and Information Service. National Environmental Satellite, Data, and Information Services (NESDIS). Advanced Very High Resolution Radiometer – AVHRR. Consulted on 07/07/2011. http://noaasis.noaa.gov/NOAASIS/ml/avhrr.html

Qin Z., Xu B., Zhang W., Li W. and Zhang H., 2004. Comparison of split windows algorithms for land surface temperature retrieval from NOAA-AVHRR data. In *IEEE 2004 International Geosciencies and Remote Sensing Symposium*, VI: 3740-3743, Anchorage, Alaska.

Rivas R. and Caselles V., 2003. La ecuación de Penman-Monteith para su uso en teledetección. In: *Revista de Teledetección,* 2003, 20, p. 65-72.

Rivas R.E., 2004. Propuesta de un modelo operativo para la estimación de la evapotranspiración. Dirigida por: Vicente Caselles Miralles. Departamento de Termodinámica. ISBN: 84-370-6083-4 Universitat de València. Servei de Publicacions.

Pérez A.M., Calle, A. y Casanova J.L., 2003. Cálculo de la temperatura superficial a partir de datos Landsat TM. In: *X Congreso de Teledetección.Teledetección y Desarrollo Regional*. 2003. p. 95-98. Rosa Pérez Utrero y Pablo Martínez Cobo (Coords).

Price J.C., 1984. Land Surface temperature measuraments from the split window channels of the NOAA 7 Advanced Very High Resolution Radiometer. In: *Journal of Geophysical Research*, 89, p. 7231-7237.

Rouse J.W., Haas R.H., Schell J.A., Deering D.W. and Harlan J.C., 1974. Monitoring the vernal advancement of retro-radation of natural vegetation. In: NASA/GSFC, Type III, Final Report, Greenbelt, MD, 371.

Sellers P.J., *et al.*, 1995. Remote sensing of the land surface for studies of global change: Models-algorithms-experiments. In: *Remote Sensing of Environment*, 51, p. 3-26, 1995.

Sobrino J.A., Coll C. and Caselles V., 1991. Atmospheric correction for land surface temperature using NOAA-11 AVHRR channels 4 and 5. In: *Remote Sensing of Environment*, 38, p. 19-34.

Sobrino J.A., and Raissouni N., 2000. Toward remote sensing methods for land cover dynamic monitoring: Application to Morocco. In: *International Journal of Remote Sensing,* 21(2), p. 353-366.

Assessment of vegetation indexes from remote sensing: Theoretical basis

S.G. García Galiano

Universidad Politécnica de Cartagena, Department of Civil Engineering, R&D Group of Water Resources Management, Paseo Alfonso XIII, 52, 30203 Cartagena (Spain)

Abstract. Uncertainties in agricultural activities due to the scarcity of water and the increase in droughts could be ameliorated by considering early detection and spatio-temporal characterization of water stress conditions at a regional scale from remote sensing. Theoretical aspects of the spatio-temporal assessment of vegetation indexes related with soil moisture, based on remote sensing and meteorological data are presented.

Keywords. Remote sensing – Water stress indicators – Land surface temperature – Vegetation indexes – GIS.

Évaluation des indices de végétation par télédétection : Bases théoriques

Résumé. *Les incertitudes en la production agricole liées a la rareté de l'eau et l'augmentation des sécheresses peuvent être résolues par la détection précoce et la caractérisation spatio-temporelle du stress hydrique à échelle régionale. Les aspects théoriques de l'évaluation spatio-temporelle des indices de végétation liés à l'humidité du sol, basée sur la télédétection et les données météorologiques sont présentés.*

Mots-clés. *Télédétection – Indicateurs de stress hydrique – Température superficielle terrestre – Indices de végétation.*

I – Introduction

The potential of remote sensing in agriculture is high, because multispectral reflectance and temperatures of the crop canopies are related to photosynthesis and evapotranspiration (Basso *et al.*, 2004). Several studies present methodologies for the assessment of water stress indices from remote sensing (Moran *et al*., 1994; Fensholt and Sandholt, 2003). The classical method for the monitoring and evaluation of vegetation water stress is the combined use of land surface temperature (LST) data and multispectral reflectance of the surface, from which the normalized difference vegetation index (NDVI) is derived. The information on wavelengths of the thermal region and visible / near-infrared (NIR), is relevant and useful for the purpose of monitoring the physiological state of vegetation and its level of stress, and especially the intensity of water stress.

In the assessment of the onset, severity, and duration of water stress and drought situations, indicators can be based on meteorological and crop data, or be indicators based only on remote sensing, or be process-based indicators.

Regarding the *indicators based on meteorological data*, the Crop Water Stress Index (CWSI) proposed by (Moran *et al.*, 1994), is widely applied. But the CWSI index, useful for surfaces completely covered with vegetation, requires a great deal of information in order to be applied.

As for *indicators based on remote sensing*, different methodologies of operational assessment of indices related with water deficit of soil and vegetation stress, soil moisture, could be applied. However, remote sensing-based products must be calibrated with ground data (ground truth). There will be a literature review of the main sensors currently used in relation to soil moisture estimation from remote sensing.

Soil moisture estimates can be obtained from various satellites, such as ERS SAR (European Remote Sensing Satellites, Synthetic Aperture Radar), Radarsat, ENVISAT ASAR, ADEOS II and EOS PM sensor AMSR (Advanced Microwave Scanning Radiometer). But most of them do not have temporal resolutions appropriate for monitoring highly dynamic processes. Among the latest tools that are available, the MIRAS (Microwave Imaging Radiometer using Aperture Synthesis) sensor of SMOS (Soil Moisture and Ocean Salinity) mission of the European Space Agency (ESA, 2009) should be highlighted. In all cases, the indicators (or variables) derived from remote sensing data must be validated *in situ* (ground truth).

In the case of *indicators estimated from remote sensing*, there indices that include ratios of two or more bands in the visible and NIR wavelengths (such as NDVI, etc.), and those obtained from the interpretation of LST-NDVI trapezoid *(Vegetation Index/Temperature Trapezoid*). These last include the Water Deficit Index (WDI) proposed by Moran *et al.* (1994) considering the Soil Adjusted Vegetation Index (SAVI) (Huete, 1988). The WDI index has been used to estimate evapotranspiration rates for mixed surfaces. WDI index reaches a value of 1 for conditions of extreme stress of the vegetation, and 0 for crop evaporation to its potential rate. The WDI index has been reformulated by Verstraeten *et al.* (2001), considering only terms of LST and air temperature.

Then Wang (2001) proposed the Vegetation Temperature Condition Index (VTCI), in which the LST-NDVI space behaved like a triangle. This methodology has been widely used in the U.S. Southern Plains (Wan *et al.,* 2004).

The Temperature-Vegetation Dryness Index (TVDI), proposed by Sandholt *et al.* (2002), is obtained from space LST-NDVI and can be used as an indicator of soil moisture and hence the vegetation water stress. Particularly in the rainy season, indices related to soil moisture obtained from wavelengths in the infrared short-wave and NIR can be a valuable supplement to the method based on LST-NDVI space interpretation. Since LST is very sensitive to atmospheric effects and clouds, the use of the SIWSI (Shortwave Infrared Water Stress Index) index, using near-infrared data (Fensholt and Sandholt, 2003) has been considered. According to these authors, working in areas of West Africa, the SIWSI is strongly related to soil moisture, and can be obtained even in the presence of clouds. Although from previous studies in Southeastern Spain (Garcia *et al*., 2006) it is not an appropriate index in semi-arid watersheds.

The STI Index (Standardized Thermal Index), obtained from data of air temperature and LST, may also constitute a relevant indicator of relative deficit of soil moisture (Park *et al*., 2004).

Finally, *indicators based on processes* are regarding with the modeling of actual evapotranspiration (ET_{act}). The methods considered simulate the mass and energy transfer between the atmosphere and surface.

II – Indices based on ratios of two or more bands in the visible and NIR wavelengths

1. NDVI (Normalized Difference Vegetation Index)

The Normalized Difference Vegetation Index (NDVI, Kriegler, 1969; Rouse *et al*., 1973), is based on the assumption that the vegetation subject to water stress presents a greater reflectivity in the visible region (0.4-0.7 μ) of the electromagnetic spectrum and a lower reflectance in the NIR region (0.7-1.1 μ). The NDVI is obtained by the following equation, where NIR is the near-infrared reflectivity and R corresponds to the red region of the electromagnet spectrum.

$$NDVI = \frac{NIR - R}{NIR + R} \quad (1)$$

This index could be easily derived with the satellite information, using bands 1 and 2 in the case of AVHRR sensor (NOAA), or bands 3 and 4 in the case of ETM+ (Landsat). NDVI vary between -1 and 1.

2. RVI (Ratio Vegetation Index)

This RVI (Ratio Vegetation Index, Jordan, 1969), is estimated as,

$$RVI = \frac{NIR}{R} \tag{2}$$

3. GNDVI (Green Normalized Difference Vegetative Index) and DVI (Difference Vegetation Index)

The GNDVI (Green Normalized Difference Vegetative Index) is a modification of NDVI where the Red band is substituted by the reflectance in the Green band (Gitelson *et al*., 1996).

In the case of DVI (Difference Vegetation Index, Richardson and Everitt, 1992), is estimated as follows,

$$DVI = NIR - R \tag{3}$$

4. SAVI (Soil Adjusted Vegetation Index)

The SAVI (Soil Adjusted Vegetation Index) proposed by Huete (1988), takes into account the optical soil properties on the plant canopy reflectance. SAVI is involving a constant *L* to the NDVI equation, and with a range -1 to +1, is expressed as follows,

$$SAVI = \frac{NIR - R}{NIR + R + L}(1 + L) \tag{4}$$

Two or three optimal adjustment for *L* constant (*L*=1 for low vegetation densities; *L*=0.5 for intermediate vegetation densities; *L*= 0.35 for higher densities), are suggested by Huete (1988).

5. TSAVI (Transformed Adjusted Vegetation Index)

The TSAVI (Transformed Adjusted Vegetation Index) original method was modified by Baret and Guyot (1991), as follows,

$$TSAVI = a\frac{NIR - aR - b}{aNIR + R - ab + \chi(1 + a^2)} \tag{5}$$

where *a* and *b* are soil line parameters, and *X* is 0.08. TSAVI varies from 0 for bare soil to 0.7 for very dense canopies (Baret and Guyot, 1991).

III – Interpretation of LST – NDVI space

The combination of LST and NDVI can provide information about the condition of vegetation and moisture on the surface. The combined information on the wavelengths of the thermal region and the visible/NIR region has proved satisfactory for monitoring vegetation conditions and stress, especially water stress. Numerous studies have provided different interpretations of space LST-NDVI, based on a wide range of vegetation types and crops, climate, and different scales.

The NDVI is a rather conservative indicator of water stress, because the vegetation remains green after the start of this stress. By contrast, the LST increases rapidly with the water stress

(Sandholt *et al*., 2002). For a given dry zone, the relationship between LST and the NDVI is characterized by a cloud of dispersion in the LST-NDVI space, the highest values of LST correspond to the lowest values of NDVI (Nemani and Running, 1989). This relationship is often expressed by the slope of a line fitted to the dry edge of the space LST-NDVI.

Numerous studies have focused on the relationship between LST and the NDVI, to provide indirect information about the vegetation stress and the soil moisture conditions. Nemani and Running (1989) related the slope LST-NDVI to stomatal resistance and evapotranspiration of a deciduous forest. Boegh *et al*. (1998) and Jiang and Islam (1999), related the slope LST-NDVI to surface evapotranspiration. The analysis of LST-NDVI space was also used to derive information on conditions of regional soil moisture (Carlson and Gillies, 1993; Goetz, 1997, Goward *et al*., 2002 and Sandholt *et al*., 2002).

Often the estimate of the slope LST-NDVI is not direct (Troufleau and Soegaard, 1998), typically due to the significant variability caused by surface heterogeneity (Czajkowski, 2000). The scattering cloud formed by the LST and NDVI (or vegetation index) both derived from remote sensing, often results in a triangular (Price, 1990, Carlson *et al*., 1994) or trapezoidal (Moran *et al*., 1994) shape, if the data represent a full range of vegetation covers and soil moisture content. Different types of surfaces can have different slopes LST-NDVI and intercept the atmospheric conditions and surface moisture equally; the choice of scale can influence the shape of the relationship between these variables (Sandholt *et al*., 2002).

The vegetation index is linearly related to vegetation cover, and the gradient LST-air temperature is as a function of vegetation index. Assuming these premises, Moran *et al.* (1994) derived the shape of LST-NDVI space from modeling and proposed a theoretical justification for the concept.

The interpretation of the LST for bare soil is not straightforward, because the measured temperature integrates both the temperature of the soil surface temperature and vegetation temperature, and the components cannot be linearly related. Other studies have shown that, at least for well irrigated areas, the relationship between LST and the NDVI is more directly related to the moisture of the soil surface (Friedl and Davis, 1994).

Moran *et al.* (1994) combined the method of LST-NDVI space with standard meteorological data, as well as remote sensing data, to estimate the Water Deficit Index (WDI). They used the temperature difference between LST and air temperature ($\Delta T_s = LST - T_a$) and its relationship to vegetation index.

Sandholt *et al.* (2002) presented a simplification of the WDI index, which considers the variations in air temperature, water balance and atmospheric conditions to estimate the LST-NDVI space. The method is conceptually and computationally straightforward, and only uses information from satellites to define the Temperature-Vegetation Dryness Index (TVDI).

Other authors, such as Prihodko and Goward (1997), proposed the Temperature-Vegetation Index (TVX), estimated as a slope in the LST-NDVI space for a homogeneous area with little or no variation in surface moisture conditions. This method, like that proposed by Sandholt *et al.* (2002), does not requires auxiliary data. This is an advantage over other methods for defining the limits of LST-NDVI space, with high requirements of detailed information about weather conditions, including vapor pressure deficit, wind speed and surface resistance.

Adapting the method proposed by Sandholt *et al.* (2002), described above, the location of a pixel in the LST-NDVI space is determined by several factors:

(i) *Vegetation cover*. The vegetation cover does not necessarily have to be related to spectral vegetation indices through a simple linear transformation. Furthermore, the fraction of vegetation cover affects the amount of bare soil and vegetation, visible by the sensor. Thus the LST can be affected by differences in temperature radiated by the bare soil and by sparse vegetation

(ii) *Evapotranspiration (ET).* The evapotranspiration can control the LST by the surface energy balance. To lower evapotranspiration, more energy will be available for heating the surface. The stomatal resistance, which characterizes the control of the plants to water vapor transfer by transpiration, is a key parameter in the estimation of ET. With greater stress of plants, there is therefore more resistance of the plants to water transfer. This resistance can be expressed in terms of soil factors (soil moisture or soil water potential) and of climate factors (radiation, relative humidity and air temperature).

(iii) *Thermal properties of the surface*. In the case of partially vegetated surfaces, LST is influenced by the heat capacity and thermal conductivity of the soil. These properties are a function of soil type, and change with the soil moisture.

(iv) *Net radiation*. The available energy, incident on the surface, affects the LST. The radiation control of LST implies that areas with high albedo values present low temperatures. The albedo is controlled by the type of soil, surface soil moisture and vegetation cover.

(v) *Weather conditions and surface roughness*. The ability to transfer energy from the surface to the atmosphere is an important factor in controlling the LST. The concept of *surface resistance* is used to quantify this ability to transfer sensible and latent heat (evaporation). This resistance depends on the surface roughness, wind speed and atmospheric stability conditions. Under similar conditions of leaf area index and water availability, the vegetation cover with high roughness (forests) and low surface resistance will have lower LST than surfaces with low roughness (low vegetation) and higher surface resistance. This influences the shape of LST-NDVI space.

The above-mentioned factors have been summarized in Fig. 1. It is clear that the relationship between LST and surface soil moisture is not straightforward. For bare soil with constant irradiance, the LST is defined primarily by the soil moisture content, via control of evaporation and thermal properties of the surface (Sandholt *et al*., 2002).

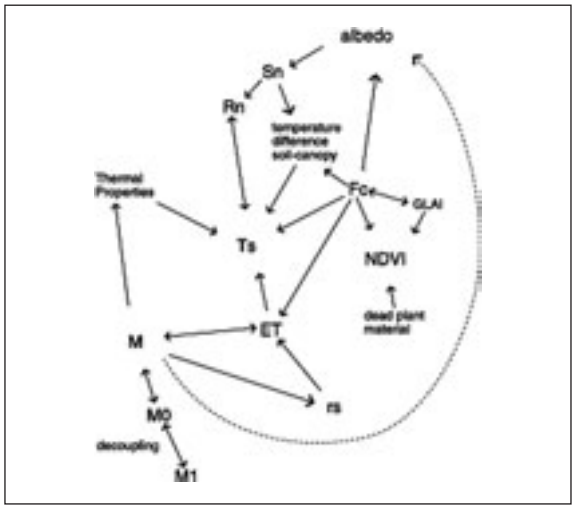

Fig. 1. Factors for the definition of LST of the illuminated surface (adapted from Sandholt *et al*., 2002).

From Fig. 1 above, variables enclosed by the circle can be estimated using satellite data. S_n = shortwave net radiation; R_n = net radiation; *GLAI* = leaf area index; F_c = fraction of soil covered

by vegetation; *ET* = evapotranspiration; *rs* = stomatal resistence; *M1* = soil moisture content (root zone); *M0* = moisture content of top soil.

Figure 2 depicts the concept of LST-NDVI space. The left edge represents bare soil from dry to wet (top-down) range. As the amount of green vegetation increases, the NDVI value also increases along the X axis and therefore the maximum LST decreases. For dry conditions, the negative relationship between LST and NDVI is defined by the upper edge, which is the upper limit of LST for a given type of surface and climatic conditions (Sandholt *et al*., 2002).

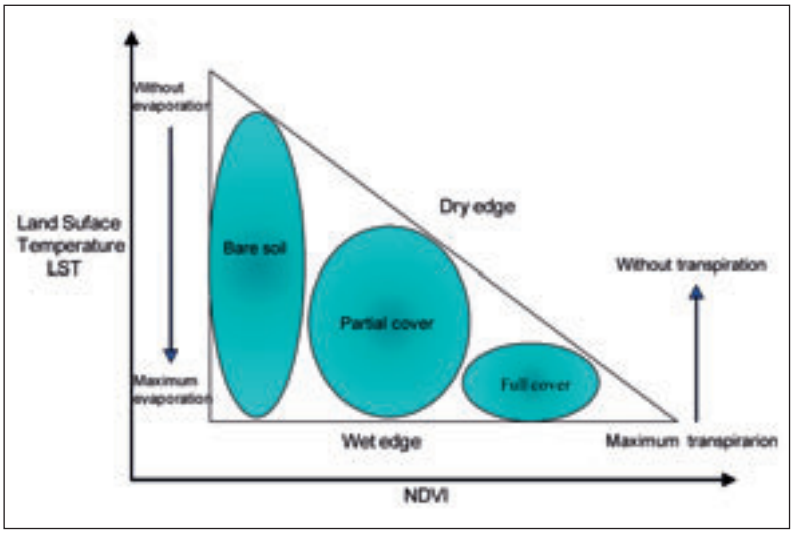

Fig. 2. Simplified LST/NDVI space (adapted from Lambin and Ehrlich, 1996 in Sandholt *et al*., 2002).

1. TVDI index

For deriving information regarding with content of surface soil moisture, Sandholt *et al.* (2002) proposed an index of aridity (TVDI), that takes values of 1 for the dry edge (limited water availability) and 0 for the wet edge (maximum evapotranspiration and thereby unlimited water availability).

The TVDI is inversely related to soil moisture, where high values indicate dry conditions and low values wet conditions. This is based on the fact that the LST is mainly controlled by the energy balance and thermal inertia, factors influencing moisture conditions at the surface and in the root zone (Andersen *et al*., 2002).

Following the concept in Fig. 3, the value of TVDI for a given pixel in the LST-NDVI space, is calculated as the ratio of lines A and B, and therefore calculated using the following equation (Sandholt *et al.* 2002),

$$TVDI = \frac{A}{B} = \frac{LST - LST_{\min}}{a + bNDVI - LST_{\min}} \quad (6)$$

where LST_{min} is the minimum LST in the triangle, defining the wet edge, and LST corresponds to the pixel. Then, *a* and *b* are the coefficients of the regression line that define the dry edge, as follows,

$$LST_{\max} = a + bNDVI \quad (7)$$

where LST_{max} is the maximum LST for a certain NDVI.

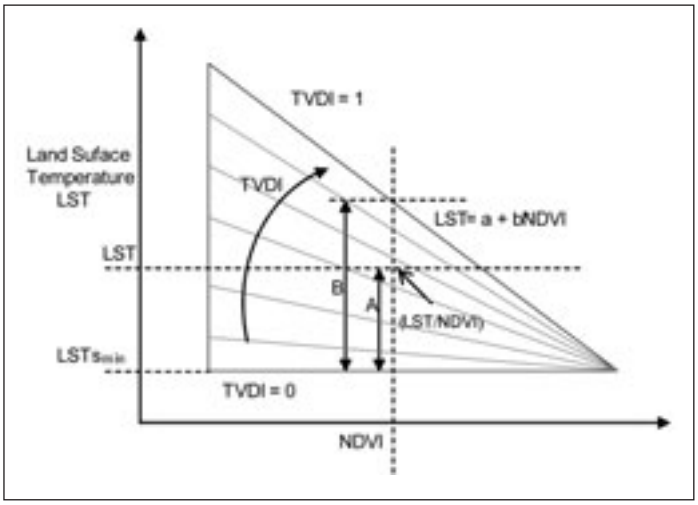

Fig. 3. Definition of TVDI index (adapted from Sandholt *et al*., 2002).

The parameters *a* and *b* are estimated based on pixels from an large enough area to represent the full range of surface soil moisture content, from wet to dry, and from bare soil to fully vegetated surfaces.

Uncertainty about TVDI is greater in the high range of NDVI, where the TVDI isolines are grouped. The simplification of representing LST-NDVI with a triangle instead of a trapezoid (eg Moran *et al*., 1994) may add uncertainty to TVDI estimation for high values of NDVI. The wet edge is also modeled as a horizontal line as opposed to an inclined one, as in the trapezoidal method, which can lead to an overestimation of TVDI for low NDVI.

The TVDI isolines correspond to the TVX index, proposed by Prihodko and Goward (1997), thus being able to estimate such TVDI isolines as multiple superimposed TVX lines. For drier conditions, several studies of LST-NDVI spaces present steep slopes (eg, Goetz, 1997 and Nemani *et al*., 1993), which is consistent with TVDI. Since TVDI can be estimated for each pixel, the spatial resolution of the data is fully maintained. TVX requires an area wide enough for determination of the slope in the LST-NDVI space.

The main advantages of TVDI are: (i) its simplicity of calculation; and (ii) its derivation from satellite data alone regardless of factors such as weather, vapor pressure deficit, wind speed and surface resistance. However, this approach requires a large number of remote sensing observations to accurately define the limits of that space (Sandholt *et al*., 2002).

2. Water Deficit index

The Water Deficit Index (WDI, Moran *et al*. 1994), to estimate evapotranspiration in both areas completely covered by vegetation or partially covered, is based on the interpretation of the trapezoid formed by the relationship between the difference in LST and air temperature versus vege-

tation cover fraction (or vegetation index). The WDI quantifies the relative rate of latent heat flux, so it shows a value of 0 for fully wet surface (evapotranspiration only limited by the atmospheric demand), and 1 for dry surfaces where there is no latent heat flux.

The WDI index could be expressed as follows,

$$WDI = 1 - \frac{ET_{act}}{ET_{pot}} = 1 - \left[\frac{(LST_{\max} - T_a) - (LST - T_a)}{LST_{\max} - T_a) - (LST_{\min} - T_a)} \right] \quad (8)$$

where LST_{max} and LST_{min} are maximum and minimum LST respectively; ET_{act} and ET_{pot} represent actual and potential evapotranspiration respectively, found for a given vegetation cover (or vegetation index) in the left and right edges of the trapezoid VITT (Vegetation index versus difference of temperature). Then, T_a represents air temperature. Verstraeten *et al.* (2001) reformulated the WDI index equation, based on the trapezoid, considering the difference of temperature on the ordinate axis and the vegetation index on the abscissa axis.

IV – Other indexes

1. STI index

The Standardized Thermal Index (STI) describes the deviation experienced LST with respect to the air temperature, as the drought conditions are accentuated (Park *et al*., 2004). The STI index is based on the hypothesis that water-stressed areas present low values of NDVI and temperature gradients between the surface and the air, higher than in non-drought conditions. Therefore, the variation of this gradient will be inversely related to soil moisture and evapotranspiration of the area, and directly related to water stress.

The indicator ranges between 0 and 1, and it is defined by the following equation (Park *et al*., 2004):

$$STI = \frac{(LST - T_{air_{mean}})_{acum}}{(LST + T_{air_{mean}})_{acum}} \quad (9)$$

where $T_{air\ mean}$ is the mean air temperature. The STI index values show a significant correlation with the deviation of the NDVI. This demonstrates that higher values of STI correspond with more severe droughts.

Several studies have shown that the cumulative deviations of LST present significant negative relationships with soil moisture content and the ratio ET_{act}/ET_{pot}, while they have positive relationships with the ration moisture deficit/ET_{pot}. Then, it was found that STI values of 0.2 correspond to a decline of 15% in NDVI, making this the threshold for thermal detection of drought conditions.

2. SIWSI index

Physical models based on radiative transfer have shown that changes in water content of plant tissues present a large effect on leaf reflectance in several regions of the spectrum between the wavelengths of 0.4 to 2.5 mm. A major absorption value is presented in these wavelengths by foliar surfaces in well-hydrated tissues.

The reflectance is inversely related to water content (Ceccato *et al*., 2001), therefore an increase in the value of reflectance at these wavelengths implies in most cases a plant response to some type of stress, including water stress (Carter, 1994). In this case, it is possible to obtain a direct meas-

urement of water content in plants. The region of the spectrum in which these changes occur is the short-wave infrared range 1.3-2.5 mm (SIR, Short Infrared), where the amount of water available in the internal structure of the leaf controls the spectral reflectance (Tucker, 1980). To illustrate this fact, Fig. 4 represents the location of the bands 5 and 6 of MODIS sensor (TERRA satellite of NASA), and the reflectance of a vegetated surface with different soil moisture content (CW).

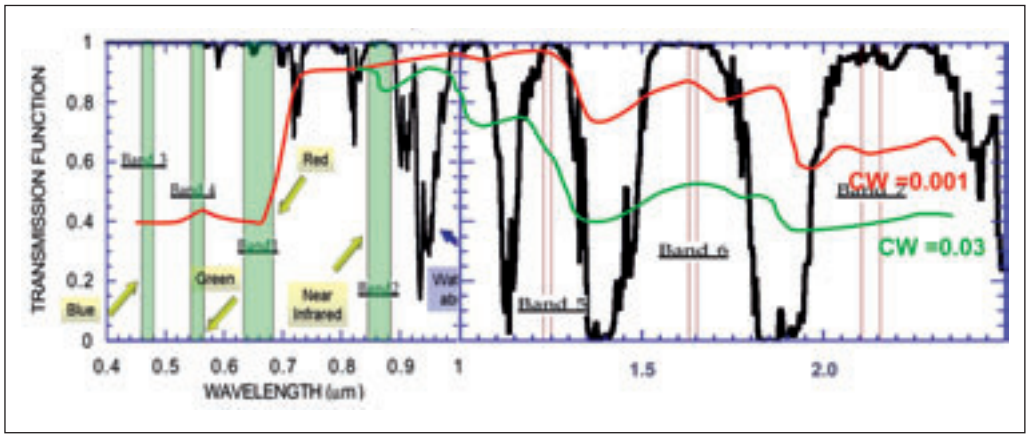

Fig. 4. Representation of MODIS sensor bands (source: Fensholt and Sandholt, 2003).

The reflectance of bare soil, leaf biochemical parameters, internal structure, leaf area index and the influence of the atmosphere affect the value of reflectance measured by satellite. Therefore, the influence of water in the tissues of the plant is needed for it to be independent of other factors. The SIWSI index with its formulation seeks to achieve this objective, and can be expressed considering the 6 band (eq. 10) or 5 band (eq. 11) of MODIS, which, as was seen from Fig. 4, can discern these differences,

$$SIWSI(6,2)= (r_6 - r_2)/((r_6+r_2) \quad (10)$$

$$SIWSI(5,2)= (r_5 - r_2)/((r_5+r_2) \quad (11)$$

where ρ is the reflectance in the spectral range of MODIS 841 a 876 nm in the band 2, 1230 a 1250 nm in the band 5 and 1628 to 1652 nm in the band 6. The SIWSI values from both equations are normalized, varying from -1 to 1. A positive value represents water stress on vegetation.

V – Conclusions

Some of the most widely used indicators, based on remote sensing, to assess water stress of vegetation, have been presented. It is important that the results of these methodologies are contrasted with the ground truth.

Acknowledgments

The funding from EU Project TELERIEG SUDOE INTERREG IV B, as well as the support from Project CGL2008-02530/BTE financed by the State Secretary of Research of Spanish Ministry of Science and Innovation (MICINN), are acknowledged.

References

Andersen J., Sandholt I., Jensen K.H., Refsgaard J.C. and Gupta H., 2002. Perspectives in using a remotely sensed dryness index in distributed hydrological models at the river-basin scale. In: *Hydrological Processes*, 16, p. 2973-2987.

Baret F. and Guyot G., 1991. Potentials and limits of vegetation indices for LAI and APAR assessment, In: *Remote Sensing of Environment*, 35, p. 161-173.

Basso B., Cammarano D. and De Vita P., 2004. Remotely sensed vegetation índices: theory and applications for crop management. In: *Rivista Italiana di Agrometeorologia*, (1), p. 36-53.

Boegh E., Soegaard H., Hanan N., Kabat P. and Lesch L., 1998. A remote sensing study of the NDVI-Ts relationship and the transpiration from sparse vegetation in the Sahel based on high resolution satellite data. In: *Remote Sensing of Environment*, 69, p. 224-240.

Carlson T.N. and Gillies R.R., 1993. A physical approach for inverting vegetation index with surface radiometric temperature to estimate surface soil water content. In: *Proc. Workshop on Thermal Remote Sensing of the Energy and Water Balance over Vegetation in Conjunction with Other Sensors*, La Londe Les Maures, France, 20-23 September 1993.

Carlson T.N., Gillies R.R. and Perry E.M., 1994. A method to make use of thermal infrared temperature and NDVI measurements to infer surface soil water content and fractional vegetation cover. In: *Remote Sensing Reviews*, 9, p. 161-173.

Carter G.A., 1994. Ratios of leaf reflectances in narrow wavebands as indicators of plant stress. In: *International Journal of Remote Sensing*, 15, p. 697-703.

Ceccato P., Flasse S., Tarantola S., Jacquemoud S., and Gregoire J.M., 2001. Detecting vegetation leaf water content using reflectance in the optical domain. In: *Remote Sensing of Environment*, 77, p. 22-33.

Czajkowski K.P., 2000. Thermal remote sensing of near-surface water vapor. In: *Remote Sensing of Environment*, 79 (1-2), p. 253-265.

ESA, 2009. ESA's Water Mission SMOS BR-278. European SA, BR-278, May 2009.

Fensholt R. and Sandholt I., 2003. Derivation of a shortwave infrared water stress index from MODIS near- and shortwave infrared data in a semiarid environment. In: *Remote Sensing of Environment*, 87 (1), p. 111-121.

García Galiano S.G., González Real M.M., Baille A. and Martínez Álvarez V., 2006. Desarrollo de un sistema de alerta temprana frente a sequías a nivel regional para las cuencas del Río Júcar y Río Segura. Informe Final. Dirección General del Agua, Ministerio de Medio Ambiente.

Gitelson A., Kaufman Y. and Merzylak M., 1996. Use of a green channel in remote sensing of global vegetation from EOS-MODIS. In: *Remote Sensing of Environment*, 58, p. 289-298.

Goetz S.J., 1997. Multisensor analysis of NDVI, surface temperature and biophysical variables at a mixed grassland site. In: *International Journal of Remote Sensing*, 18, p. 71-94.

Goward S.N., Xue Y. and Czajkowski K.P., 2002. Evaluating land surface moisture conditions from the remotely sensed temperature/vegetation index measurements: An exploration with the simplified simple biosphere model. In: *Remote Sensing of Environment*, 79, p. 225-242.

Huete A., 1988. A soil adjusted vegetation index (SAVI). In: *International Journal of Remote Sensing*, 9, p. 295-309.

Jordan C.F., 1969. Derivation of leaf area index from quality measurements of light on the forest floor. In: *Ecology*, vol. 50, p. 663-666.

Kriegler F.J., Malila W.A., Nalepka R.F. and Richardson W., 1969. Preprocessing transformations and their effects on multispectral recognition, in: *Proceedings of the Sixth International Symposium on Remote Sensing of Environment*, University of Michigan, Ann Arbor, MI, p. 97-131

Moran M.S., Clarke T.R., Inoue Y. and Vidal A., 1994. Estimating crop water deficit using the relation between surface-air temperature and spectral vegetation index. In: *Remote Sens. Environ.,* 49, p. 246-263.

Nemani R.R and Running S.W., 1989. Estimation of regional surface resistance to evapotranspiration from NDVI and thermal IR AVHRR data. In: *Journal of Applied Meteorology*, 28, p. 276-284.

Nemani R., Pierce L., Runnin, S. and Gowar, S., 1993. Developing satellite-derived estimates of surface moisture status. In: *Journal of Applied Meteorology*, 32 (3), p. 548-557.

Park S., Feddema J.J., and Egbert S.L., 2004. Impacts of hydrologic soil properties on drought detection with MODIS thermal data. In: *Remote Sensing of Environment*, 89, p. 53-62.

Price J.C., 1990. Using spatial context in satellite data to infer regional scale evapotranspiration. In: *IEEE Transactions on Geoscience and Remote Sensing*, 28, p. 940-948.

Prihodko L. and Goward S.N., 1997. Estimation of air temperature from remotely sensed surface observations. In: *Remote Sensing of Environment*, 60 (3), p. 335-346.

Richardson A.J. and Everitt J.H., 1992. Using spectra vegetation indices to estimate rangeland productivity. In: *Geocarto International*, 1, p 63-69.

Rouse J.W., Haas R.H., Schell J.A. and Deering D.W., 1973. Monitoring vegetation systems in the great plains with ERTS. In: *Third ERTS Symposium,* NASA SP-351 I, p. 309-317.

Sandholt I., Rasmussen K. and Andersen J., 2002. A simple interpretation of the surface temperature/vegetation index space for assessment of surface moisture status. In: *Remote Sensing of Environment,* 79 (2-3), p. 213-224.

Troufleau D. and Soegaard H., 1998. Deriving surface water status in the Sahel from the Pathfinder AVHRR Land data set. In: *Physics and Chemistry of the Earth*, 23 (4), p. 421-426.

Tucker C.J., 1980. Remote sensing of leaf water content in the near infrared. In: *Remote Sensing of Environment,* 10, p. 23-32.

Verstraeten W.W., Veroustreaete F., and Feyen J., 2001. Monitoring water limited carbon mass fluxes over Europe using NOAA-AVHRR imagery and an adapted PEM Model C-FIX.

Wang C., Qi S., Niu Z., and Wang J., 2004. Evaluating soil moisture status in China using the temperature-vegetation dryness index (TVDI). In: *Canadian Journal of Remote Sensing*, 30(5), p. 671-679.

Applications of remote sensing of medium resolution

Estimation of irrigated crops areas: Generation of water demand scenarios

S. Montesinos and L. Fernández

GEOSYS S.L., Sector Foresta 23, locales 7 y 8. 28760 Tres Cantos, Madrid (Spain)

Abstract. The study of the evolution of agricultural demand is one of the most significant aspects for water management, not only due to the specific weight that it represent inside the global river basin demand, but also to the difficulty to estimate it. The irrigated area map is elaborated from digital processing of available satellite images, and is based in the analysis, interpretation and classification of vegetation index maps, where numerical information is collected and is linked with the photosynthetic activity rate, vegetation cover vigour and vegetation vigour within each crop.

Keywords. Water demand – Remote sensing – Crop maps – Vegetation index.

Estimation des zones irriguées : la generation de scénarios de demande en eau

Résumé. *L'étude de l'évolution de la demande agricole est l'un des aspects les plus importants pour la gestion de l'eau, non seulement par son poids spécifique dans la demande globale dans un bassin versant, mais aussi du à la difficulté de son estimation. La cartographie de la superficie irriguée se fait à partir du traitement numérique de l'imagerie satellitale disponible et est basée sur l'analyse, l'interprétation et la classification des cartes d'indice de végétation dans lesquelles l'information numérique est recueilli liée au taux d'activité photosynthétique et à la vigueur de la végétation dans chaque parcelle et pour chaque culture.*

Mots-clés. *Demande en eau –Télédétection – Cartes des cultures – Indice de végétation.*

I – Introduction

The evaluation of the evolution of water demand over time is one of the aspects that produces major deviations and errors in the usual process of restoration of the natural regime of the contributions.

The study of the evolution of agricultural demand is one of the most significant aspects, not only because the specific weight that it represents inside the global river basin demand, but also due to the difficulty to estimate it.

Mapping of irrigated areas is made from digital image processes based on available satellite images, as well as in the analysis, interpretation and classification of vegetation index maps, where numerical information is collected and linked to the photosynthetic activity rate, vegetation cover vigour and vegetation vigour within each crop.

Vegetation indexes are calculated by reference with reflectivity values, collected by satellite, within the visible and near and medium infrared spectrums:

– Red visible, by corresponding to the absorption range of chlorophyll, to differentiate the vegetation type. This band records the reflected energy in the visible region corresponding to the red where chlorophyll pigments of the vegetation reaches its maximum absorption. Green and vigorous plants, with high rates of photosynthetic activity, absorb a very large amount of light within this range, being quite reduced the values of reflected radiation. This makes that surface with irrigated crops being identifiable in this spectrum band for representing low digital values respect to the rest of surfaces.

– Near reflected infrared, indicator of the plant biomass. This bands picks up the electromagnetic radiation reflected in the near infrared. Terrestrial surfaces with high biomass density reflect around the 45% of the received radiation. Surfaces with irrigated crops are characterised by a higher vegetation cover and a higher biomass content that non irrigated crops, and they are identified in this band for presenting very high digital values in comparison to the rest of surfaces.

– Near reflected infrared, sensible to moisture content of vegetation. Water in plants and soils absorbs the most of the radiation reaching at Earth surface, being the reflected radiation around the 30% of the received. Surfaces with irrigated crops can be discriminated in this bands for representing digital values lowest than the rest of surfaces.

II – Methodology

The methodology for each irrigated area consists of:

– Development of infrared colour compositions to each date.

– Calculation of vegetation indexes.

– Determination of thresholds for discrimination between irrigated vegetation and other types of surfaces.

1. Development of infrared colour compositions

The infrared colour composition is the combination in a single image of near infrared, visible and green visible bands, associating each band to the primary colours (RGB).

The higher photosynthetic activity rate of plants, their fraction of vegetation cover over the ground or the moisture present in the outer tissues of the plant, the more intense will be the red colour that is seen in these bands combination (Fig. 1). According to this combination:

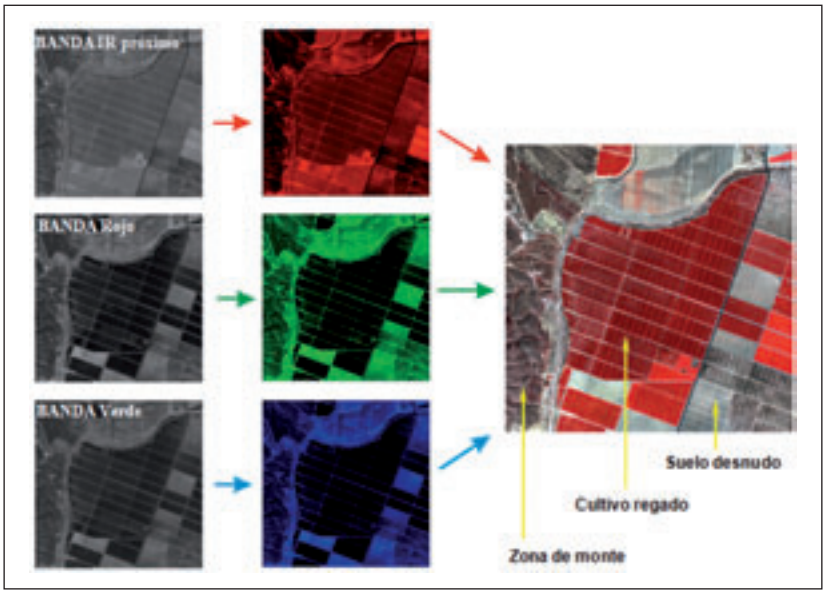

Fig. 1. Sheme of infrared false colour composition.

– Irrigated crop areas appear in intense red shade.

– Areas occupied by natural vegetation appear in green or greyish shades.

– Surfaces of stubble or bare soil appear like light grey or white shades.

For the discrimination of crops under plastic or greenhouses it necessary to use a different methodology based on the detection of the response produced by the plastic, which produces a high reflectance of light in a very specific wavelength.

It uses two bands of the visible spectrum (bands 1 and 3) and the near reflected infrared band (band 7) preparing a composition that allow to discriminate areas occupied by crops under plastic appearing in deep blue and purple shades (Fig. 2).

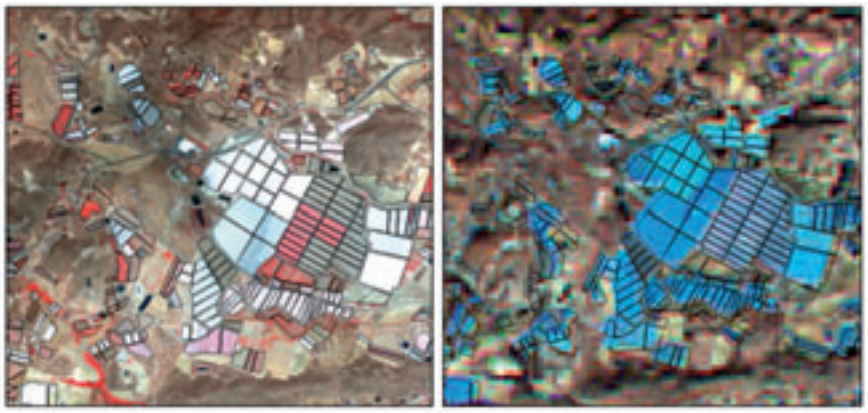

Fig. 2. Example of false infrared colour composition (right) and composition to plastic detection (right image).

2. Calculation of vegetation indexes

A *vegetation index* is a mathematical algorithm applied over stored values of two or more bands. They are used to discriminate different covers that present a very different behaviour in terms of reflectivity in these bands.

For the identification of areas occupied by crops with significant vegetation vigour and significant vegetation cover, maps have been prepared by calculating *Normalised Difference Vegetation Index, NDVI* over each one of these irrigated areas.

The NDVI is a relationship between pixel values of near infrared band and pixel values of visible red band, in the words:

$$NDVI = \frac{NearIR - Visible\,red}{NearIR + Visible\,red} \times 100$$

NDVI is a sensitive indicator of vegetation presence and its conditions. The spectral response of terrestrial surface in these two bands of electromagnetic spectrum is enlarged in the NDVI. Photosynthetically active vegetation areas with high coverage present high values of NDVI due their high electromagnetic reflectance in the range of near infrared and their low reflectance in the visible range. Bare soil and water presents very low NDVI values. Figure 3 provides and example of general map of vegetation index.

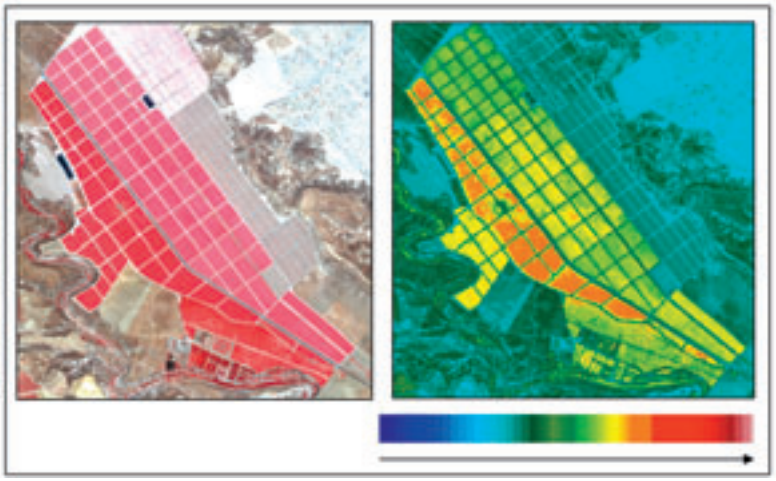

Fig. 3. Elaboration of NDVI map.

Moreover, for the delimitation of greenhouses and crops under plastic, an index called ICP *(Index of Crop Under Plastic)* is used. The mathematical formula, for Landsat bands, is presented below:

$$ICP = (Band1\text{-}Band7) * Band1 * Band4$$

Being:

Band 1: Blue band.

Band 7: Medium infrared band.

Band 4: Near infrared band.

ICP is designed so that pixels corresponding to areas covered by pure plastic reach values of greater magnitude than most of other studied surfaces in the area (Fig. 4).

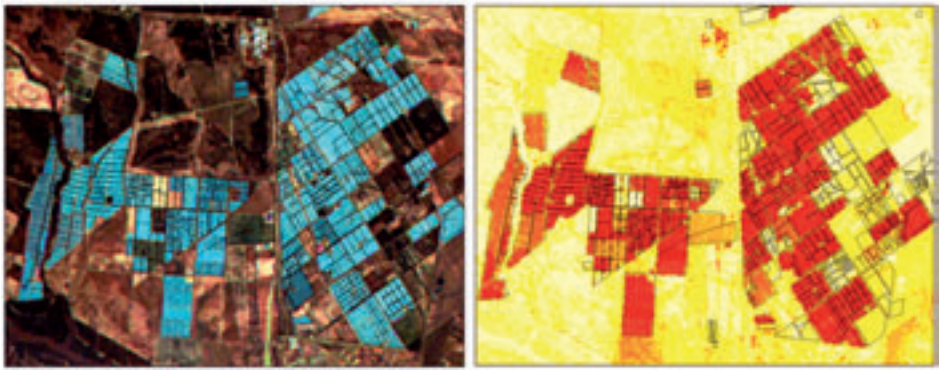

Fig. 4. Elaboration of ICP map.

Discrimination capacity of crops under plastic of this index is very high, particularly in areas occupied by greenhouses or big tunnels. However, in small plots located in borders and in exploitations with small tunnels with less density of plastic, values obtained by calculating indexes may be confused with those appeared in areas with high reflectivity like beach or dunes, industrial areas or urban areas.

3. Territorial segmentation

Prior to the definition of thresholds, a territorial segmentation must be carried out in order to define areas where agronomic traits (type of existing crops and phenological development) are as much homogeneous as possible.

The objective of this process is to minimize errors produced trying to extrapolate criteria of irrigated identification, which are adopted based on a series of concrete measures over a large territory. For this, the study area is divided in different units where climatic and environmental characteristics, as well as agricultural practices and crops typology are similar.

The process of elaboration of irrigated area maps is developped for each of the areas resulting from the territory segmentation.

4. Discrimination between irrigation and other types of surfaces

After obtaining both values of NDVI and ICP for different dates, cut-off values are defined to keep those that are interesting (those that characterize irrigated crops or crops under plastic) and discard the values of covertures not interesting.

The threshold of cut-off is a minimum value inside the index map that our unit (pixel) should have to be classified as irrigated crop or crop under plastic.

This will result in obtaining maps of irrigated areas and maps of crops under plastic for each one of the areas defined from the territorial segmentation. The union of these partial maps allows the production of irrigated area maps for each analyzed date.

III – Conclusions

The main features that support the remote sensing technique in such type of studies are:

(i) *Objectivity*. Data provided are digital images (representation of an object by a two-dimensional numerical matrix) obtained by spatial international agencies (ESA, NASA, etc.) and are commercially available by any citizen.

(ii) *Continuity of data*. Data provided by satellites are not extrapolated or interpolated from punctual observations, as with statistical techniques, but are a discretization of continuous space observed variables in units called pixels that generate a digital image.

(iii) *Frecuency of observations*. Because theie orbital models, satellites fly the same area periodically, allowing us to obtain periodical observations of an area. This means that current orbiting satellites, Landsat series per example, provides one observation over a particular area every 16 days, or 22 observations per year or 440 observations over the last 20 years. SPOT series of satellites, do it every 26 days or 14 times a year or 280 times in the last 20 years.

(iv) *Multispectrality of observation*. Sensors on board satellites capture data no only in the visible regions of spectrum (which are captured by the human eye or by aerial photography) but also in the infrared spectral region, allowing us to "see" invisible things for human eye.

(v) *Multiscale Observation*. With current orbiting satellites, it is possible to approach studies from 1:150.000 scales (from images with 30 meters of spatial resolution for a maximum tolerable error of 0.2 mm) to scales of 1:3.500 (from QuickBird images with 70 cm of spatial resolution).

(vi) *Low cost of data acquisition*. Prices of acquisition of satellite images ranging from a mission to another (Landsat, SPOT, QuickBird...), and even if it is a modern image or 10 years image, range from € 23/km^2 of QuickBird, to € 2.00 km^2 for SPOT schedule image with 2.5 m of spatial resolution, to € 0.05 km^2 current Landsat image, with 7 spectral bands and 30 m of spatial resolution.

Regardless the methodology (photointerpretation or digital analysis) used to extract information contained in the satellite images, space remote sensing is a powerful, dynamic and objective source of data for the estimation of irrigated areas and for the monitoring of their evolution through time.

Remote sensing based water balance to estimate evapotranspiration and irrigation water requirements. Case study: Grape vineyards

I. Campos*, L. Boteta, C. Balbontín*, M. Fabião**, J. Maia** and A. Calera***

*Sección de Teledetección y SIG. Instituto de Desarrollo Regional, Universidad de Castilla-La Mancha, Campus Universitario S/N, 02071, Albacete (Spain)
**Centro Operativo e de Tecnologia de Regadio, COTR, Quinta da Saúde, Beja (Portugal)

Abstract. In this paper the basis for the incorporation of remote sensing data into a soil water balance through the relationship between the basal crop coefficient (Kcb) and vegetation indices (VI) for grape vineyards is described. The remote sensing soil water balance has been applied in previous studies obtaining accurate estimates of actual evapotranspiration and crop coefficient in grape vineyard, and this methodology is evaluated in order to estimate irrigation necessities in an irrigated vineyard in Albacete, Spain. The model was also applied in vineyards under high deficit irrigation management. The model results: total irrigation necessities, crop evapotranspiration, and water stress coefficient (Ks) are analyzed. The evolution of Ks was compared with experimental measurements of stem water potential (ψs). Ks calculated present values between 0.2 and 0.4 during July and August, indicating severe stress levels. The ψs tendency coincides with the modelled Ks, showing a parallel evolution and values of about -1.4 MPa during the stress period. The evidences presented indicate that Kcb derived from VI overestimate the actual crop coefficient under water stress conditions. In these cases, it is therefore essential to properly estimate the stress coefficient in order to accurately estimate actual crop evapotranspiration and crop coefficient.

Keywords. Vineyard – Evapotranspiration – Vegetation indices – Basal crop coefficient – Soil water balance – Crop water necessities.

Bilan hydrique fondé sur la télédétection pour estimer l'évapotranspiration et les besoins en eau d'irrigation. Étude de cas sur des vignobles

Résumé. *Dans cet article sont décrits les fondements pour l'incorporation des données issues de la télédétection dans un bilan hydrique du sol à travers la relation entre le coefficient de base de la culture (Kcb) et les indices de végétation (VI) pour des vignobles. On a utilisé le bilan hydrique du sol par télédétection dans des études préalables, ce qui a permis d'obtenir des estimations exactes de l'évapotranspiration réelle et du coefficient des cultures pour des vignobles, et cette méthodologie est évaluée afin d'estimer les besoins en irrigation dans un vignoble à Albacete, Espagne. Le modèle a aussi été appliqué dans des vignobles conduits sous irrigation fortement déficitaire. Comme résultats du modèle, les besoins en irrigation totale, l'évapotranspiration des cultures, et le coefficient de stress hydrique (Ks) ont été analysés. L'évolution de Ks a été comparée aux mesures expérimentales de potentiel hydrique au niveau des tiges (ψs). Ks a pris des valeurs actuelles allant de 0,2 à 0,4 pendant juillet et août, indiquant des niveaux de stress sévères. La tendance ψs coïncide avec le Ks modélisé, montrant une évolution parallèle et des valeurs d'environ -1,4 MPa pendant la période de stress. Les résultats présentés indiquent que le Kcb dérivé de VI surestime le coefficient réel des cultures en conditions de stress hydrique. Dans ces cas, il est donc essentiel d'estimer de façon appropriée le coefficient de stress afin d'évaluer avec exactitude l'évapotranspiration réelle des cultures et le coefficient des cultures.*

Mots-clés. *Vignobles – Évapotranspiration – Indices de végétation – Coefficient de base de la culture – Bilan hydrique du sol – Besoins en eau des cultures.*

I – Introduction

Precise information about crop water necessities, adapted to the actual crop development and meteorological conditions, and its knowledge on near-real time is a paramount in agriculture. Remote sensing data, obtained from space, aerial or terrain platforms could provide significant advances for this purpose. During the last decades some research efforts have been conducted to develop and to evaluate specific algorithms, models, and indicators for agronomic applications based on remote sensing data, as well as to provide easy and near-real time access to this information.

One of the most accepted methodologies for the estimation of crop water requirements is the use of reference evapotranspiration and a crop coefficient (FAO-56 methodology) (Allen *et al.*, 1998). Estimation of the crop coefficient (Kc) is required to calculate crop evapotranspiration and maintaining a soil moisture balance as described by the FAO56 methodology. A large amount of research has been conducted to estimate the standard values and temporal evolution of Kc, but the adaptation to local crop varieties, management practices and climate is always recommended.

For grapevines crops, such as many woody crops, local practices can largely vary many parameters related to crop evapotranspiration such as canopy cover, inter-rows vegetation and irrigation frequency. The review of vineyard Kc values obtained by field crop evapotranspiration measurements reveal Kc values ranging between 0.5 (Campos *et al.*, 2010; Montoro, 2008) to up to 0.9 (Teixeira *et al.*, 2007; Williams and Ayars, 2005) in irrigated row vineyards. This range is greater if we consider the mean values of 0.2 published by Oliver and Sene (1992) for rainfed bush vineyards.

Numerous studies rely on the capability of multispectral vegetation indices (VI) to assess vegetation development and so to estimate Kc. Several authors have reported relationships between Kc and VI and applications of this methodology (Bausch and Neale, 1987; Choudhury *et al.*, 1994; Duchemin *et al.*, 2006; Er-Raki *et al.*, 2007; González-Dugo and Mateos, 2008; González-Piqueras, 2006; Hunsaker *et al.*, 2003; Jayanthi *et al.*, 2007). These previous studies developed relationships between vegetation indices and basal crop coefficient for herbaceous crops, but the development and applications of this relationship for fruit trees was on the border of knowledge for this methodologies.

This paper aims to communicate an illustrative explanation about the practical application of remote sensing based soil water balance for grape vineyards and some of the most recent research applied to remote sensing soil water balance in grape vineyards are presented and analyzed.

II – Remote sensing soil water balance basis

1. Soil water balance in the root zone

The soil water balance (SWB) described in the FAO-56 methodology and reproduced in this work is a one layer soil water balance (performed in the plant root zone) with additions to simulate soil evaporation from the surface layer. SWB formulation for the root zone is presented in (Equation 1). $D_{r,i}$ and $D_{r,i-1}$ referring to the soil moisture depletion on the day and previous day time step. Runoff from the soil (RO) in the study field must be evaluated, further for great slopes and rain intensities and precipitation (P) can be measured by automatic weather stations. Capillary rise (CR) from groundwater table could be an important input in determined areas, but is semiarid regions this factor can be considered insignificant. Evenly, deep percolation (DP_i) is an important component in the soil water balance under high irrigation or precipitation regimes. For water necessities assessment Irrigation (I_i) is derived as residual in the formulation, but it requires the measurement or estimation of crop evapotranspiration (ET).

$$D_{r,i}=D_{r,i-1}-(P-RO)_i-I_i-CR_i+ET+DP_i \quad \text{(Equation 1)}$$

For practical applications in operatives scenarios SWB is initialized for conditions of full watered soil profiles, which can occur after precipitation events. Thus, soil water balance is sometimes computed for periods longer than crop development seasons, even in the absence of vegetation cover, being ET mainly attributable to soil evaporation under these conditions. For practical considerations about soil evaporation estimation, the reader is referred to Torres and Calera (2010).

2. "Two steps" methodology for crop evapotranspiration estimation

A theoretical approach towards estimating crop evapotranspiration (ET) is given by the Penman-Monteith combination equation (Equation 2). The crop coefficient (Equation 3) (Allen *et al.*, 1998) is the ratio between crop evapotranspiration and reference crop evapotranspiration (ETo), which may be computed by means of the FAO56 Penman-Monteith equation (Equation 4) (Allen *et al.*, 1998). The variables utilized in the formulation of evapotranspiration are net radiation (R_n) heat flux into the soil (G), air density (ρ_a), specific heat of air (c_p), vapor pressure deficit (e_s-e_a), the thermodynamic psychrometric constant (γ), aerodynamic resistance (r_a), canopy resistance (r_c), wind speed adjusted to 2 m of height (u_2), air temperature (T) and saturation slope vapor pressure curve at air temperature (Δ). ETo formulation is the application of the generic Penman-Monteith combination equation to an ideal reference grass surface, the "reference surface". This adaptation includes the use of constant values and imposes the measurement or simulation of the parameter for this surface and the specific conditions described in the FAO-56 manual.

$$ET=\frac{\Delta(R_n-G)+\rho_a c_p (e_s-e_a)/r_a}{\Delta+\gamma(1+r_c/r_a)} \quad \text{(Equation 2)}$$

$$Kc=\frac{ET}{ETo} \quad \text{(Equation 3)}$$

$$ETo=\frac{0.408\Delta(R_{no}-G_o)+\gamma(\frac{900}{T+273})u_2(e_s-e_a)}{\Delta+\gamma(1+0.34u_2)} \quad \text{(Equation 4)}$$

The model proposed in FAO-56 for ET estimation and resumed in (Equation 3) is entitled the "Two step" methodology because it conceptually decouples ET in two components, mainly related to atmospheric demand, ETo, and mainly related to surface (canopy) properties, Kc. This approach was improved by calculating Kc as the sum of a basal crop coefficient (Kcb), related to plant transpiration, and an evaporation coefficient (Ke), linked to soil evaporation (Wright, 1982). In particular, we recommend the use of the dual crop coefficient approach and adjustments to Kcb to account for water stress in the root zone, modeled as Ks (Allen *et al.*, 1998), (Equation 5). Actual crop evapotranspiration resulting with this formulation taking into account the presence of water stress is named ETadj.

$$ETadj=(Ke+KcbKs)ETo \quad \text{(Equation 5)}$$

In the FAO-56 methodology Ke is calculated using a parallel water budget in the top soil layer. The use of the stress coefficient confers additional capabilities to the SWB methodology because the model is able to simulate ET reduction under water stress conditions and the irrigation depth and frequency can be adapted to attach the desired water stress level.

A. FAO-56 Crop water stress sub-model

The coefficient K_s is estimated using the expression presented in (Equation 6) where TAW is the total available water in the root zone (mm). RAW is the proportion (p) of TAW that is used by a given crop without reduction of transpiration and $D_{r,i}$ is the water depletion for day i (mm) derived from the soil water balance (Equation 1).

$$K_s = 1 \qquad if\ D_{r,i} \leq RAW$$
$$K_s = \frac{TAW\text{-}D_{r,i}}{TAW\text{-}RAW} = \frac{TAW\text{-}D_{r,i}}{(1\text{-}p)\,TAW} \qquad if\ D_{r,i} > RAW \qquad \text{(Equation 6)}$$

TAW value is estimated using the expression presented in (Equation 7) where Z_r is the depth of the root zone, θ_{FC} is the water content in the soil layer at field capacity ($cm^3\ cm^{-3}$); θ_{WP} is the water content in the soil layer at wilting point ($cm^3\ cm^{-3}$).

$$TAW = 1000\ Z_r\ (\theta_{FC} - \theta_{WP}) \qquad \text{(Equation 7)}$$

The formulation used to estimate Ks is strongly dependent on TAW, and consequently on root depth. In woody and perennial crops such as in vineyards the roots explore important volumes of soil extracting water up to 2 m depth (Pellegrino *et al.*, 2004). The water storage in the soil profile supposes an important source of resources and could suppose near to 50% of total water necessities in irrigated vineyards (Campos *et al.*, 2010). It is therefore essential to properly estimate roots depth and total available water in the root zone for an adequate estimation of irrigation necessities and plant water stress, being this factor one of the greatest uncertain sources for the model application.

3. Remote sensing inputs in the "Two steps" methodology

The assimilation of remote sensing inputs in the SWB model described in this work is based on the relationship between VI and the basal crop coefficient Kcb, which is defined as the ratio of the crop evapotranspiration over the reference evapotranspiration when the soil surface is dry but transpiration is occurring at potential rate (Allen *et al.*, 1998). Thus, the Kcb derived from VI relationships, Kcbrf in this paper, and experimental Kc will coincide only for the period with minimum soil evaporation and free of water stress in the root zone, see (Equation 5). And for a complete comparison during the entire growing season Ke and Ks must be added to the modeled Kc.

Neale *et al.* (1989) proposed the development of this relationship by means of linear scaling relating the average VI of dry tilled bare soil for the site (VImin) with the Kcb value for dry bare soil (Kcb,min) and the average maximum VI value for the site at effective cover (VImax) with the Kcb value at effective cover (Kcb,max) (Equation 8).

$$Kcb = Kcb,max \cdot \left[1 - \frac{\left(1 - Kcb,min\right) \cdot \left(IVmax - IV\right)}{IVmax - IVmin} \right] \qquad \text{(Equation 8)}$$

This relationship has been considered non-linear for the NDVI such as other VI (Choudhury *et al.*, 1994) and the formulation is rewritten accounting for this effect including an exponent η (Equation 9) (González-Dugo *et al.*, 2010).

$$Kcb = Kcb,max \cdot \left[1 - \left(\frac{IVmax - IVmin}{IVmax - IVmin} \right)^{\eta} \right] \qquad \text{(Equation 9)}$$

Other approaches relay on the use of empirical relationships correlating experimental Kc values obtained with minimum soil evaporation and free of water stress in the root zone (analogous to experimental Kcb) with the VI obtained in the plot. This is the method used to derive the relationship between VI and Kcb in a row vineyard (Campos *et al.*, 2010) presented in (Equation 10).

$$K_{cb} = 1.44NDVI - 0.10 \quad \text{(Equation 10)}$$

III – Remote sensing SWB approaches in grape vineyards

1. Case study I. Crop coefficient and irrigation necessities estimation in irrigated vineyard in Albacete, Spain

In this case study we will analyze the crop evapotranspiration data obtained in a drip irrigated vineyard located in Albacete, Spain, using Eddy Covariance flux measurements. For additional information about the measurements methodologies, flux corrections and postprocessing, crop management and climatic conditions the reader is referred to Balbontín *et al.* (2011) and Campos *et al.* (2010). Measured crop evapotranspiration in the studied vineyard has been modeled by using the approach described in this paper and the results are published in Campos *et al.* (2010). In this work, we reanalyze these data improving the methodology proposed before by including the modifications to the FAO-56 soil evaporation sub-model proposed by Torres and Calera (2010).

The Kc modeled using the proposed methodology, including the modifications remarked before, following the measured Kc values increasing its value from the beginning of June to early July (Fig. 1) when the vegetation growth was stopped due to mechanical pruning. The variability in measured Kc after that date was affected by the irrigation events (22 mm every 12 days). After each irrigation event, a sudden increase in the Kc can be observed due to the presence of increased soil evaporation with a subsequent dry down period and decrease in the Kc lasting typically 3-4 days, these tendencies was reproduced by the model, Fig. 1, and the similarity between both modeled and measured coefficients was evident during the whole campaign, being RMSE=0.07. Both tendencies are even more similar outside of these drying periods, for which soil evaporation can be neglected and measured Kc is essentially equal to Kcb, and thus this similarity reinforces the capability of a VI based model to estimate Kcb in vineyards.

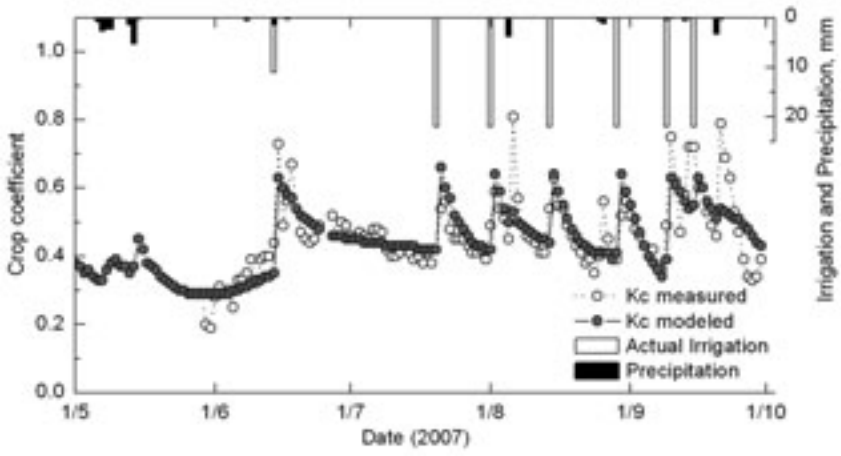

Fig. 1. Comparison of measured Kc and modeled Kc values in a drip irrigated vineyard in Albacete, Spain.

The same model formulation used to estimate ET and the showed vineyard crop coefficient were inverted to estimate vineyard irrigation necessities during the vines growing season. In this simulation the maximum irrigation depth (maximum irrigated volume per irrigation event) were limited to 22 mm according to farming practices. Total irrigation necessities during the vines growing season was estimated in 132 mm, resulting in a low difference with respect to the actual irrigation measured in the field, 143 mm. Interesting discrepancies between the actual irrigation manage and the models results were the start date of the irrigation campaign and the irrigation frequency during that. The farming practices include one irrigation event during mid June besides to soil depletion simulated by the model indicating significant levels of water available for the plants until early August, Fig. 2. Irrigation frequency is limited in the studied plot to one event every 12-14 days. This frequency seems to not be enough for the vineyard requirements during the campaign. Nevertheless, the vines water status was evaluated during the campaign using a pressure chamber and only low levels of water stress in certain dates (August 30th) was detected, in accordance with the stress coefficient predicted by the model, being Ks greater than 0.9 during the whole analyzed period.

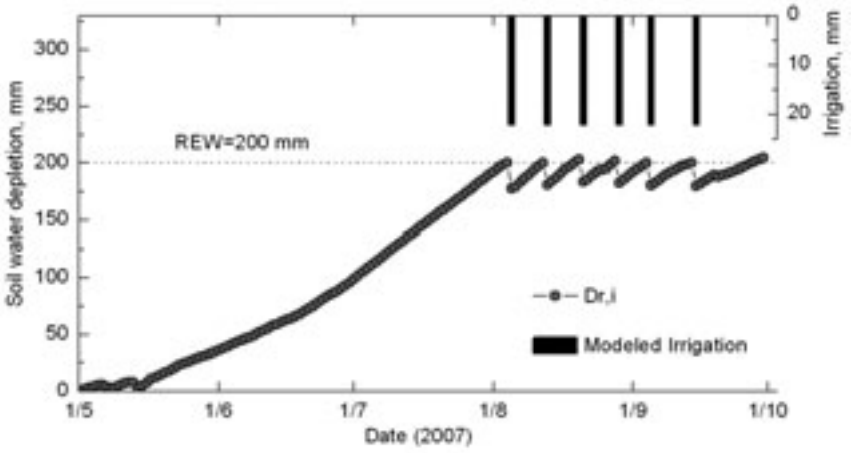

Fig. 2. Date and depth of irrigation necessities simulated by the model and measured in the field plotted along with soil water depletion (Dr,i) during the vines growing season modelled using the irrigation necessities predicted by the model. In the graphic is also shown the value of readily available water (REW).

The results presented before were obtained in conditions of no water limitations for the plants. Under water stress conditions, Kc measurements are expected to be lower than Kcb derived from its relationships with VI. In line with this theory, Silvestre *et al.* (2009) found an overestimation of measured ET, in water stressed vineyards when the expression Kcbrf*ETo is applied and proposed the inclusion of a stress coefficient derived from sap-flow measurements to correct that. O'Connell *et al.* (2010) found a strong relationship between NDVI and the ET/ETo ratio (experimental Kc) calculated using the model METRIC (Allen *et al.*, 2007) in vineyards. In this experiment, the Kc-NDVI observations that fall below the mean Kc-NDVI line are subjected to increasing levels of water stress.

NDVI such as other multispectral vegetation indices are not sensitive to water stress, at least not prior to structural changes, such as plant defoliation induced by water stress. Thus, dual crop coefficient methodology improved with remote sensing data provides, through the expression

Kcbrf*Eto, that maximum or "potential" rate of transpiration of the actual canopy. This potential transpiration will only coincide with real transpiration in absence of stress, being real transpiration lower than potential under water stress conditions. The model is able to estimate that effect by including in the formulation the stress coefficient presented before.

2. Case study II. SWB in vineyards under high deficit irrigation in the Alentejo, Portugal, preliminary results

In this case study, we will analyze the remote sensing SWB model results in two commercial vineyards under high deficit irrigation management during two consecutive years in the Alentejo, Portugal. The study plots are named P1 and P2 in this project. The model results analyzed here are crop evapotranspiration, soil moisture and water stress coefficient (Ks). The evolution of Ks was compared with experimental measurements of midday stem water potential (ψs).

The comparison of total irrigation requirements with respect to the actual irrigation volumes, Table 1, shows a water deficit in all plots and all periods analyzed, being applied volumes less than 50% of the total requirements estimated in P1 and less than 60% in P2. This result is consistent with the strategy of deficit irrigation imposed by farmers. The inclusion of real irrigation data in the model leads to reduced crop evapotranspiration as a result of water stress. ETadj cumulated during the growing season, April 15 to September 15, is less than 60% of the estimated maximum evapotranspiration, simulated under conditions of no water stress, and less than 80% in plot P2, Table 1.

Table 1. Seasonal cumulated values of total irrigation necessities, actual irrigation measured in the plot, maximum evapotranspiration and adjusted evapotranspiration accounting for water stress

	Total irrigation necessities, mm		Actual irrigation, mm		Maximum ET, mm		ETadj, mm	
	Year 2008	Year 2009	Year 2008	Year 2009	Year 2008	Year 2009	Year 2008	Year 2009
P1	300	360	102	177	505	540	320	366
P2	240	300	115	193	433	470	317	369

The model results indicate that soil moisture content is clearly below the RAW limit for much of the campaign. This causes a reduction in crop evapotranspiration, ETadj, Fig. 3, reaching values lower than 2 mm. ETadj increases after irrigation events due to the evaporation from the soil. During the 2009 campaign, irrigation events are more frequent in both plots resulting in higher ETadj values, Fig. 3.

The main strength of the remote sensing based SWB is the ability to analyze the relationship between the maximum irrigation needed and real irrigation applied, allowing to estimate the amount of water required to return the plants to a status of water "comfort" (free of water stress). For irrigation management and recommendations purposes, it is interesting to estimate the coefficient of stress and its simulation under different irrigation management scenarios, but its estimation and interpretation must be evaluated against crop evapotranspiration measurements and field estimators of plant water status, such as midday stem water potential, ψs.

The evolution of ψs measured in the study plots during the campaigns show a clear downward trend, Fig. 4. At the end of the season, in the period from DOY 190 to DOY 230, ψs values in all plots become stable around -1.3 or -1.4 MPa. ψs values in P2 plot during the 2008 campaign did not reach the stability around this minimum value in the indicated period and ψs values continued declining as low as values of -1.5 MPa. The low values obtained in the field indicate severe water stress conditions in the cases studies presented.

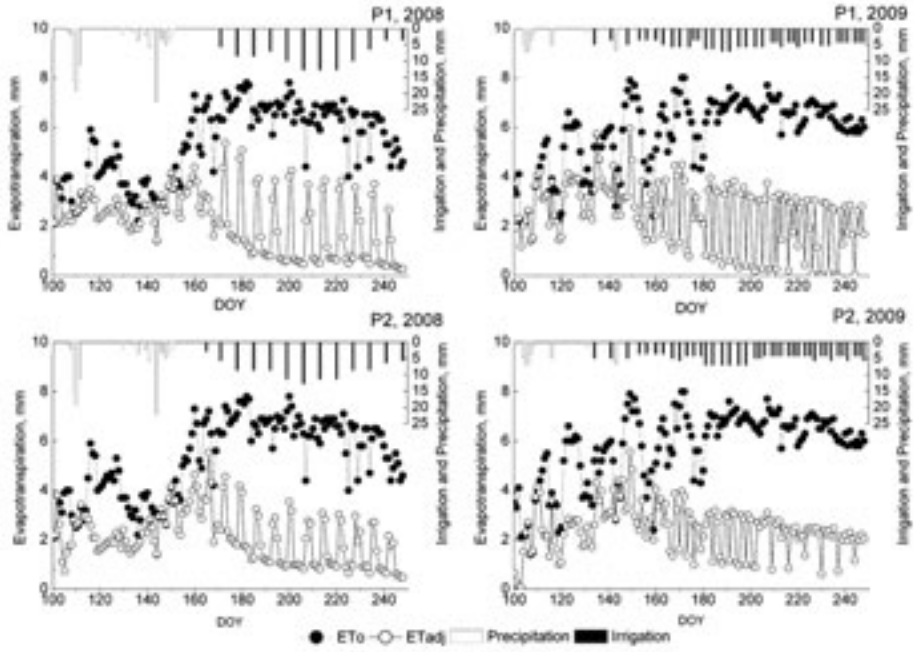

Fig. 3. Reference crop evapotranspiration (ETo), modeled adjusted evapotranspiration (ETadj), precipitation (P) y and actual irrigation in P1 and P2 during both analyzed periods.

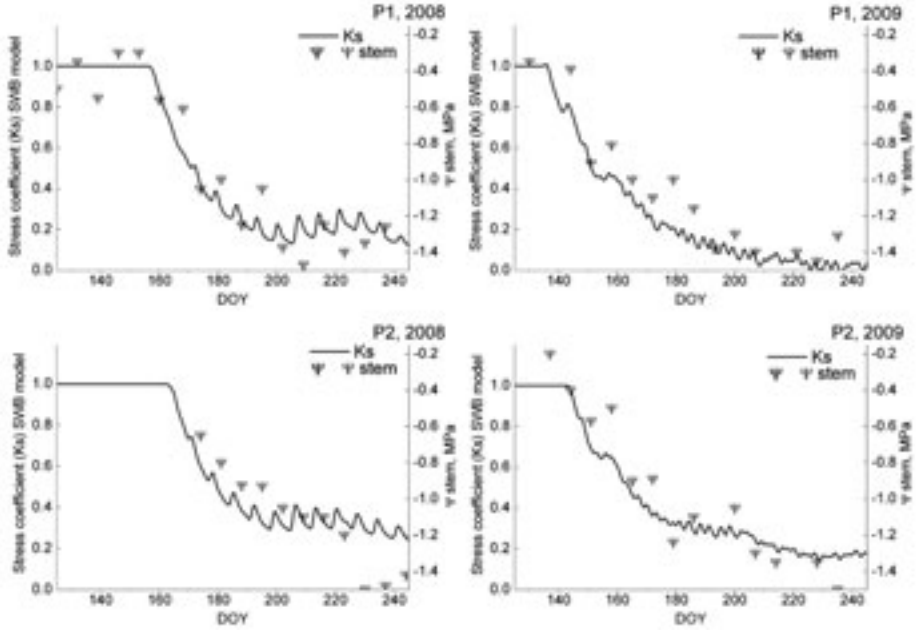

Fig. 4. Crop water stress estimated following the SWB approach plotted along with midday stem water potential measured in the field.

The temporal evolution of Ks estimated using the SWB model and ψs values show a parallel evolution in both plots during the two years analyzed,. The results indicate that the simulated stress coefficient has low sensitivity to ψs values lower than -1.4 MPa. For the periods in which the model does not detect water stress (beginning of the campaign) ψs values ranged between -0.3 and -0.5 MPa. It should be noted that ψs measurements have been obtained under different meteorological conditions (air temperature, vapour pressure deficit and illumination) and phenological stages, and the effect of these variables in ψs has not been evaluated in this work.

IV – Conclusions and remarks

Grape vineyards basal crop coefficient can be derived from its relationships with multispectral vegetation indices, measured using satellite images. This "spectral" or "remote sensing based" basal crop coefficient is adapted to the actual crop development and presents a fast, effective and precise method to estimate this parameter in great areas.

For an accurate estimation of experimental crop coefficient in vineyards, evaporation and stress coefficient must be added, using the formulation described in the text. The soil water balance in the root zone is needed for the estimation of the stress coefficient and this balance allows to estimate crop irrigation requirements with adequate precision for irrigated vineyards, such as it is presented in the text.

The methodology described in this paper has been tested in previous studies for grape vineyards, under different irrigation regimens and vegetation management (bush and row trellis system), but more experiments are necessary especially those centered in the study crop evapotranspiration under water stress conditions, evaluating the capacity of the soil water balance and water stress models. Additionally, a synergistic combination of this approach with those models estimate crop water stress using physiological measurements or are based on surface energy balance models (SEB), that provide real evapotranspiration, could be a future research line. The knowledge of the maximum transpiration rate from Kcb-VI procedure, combined with water stress or real evapotranspiration estimates, could provide an operational method for the assessment of irrigation recommendation on grape vineyards.

Acknowledgments

This work was supported by the project "Telerieg" from the Interreg IVB SUDOE Programme. The authors are particularly grateful to the farmers for their help, permission and collaboration during the data collection phase.

References

Allen R.G., Pereira L.S., Raes D. and Smith M., 1998. Crop evapotranspiration: Guidelines for computing crop requirements. *Irrigation and Drainage Paper No. 56*, FAO, Rome, Italy.

Allen R.G., Tasumi M. and Trezza R., 2007. Satellite-based energy balance for mapping evapotranspiration with internalized calibration (METRIC)-Model. In: *Journal of Irrigation and Drainage Engineering,* 133, p. 380-394.

Balbontín C., Calera A., González-Piqueras J., Campos I., Lopéz M.L. and Torres E., 2011. Comparación de los sistemas de covarianza y relación de Bowen en la evapotranspiración de un viñedo bajo clima semiárido. In: *Agrociencia*, 45, p. 87-103.

Bausch W.C. and Neale C.M.U., 1987. Crop coefficients derived from reflected canopy radiation – A concept. In: *Transactions of the ASAE*, 30, p. 703-709.

Campos I., Neale C.M.U., Calera A., Balbontin C. and González-Piqueras J., 2010. Assesing satellite-based basal crop coefficients for irrigated grapes (*Vitis vinifera* L.). In: *Agricultural Water Management*, 98, p. 45-54.

Choudhury B.J., Ahmed N.U., Idso S.B., Reginato R.J. and Daughtry C.S., 1994. Relations between evaporation coefficients and vegetation indices studied by model simulations. In: *Remote Sensing of Environment*, 50, p. 1-17.

Duchemin B., Hadria R., Er-Raki S., Boulet G., Maisongrande P., Chehbouni A., Escadafal R., Ezzahar J., Hoedjes J.C.B., Kharrou M.H., Khabba S., Mougenot B., Olioso A., Rodríguez, J.C. and Simmoneaux V., 2006. Monitoring wheat phenology and irrigation in central Morocco: On the use of relationships between evapotranspiration, crop coefficients, leaf area index and remotely-sensed vegetation indices. In: *Agricultural Water Management,* 79, p. 1-27.

Er-Raki, S., Chehbouni, A., Guemouria, N., Duchemin, B., Ezzahar, J. and Hadria, R., 2007. Combining FAO-56 model and ground-based remote sensing to estimate water consumptions of wheat crops in a semi-arid region. In: *Agricultural Water Management*, 87, p. 41-54.

González-Dugo M., González-Piqueras J., Campos I., Balbontin C. and Calera A., 2010. *Estimation of Surface Energy Fluxes in Vineyard Using Field Measurements of Canopy and Soil Temperature, Remote sensing and hydrology*. IAHS, Jackson Hole (WY). USA.

González-Dugo M.P. and Mateos L., 2008. Spectral vegetation indices for benchmarking water productivity of irrigated cotton and sugarbeet crops. In: *Agricultural Water Management*, 95, p. 48-58.

González-Piqueras J., 2006. Crop Evapotranspiration by means of remote sensing determination of the crop coefficient. Regional Scale Application: 08-29 Mancha Oriental aquifer, Universitat de València.

Hunsaker D.J., Pinter P.J., Barnes E.M. and Kimball B.A., 2003. Estimating cotton evapotranspiration crop coefficients with a multiespectral vegetation index. In: I*rrigation Science*, 22, p. 95-104.

Jayanthi H., Neale C.M.U. and Wright J.L., 2007. Development and validation of canopy reflectance-based crop coefficient for potato. In: *Agricultural Water Management*, 88, p. 235-246.

Montoro A., López Urrea R., Mañas F., López Fuster P. and Fereres E., 2008. Evaporation of Grapevines Measured by a Weighing Lysimeter in La Mancha, Spain. In: *Acta Hort.* (ISHS), 792, p. 459-466.

Neale C.M.U., Bausch W.C. and Heerman D.F., 1989. Development of reflectance-based crop coefficients for corn. In: Transactions of the ASAE, 32, p. 1891-1899.

O'Connell M., Whitfield D., Abuzar M., Sheffield K., McClymont L. and McAllister A., 2010. Satellite remote sensing crop water requirement in perennial horticultural crops. Australian Irrigation Conference 2010: One Water Many Futures, Sydney, Australia.

Oliver H.R. and Sene K.J., 1992. Energy and water balances of developing vines. In: A*gricultural and Forest Meteorology*, vol. 61 (3-4), p. 167-185.

Pellegrino A., Lebon E., Voltz M. and Wery J., 2004. Relationships between plant and soil water status in vine (*Vitis vinifera* L.). In: Plant Soil, 266, p. 129-142.

Silvestre J., Conceição N., Fabião M., Boteta L. and Ferreira I., 2009. Comparação de técnicas para a medição da evapotranspiração em vinha. In: 1.º Congresso Internacional dos Vinhos do Dão, Viseu, Portugal.

Teixeira A.H.d.C., Bastiaanssen W.G.M. and Bassoi L.H., 2007. Crop water parameters of irrigated wine and table grapes to support water productivity analysis in the São Francisco river basin, Brazil. In: *Agricultural Water Management*, 94, p. 31-42.

Torres E.A. and Calera A., 2010. Bare soil evaporation under high evaporation demand: a proposed modification to the FAO-56 model. In: *Hydrological Sciences Journal*, 55, p. 303-315.

Williams L.E. and Ayars J.E., 2005. Grapevine water use and the crop coefficient are linear functions of the shaded area measured beneath the canopy. In: *Agricultural and Forest Meteorology*, 132, p. 201-211.

Wright J.L. 1982. New Evapotranspiration Crop Coefficients. In: *Journal of the Irrigation and Drainage Division,* 108, p. 57-74.

Models for assessment of actual evapotranspiration from remote sensing: Theoretical basis

S.G. García Galiano* and A. Baille**

*Universidad Politécnica de Cartagena, Department of Civil Engineering, R&D Group of Water Resources Management, Paseo Alfonso XIII, 52, 30203, Cartagena (Spain)
**Universidad Politécnica de Cartagena, Department of Agricultural and Food Engineering, Paseo Alfonso XIII, 48, 30203, Cartagena (Spain)

Abstract. In the evaluation of the onset, severity and duration of situations of water stress and droughts, indicators based on processes with intensive use of remote sensing can be used. In the monitoring of agricultural activities as well as the management of water and forest resources, spatio-temporal distributions of information of actual evapotranspiration (ET_{act}) are crucial. This work presents the theoretical aspects of spatio-temporal assessment of ET_{act} process, from remote sensing and meteorological data.

Keywords. Remote sensing – GIS – Actual evapotranspiration – Land surface temperature – NDVI.

Modèles pour l'évaluation de l'évapotranspiration réelle à partir de la télédétection : bases théoriques

Résumé. *L'apparition, la sévérité et la durée du stress hydrique et de la sécheresse, peuvent être évalués au moyen d'indicateurs basés sur les données de télédétection. Pour le suivi de la productivité agricole et pour la gestion des ressources hydriques, la distribution spatio-temporelle de l'évapotranspiration réelle, ET_{act}, est d'une grande importance. Cet article présente les aspects théoriques de l'évaluation spatio-temporelle de ET_{act}, à partir de la télédétection et des données météorologiques.*

Mots-clés. *Télédétection – GIS – Evapotranspiration réelle – Temperature de la superficie terrestre – NDVI.*

I – Introduction

The monitoring and modelling of land surface and vegetation processes is an essential tool for the assessment of water and carbon dynamics of terrestrial ecosystems (Verstraeten *et al.*, 2008). Several studies present the state of the art in the field of estimation of actual evapotranspiration (ET_{act}) from remote sensing (Couralt *et al.*, 2005; Olioso *et al.*, 2005; García *et al.*, 2006; Carlson, 2007). The spatial pattern of daily ET_{act} is important not only for the estimation of crop water requirements and water consumption, the analysis of climate processes, weather forecasting, the study of soil salinisation, and assessing aquifer recharge (SIRRIMED D4.3, 2011), but also for studies of the hydrological cycle at basin scale.

The spatio-temporal assessment of ET_{act} depends on the water status and the energy processes. These processes, in turn, are dependent on land use, distribution of rainfall and irrigation supply, soil properties and climatic factors. There is a need for development of an operational monitoring of ET_{act}.

A brief introduction of models for the estimation of ET_{act} are presented. These are based on balance of surface energy, surface temperature, derivations of the residual model, the relationship between vegetation indexes and land surface temperature (LST), and indirect methods (SVAT).

II – Classification of methodologies for estimation of ET_{act}

1. Models based on surface energy balance

The energy balance equation, without advection, is expressed as:

$$R_N = \lambda ET + H + G + PH \quad (1)$$

where R_N is the net radiation, λET is the latent heat flux or ET_{act} (λ latent heat of vaporization and ET flux of evaporated water), H is the sensible heat flux, G is the soil heat flux, and PH the energy used in the photosynthesis process. The magnitude order of PH is generally small, it is therefore negligible. The residual equation is usually used for the estimation of λET considering the following equation (Choudhury, 1994),

$$\lambda ET = R_N - G - H \quad (2)$$

However, when ET-retrieval methods from remote sensing are used, several uncertainties arise in the parameterization of the energy term ($R_N - G$), and especially of the term G, which can reach high values in arid and semiarid countries (SIRRIMED D4.3, 2011).

2. Models based on land surface temperature: derivations of the residual method

The surfaces where evapotranspiration occurs present a reduction in the temperature with respect to the non-evaporative surfaces. The level at which you set the surface temperature is an indicator of the distribution of the surface energy available for processes such as the flow of sensible and latent heat to the atmosphere, sensible heat flux to the ground and radiation into the atmosphere. The LST is a piece of readily-available remote sensing data. So, another expression derived from the residual equation, and known as "simplified equation", was considered for the assessment of ET_{act} (Jackson *et al.*, 1977; Delegido *et al.*, 1993),

$$ET_d = R_{Nd}^{*} - B \cdot (LST - T_a)_i \quad (3)$$

where ET_d is the daily actual evapotranspiration and R_{Nd}^{*} is the daily net radiation (both in mm/day), B is an empirical constant, and $(LST - T_a)_i$ is the difference between land surface and air temperature, both measured around noon.

For the determination of the constant B, measures of: evapotranspiration (lysimeter, method of "eddy-correlation", method of Bowen), daily net radiation, daily mean air temperature and LST (which is obtained through remote sensing) are all needed. With these data, the constant B is calculated from the regression line (ET_d - R_{Nd}^{*}) as a function of $(LST - T_a)_i$. Once B is obtained, it is possible to use the simplified equation for estimating evapotranspiration from LST, T_a and R_{Nd} data.

Later, this equation was improved by introducing a second parameter, A (Seguin, 1993):

$$ET_d = R_{Nd}^{*} + A - B\,(LST - T_a)_i \quad (4)$$

Net radiation data are difficult to obtain from conventional weather stations, which could therefore be a drawback for the simplified method. But, nowadays, estimation of net radiation could be obtained considering remote sensing data. However, the equation was modified to obtain an expression depending on global radiation (which is easier to get). The ET_0 is obtained with the following equation (Caselles *et al.*, 1992),

$$ET_0 = A \,.\, T_a^{máx} \,.\, R_g + B \,.\, R_g + C \quad (5)$$

where ET_0 is the reference crop evapotranspiration, $T_a^{máx}$ is the maximum air temperature, R_g daily global radiation, and *A*, *B* and *C* are empirical coefficients. There are several methods for estimating $T_a^{máx}$ and R_g from information obtained by remote sensing (Dedieu *et al.*, 1987).

3. Models based on the relationship between vegetation indexes and land surface temperature

A negative linear relationship between LST and vegetation indices (such as NDVI Normalized Vegetation Index), is generally observed. The LST decreases as the density of vegetation increases, which is explained by the cooling caused by ET_{act} (Caselles *et al.*, 1998). The slope of this linear relationship varies depending on the soil water availability, which depends on water balance (rainfall and evaporation).

There are several water stress indices based on remote sensing of LST, associating the ET_{act} with potential ET (ET_{pot}) to assess water requirements.

One of the first that was developed is the **CWSI** (Crop Water Stress Index), expressed as (Jackson *et al.*, 1981),

$$\frac{ET_{act}}{ET_{pot}} = \frac{LST - LST_{\max}}{LST_{\min} - LST_{\max}} = 1 - CWSI \tag{6}$$

where ET_{act} is the actual evapotranspiration, ET_{pot} is the potential evapotranspiration, LST_{max} is the maximum *LST* in the study area, and LST_{min} is the minimum *LST* in the study area (Jackson *et al.*, 1981). This index is reliable only for surfaces with full cover of vegetation.

For composite surfaces (only partially covered by vegetation), a graphical method of *VITT trapezoid* (Vegetation Index/Temperature Trapezoid), presented in Fig. 1, is used. With this method it is possible to estimate the *WDI index* (Water Deficit Index, Moran *et al.*, 1994).

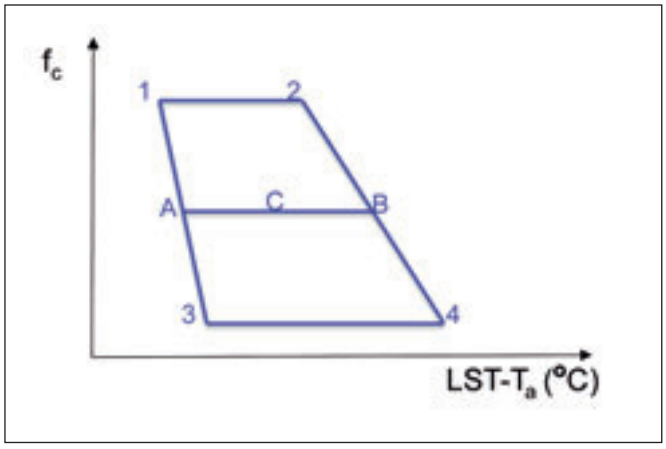

Fig. 1. VITT trapezoid (Vegetation Index-Temperature Trapezoid). Example for MODIS data, for Jucar River basin.

4. Indirect methods. SVAT Model

These methods are based in Soil-Vegetation-Atmospheric Transfer (Soil-Vegetation-Atmosphere Transfer, SVAT) models. The SVAT models require data from different wavelengths (while the methods mentioned thus far require mainly data in the thermal infrared or IRR), to calculate land surface characteristics such as albedo, emissivity and leaf area index (LAI) (Courault *et al.*, 2003).

Although SVAT models are designed to be coupled with atmospheric models, they can also be used to study the processes of evapotranspiration in an "off-line" mode (Bastiaanssen *et al.*, 2005). These models are suitable for ET evaluation in precision irrigation for short periods of time (hours), but have the disadvantage of requiring more initial data.

III – Algorithms derived from the residual method

All the selected algorithms are derived from the *residual method*. Once all the terms of surface energy balance equation have been estimated, ET_{act} is evaluated as the residual of the equation. The methodologies considered could be classified into two groups:

(i) Methods with direct estimation of sensible heat flux (Hs), estimating ET as the residual term of the surface energy balance equation:

– SM method (Simplified method),

– SEBAL model (Surface Energy Balance Algorithm for Land), and

– TSEB (Two Source Energy Balance model).

These are a direct application of the residual method, where:

$$\lambda ET = R_N - H_s - G \tag{7}$$

(ii) Methods with direct estimation of evaporative fraction (EF), and therefore ET_{act} (without estimation of H_s):

– Simplified SEBI method, S-SEBI (Soil Energy Balance Index), and

– JIC method (proposed by Jiang and Islam, 2001).

Where:

$$\lambda ET = EF \cdot (R_N - G) \tag{8}$$

Three of these methods (S-SEBI, SEBAL and JIC) are based on the contrast between the pixels of the wet zone and the dry zone. These methods require a prior graphical representation and interpretation of the data, therefore they are also named *graphical methods*. The net radiation R_N, at daily scale, as well as the flux of soil heat G, are needed for ET_{act} estimation.

1. The simplified method

In the simplified method, proposed by Carlson *et al.* (1995), the net daily evapotranspiration integrated in the surface ET_d, is estimated from a few data: *LST* near noon, when the satellite passes ($T_{s,i}$), air temperature ($T_{a,i}$), and net radiation expressed as the integrated value over 24 hours ($R_{n,d}$), as follows

$$R_{n,d} - \lambda ET_d = B \cdot (T_{s,i} - T_{a,i})^n \tag{9}$$

where B and n are parameters to be defined. $R_{n,d}$ and λET are expressed in cm day^{-1}. The term on the right of equation (9), represents an approximation of the daily sensible heat flux $H_{s,d}$,

assuming that the soil heat flux is negligible at daily scale ($G_d \approx 0$). The term B could be considered as a coefficient of sensible heat flux transference by convection and n is a correction factor to take the stability of the atmosphere into account. An *unstable* situation (during the day, when the warmer air is below the cooler air), tends to increase the sensible heat flux, while the reverse situation (*stable* atmosphere), tends to inhibit this flux. Carlson *et al.* proposed a relationship among the *B* and *n* parameters, the vegetation fraction F_v and the corrected NDVI N^*, using the results from a SVAT simulation.

This method requires the following data: (i) spectral radiances in the red and NIR (for NDVI estimation), and *LST*, from remote sensing; and (ii) air temperature at surface level.

The main advantage of the simplified method is its simplicity. The drawback is its lack of precision, since the *B* and *n* parameters depend not only on the vegetation cover, but also of roughness height, wind velocity, and water status of soil and vegetation.

2. The SEBAL method

The SEBAL method developed by Bastiaanssen *et al.* (1998) is a direct application of the residual method, combining an empirical and physical parameterization. The input data include local meteorological data (mainly wind velocity), and remote sensing data (radiances and *LST*). From these data, the net radiation (R_n), NDVI, albedo (α), roughness height (z_0) and soil heat flux (G), are estimated. The sensible heat flux is estimated by contrasting two sites (one site of wet soil or with vegetation without water stress, and another site of dry soil). ET_{act} is derived as the residual term of the surface energy balance.

3. The TSEB algorithm

So far, the models presented consider a single source of water vapour at the surface. They do not distinguish contributions of vegetation and soil in the surface fluxes. Therefore, the use or the water stress of vegetation cannot be separated. In the models with the approach known as "Two sources" (Norman *et al.*, 1995; Kustas *et al.,* 2003; Melesse *et al.,* 2005), the estimation of surface energy balance at the surface is divided into two parts: one is related with the vegetation, and the other with the soil.

This model can reach, in certain cases, high accuracy (up to 90%), but it is more complex than other approaches, and requires very accurate *LST* information.

4. The S-SEBI algorithm

The S-SEBI scheme, proposed by Roerink *et al.* (2000), defines two temperature thresholds for a given surface albedo value: a maximum temperature, which corresponds to completely dry areas and a minimum temperature corresponding to surfaces that evaporate freely. These temperatures define the variation range of *LST* over the whole image, and are used for defining the evaporative fraction (*EF*). In the SEBI (Surface Energy Balance Index) method, the evapotranspiration estimated from the evaporative fraction is defined as follows,

$$EF = \frac{\lambda ET}{R_N - G} = \frac{\lambda ET}{\lambda ET + H_S} \tag{10}$$

The S-SEBI method presents two main advantages:

(i) It is a self-sufficient method while satellite data is available, and needs no ground measurement data.

(ii) From a physical point of view, and comparing it with the methods that determine a single temperature for both dry and wet conditions, the S-SEBI method is more realistic because it determines the value of these temperatures as a function of albedo.

The data required for the application of this method are: spectral radiances in the visible, near infrared and thermal infrared.

5. The JIC algorithm

The method proposed by Jiang *et al.* (2004), or the JIC method, is based on the analysis of LST-NDVI space. This space (triangular or trapezoidal form), delimited by the distribution of pixels, has a linear relationship with the surface fluxes of energy.

Figure 2 below presents an example of *LST*-NDVI space obtained from remote sensing. This triangle defines the limits for the evaporative fraction (*EF*). The estimation of latent heat flux is restricted in this space, which is the key to this method. From this space, the EF is linearly related with LST for a certain NDVI.

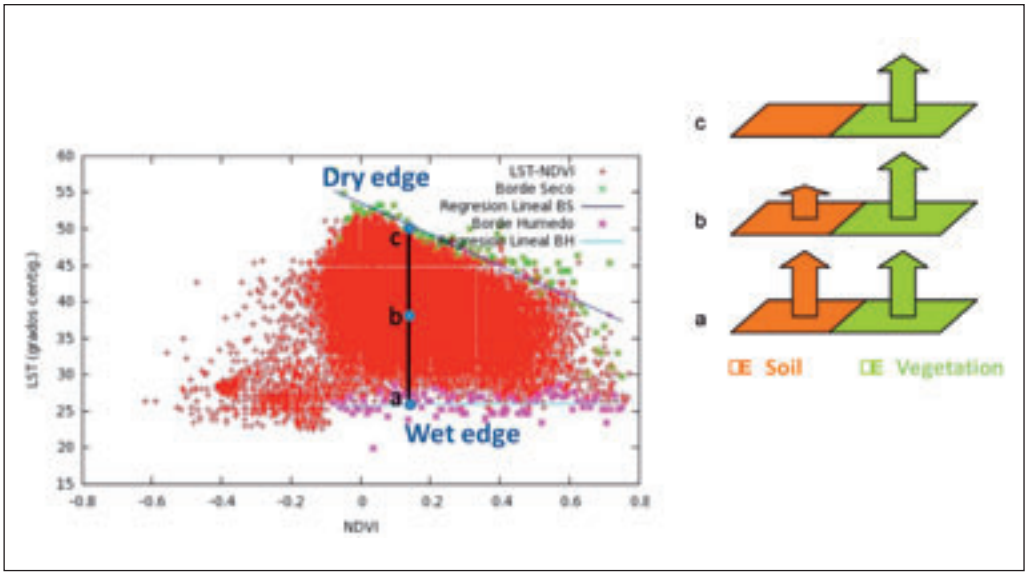

Fig. 2. Conceptual interpretation of LST *vs* NDVI (adapted from Jiang *et al.*, 2004). Example from MODIS data.

In this method, ET_{act} is based in the *Priestley-Taylor* equation and a relation between *LST* and NDVI (Jiang and Islam, 2001), is estimated as follows:

$$\lambda ET = \phi \frac{\Delta}{(\Delta + \gamma)} (R_N - G) \tag{11}$$

where Φ corresponds to *EF* value, Δ is the slope of the vapour pressure curve, γ the psychometric constant and R_N represents net radiation.

In conditions without convection and advection,

$$ET \leq (R_N - G) \tag{12}$$

Therefore, Φ presents the following range corresponding to minimum and maximum values of ET_{act}, respectively.

$$0 \leq \phi \leq \frac{\Delta}{(\Delta + \gamma)} \tag{13}$$

Each pixel of this LST-NDVI space has an associated specific Φ defined by:

$$\phi = \phi_{\max} \frac{LST_{\max} - LST}{LST_{\max} - LST_{\min}} \tag{14}$$

where Φ_{max} = 1.26 corresponds to bare soil, LST_{max} is the maximum LST for NDVI = 0, and LST_{min} the minimum LST. Then, a spatial distribution of Φ is obtained for each date.

The following equation represents the evaporative fraction (EF),

$$EF = \phi \frac{\Delta}{(\Delta + \gamma)} \tag{15}$$

where the psychometric constant is a function of atmospheric pressure.

The net radiation is estimated considering ground meteorological data, remote sensing data, and topographical attributes derived from a Digital Elevation Modelo (DEM), applying the following equation,

$$R_N = (1 - \alpha)\, R_s + R_L^{\downarrow} + R_L^{\uparrow} \tag{16}$$

where R_s is the solar radiation (or downward short wave radiation), $R_L^{\downarrow}$ and $R_L^{\uparrow}$ are downward and upward long wave radiation respectively. They were estimated considering the Stefan Law, with the clear sky emissivity calculated from an empirical relationship with e_a, and the surface emissivity.

IV – Conclusions

The monitoring of agricultural activities, land management, food security research, pollution detection, nutrient flows, fire detection, and carbon balance as well as hydrological modelling, require the estimation of evapotranspiration at different spatio-temporal resolutions. Several methods for the estimation of ET_{act}, considering an intensive use of remote sensing of earth systems, were presented. It is recommendable to validate the results of these methodologies with *in situ* data or ground truth.

Acknowledgments

The funding from EU Project TELERIEG (SUDOE INTERREG IV B Programme), as well as the support from Project CGL2008-02530/BTE financed by the State Secretary of Research of Spanish Ministry of Science and Innovation (MICINN), are acknowledged.

References

Bastiaanssen W.G.M., Menenti M., Feddes R.A. and Holtslag A.A.M., 1998. A remote sensing surface energy balance algorithm for land (SEBAL). 1. Formulation. In: *J. Hydrol.*, 212/213, p. 198-212.

Bastiaanssen W.G.M., E. Noordman J.M., Pelgrum H., Davids G., Thoreson B.P. and Allen R.G., 2005. SEBAL model with remotely sensed data to improve water-resources management under actual field conditions. In: *J. Irrig. Drainage Engin.*, 131, p. 85-93.

Caselles V., Artigao M., Hurtado E., Coll C. and Brasa A., 1998. Mapping actual evapotrasnpiration by combining Landstat TM and NOAA-AVHRR images: application to the Barrax area, Albacete, Spain. In: *Remote Sensing of Environment*, 63, p. 1-10.

Caselles V., Delegido G., Sobrino J. and Hurtado E., 1992. Evaluation of the maximum evapotranspiration over the La Mancha region, Spain, using NOAA AVHRR data. In: *International Journal of Remote Sensing*, 13 (5), p. 939-946.

Carlson T.N., William J.C. and Gillies R.R., 1995. A new look at the simplified method for remote sensing of daily evapotranspiration. In: *Remote Sens. Environ.*, 54, p. 161-167.

Carlson T.N., 2007. An Overview of the "Triangle Method" for Estimating Surface Evapotranspiration and Soil Moisture from Satellite Imagery. In: *Sensors*, 7, p. 1612-1629.

Choudhury B., 1994. Synergism of multispectral satellite observations for estimating regional land surface evaporation. In: *Remote Sensing of Environment*, 49, p. 264-274.

Courault D., Seguin B. and Olioso A., 2003. Review to estimate evapotranspiration from remote sensing data: some examples from the simplified relationship to the use of mesoscale atmospheric models. In: *ICID workshop on remote sensing of ET for large regions,* 17th September, 2003.

Courault D., Seguin B. and Olioso A., 2005. Review on estimation of evapotranspiration from remote sensing data: From empirical to numerical modeling approaches. In: *Irrigation and Drainage Systems*, 19, p. 223-249.

Dedieu G., Deschamps P. and Kerr Y., 1987. Satellite estimation of solar irradiance at the surface of the earth and of surface albedo using a physical model applied to METEOSAT data. In: *Journal of Climate and Applied Meteorology*, 26, p. 79-87.

Delegido J. and Caselles V., 1993. Evapotranspiración. Teledetección en el seguimiento de los fenómenos naturales. In: *Climatología y Desertificación* (S. Gandía y J. Meliá, coords), Universidad de Valencia, p. 205-213.

García Galiano S.G., González Real M.M., Baille A. and Martínez Álvarez V., 2006. Desarrollo de un sistema de alerta temprana frente a sequías a nivel regional para las cuencas del Río Júcar y Río Segura. Informe Final. Dirección General del Agua, Ministerio de Medio Ambiente.

Jackson R., Reginato R. and Idso S.B., 1977. Wheat canopy temperature: a practical tool for evaluating water requirements. In: *Water Resources Research*, 13, p. 651-656.

Jackson R., Idso S., Reginato R. and Pinter, P., 1981. Canopy temperature as a crop water stress indicator. In: *Water Resources Research*, 17, p. 1133-1138.

Jiang L. and Islam S. 2001. Estimation of surface evaporation map over southern Great Plains using remote sensing data. In: *Water Resources Research*, 37(2), p. 329-340.

Jiang L., Islam S. and Carlson T.N., 2004. Uncertainties in latent heat flux measurements and estimation: implications for using a simplified approach with remote sensing data. In: *Can. J. Remote Sensing*, 30, p. 769-787.

Kustas W.P., Norman J.M., Anderson M.C. and French A.N. (2003). Estimating subpixel surface temperatures and energy fluxes from the vegetation index radiometric temperature relationship. In: *Remote Sens. Environ.*, 85, p. 429-440.

Moran M.S., Clarke T.R., Inoue Y. and Vidal A., 1994. Estimating crop water deficit using the relation between surface-air temperature and spectral vegetation index. In: *Remote Sens. Environ.,* 49, p. 246-263.

Melesse A.M. and Nangia V., 2005. Estimation of spatially distributed surface energy fluxes using remotely-sensed data for agricultural fields. In: *Hydrological Processes*, 19, p. 2653-2670.

Norman J.M., Kustas W.P. and Hume K.S., 1995. Source approach for estimating soil and vegetation energy fluxes in observations of directional radiometric surface temperature. In: *Agricultural and Forest Meteorology*, 27, p. 263-293.

Olioso A., Inoue Y., Ortega-Farias S., Demarty J., Wigneron J.-P.,Braud I., Jacob F., Lecharpentier P., Ottlé C., Calvet J.-C. and Brisson N., 2005. Future directions for advanced evapotranspiration modeling: assimilation of remote sensing data into crop simulation models and SVAT models. In: *Irrigation and Drainage Systems*, 19, p. 377-412.

Roerink G.L., Su Z. and Meneti N., 2000. S-SEBI: A simple remote sensing algorithm to estimate the surface energy balance. In: *Phys. Chem. Earth* (B), 25, p. 147-157.

Seguin B., 1993. NOAA/AVHRR data for crop monitoring at a regional level: possibilities and limits in the European context. In: *EARSel Advances in Remote Sensing*, 2 (2), p. 87-93.

SIRRIMED, 2011. Deliverable D4.3. ET-retrieval algorithms for ET-Mapping: State-of-the-Art and Tools to be used in SIRRIMED WP4 and WP5. SIRRIMED Sustainable use of irrigation water in the Mediterranean Region. FP7 Seventh Framework Programme.

Verstraeten W.W., Veroustraete F. and Feyen J., 2008. Assessment of Evapotranspiration and Soil Moisture Content Across Different Scales of Observation. In: *Sensors*, 8, p. 70-117.

Estimation of actual evapotranspiration from remote sensing: Application in a semiarid region

S.G. García Galiano and R. García Cárdenas

Universidad Politécnica de Cartagena, Department of Civil Engineering,
R&D Group of Water Resources Management, Paseo Alfonso XIII, 52, 30203, Cartagena (Spain)

Abstract. The potential of remote sensing for the recommendation and monitoring of irrigation practices is irrefutable. GIS have enabled the development of operational spatio-temporal tools for monitoring agricultural activity which can overcome the uncertainty brought about by problems related to water scarcity and increasing drought events. This paper presents an operational methodology for estimating actual evapotranspiration from Landsat images, and its application in the Region of Murcia (Spain).

Keywords. Remote sensing – GIS – Actual evapotranspiration – Land surface temperature – NDVI.

Estimation de l'évapotranspiration réelle à partir de la télédétection : application dans une région semi-aride

Résumé. *Le potentiel que représente la télédétection pour la recommandation et le suivi des pratiques d'irrigation est irréfutable. Couplées avec un SIG, les images de télédétection permettent le développement d'outils opérationnels spatio-temporels utiles pour le suivi des activités agricoles. Ce papier présente une méthodologie opérationnelle pour l'estimation de l'évapotranspiration réelle à partir d'images Landsat et son application dans la Région de Murcia (Espagne).*

Mots-clés. *Télédétection – GIS – Evapotranspiration réelle –Température de surface des terres – NDVI.*

I – Introduction

The potential of remote sensing for the recommendation and monitoring of irrigation practices is irrefutable. The context of uncertainty in the rural areas of the southwest Mediterranean area, especially in agriculture, is caused by the loss of competitiveness and abandonment of farming in many areas due to problems related to water scarcity and the increase of drought events.

The Southeastern Spanish basins are regularly affected by drought. These events affect large areas, and their severity has increased in recent years due to climate change (García Galiano *et al*., 2011). This situation endangers the continuity of significant areas of irrigation, critical in this case for the economy of the Region of Murcia. Moreover, the adjusted water allocations for irrigation in the region, coupled with quality problems that necessarily arise from the intensive use of resources, will continue setting up a situation of scarcity. It is conceivable that repeated acute episodes of lack of water for irrigation, such as those registered in recent years, will have to be faced in the coming decades with greater intensity.

As a result, the assessment and monitoring of irrigated areas presents special relevance. Remote sensing has proved to be a very efficient tool for this, allowing the estimation of vegetation indices related to the soil water content and actual evapotranspiration directly. The present study addresses the operational development in a GIS (Geographical Information System) environment, a remote sensing based methodology for estimating actual evapotranspiration and its application in the Region of Murcia.

II – Target zone and databases

1. Segura River Basin and its level of spatial disaggregation

The study area corresponds to the Segura River Basin (SRB, Spain), located in the southeastern part of the Iberian Peninsula (Fig. 1). The semiarid SRB, with an area of 18,870 km^2, presents the lowest percentage of renewable water resources of all Spanish basins and it is currently highly regulated.

The main water demand is agriculture, with a surface of more than 43% (809,045 ha) of the basin (SRBP, 1998), with one third of that surface being under irrigation (269,000 ha). Agricultural water demand from irrigated areas must be highlighted because it accounted for 85% of the total water demand in 2007 (Urrea *et al.*, 2011).

In addition, available water resources per inhabitant in the Segura River Basin (only 442 m³/inhabitant/year) are much lower than the national water scarcity threshold, which is set at 1000 m³/inhabitant/year, according to the United Nations and the World Health Organization. Water scarcity is a major issue in the Segura River Basin. Consequently, water transfer from the Tajo River Basin, supplemented with desalinization, are real options for increasing water resources in the basin.

The SRB is controlled by head water reservoirs, where natural runoff is regulated, and by reservoirs that store the water resources from the Tajo River Basin. With the aims of planning and managing water resources, and considering the specificities of the basin, several levels of spatial disaggregation are identified: hydraulic zones, systems of exploitation of resources, and units of exploitation. The evaluation of resources and demands and possibilities of management, considering the hydraulic infrastructures of the basin, are analyzed from the disaggregation into hydraulic zones and sub-zones according to the Segura River Basin Management Plan (SRBP, 1998). The hydraulic zones (Fig. 1) were defined considering topographical criteria (basins and sub-basins) and administrative limits. There are fourteen hydraulic zones in the SRB.

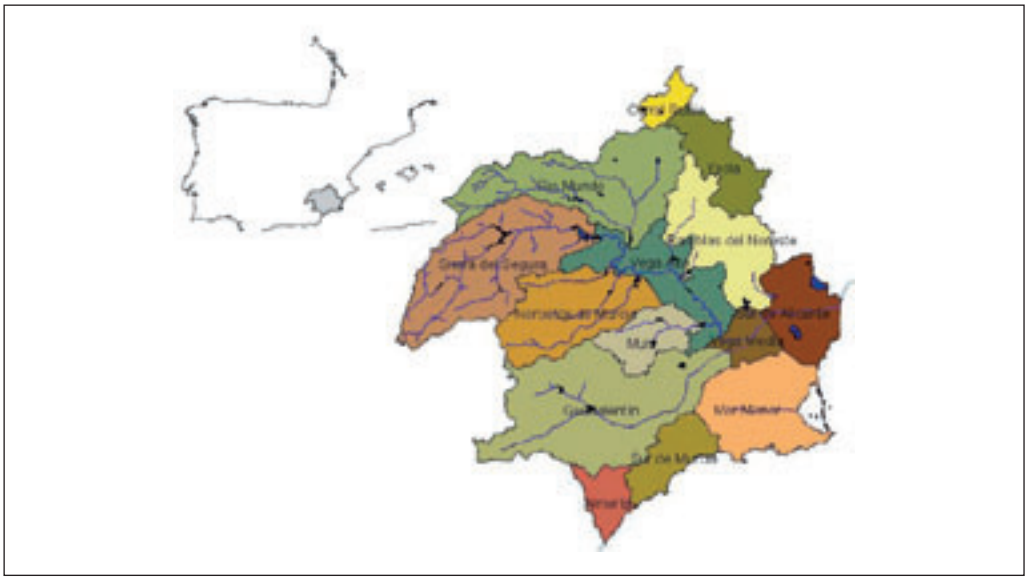

Fig. 1. Location of the Segura River Basin, and hydraulic zones (Source: Hydrographic Confederation of Segura River Basin (CHS), Ministry of Environment, Marine and Rural Affairs).

Based on these hydraulic zones, the CHS defined several Systems of Exploitation of Resources (SER). These SER are further aggregated in the frame of the Segura River Basin Drought Action Plan (SRBDAP, 2007).

Finally, considering the water demands and sources, several spatial disaggregation schemes could be identified for the basin, each one corresponding to specific objectives. For example, the Spanish Institute of Statistics (INE) identifies *agricultural areas* (Fig. 2). In turn, these areas can be identified as rain fed or *irrigated-zones*, and the latter can be further identified into irrigated zones using the Basin System resources or the water supplied by ATS. The CHS in turn, consider the use of *UDAs* (Units of Agriculture Demands).

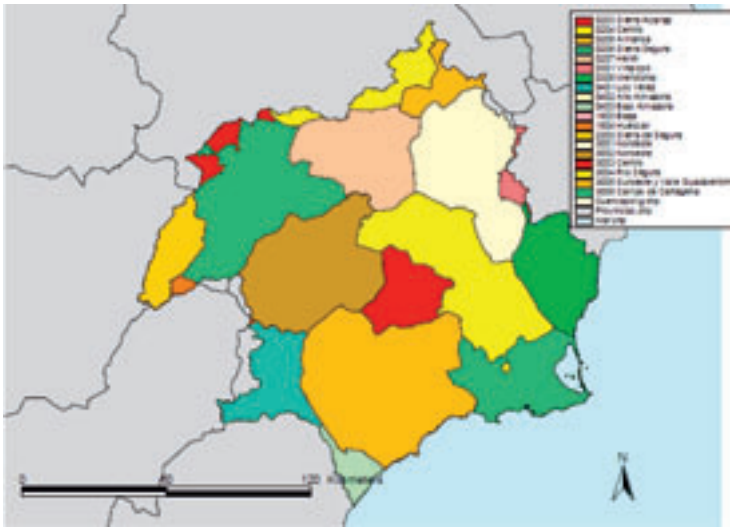

Fig. 2. Spatial disaggregation of agricultural zones [Source: National Institute of Statistics (INE, Spain)].

2. Datasets: Collection of spatio-temporal information

Several sources of information were considered: the National Plan of Remote Sensing (PNT), the CHS water agency, the Instituto Murciano de Investigación Agraria y Alimentaria (IMIDA), as well as information freely accessible on the Internet.

The satellite data used corresponded to Landsat 5 TM (TM5), Spot 5, and MODIS data. However, the work was mainly based on Landsat 5 TM and MODIS data. The MODIS (Moderate Resolution Imaging Spectroradiometer) is a sensor, on the TERRA (EOS AM) and AQUA (EOS PM) platforms of NASA.

The Landsat images cover a total surface of 185x185 km^2. These images were geometrically rectified, and georeferenced considering the ETRS-89 system with UTM projection by the Instituto Geográfico Nacional (IGN).

For considering the whole SRB in a specified date, the acquisition of the following four images are needed: 199-33, 199-34, 200-33, and 200-34 (Fig. 3). A time lag between 199-33/1999-34 and 200-33/200-34 will be identified. Therefore, it is not possible to study the whole basin for the same date. The Region of Murcia is included in the spatial framework of 199-33 and 199-34 images.

For this study, the zones 199-33, 199-34, 200-33 and 200-34 were considered for the years 2008 and 2009. Some of these images present a high percentage of cloudiness, especially in the case of 2008. For filtering clouds a methodology proposed by IGN was considered. This methodology of filtering is based in the difference between a reference image and the image to be evaluated (excluding false positives, fixing a threshold in the thermal band).

Time series of meteorological information (air temperature, relative humidity, atmospheric water vapour, etc.), were collected for the same time period from the IMIDA and the National Agency of Meteorology (AEMET, Agencia Estatal de Meteorología). The IMIDA institute is responsible for the management of several meteorological and agrometeorological networks, with more than 100 gauging stations in the Region of Murcia (and more than 30 stations of radiation measures). Fig. 4 below represents the spatial distribution of stations for the Region of Murcia.

Fig. 3. Distribution of Landsat images over Spain.

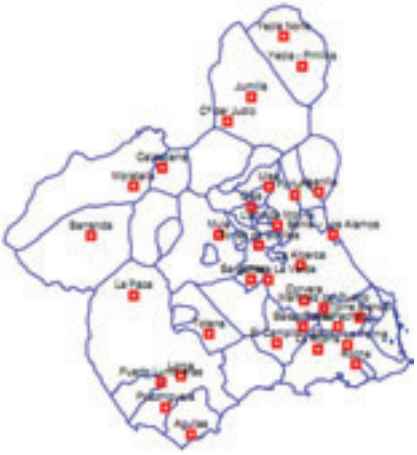

Fig. 4. Meteorological stations in the Murcia Region. Source: IMIDA on line.

The dataset was completed including products of MODIS images, provided by the TERRA MODIS satellite (NASA), corresponding to the same date as the TM5 images. The land surface temperature (LST) product presents a spatial resolution of 1 by 1 km. The MODIS images are available for free on the Internet (http://ladsweb.nascom.nasa.gov/data/).

Additional spatial information was collected and processed below GIS, in the present work, corresponding to channel network, UDAs, and administrative limits for SRB.

III – Methodological aspects

1. Estimation of time evolution of NDVI

Several vegetation indexes were considered, based in the interpretation of space conformed by LST and NDVI. Then, the water susceptibility (Giraut *et al*., 2000) could be estimated based on cover of plant biomass based on NDVI (combination of bands 3 and 4); index of soil dryness (combination of bands 2 and 5), and cover of water surface (discrimination of band 7).

NDVI was derived from reflectance values in the Red (B3) and infrared (B4) region of the electromagnetc spectrum of TM5 images, as follows:

$$NDVI = (B4 - B3) / (B4 + B3) \quad (1)$$

The range of NDVI correspond from -1 to 1, but for this study the range 0 (bare soil) to 1 (soil with maximum plant biomass), was considered. Then, negative values represent water. Fig. 5 shows the spatial distribution of NDVI for two dates (14/02 and 24/07 of 2009), in the Region of Murcia.

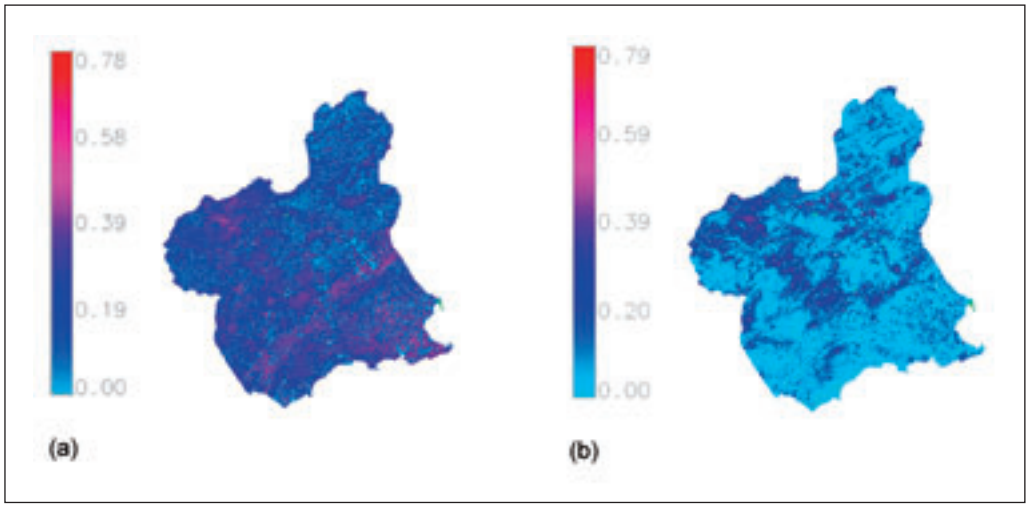

Fig. 5. Spatial distribution of NDVI for the Region of Murcia, from TM5: (a) 14/02/2009 and (b) 24/07/2009.

2. Estimation of time evolution of LST

The LST was estimated from band 6 of Landsat, with spatial resolution of 120 m. The LST spatial distribution in combination with vegetation indexes will be considered in the estimation of indicators related with soil moisture (Sandholt *et al*., 2002) and actual evapotranspiration (Jiang and Islam, 2001). The LST spatial distributions from TM5 were contrasted with the LST product provided by MODIS sensor. SPOT images do not present thermal band.

In the following paragraphs, the methodology for the estimation of LST from Landsat is presented. The geometric correction was not needed for Landsat images, because they correspond to PNT, and the corrections were already made. The signals received by the thermal sensors (TM5) can be converted to at-sensor radiance (L_{sensor}), according to the corrections proposed by Voogt and Oke (2003):

(i) Spectral radiance conversion to at-sensor brightness temperature,

(ii) Correction by atmospheric absorption and re-emission,

(iii) Correction by surface emissivity, and

(iv) Correction by surface roughness.

In the case of correction (i), the signal received from the thermal sensor could be converted to different parameters for the LST estimation,

$$L_{sensor} = gain.DN + bias \quad (2)$$

where L_{sensor} is the spectral radiance of thermal band, *DN* is the digital number of a given pixel (in this case, each pixel of TM5 band 6), *gain* is the slope of the radiance/*DN* conversion function depending of the band (for band 6, the *gain* is 0.055158), and *bias* is the intercept of the radiance/*DN* conversion function; it is a constant depending on the band (*bias*=1.238 for TM5 band 6)

$$T_{sensor} = \frac{K_2}{\ln\left(\frac{K_1}{L_{sensor}} + 1\right)} \quad (3)$$

where T_{sensor} represents the at-sensor brightness temperature (K) with K_1 = 607.76 W/(m^{2}sr.μm) and K_2 = 1260.56 K as prelaunch calibration constants for TM5 (Landsat Project Science Office, 2002), and L_{sensor} estimated above.

To obtain LST, the following steps correspond to correction (ii) to (iv), the single-channel algorithm proposed by Jiménez-Muñoz and Sobrino (2003) must be applied.

$$T_s = \gamma\left[\varepsilon^{-1}\left(\psi_1 L_{sensor} + \psi_2\right) + \psi_3\right] + \delta \quad (4)$$

with

$$\gamma = \left\{\frac{c^2 L_{sensor}}{T_{sensor}^2}\left[\frac{\lambda^4}{c_1} L_{sensor} + \lambda^{-1}\right]\right\}^{-1} \quad (5)$$

$$\delta = -\gamma\, L_{sensor} + T_{sensor} \quad (6)$$

where T_s is the LST in K, ε is the ground surface emissivity, c_1 = 1.19104.10^8 (W μm^{4}m^{-2}sr^{-1}), and c^2 = 14387.7 (μm K), λ is the effective wave length (μm) corresponding to band 6.

The following equations represent the correction by total atmospheric water vapour content (*w in* grs/cm^2), therefore the atmospheric functions (ψ_1, ψ_2 and ψ_3) depend only on *w*, particularized for TM/ETM+ 6 data, as follows,

$$\begin{aligned}\psi_1 &= 0.14714w^2 - 0.15583w + 1.1234\\ \psi_2 &= -1.1836w^2 - 0.37607w - 0.52894\\ \psi_3 &= -0.04554w^2 + 1.8719w - 0.39071\end{aligned} \quad (7)$$

For the estimation of atmospheric water vapour, external data are needed. In this case, the MODIS Terra Level 2 Water Vapour product MOD05_L2 (Gao and Kaufman, 1998), could be used because the hour the satellite passes over the Iberian Peninsula is similar to Landsat. But the MODIS data are available from 2000, therefore for previous years the AVHRR sensor of NOAA satellite could be considered.

However, in the present work the maps of water vapour (grs/cm^2) were generated from monthly values provided for typical clear days by the SoDA Project (http://www.soda-is.com) stations in different parts of the Region of Murcia, according to Remund *et al.* (2003).

The last step for the estimation of LST from Landsat is the calculation of the surface emissivity (ε). The ε values could be obtained for example based on classification image, based on NDVI

image or based on the ratio values of vegetation and bare ground (Zhang *et al*., 2006). In this work, the ε values are estimated in function of NDVI (Valor and Caselles, 1996) as follows,

$$
\begin{aligned}
&-1 < NDVI < -0.18 \quad \varepsilon = 0.985 \\
&-0.18 < NDVI < 0.157 \quad \varepsilon = 0.955 \\
&0.157 < NDVI < 0.727 \quad \varepsilon = 1.0094 + 0.047 \ln(NDVI) \\
&0.727 < NDVI < 1 \quad \varepsilon = 0.99
\end{aligned}
\tag{8}
$$

Fig. 6 presents an example of the application of the methodology described in the estimation of LST for Murcia Region (date 24/07/2009).

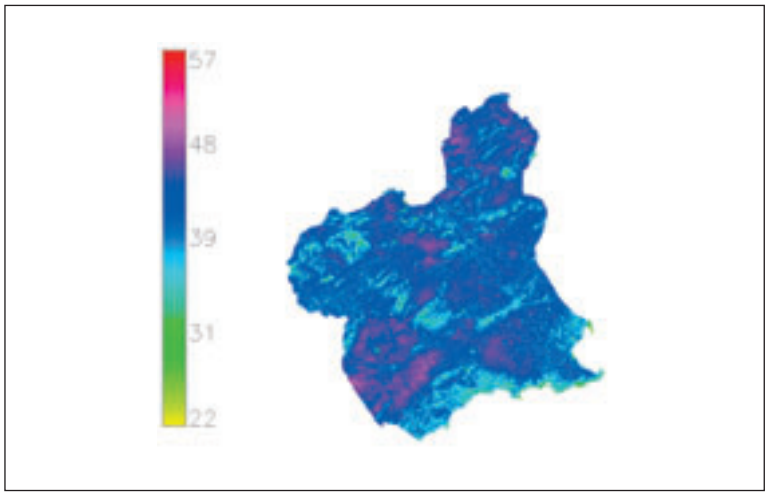

Fig. 6. Spatial distribution of LST (ºC) for date 24/07/2009 (LSTD20090724).

The results of NDVI and LST derived from TM5 could be compared with the corresponding products from MODIS TERRA. In this case, the product MOD11A1 (daily LST with spatial resolution 1x1 km) and product MOD09GA (daily reflectances with spatial resolution 500x500 m), could be used. From MOD09GA the NDVI is estimated, combining bands 1 and 2, as *NDVI* = (*B2–B1*)/(*B2+B1*). From the comparison of images, the differences detected are neglectable.

IV – Application of JIC Algorithm derived from the residual method

An algorithm derived from the *residual method*, proposed by Jiang *et al.* (2004) or the JIC method, was selected. In the JIC method, the ET_{act} is based on the direct estimation of the evaporative fraction (EF), without estimation of H_s, as follows

$$\lambda ET = \phi \frac{\Delta}{(\Delta + \gamma)} (R_N - G) \tag{9}$$

where ¦ is the evaporative fraction (EF), Δ is the slope of the vapour pressure, γ the psychrometric constant, R_N is the net radiation, and *G* is the flux of soil heat.

This method requires a prior graphical representation and interpretation of LST-NDVI space. This space (triangular or trapezoidal in form), delimited by the distribution of pixels, has a linear relationship with the surface fluxes of energy. Each pixel of the space presents a specific Φ defined by,

$$\phi = \phi_{\max} \frac{LST_{\max} - LST}{LST_{\max} - LST_{\min}} \tag{10}$$

where Φ_{max} = 1.26 corresponds to bare soil, LST_{max} is the maximum LST for NDVI = 0, and LST_{min} the minimum LST. Then, a spatial distribution of Φ is obtained for each date.

The following equation represents the evaporative fraction (EF),

$$EF = \phi \frac{\Delta}{(\Delta + \gamma)} \tag{11}$$

where the psychrometric constant is a function of atmospheric pressure by the following equation,

$$\gamma = 0.665.10^{-3} P \tag{12}$$

where *P* is the atmospheric pressure (kPa), depending on height (on normal climatology conditions), as:

$$P = P_0 e^{\left(-\frac{z}{8000}\right)} \tag{13}$$

where *z* is the height in meters above sea level, and P_0 atmospheric pressure (kPa) at sea level.

The Δ is the slope of the vapour pressure, is estimated as follows,

$$\Delta = \frac{4098 * 0.6108}{(T_a + 237.3)^2} \exp\left(\frac{17.27 T_a}{T_a + 237.3}\right) \tag{14}$$

The maps of relative humidity (*HR*) and air temperature are obtained from meteorological stations. Fig. 7, presents an example ot *HR* and T_a maps, for the date 24/07/2009. From these maps, the spatial distributions of e^* (saturated vapour pressure) and e_a (air vapour pressure), were derived.

The saturated vapour pressure (e^*) could be estimated only depending on surface temperature (LST), and, finally the e_a is estimated from *HR* (%) and e^*, as follows,

$$e_a = \frac{HR\ e^*}{100} \tag{15}$$

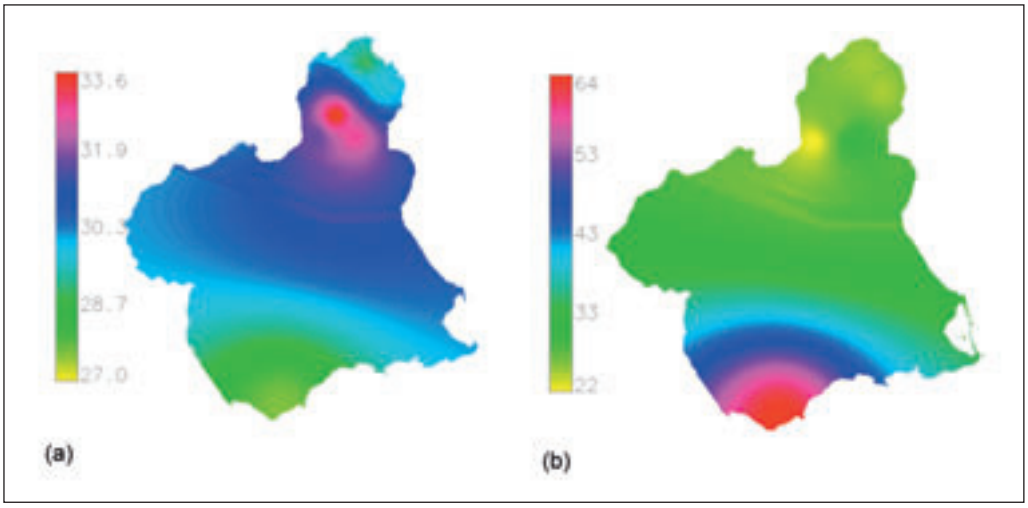

Fig. 7. Mean daily spatial distribution for the Region of Murcia: (a) T_a (ºC), and (b) *HR*.

V – Estimation of net radiation

The net radiation (R_N, $Wm^{-2}day^{-1}$) is estimated considering ground meteorological data, remote sensing data, and topographical attributes derived from a Digital Elevation Model (DEM), applying the following equation,

$$R_N = R_s^{\downarrow} + R_s^{\uparrow} + R_L^{\downarrow} + R_L^{\uparrow} = (1-\alpha)R_s^{\downarrow} + R_L^{\downarrow} + R_L^{\uparrow} \quad (16)$$

where $R_s^{\downarrow}$ and $R_s^{\uparrow}$ are downward and upward shortwave solar global radiation, respectively, $R_L^{\downarrow}$ and $R_L^{\uparrow}$ are downward and upward long wave radiation, respectively. They were estimated considering the Stefan Law, with the clear sky emissivity calculated from an empirical relationship with e_a, and the surface emissivity.

1. Estimation of ($Rs^{\downarrow}$ + $Rs^{\uparrow}$) shortwave net radiation

The diffuse, direct (beam) and ground reflected solar irradiation for given day, latitude, surface and atmospheric conditions, could be estimated for clear-sky and overcast atmospheric conditions with the *r.sun* model below GRASS GIS (GRASS, 2011). Therefore, the term ($R_s^{\downarrow}$ + $R_s^{\uparrow}$) or net balance of shortwave global radiation is derived from the results of the *r.sun* command.

The *r.sun* model considers all relevant input parameters as spatially distributed entities to enable computations for large areas with complex terrain (Šúri and Hofierka, 2004). Conceptually, the model is based on equations of European Solar Radiation Atlas (ESRA). As an option, the model considers a shadowing effect of the local topography. The *r.sun* works in two modes. In the first mode it calculates a solar incidence angle (degrees) and solar irradiance values (Wm^{-2}) for the set local time. In the second mode, used in the present work, daily sums of solar radiation ($Whm^{-2}day^{-1}$) are computed within a set day.

The input data correspond to:

– A DEM (meters) and topographical attributes such as slope and aspect (both in decimal degrees), are used. In this case, a DEM with a spatial resolution of 30 m was considered. The

topographical attributes were derived from the DEM, applying the GRASS GIS command *r.slope.aspect*. Fig. 8, below, presents the DEM and aspect maps for the Region of Murcia.

– Latitude map (decimal degrees, from -90º to 90º), is the other map required.

Then, the spatial distribution of slope and latitude are presented in Fig. 9.

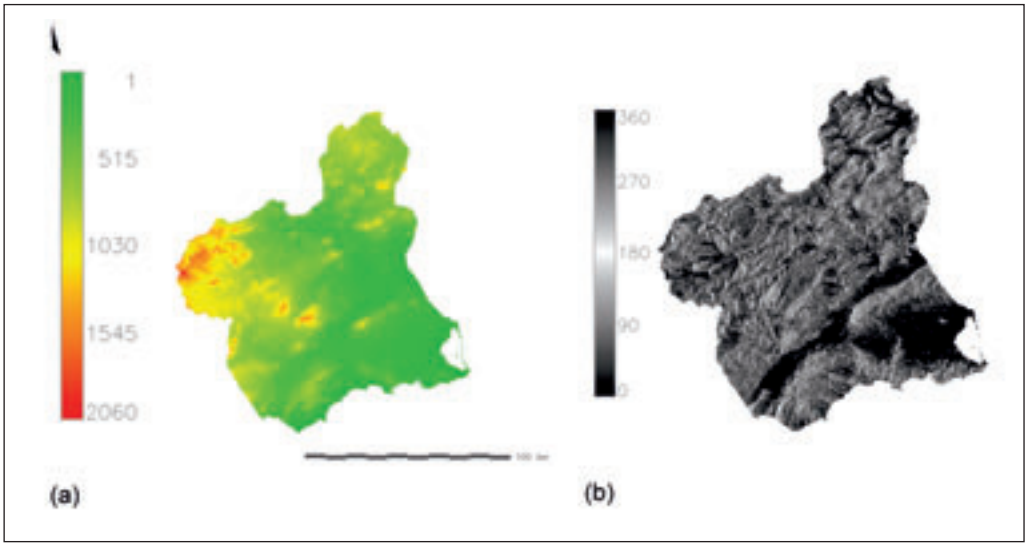

Fig. 8. Spatial distributions for the Region of Murcia: (a) DEM (m), and (b) aspect (grades from East).

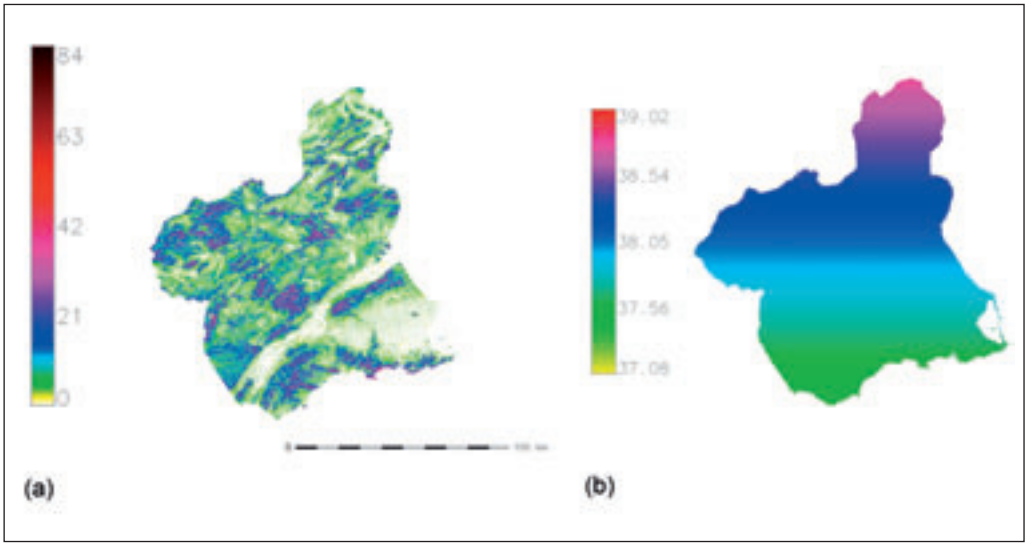

Fig. 9. Spatial distributions for the Region of Murcia: (a) slope, and (b) latitude.

– The *link turbidity* values, through SoDa Webpage (http://www.helioclim.net) were obtained at monthly scale for the 34 stations considered in the present study. The spatial distributions of monthly mean turbidity were obtained by interpolation.

– The *albedo* indicates the percentage of irradiation reflected depending on the surface. In this case, the spatial distribution of albedo was derived from MODIS MOD43B3 product.

– The *day* corresponds to Julian day of the year (1 to 365).

From the results of this command, the shortwave net radiation could be estimated from direct, diffuse and reflected radiation as follows,

$$R_N = R_{direct} - R_{diffuse} - R_{reflected} \tag{17}$$

2. Estimation of longwave net radiation

The longwave net radiation could be estimated by a balance between the radiation emitted by the sky and the reflected by earth's surface (Law of Stefan-Boltzmann), as follows,

$$R_L^{\downarrow} - R_L^{\uparrow} = \sigma \varepsilon_a T_a^4 - \sigma \varepsilon_s LST^4 \tag{18}$$

where $\sigma = 5.67.10^{-8} Wm^{-2}K^{-4}$ is the constant of Stefan-Boltzmann, T_a (K), LST (K), ε_s is surface emissivity (or ε), and ε_a is the atmospheric emissivity estimated as,

$$\varepsilon_a = \left[1 - (1+\xi)\exp\left[-(1.2+3\xi)^{1/2}\right]\right] \text{ ó } \varepsilon_a = 0.56 + 0.259\sqrt{e_a} \tag{19}$$

$$\xi = 46.5\frac{e_a}{T_a} \tag{20}$$

where e_a is the air vapour pressure (kPa).

The heat flux from the soil G varies throughout the day, but its value is too small in comparison with R_N or λET. Therefore in the present work, the G value was not considered. However, the relation among R_N, NDVI, and G could be estimated by the equation from Moran *et al.* (1989).

$$G = 0.583\exp\left[(-2.13NDVI)R_N\right] \approx 0 \tag{21}$$

Therefore, the actual evapotranspiration ($Wm^{-2}day^{-1}$) will be,

$$\lambda ET = \phi \frac{\Delta}{\Delta + \gamma}\left(R_N - G\right) \tag{22}$$

And for the result expressed in mm/day, it is necessary to divide eq. (9) by 3047.6 factor. A schema of the developed methodology is presented in Fig. 10, and an example of spatial distributions of R_N and ET_{act} for the 24/07/09, are presented in Fig. 11.

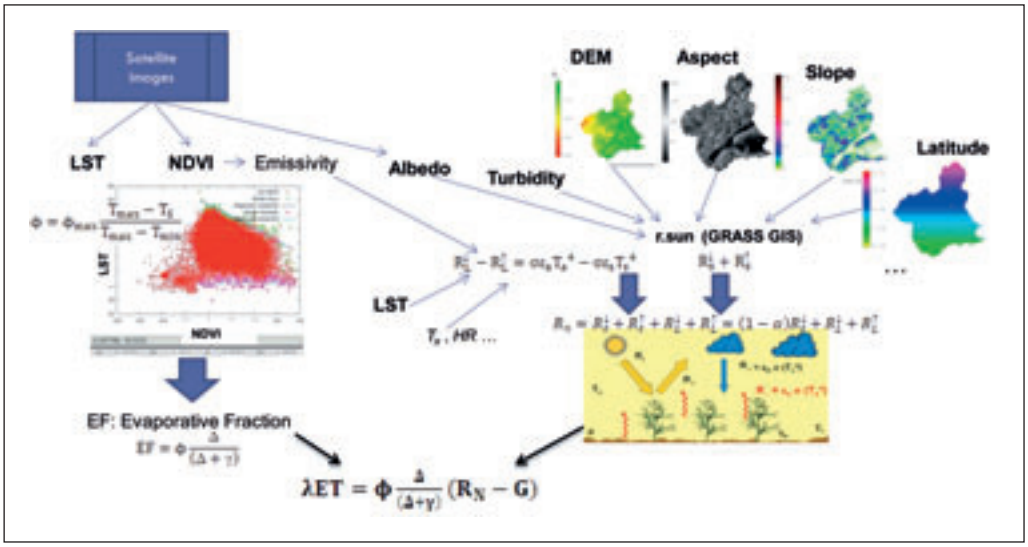

Fig. 10. Schema of the developed methodology.

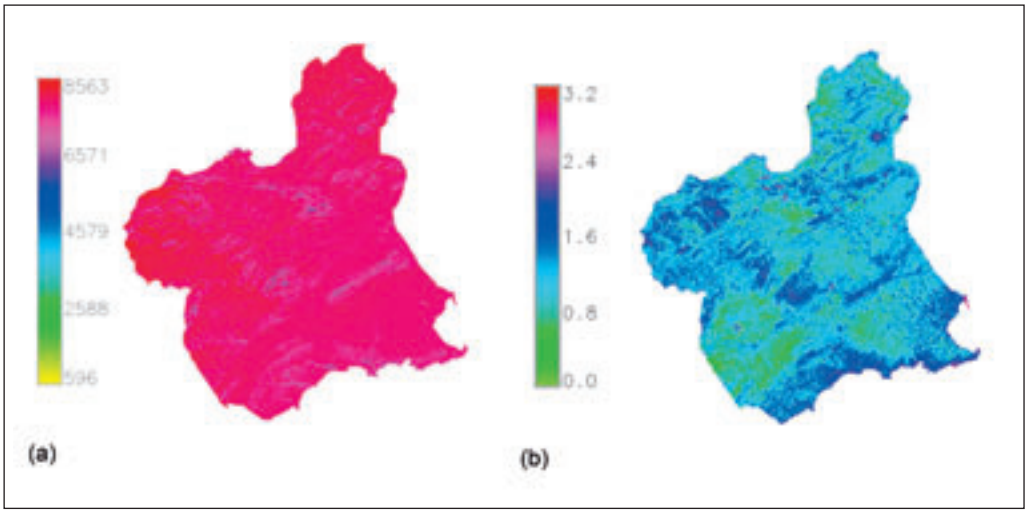

Fig. 11. Spatial distributions for the Region of Murcia: (a) R_N net radiation ($Wm^{-2}day^{-1}$), and (b) ET_{act} (mm/day).

VI – Conclusions

Climate change and variability predict a plausible negative scenario for the frequency and severity of drought events over the Segura River Basin (Garcia Galiano *et al*., 2011). This situation endangers the continuity of significant irrigated areas in the Region of Murcia, which are important for the Region's economy. The monitoring of irrigated areas from remote sensing and direct estimation of actual evapotranspiration constitute valuable information for farmers. The method-

ology presented for estimating ET_{act} has been incorporated to GIS environment. Subsequently, the incorporation of the DEM and the derived topographical attributes have improved the spatial distributions of radiation estimates. These types of solutions are affordable from an operational point of view, for making recommendations of irrigation practices and schedules for farmers.

Acknowledgments

The funding from EU Project TELERIEG (Programme SUDOE INTERREG IV B), as well as the support from Project CGL2008-02530/BTE financed by the State Secretary of Research of Spanish Ministry of Science and Innovation (MICINN), are acknowledged.

References

Gao B.-C. and Kaufman Y.J., 1998. *The MODIS Near-IR Water Vapor Algorithm. Algorithm Technical Background Document. Product ID: MOD05 - Total Precipitable Water.* p. 1-23. On line *http://modis-atmos.gsfc.nasa.gov/_docs/atbd_mod03.pdf*

García Galiano S.G., Giraldo Osorio J.D., Urrea Mallebrera M., Mérida Abril A. and Tetay Botía C., 2011. Assessing drought hazard under non-stationary conditions on South East of Spain. In: *Risk in Water Resources Management*. (Eds. G. Blöschl, K.Takeuchi, S.Jain, A. Farnleitner, A. Schumann). IAHS Publ. 347, IAHS Press, CEH Wallingford, Oxfordshire, United Kingdom, p. 85-91.

Giraut M., Minotti P. and Ludueña S., 2000. Integración de imágenes SAC-C, LANDSAT, y SPOT pancromático para la determinación de susceptibilidad hídrica. In: *IX Simposio Latinoamericano de Percepción Remota*, p. 1-8. On line *http://www.hidricosargentina.gov.ar/selper_bol_giraut.pdf*

Grass, 2011. *GRASS (Geographic Resources Analysis Support System) GIS 6.4.2svn Reference Manual.* On line *http://grass.osgeo.org/grass64/manuals/html64_user/index.html*

Jiang L. and Islam S. 2001. Estimation of surface evaporation map over southern Great Plains using remote sensing data. In: *Water Resources Research*, 37(2), p. 329-340.

Jiang L., Islam S. and Carlson T.N., 2004. Uncertainties in latent heat flux measurements and estimation: implications for using a simplified approach with remote sensing data. In: *Can. J. Remote Sensing*, 30, p. 769-787.

Jiménez-Muñoz J.C. and Sobrino J.A., 2003. A generalized single-channel method for retrieving land surface temperature from remote sensing data. In: *Journal of Geophysical Research*, 108, 1.

Landsat Project Science Office 2002. Landsat 7 Science Data User's Handbook. Goddard Space Flight Center, Greenbelt, M.D.

Remund J., Wald L., Lefevre M., Ranchin T. and Page J., 2003. Worldwide Linke turbidity information. Proceedings of ISES Solar World Congress, 16-19 June 2003, Göteborg, Sweden). CD-ROM published by International Solar Energy Society. On line: *http://hal.archives-ouvertes.fr/docs/00/46/57/91/PDF/ises2003_linke.pdf*

Sandholt I., Rasmussen K. and Andersen J., 2002. A simple interpretation of the surface temperature/vegetation index space for assessment of surface moisture status. In: *Remote Sensing of Environment*, 79 (2-3), p. 213-224.

SRBDAP, 2007. *Segura River Basin Drought Action Plan*. Hydrographic Confederation of Segura River Basin (CHS), Ministry of Environment, Marine and Rural Affairs, Spain.

Šúri M. and Hofierka J. 2004. A new GIS-based solar radiation model and its application to photovoltaic assessments. In: *Transactions in GIS*, 8(2), p. 175-190.

Urrea Mallebrera M., Mérida Abril A. and García Galiano S.G., 2011. Segura River Basin: Spanish Pilot River Basin Regarding Water Scarcity and Droughts. In: *Agricultural Drought Indices. Proceedings of the WMO/UNISDR Expert Group Meeting on Agricultural Drought Indices*. S. Mannava V.K., R.P. Motha, D.A. Wilhite and D.A. Wood (eds.), 2-4 June 2010, Murcia, Spain: Geneva, Switzerland: World Meteorological Organization. AGM-11, WMO/TD No. 1572; WAOB-2011. 219 p. 2-12.

Valor E. and Caselles V., 1996. Mapping land surface emissivity from NDVI: Application to European, African, and South American Areas. In: *Remote Sensing of Environment*, 57 (3), p. 167-184.

Voogt J.A. and Oke T.R., 2003. Thermal remote sensing of urban climates. In: *Remote Sensing of Environment*, 86 (3), p. 370-384.

Zhang J., Wang Y. and Li Y., 2006. A C++ program for retrieving land surface temperature from the data of Landsat TM/ETM+ band 6. In: *Computers & Geosciences*, 32, p. 1796-1805.

Applications of remote sensing of high resolution

Thermostress. An automatic imaging process for assessing plant water status from thermal photographs

M.A. Jiménez-Bello, C. Ballester, J.R. Castel and D.S. Intrigliolo

IVIA, Ctra Moncada-Náquera km 4.500, P.O. Box 46113 Moncada, Valencia (Spain)

Abstract. Leaf temperature can be used for monitoring plant water status. Nowadays, by means of thermography, canopy temperature can be remotely determined. In this sense, it is crucial to automatically process the images. In the present work, a methodology for the automatic analysis of frontal images taken on individual trees was developed. The camera used in this investigation took at the same time thermal and visible scenes, so it was not necessary to overlap the images. During the processing in batch no operator participated. This was done by means of a non supervised classification of the visible image from which the presence of sky and soil was detected. In case of existence, a mask was performed for the extraction of intermediated pixels to calculate canopy temperature by means of the thermal image. Sunlit and shady leaves could be detected and isolated. Thus, the procedure allowed to separately determine canopy temperature either of the more exposed part of the canopy or of the shaded portion. The methodology developed was validated using images taken in several regulated deficit irrigation trials in persimmon and two citrus trees cultivars (Clementina de Nules and Navel Lane-Late). Overall, results indicated that similar canopy temperatures were calculated either by means of the automatic process or the manual procedure. In addition, differences in midday stem water potential and stomatal conductance among irrigation treatments were associated with differences in canopy temperature in persimmon trees. The procedure here developed here allowed to drastically reduce the time amount used for image analysis also considering that no operator participation was required. Indeed, the tool here proposed will facilitate further investigations in course for assessing the feasibility of using thermography for detecting plant water status in woody perennial crops with discontinuous canopies

Keywords. Image analysis – Regulated deficit irrigation – Thermography – Water relations.

Thermostress. Un traitement automatique d'images pour évaluer l'état hydrique des plantes à partir de photographies thermiques

Résumé. *La température de la feuille peut être utilisée pour le suivi de l'état hydrique des plantes. De nos jours, à l'aide de la thermographie, la température du couvert végétal peut être déterminé par télédétection. Dans ce sens, le traitement automatique des images est crucial. Dans le présent travail, on a développé une méthodologie pour l'analyse automatique d'images frontales concernant les arbres pris individuellement. La caméra utilisée pour cette étude a pris en même temps des images dans les spectres thermique et visible, donc il n'était pas nécessaire de superposer les images. Le traitement en lots s'est fait sans opérateur. Ceci a été réalisé par classification non supervisée de l'image du visible à partir de laquelle on détectait la présence de ciel et de sol. S'il existait, un masque était appliqué pour l'extraction de pixels intermédiaires afin de calculer la température du couvert végétal à l'aide de l'image thermique. Les feuilles ensoleillées et ombragées pouvaient être détectées et isolées. Ainsi, la procédure permettait de déterminer séparément la température du couvert soit pour la partie la plus exposée de ce couvert, ou pour la partie ombragée. La méthodologie développée a été validée en utilisant des images prises lors de plusieurs essais d'irrigation déficitaire régulée sur plaqueminiers et sur deux cultivars d'agrumes (Clémentine de Nules et Navel Lane-Late). Dans l'ensemble, les résultats ont indiqué que l'on calculait des températures de couvert semblables soit par le traitement automatique ou par la procédure manuelle. En outre, des différences de potentiel hydrique des tiges à midi et de conductance stomatale parmi les traitements d'irrigation ont été associées à des différences de température du couvert chez les plaqueminiers. La procédure développée ici a permis de réduire drastiquement le temps pour analyser l'image et il convient également de considérer qu'aucun opérateur n'était requis. En fait, l'outil proposé ici facilitera les recherches en cours pour évaluer la faisabilité d'utiliser la thermographie pour détecter l'état hydrique des plantes chez des cultures arborées pérennes présentant un couvert discontinu.*

Mots-clés. *Analyse d'images – Irrigation déficitaire régulée – Thermographie – Relations hydriques.*

I – Introduction

Efficient irrigation scheduling procedures requires the analysis of plant water status. Leaf water potential measured with the pressure chamber, either at predawn or at midday, has long been used as a plant water stress indicator. However this measurement is quite time and labor consuming what often limits its use.

Transpiration is an endo-energetic thermodynamical process. When water is transpired by plants, the latent heat of evaporation is drawn from them, decreasing thereby their temperature.

Plants under soil water limitations often respond decreasing stomatal conductance (gs), reducing hence transpiration. This implies that canopy temperature should raise in plants grown under soil water limitations. Therefore infrared sensing of the canopy temperature can be used to estimate stomatal conductance and plant evapotranspiration (Merlot *et al.*, 2002; Jones *et al.*, 2002).

Infrared thermography is a powerful tool to estimate crop temperatures. Hand-operated cameras allow taking images of individual plants or even portions of them, achieving higher spatial resolution. For instance, images can capture different tree positions (shady, sunlit or zenithal position). Subsequently, images are processed, without the need of georeferentiation if crops are identified previously in the field and linked to their corresponding images. In order to make this technique more useful for assessing crop water status, the automation of the images analysis is required. This is particular important in the case of woody perennial crops that often have discontinuous canopies (i.e. ground cover is below 100%). In this case images can contain both canopy and soil portions that need to be separated. In this work, a methodology has been developed where vegetation temperature is calculated with the help of a color image. The camera used takes a color and infrared image at the same time, and therefore no alignment techniques are necessary. Objects in the scene are classified into classes using an unsupervised classification method of the color image. Classes are identified by means of its vector in the Red, Green and Blue model (RGB) and they are grouped according to their intensity. In this way, no operator participates in the analysis phase and images are processed in a sequential way. If sky or soil appear in the scene these classes are identified and removed from the analysis. Temperature can be calculated from the sunlit or shady leaves or from both together. The methodology has been implemented using ArcGIS 9.x (ESRI, Redlands, USA) a commercial software and its developing platform named ArcObjects. Examples of the validation of this procedure are reported and results obtained in different irrigation trials are also presented and briefly discussed.

II – Material and methods

1. Experimental orchards

The experiment was performed during 2009 in a commercial orchards of Persimmon (*Diospyros kaki* L.f.), located in Manises, (Valencia, Spain). The orchard was planted in 2001 with the cv 'Rojo Brillante' grafted on *Diospyros lotus* at 5.5 x 4 m. During the experimental period trees had, on average, a shaded area of 39%.The soil was sandy loam to sandy clay loam, calcareous; with an effective depth of 0.8 m. Trees were drip-irrigated with two laterals per row and 8 emitters (4 l/h) per tree. Two irrigation treatments were applied in this orchard: (i) Control, irrigated at 100% of the estimated crop evapotranspiration (ETc) defined by Allen *et al*. (1998); during the whole season with a total amount of water applied of 487 mm; and (ii) RDI, irrigated at 50% of ETc from July (DOY 185) to August (DOY 230) with a total amount of water applied of 429 mm. The statistical design was a complete randomized plot with three replicates plot per treatment and 6-7 sampling trees per replicate.

2. Plant water status determinations

Stem water potential (Ψs) was measured weekly at solar midday (14:00 h) using a pressure chamber (Model 600 Pressure Chamber Instrument, Albany, USA), following recommendations of Turner (1981) in three mature leaves of two trees per replicate plot. In the case of NLL and three trees per replicate plot, in the case of CN and Persimmon, were enclosed in plastic bags covered with silver foil at least two hours prior to the measurements. Mean values of Ψs for each tree were compared with the thermal image analysis.

Stomatal conductance (gs) was measured with a leaf porometer (SC 1 Porometer, Decagon, WA, USA) in the same trees where Ψs was determined. Gs of each tree was determined as the mean value of five measurements in five different fully exposed leaves. These mean values were used for comparison with the thermal image analysis.

Thermal images were taken with an infrared thermal camera TH9100 WR (NEC San-ei Instruments, Tokyo, Japan) with a precision of 2ºC or 2% of reading. The camera had a visible of 752 x 480 pixels and a 320 x 240 pixel microbolometer sensor, sensitive in the spectral range of 8 and 14 μm and a lens with an angular field of view of 42.0º x 32.1º. Emissivity used was 0.98, value that can be assumed for the healthy vegetation (Monteith and Unsworth 2008). Images were registered in a proprietary format denominated SIT where information is arranged in sections. Temperature is stored in a file of type "band sequential" (bsq) of 16 bits with temperature stored on 14 bits. Information referred to RGB format has a JPG format. Thermal images were taken at noon in both, sunlight and shaded sides of all the trees where Ψs and gs were measured.

II – Methodology developed

For the image analysis the ArcGIS 9.3 software (ESRI, Redlands, USA) was used. This software has an application called "Geoprocessing" which is a set of windows and dialog boxes used to manage and build models that execute a sequence of tools. These models can be customized and run by means of programming languages like Microsoft Visual Basic. In addition, it is possible to connect with a database (DB) to feed the processes developed in the ArcGIS environment and to store the results on the DB. The analysis process included the following steps (see algorithm in Fig. 1).

Images were catalogued and stored in the DB. Each image was clearly identified with the date and hour, treatment, replicate, tree and position (sunlit or shadow). Images were selected by means of a query to the DB. This allows to analyse all the images captured in a day or for a selected irrigation treatment.

The SIT image format was exported to a standard format compatible with the software used. For that purpose, pixels with thermal information image were exported to the bsq format (ESRI, 2007) and pixels with RGB information were exported to JPG format.

Thermal images were reclassified assigning to each pixel the corresponding temperature, in a binary code, according to the scale used by the camera. In this case, temperature range was -50ºC to 130ºC and pixel temperature was calculated by the equation: T (ºC) = 40 + (DN × 180)/16.384, where DN is the 14 bits value, 40 is the temperature value for DN = 0, 180 is the temperature range and 16,384 the possible values of a 14 bits pixel.

Non supervised pixel classification of the RGB image was performed (Lillesand *et al.*, 2004). The reason was to avoid the presence of an operator in the spectral signatures selection phase. Normally, up to six classes appeared in a scene: clear sky, clouds, shadows, soil, shady vegetation and sunlit vegetation. In a supervised process, the operator has to assign a representative area to the classes presented in the image. Successively, the operator should calculate, for each selected class, a spectral signature in RGB. This consists of a vector of three dimensions where

Fig. 1. Flux diagram of the whole automatic thermal image processing algorithm.

each component represents the red, blue and green bands. This process has to be repeated for each single image analysis considering that scene features might differ among days and even among scenes taken in a same day. The possible number of different classes in a scene was tested concluding that, for more than 7 classes, the algorithm did not find enough pixels to identify a new class. The above mentioned six classes were identified, assigning the extra class to pixels of vegetation. In the absence of clouds and when the sky had different levels of intensity, the extra class was assigned to sky. An example of this classification, is shown in Fig. 2 where a photograph taken in the Persimmon orchard has been included.

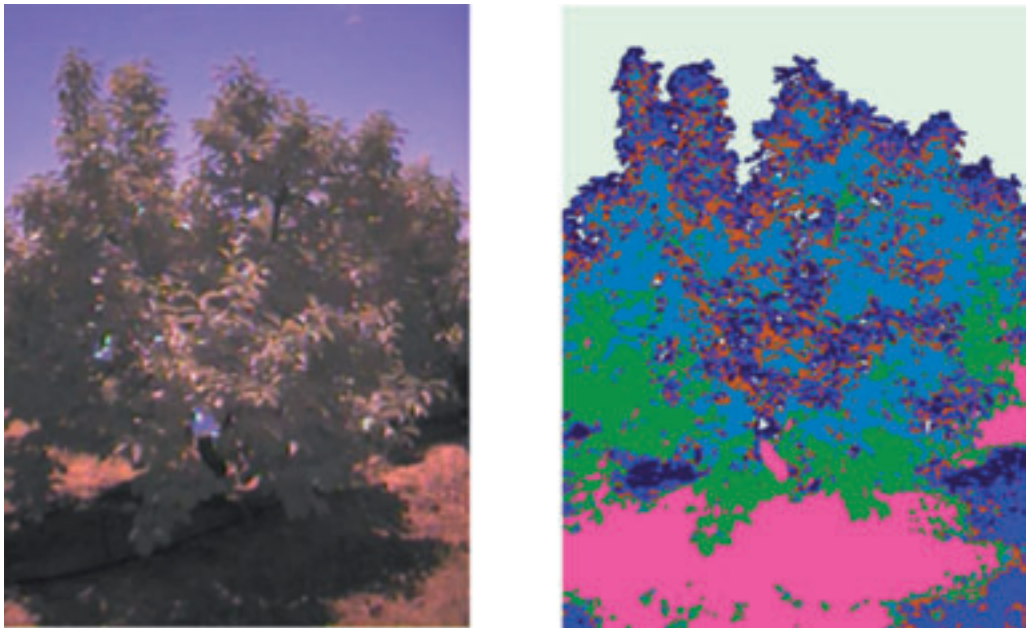

Fig. 2. Classification non supervised in seven classes of a RGB image of a persimmon tree.

Once the classes where set up, image was classified using a Maximum Likelihood Classification algorithm based on the Bayes theorem considering that each class is normally distributed in a multidimensional space (Lillesand *et al.*, 2004). The tool implemented in ArcGIS offered us the possibility of produce a raster file with 14 levels showing the interval of confidence of the pixel classification. For the images where neither sky nor soil were captured, captured, classes were assigned within the shady and sunlit vegetation, representing the intermediate classes vegetation with different illumination intensities.

For each class, the RGB vector module was calculated. Each coordinate vector was defined by the pixel value in the RGB bands. These classes are ordered according to their intensity. The darkest classes, usually represent shadows, have a lower value.

Due to the low sky emissivity in clear days (Wunderlich, 1972), pixels composing the sky classes show a lower average temperature and higher standard deviation than the other classes. In the case that sky would had been photographed, gravity centers of the darkest class and sky can be calculated and a polygonal can be created to overlap the intermediate pixels existing between both classes. The rest of pixels can then be excluded from the analysis to avoid possible errors in pixel

classification (e.g., a sunlit soil zone could be misclassified as vegetation). The width of the mask was set taking into account the average distance from the camera to the tree and the camera field of view which determined the scale and the size of the photographed scene. This area must be lower than the canopy diameter, thus the target tree can be properly analysed (Fig. 4).

Fig. 3. Polygonal mask applied to a scene with sky and shadows.

When sky was not detected in the scene, masking was not applied, nevertheless, a mask can be forced to include only an image zone. In the case that the mask was applied, the shadiest class gravity center was calculated. The image orientation (vertical or horizontal) was determined and the midpoint of the opposite edge was chosen as reference to build the polygon mask.

When sunlit leaves were chosen for temperature calculation, pixels with highest RGB module were selected. In case all pixels need to be included the whole selectable classes can be easily taken into account. The minimum (Tmin, ºC), maximum (Tmax, ºC), average (Tc, ºC) and standard deviation (Tstd, ºC) of selected pixels were calculated. It is possible to exclude from the calculation those pixels not to be classified, for example those below a certain degree of confidence, making a mask with the confidence raster produced during the classification process. Output results were stored in the database together with Ψs and gs determined for each crop and date.

III – Results and discussion

1. Thermostress validation

The ANOVA results indicated that there were no statistically significant differences between canopy temperatures obtained either via automatic or manual procedures (P values of 0.427). The slopes of the linear regressions between pairs of Tc computed either manually or automatically were not different from 1 (Fig. 4).

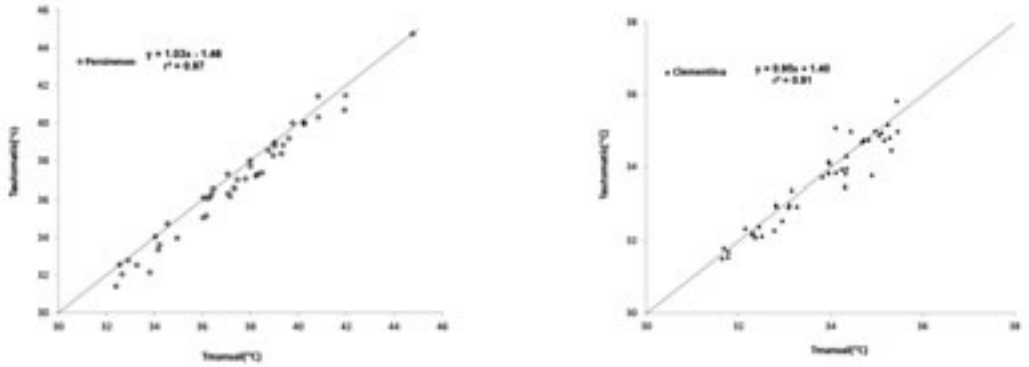

Fig. 4. Comparison of manual and automatic procedures of average canopy temperatures (Tc) calculation for a representative day in persimmon (DOY 204) and clementine (DOY 215). The solid line represents the 1:1 relationship.

However, the intercept ("a") was -1.46 indicating a general underestimation of the Tc when automatically calculated. This underestimation occurred in 36 images out of 44 that were taken to deliberately capture the whole tree. The reason for this underestimation is due to the fact that when the mask is created, some leaf pixels close to sky, together with some sky pixels misclassified as leaves, are included in the average Tc computation. Since the sky has a lower emissivity than the leaves, this lead to an underestimation of temperature calculated automatically. This fact can be seen in Fig. 5 where the T raster computed by means of a mask manually performed by an operator (Fig. 5A) and the T raster computed with a mask automatically created detecting the shadow and the sky (Fig. 5B) are shown. The darkest pixels represent the lower temperatures. They are located on the canopy outline with the sky as background. This issue could be overcome taking photographs with higher resolution, where sky and leaves could be more clearly separated.

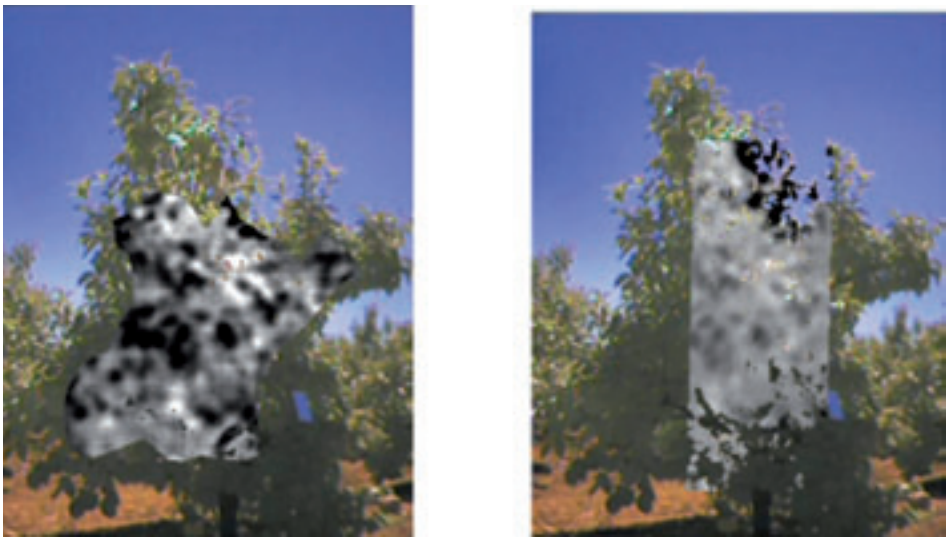

Fig. 5. Tc calculated by different types of masks in a persimmon tree. (A) The mask is manually created by an operator. The operator draws the mask following the tree outline avoiding sky pixels selection. (B) The mask is created automatically after sky and shadow detection. Pixels close to the tree outline are also selected.

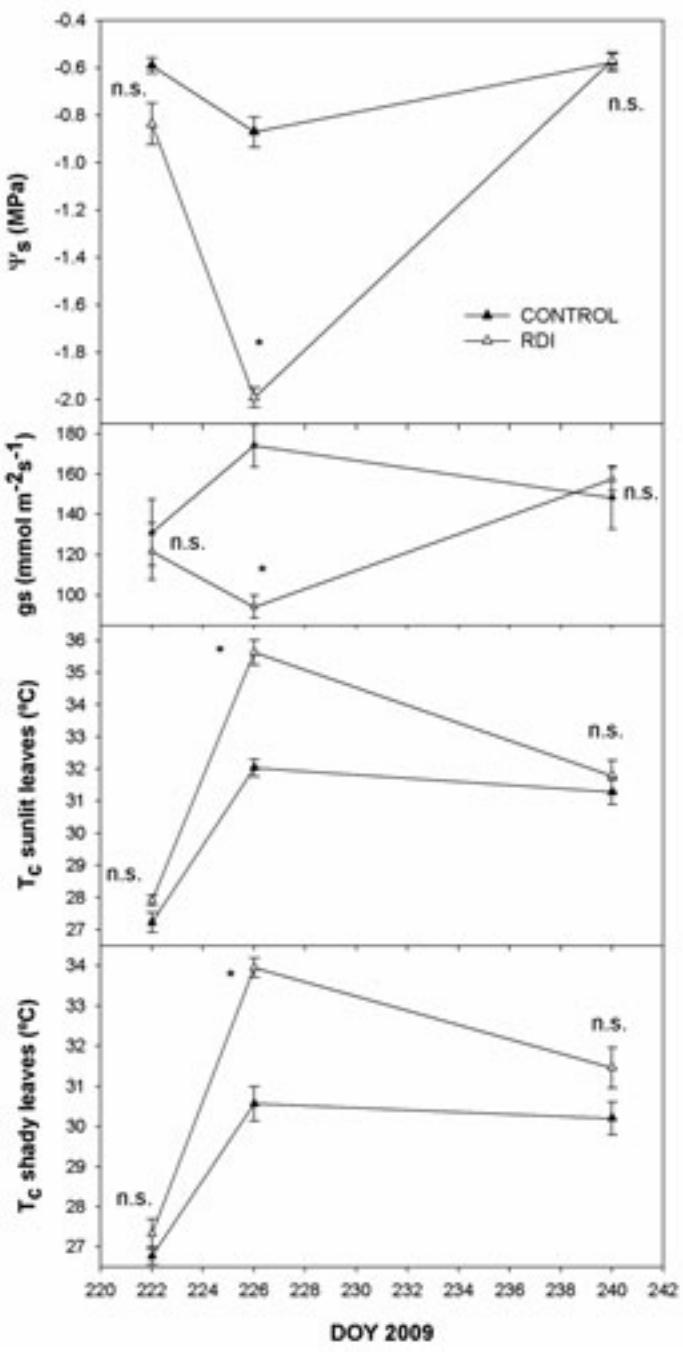

Fig. 6. Evolution of stem water potential (ψs), conductance (gs) and temperature from the sunlit and shady side of the canopy during the period of water restrictions in 2009. * and ns denote significant differences at P<0.05 and non significant differences, respectively, by Dunnett's test.

2. Thermostress application

The Thermostress procedure was applied to obtain canopy temperatures of kaki trees under different irrigation regimes (Fig. 6) During the period of water restrictions Control trees maintained ψs values around -0.70 MPa whilst RDI trees reached values of -1.99 MPa. Differences of 1.12 MPa on average between RDI and Control trees (DOY 226) resulted in a reduction of 46% for the gs in the water stressed treatment (174 mmol m^{-2} s^{-1} for the Control treatment and 94 mmol m^{-2} s^{-1} for the RDI trees). This gs reduction in the RDI trees was reflected in a high temperature of the canopy from these trees. Pictures from both sides of the trees (sunlit and shady side) detected the temperature increase. In pictures from the sunlit side, on average, Control trees had a temperature of 32ºC while RDI trees had a temperature 3.6ºC higher. The difference of temperature between treatments when pictures were taken from the shady side was similar, 3.4ºC, showing in this case Control trees temperatures of 30.6ºC. When water restrictions finished and irrigation was resumed to normal dose RDI trees returned to ψs, gs and canopy temperature values similar to Control trees (DOY 240).

IV – Conclusions

A routine for automatic canopy temperature extraction based on an unsupervised classification method of the color image has been developed and validated. This automatic process allows obtaining quickly canopy temperature data from experiments or commercial situations, drastically reducing the time consumed for images analysis eliminating in addition any subjectivity due to the operator analysis. Indeed, the procedure here developed might facilitate the adoption of the thermography for crop water stress detection and irrigation scheduling. At a commercial scale it is important to automate the information extraction process in order to be able to actuate on irrigation controllers. The routine proposed might serve as a first step in order to finally incorporate canopy temperature determinations by thermography in the irrigation scheduling automation.

Acknowledgements

This research was supported by funds from projects TELERIEG (Programme Interreg IVb Sudoe) and Rideco-Consolider CSD2006-0067.

References

Lillesand T.S., Kiefer R.W., Chipman J.W., 2004. *Remote Sensing and Image Interpretation*, 5th ed. John Wiley and Sons Inc., New York.

Mazomenos B., Athanassiou C.G., Kavallieratos N., and Milonas P., 2004. Evaluation of the major female *Eurytoma amygdali* sex pheromone components, (Z,Z)-6,9- tricosadiene and (Z,Z)-6-9-pentacosadiene for male attraction in field tests. In: *Journal of Chemical Ecology,* 30, p. 1245-1255.

Merlot S., Mustilli A.C., Genty B., North H., Lefebvre V., Sotta B., Vavasseur A., Giraudat J., 2002. Use of infrared thermal imaging to isolate *Arabidopsis mutants* defective in stomatal regulation. In: *Plant Journal*, 30, p 601-609.

Monteith J.L., Unsworth M.H., 2008. *Principles of Environmental Physics*. Elsevier/Academic Press, p. 440.

Jones H.G., Stoll M., Santos T., de Sousa C., Chaves M.M., Grant O.M., 2002. Use of infrared thermography for monitoring stomatal closure in the field: application to grapevine**.** In: *Journal of Experimental Botany,* 53, p. 2249-2260.

Turner N., 1981. Techniques and experimental approaches for the measurement of plant water status. In: *Plant Soil,* 58, p. 339-366.

Wunderlich W.O. 1972. Heat and mass transfer between a water surface and the atmosphere. Lab. Report No. 14, Tennessee Valley Authority Engineering Laboratories, Norris, TN.

The use of multispectral and thermal images as a tool for irrigation scheduling in vineyards

J. Bellvert and J. Girona[1]

Irrigation Technology, Institut de Recerca i Tecnologia Agroalimentàries (IRTA)
Centre UdL-IRTA, 25198 Lleida, Spain
[1]E-mail: joan.girona@irta.es

Abstract. Multispectral and thermal imagery were studied to evaluate the relationship between grapevine water status and "Plant Cell Density" index (PCD) and "Crop Water Stress" index (CWSI). Grapevine water status was determined with a pressure chamber by measuring the leaf water potential (Ψ_{leaf}) of 184 grapevines distributed homogeneously within a 11 ha vineyard. Image acquisitions and Ψ_{leaf} measures were obtained simultaneously at noon. Results showed that PCD could be useful to discriminate well-watered zones in a vineyard. However the relationship between PCD *vs* Ψ_{leaf} seemed to vary between different zones of the vineyard. This inconvenient did not exist with CWSI. The relationship between Ψ_{leaf} and "crop-air temperature differential" was strong and presented a high coefficient of determination (r^2 = 0.714; P < 0.0001) at noon. Accordingly, this methodology showed potential to be used as a tool for irrigation scheduling. Further studies should be directed to explore the convenience of CWSI measured at other moments of the day and the optimal thermal image resolution to obtain the best results.

Keywords. *Multispectral imagery – Thermal imagery – Crop water stress index – Leaf water potential.*

L'utilisation des images multispectrales et thermiques comme outil pour la programmation de l'irrigation chez les vignobles

Résumé. *Des images multispectrales et thermiques ont été étudiées pour évaluer la relation entre l'état hydrique de la vigne et le "Plant Cell Density" index (PCD) et le "Crop Water Stress" index (CWSI). L'état hydrique de la vigne est déterminé en mesurant le potentiel hydrique de la feuille (Ψ_{leaf}) avec une chambre à pression. Sur une vigne de 11 ha on a étudié 184 plantes distribuées régulièrement dans l'espace. La prise des images et le potentiel hydrique ont été pris simultanément à midi. Les résultats ont indiqué que, bien que le PCD s'est montré utile pour discriminer les zones les plus favorables d'état hydrique, on a trouvé que la relation PCD vs Ψ_{leaf} peut varier d'une zone de la vigne à une autre. Par contre, cet inconvénient n'a pas apparu quand on a utilisé le CWSI. En effet, la relation entre Ψ_{leaf} et le différentiel de température entre l'air et la culture était très étroite et présentait un coefficient de détermination (r^2=0,714 ; P<0,0001) très élevé à midi. Or, cette méthodologie du CWSI a montré un grand potentiel pour être utilisé dans la programmation d'irrigation dans le vignoble. Afin d'obtenir les meilleurs résultats, les prochains travaux chercheront à identifier le meilleur moment de la journée pour calculer le CWSI et définir la résolution optimale des images thermiques.*

Mots-clés. *Images multispectrales – Images thermiques – Crop water stress index – Plant cell Density – Potentiel hydrique de la feuille.*

I – Introduction

Vineyards present a natural spatial variability. Different responses of grapevines are commonly found in different zones, and these can be explained by a number of parameters either physical (topography, soil properties, etc.) or management (pruning, training system, irrigation, fertilization, etc.). Thus, there exist a wide range of variation in yield and also in different berry composition parameters within-vineyard. One of the main priorities for wine grapegrowers, is to obtain uniform yields and batches of berry composition. Until now, this has been achieved by *zonal vine-*

yards management in which, individual blocks are split into zones of similar characteristics and managed and harvested differentially (Bramley and Hamilton, 2004a).

Many authors have shown the direct effect of grapevine water status on both yield and berry composition (Ojeda *et al.*, 2002; Girona *et al.*, 2009; Esteban *et al.*, 1999; Basile *et al.*, 2011). This general concept has led to the use of irrigation to help solving heterogeneity problems into blocks. Regulated Deficit Irrigation (RDI) is a technique that can improve berry composition parameters without affecting yield. However, an adequate management of RDI in each zone of the vineyard is not easy and has to be determined individually as a function of vine water status. In fact, speaking in terms of precision viticulture (PV), the ideal would be to apply the necessary water for each vine of the plot by knowing its water status. A good indicator for irrigation scheduling is the leaf water potential (Ψ_{leaf}) (Girona *et al.* 2006). However, this method presents the inconvenience that has to be measured manually with a pressure chamber in a reduced span of time at noon and thus it results impractical in large commercial blocks. This is the reason why other alternatives which could replace Ψ_{leaf} have to be investigated. Remote sensing technology for crop-management applications which has increased considerably during last years, can be a candidate to explore.

Multispectral images have been widely used for studying qualitative and quantitatively the vegetative status of different crops. Normalized Differences Vegetation Index (NDVI) or Plant Cell Density (PCD) can be obtained by combining mathematically different wavebands. Acevedo-Opazo (2008) used high resolution multi-spectral images to define different irrigation zones and to relate NDVI with plant water status.

On the other hand, thermal images are currently presented as a promising technology to derive plant water status. In fact, in 1970's Gates (1964) and Jackson *et al.* (1977) demonstrated that leaf temperature (T_{leaf}) could be used as plant water status indicator. Jackson *et al.* (1988) and Idso *et al.* (1981) obtained a normalized index denominated "Crop water stress" index (CWSI) to overcome the effects of other environmental parameters affecting the relation between stress and plant temperature.

Although there are a number of studies that have related CWSI or NDVI with plant water status, no study have found sound relationships between Ψ_{leaf} and either vegetative indices or temperature within the whole block. The objective of this study was to evaluate both methods (multispectral and thermal imagery) as an indicator of Ψ_{leaf}.

II – Materials and methods

A case study was carried out on a 16-years old `Pinot noir´ wine grape (*Vitis vinifera* L.). The 11-ha commercial vineyard was located at 41º39'58"N, 00º30'10"E (WGS84, UTM zone 31N) in Raïmat, Lleida, Catalonia, Spain.

In 2008, four flights were done with a four waveband multispectral camera (DMS2C-2K System) corresponding to the infra-red, red, green and blue wavelengths. The camera image resolution was 2048 x 2048 pixels with 14-bit digitization and optical focal length of 24-28 mm, yielding a ground-based spatial resolution of 50 cm at 1 km altitude. Flights were done by the company RS Teledetección by using a light aircraft (CESSNA C172S EC-JYN). The ratiobased vegetation index PCD was obtained according to Equation 1:

$$PCD = \frac{\varphi_{NIR}}{\varphi_{RED}} \quad (1)$$

where φ_{NIR} and φ_{RED} are spectral reflectance measurements acquired in the near-infrared (760-900 nm) and red (630-690 nm), respectively.

Therefore, in 2009 a thermal image was acquired the 31st july at noon, with a thermal sensor Miracle 307 KS (Thermoteknix Systems, UT) installed on board an unmanned aerial vehicle (UAV) (Quantalab, IAS-CSIC Córdoba, Spain). Image resolution was 640 x 480 pixels and spectral response in the range 7.5-13 µm. The camera was equipped with 45º FOV lens, yielding 30-40 cm spatial resolution at 150 m altitude.

During all 2009 season, four infrared temperature (IRT) sensors (model PC151HT-4; Pyrocouple, Calex Electronics) were placed 1 m above the grapevines with different irrigation treatments (well-watered and stressed) (Sepulcre-Canto *et al.*, 2006), recording mean leaf temperature every 5-min with a datalogger (model CR200X,Campbell Scientific, Logan, UT). This data was used to calculate the CWSI as follows:

$$CWSI = \frac{(T_c - T_a) - (T_c - T_a)_{LL}}{(T_c - T_a)_{UL} - (T_c - T_a)_{LL}} \quad (2)$$

where (Tc-Ta) is the difference between canopy and air temperature, $(T_c\text{-}T_a)_{LL}$ is the expected lower limit of $(T_c\text{-}T_a)$ in the case of a canopy which is transpiring at the potential rate, and $(T_c\text{-}T_a)_{UL}$ expected differential in the case of a non-transpiring canopy. The lower and upper limits of Tc-Ta were obtained following the methodology of Idso *et al.* (1981).

1. Leaf water potential (Ψ_{leaf}) measurements

At the same time of the images acquisitions, 184 Ψ_{leaf} were measured in a regular grid around the vineyard. Determinations of Ψ_{leaf} were performed with a pressure chamber (Scholander *et al.*, 1965) (Soil Moisture plant water status console 3005 Corp. Sta. Barbara, CA, USA) following the recommendations of Turner and Long (1980). All measurements were done at noon (less than 1 hour) selecting one wee-lit leaf.

2. Image processing

Thermal imagery acquisition and geometric, radiometric and atmospheric corrections were processed by Quantalab, IAS-CSIC of Córdoba. The methodology for obtaining surface temperature by removing atmospheric effects using a single-channel atmospheric correction is explained in Berni *et al.* (2009). Pixel data from each measured vine was extracted and averaged avoiding obtaining pure soil pixels. Analysis for multispectral images was carried out in ArcMap (version 9.3; ESRI Inc. Redlands, CA, USA) using the Spatial Analyst extension. On the other hand, thermal images were processed with ENVI 4.7 (ITT Visual Information Solutions, 2009).

III – Results and discussion

1. Multispectral images

Table 1 showed a high variability of vine water status within-vineyard which increased along the season. The most stressed grapevines were found in the last day of measurement (beginning August), reaching minimum values of -1.4 MPa. A previous study carried out in this same plot, indicated that spatial heterogeneity of grapevine water status was stable and followed very similar patterns over the time. It also demonstrated that the more stressed grapevines were localized in zones with shallower soils and with less soil water holding capacity.

Similarly to Ψ_{leaf}, PCD index also presented high variability within-vineyard, although this variability remained stable along the season. The highest differences between maximum and minimum PCD values were found at the end of the vegetative growing period (end July). This was

Table 1. Descriptive statistical analysis and relationships between leaf water potential (Ψ_{leaf}) and plant cell density (PCD) index measurements in a vineyard of 11 hectares in Raïmat (Lleida, Spain). Significant differences among Ψ_{leaf} and PCD based on Duncan's test at P < 0.05

2008	Average	Stand. Desv.	Min.	Max.	C_v
Ψ_{leaf}					
Day 1	-0.81	0.15	-1.15	-0.48	19.01
Day 2	-0.69	0.12	-1.08	-0.45	17.25
Day 3	-0.62	0.11	-0.94	-0.41	17.69
Day 4	-0.79	0.20	-1.42	-0.44	25.63
PCD					
Day 1	130.50	43.09	44.50	229.18	33.02
Day 2	129.15	43.08	48.58	216.54	33.36
Day 3	126.93	46.81	33.37	222.97	36.87
Day 4	120.96	39.41	44.56	213.59	32.58
	Day 1	**Day 2**	**Day 3**	**Day 4**	
r^2	0.215	0.105	0.196	0.046	
Pr>F	<.0001	<.0001	<.0001	n.s	

explained because at that moment, the most stressed vines throughout the season had less vigour than fully irrigated grapevines. Visually, from maps as showed in Fig. 1, it seemed that there was a relationship between both analyzed parameters, except for the fourth day. However, statistical analysis did not indicate this perception.

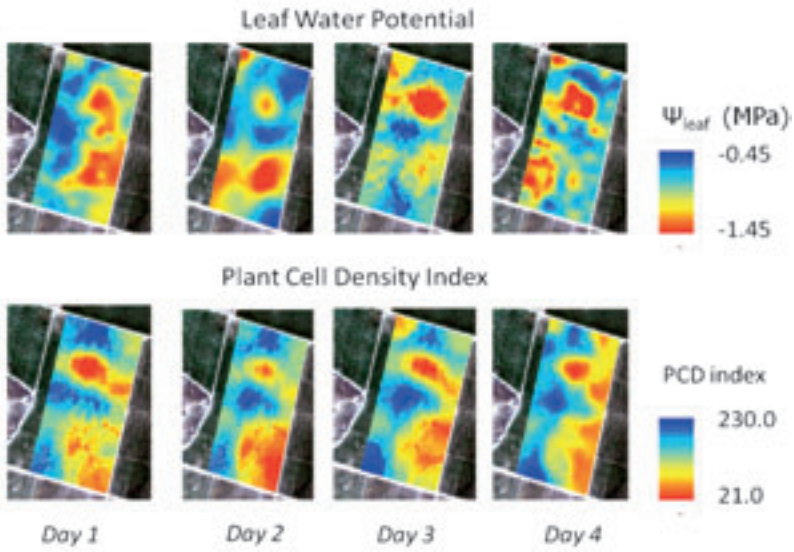

Fig. 1. Leaf water potential (Ψ_{leaf}) measured with pressure chamber and plant cell density (PCD) maps obtained in four different days during 2008.

Relationships were slightly low in all cases, although significant (P<0.0001), with the exception of the 4th day which presented a non-significant relationship (Table 1). This was explained due to grapevine pruning management. It is well-known that these vegetative indices obtained from air-

borne multispectral imagery are very sensitive to crop cultural practices (Bramley *et al.*, 2011). For instance, in our studied block, a mechanical pruning was made in half part of the block two days before of the 4th image acquisition. Then, PCD values were considerably reduced in that zone due to the lower reflected near infrared by leaves because of less canopy vigor. On the other hand, an improvement of grapevine water status was achieved in that zone, obtaining maximum values of Ψ_{leaf} of -0.44 MPa.

Results of this study demonstrated that structural vegetative indexes are not always related to plant water status indicators because they are mainly giving information about the canopy size. Well-watered grapevines along the season will be more vigorous, but is also possible that vines with higher vigour may have increased transpiration, and consequently this would lead to lower Ψ_{leaf} due to increased water loss though transpiration (Rossouw, 2010). Then, these indices demonstrated to be highly stable in detecting water stress variations on time but also very sensitive to the intersection of cultural practices and pathogen effects.

2. Thermal images

In 2009, vine water status variability was slightly high at moment that Ψ_{leaf} were measured. Spatial distribution of vine water status was shown in the two maps of Fig. 2. Coefficient of variation (C_v) was 20.97, ranging from -0.6 MPa to -1.7 MPa. High image resolution was showed in the thermal mosaic, where was possible to distinguish pure crown temperature pixel from grapevines and soil pixels. Visually, it seems clear the relationship between both parameters. Blue color zones of Ψ_{leaf} map represented zones with well-watered grapevines, which in theory had a higher stomatal conductance and a major transpiration which is directly affected by lower leaf temperatures. On the other hand, more stressed grapevines (represented in red color), depending on the variety, close the stomata to avoid water losses and consequently, T_{leaf} increases.

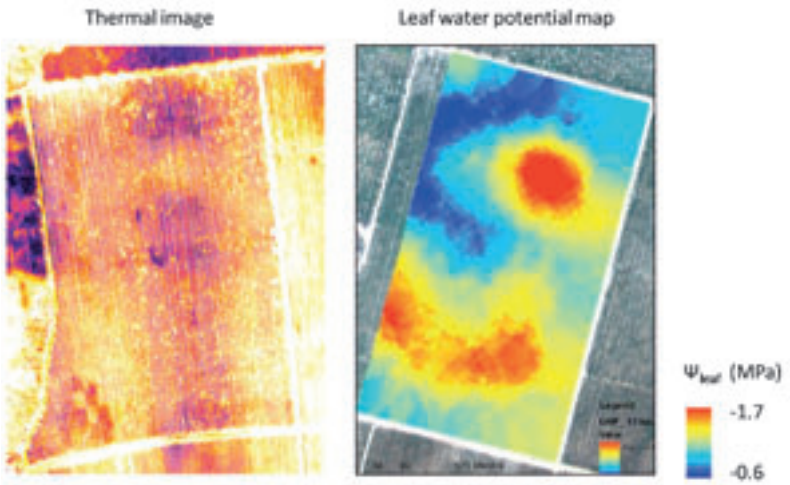

Fig. 2. Thermal mosaic from the overlapping of thermal images obtained from an UAV at noon. Leaf water potential (Ψ_{leaf}) map measured at noon.

Relationship between Ψ_{leaf} and crop-air temperature differential in the whole block presented a high significant degree of determination (r^2 = 0.714, P < 0.0001) at noon. According to the most recent literature [Grimes and Williams (1990); Peacock *et al.* (1998); Choné *et al.* (2001); Williams

and Araujo (2002) and Girona *et al.* (2006)], a reasonable threshold of Ψ_{leaf} for well-irrigated grapevines would be around -0.8 MPa, -1.2 MPa for moderately stressed vines, and -1.5 MPa for severe stress conditions. Then, maximum differences of (Tc-Ta) which reached until 8ºC, corresponded with the most stressed grapevines within the block, which presented Ψ_{leaf} values around -1.6 MPa. On the other hand, small differences of (Tc-Ta) corresponded with well-watered grapevines. Bearing in mind that moderately stressed grapevines starts with Ψ_{leaf} values below -1.2 MPa, results indicated that grapevine stress starts when (Tc-Ta) values are above 3ºC.

CWSI equation was obtained from IRT sensors data. Thus, relationship between CWSI and Ψ_{leaf} measurements in the whole block showed that well-watered grapevines corresponded with CWSI values below 0.5, whereas the most stressed grapevines of the block, reached until values around 1.0.

IV – Conclusions

In the present study it was demonstrated the viability of high resolution thermal imagery for detecting the level of water stress in grapevines. Further studies will be performed to develop applications useful to improve irrigation efficiency at parcel scale. However, this work showed the feasibility of this tool only at noon. In future studies we will investigate the time-window of the day in which relationships between CWSI and Ψ_{leaf} would be useful.

References

Acevedo-Opazo C., Tisseyre B., Guillaume S. and Ojeda H., 2008. The potential of high spatial resolution information to define within-vineyard zones related to vine water status. In: *Precision Agriculture*, 9, p. 285-302.

Basile B., Marsal J., Mata M., Vallverdú X., Bellvert J. and Girona J., 2011. Phenological sensitivity of Cabernet Sauvignon to water stress: vine physiology and berry composition. In: *American Journal of Enology and Viticulture*. AJEV-D-11-00003R1 (in-press).

Berni J.J., Zarco-Tejada JP., Suárez L. and Fereres E., 2009. Thermal and narrowband multispectral remote sensing for vegetation monitoring from an unmanned aerial vehicle. In: *IEEE Transactions on geosciences and remote sensing*, 47, p. 3.

Bramley R.G.V. and Hamilton R.P., 2004. Understanding variability in winegrape production systems. 2. Within vineyard variation in yield over several vintages. In: *Australian Journal of Grape and Wine Research*, 10, p. 32-45.

Bramley R.G.V., Trought MCT. and Praat J-P., 2011. Vineyard variability in Malborough, New Zealand: characterizing variation in vineyard performance and options for the implementation of precision viticulture. In: *Australian Journal of Grape and Wine Research*, 17, p. 72-78.

Choné X., van Leeuwen C., Dubourdieu D. and Guadillère J.P., 2001. Stem wáter potential is a sensitive indicator of grapevine wáter status. In: *Ann. Bot.*, 87, p. 477-483.

Esteban M.A., Villanueva M.J. and Lissarrague J.R., 1999. Effect of irrigation on changes in berry composition of Tempranillo during maduration: Sugars, organic acids, and mineral elements. In: *American Journal of Enology and Viticulture*, 57, p. 257-268.

Gates D., 1964. Leaf temperature and transpiration. In: *Agron. J.*, 56, p. 273-277.

Girona J., Mata M., del Campo., Arbonés A., Bartra E. and Marsal J., 2006. The use of midday leaf water potential for scheduling déficit irrigation in vineyards. In: *Irrigation Science*, 24, p. 115-127.

Girona J., Marsal J., Mata M., del Campo. and Basile B., 2009. Phenological sensitivity of berry growth and quality of 'Tempranillo' grapevines (*Vitis vinífera* L.) to water stress. In: *Australian Journal of Grape and Wine Research*, 15, p. 268-277.

Grimes D.W. and Williams L.E., 1990. Irrigation effects on plant water relations and productivity of 'Thompson Seedless' grapevines. In: *Crop Sci.*, 30, p. 255-260.

Idso S.B. 1981. Non-water-stressed baselines – A key to measuring and interpreting plant water-stress. In: *Agr. Meteorol.*, 27, p. 59-70.

Jackson R.D., Reginato R.J. and Idso S.B., 1977. Wheat canopy temperature – Practical tool for evaluating water requirements. In: *Water. Resour. Res.*, 13, p. 651-656.

Jackson R.D., Idso S.B., Reginato R.J. and Printer P.J., 1988. Canopy temperature as a crop water-stress indicator. In: *Water Resour. Res.*, 17, p. 1133-1138.

Ojeda H., Andary C., Kraeva E., Carbonneau A. and Deloire A., 2002. Influence of pre- and postveraison water deficit on synthesis and concentration of skin phenolic compounds during berry growth of *Vitis vinifera* cv. Shiraz. In: *American Journal of Enology and Viticulture*, 53, p. 261-267.

Peacock B., Williams L.E. and Christensen P., 1998. Water management irrigation scheduling. University of California. Cooperative Extension, Pub.

Rossouw G.C., 2010. The effect of within-vineyard variability in vigour and water status on carbon discrimination in *Vitis vinifera* L. cv Merlot. Thesis at Stellenbosch University, department of viticulture and oenology, Faculty of AgriSciences.

Scholander P.F., Hammel H.T., Bradstreet E.D. and Hemmingsen E.A., 1965. Sap pressure in vascular plants. In: *Science*, 148, p. 339-346.

Sepulcre-Canto G., Zarco-Tejada P.J., Jiménez-Muñoz J.C., Sobrino J.A., de Miguel E. and Villalobos F.J., 2006. Detection of water stress in a olive orchard with thermal remote sensing imagery. In: *Agric. For. Meteorol.*, 136, p. 31-44.

Turner N.N. and Long M.J., 1980. Errors arising from rapid water loss in the measurement of leaf water potential by pressure chamber technique. In: *Austr. J. Plant. Physiol.*, 7, p. 527-537.

Williams L.E. and Araujo F.J., 2002. Correlations among predawn leaf, midday leaf and midday stem water potential and their correlations with other measures of soil and plant water status in *Vitis vinifera*. In: *J. Am. Soc. Hort. Sci.*, 127 (3), p. 448-454.

Study of the effects of irrigation on stem water potential and multispectral data obtained from remote sensing systems in woody crops

J.J. Alarcón* and P. Pérez-Cutillas**

*Centro de Edafología y Biología Aplicada del Segura (CEBAS-CSIC),
Campus Universitario de Espinardo, 30100 Murcia (Spain)
**Instituto Murciano de Investigación y Desarrollo Agrario y Alimentario (IMIDA),
C/ Mayor s/n, La Alberca, 30150 Murcia (Spain)

Abstract. This study is part of the work carried out in experimental plots of different research centres (IMIDA, CEBAS, UPCT and IVIA) that are part of the TELERIEG project, with the aim of improving irrigation methods in irrigated crops in the region of Murcia, significantly contributing to a better management of drought. The work was carried out, on the one hand, on two parcels of citrus fruit (mandarin and grapefruit) where several different irrigation treatments were applied, which generated varying degrees of water stress on the studied trees. Three sources of irrigation water were also used, each one different in nature and quality, in order to study their impact on the development of crops. On the other hand, work was also carried out on a parcel of peach trees, where several different irrigation treatments were applied, which also generated varying degrees of water stress. This variability in tree water status was measured in the field through stem water potential at midday (Ψs), and from the air by capturing images with a multispectral camera to estimate the values of the near-infrared spectrum (NIR) and the normalized difference vegetation index (NDVI).

Keywords. Precision agriculture – Remote sensing – Drought – Water relations – Reclaimed water irrigation.

Étude des effets de l'irrigation sur le potentiel hydrique de la tige et sur les données multispectrales obtenues par télédétection dans des cultures ligneuses

Résumé. *Cette étude s'inscrit dans le cadre des recherches effectuées dans des parcelles expérimentales de différents centres de recherche (IMIDA, CEBAS, UPCT et IVIA) participant au projet TELERIEG, dont l'objectif est l'amélioration des méthodes d'irrigation des cultures irriguées dans la région de Murcie, contribuant ainsi de façon significative à la gestion de la sécheresse. Les travaux ont été réalisés, d'une part, sur deux parcelles d'agrumes (mandarine et pamplemousse) où plusieurs traitements différents d'irrigation ont été appliqués, ce qui a généré des degrés variables de déficit hydrique sur les arbres étudiés. On a également utilisé trois sources d'eau d'irrigation de nature et qualité différentes, afin d'étudier leurs effets sur le développement des cultures. Les travaux ont été aussi conduits sur une parcelle de pêchers où plusieurs traitements différents d'irrigation ont été appliqués, ce qui a généré des degrés variables de déficit hydrique sur les arbres étudiés. Cette variabilité de l'état hydrique des d'arbres a été mesurée sur le terrain à l'aide du potentiel hydrique des tiges à midi (Ψs), et à distane au moyen d'images capturées avec une caméra multispectrale, qui ont permis d'estimer les valeurs du spectre dans le proche infrarouge (NIR) et l'indice de végétation par différence normalisée (NDVI).*

Mots-clés. *Agriculture de précision – Télédétection – Sécheresse – Relations hydriques – Irrigation avec des eaux recyclées.*

I – Introduction

Agriculture has always been influenced by various climatic elements. Among them, drought is one of those which affect more negatively the production and the quality of agricultural products, especially in South-East Spain, which is characterized by semi-arid climate. Therefore, the short-

age of water for agriculture in this highly productive area periodically causes high losses that strongly affect the economy. This has led in the last decade to a major boom in the purification and reuse of reclaimed water in the Region of Murcia, a fact that highlights the importance of researching on the interaction of these low-quality waters with strategies of regulated deficit irrigation (RDI), especially in areas as South-East Spain, where water scarcity is a major issue. In recent years there has been a rapid development in terrestrial remote sensing systems, with the emergence of new sensors offering better performances, which has helped to improve research on the coverage of the Earth's surface. In the agricultural sector, these tools have contributed to the advancement of precision farming, improving the agricultural aspects, reducing the environmental impacts associated with agricultural activities and optimizing production costs.

Based on these criteria, several studies have been conducted to evaluate the effects of regulated deficit irrigation in fruit trees. One of them has been based on the effect of water of different qualities on stem water potential in citrus; another one has characterized the physiological state of peach trees. In both cases the field values have been correlated with the evolution of some parameters obtained through terrestrial remote sensing systems, i.e. high-resolution images with near-infrared data.

II – Material and methods

The trials were conducted in the summer of 2009: the first one in two commercial farms located in Molina de Segura (Murcia, Spain) and the second one in a commercial farm located in Fuente Librilla, Mula (Murcia, Spain). All these plots have been under study within the Telerieg project (SUDOE programme), along with other trials that have been carried out in different experimental plots with various fruit trees and different treatments (Fig. 1).

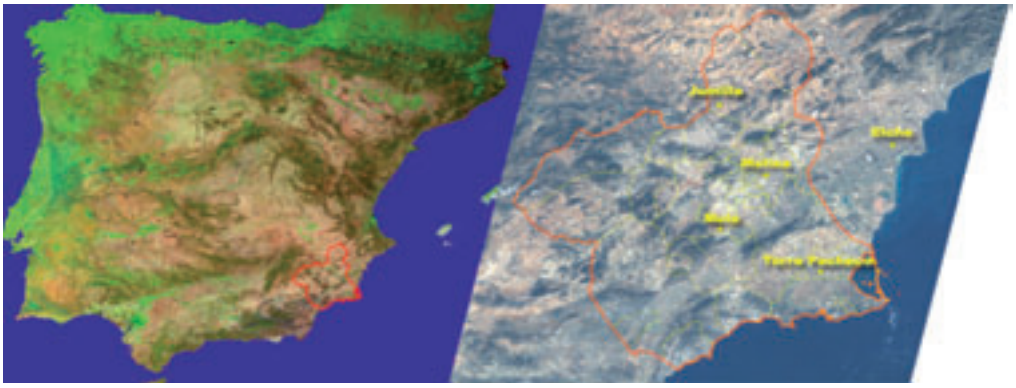

Fig. 1. Experimental plots under study within the Telerieg SUDOE project.

1. Study plots

The study on reclaimed water, conducted in Molina de Segura, was performed on two plots with different crops: a 4 years old grapefruit (cv. Star Ruby) grafted on macrophylla (Fig. 2) and a 7 years old mandarin (cv. Orogrande) grafted on Citrange carrizo (Fig. 3).

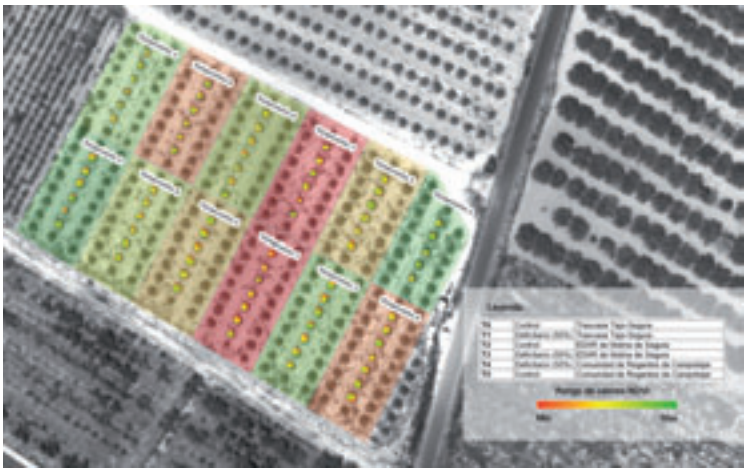

Fig. 2. Irrigation treatments on a grapefruit plot in Campotejar (Molina de Segura, Spain).

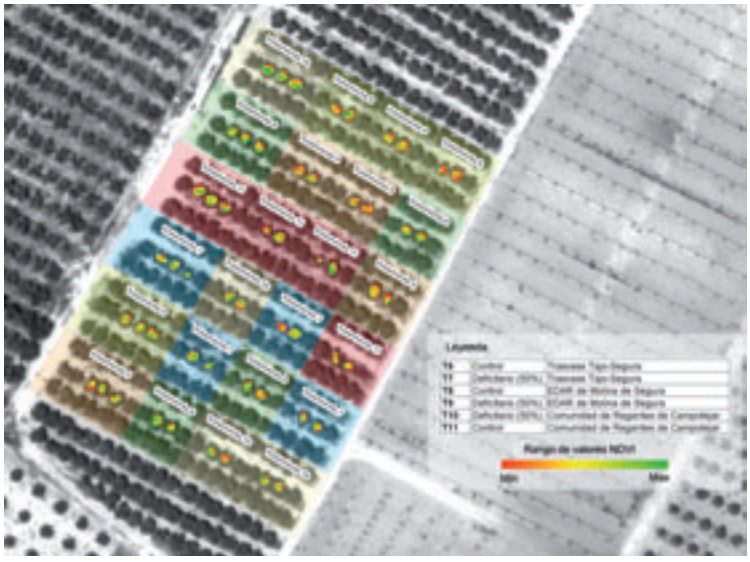

Fig. 3. Irrigation treatments on a mandarin plot in Campotejar (Molina de Segura, Spain).

Three sources of irrigation water were used: the first, from the Tajo-Segura Aqueduct, had a good agronomic quality; the second, from the WWTP of Molina de Segura, was mainly characterized by its high salinity; the third, from the Irrigation Community of Campotejar, was a blend of well water and purified wastewater used in different proportions depending on the availability of each one of them (Figs 2 and 3). Throughout the production cycle, the average value of the electrical conductivity (EC) of the different sources of water was of 1.2, 3.4 and 2.5 dS/m for aqueduct water, wastewater and community water, respectively.

Drip irrigation was used, with a single irrigation line for each row of trees and three emitters per plant, which had a rate of 4 $l \cdot h^{-1}$. There were two irrigation treatments for each quality of water: a control where watering met crop requirements (100% ETc) and a RDI treatment where the volume of water was reduced to 50%, compared to the control treatment, during the second phase of fruit growth (from late June to mid-August).

Regarding the Fuente Librilla plot, the trial was conducted on adult peach trees (*Prunus persica* L. cv. Catherine) grafted on GF677, with a 6 × 4 m planting pattern. Drip irrigation was used, with a single irrigation line for each row of trees and five emitters per plant, which had a rate of 4 l·h-1.

The experimental plot was divided equally into five irrigation treatments: a control (C), which was watered to meet crop water requirements (100% ETc) and four RDI treatments were watering was reduced respectively 70%, 60%, 50%, and 40% compared to the control treatment. The RDI period went from May 5 to June 10, 2009. To perform the trial, 21 trees randomly distributed among the different irrigation treatments were monitored (Fig. 4).

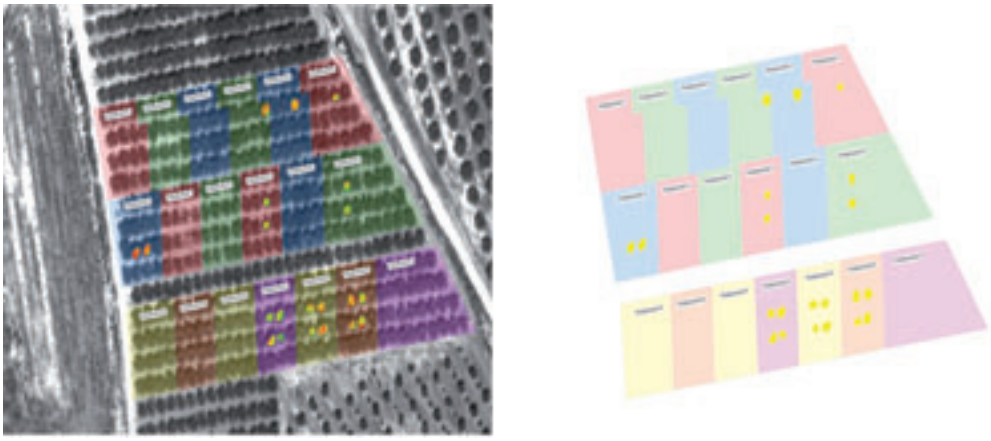

Fig. 4. Distribution of treatments and monitored trees in the experimental plot (commercial farm located in Fuente Librilla, Mula, Spain). Experimental design and aerial view.

2. Measured parameters

Both trials studied the effects of irrigation treatments on the water status of trees, aiming to establish correlations between physiological variables obtained in the field (stem water potential) and data from a series of high-resolution near-infrared images obtained through remote sensing systems.

Water status in field was determined by measuring the stem water potential at midday (Ψs) in healthy adult leaves close to the trunk, following the technique described by Scholander *et al.* (1965) and Turner (1988). A pressure chamber (Soil Moisture Equip. Corp., 3000 model, Santa Barbara CA, USA) was used as described by Hsiao (1990).

To obtain remote sensing imagery, a multispectral camera (ADS40) carried in an aircraft type Partenavia P68C was used. The resulting images had a spatial resolution of 35 cm per pixel and radiometric resolution of 16-bit sensor. The flight took place on August 14, 2009, coinciding with the field data collection.

The images from different plots were comprehensively analysed with GIS tools for obtaining infrared data. Monitored trees were mapped in the image by means of their coordinates, taken in the field with a GPS. Then, the perimeter of all crops was digitized to generate a cutting "mask" to extract data from images, but this was done after removing all outer pixels in order to minimize edge effect and leave out of the analysis the "noise" that could be produced by the "soil line" (Lychak *et al.,* 2000), i.e. values or information that do not correspond strictly to those we are looking for in the trees under study. Once these "mask" elements are better defined, we started the process of extracting data from the infrared (IR) spectrum of the captured images. This is how we obtained an index of normalized difference vegetation index (NDVI), a well-known and reliable index, backed up by numerous studies, that informs about the state of vegetation (Crippen, 1990).

Correlations between the different irrigation treatments and the various parameters measured were done through a series of statistical analysis based on the use of SPSS and R software applications.

III – Results and discussion

1. Mandarin trees

The results show that regulated deficit irrigation affected the stem water potential (Ψs) of mandarin trees, the control trees always showing higher values than those subjected to water deficit. Using the Mann–Whitney U test to compare the results obtained with different watering treatments in mandarin (control and RDI), we observed that Ψs was the only variable significantly affected by the volume of water supplied (U=2.5 p=0.001) (Table 1).

Table 1. Mann-Whitney U test for different watering treatments (control and deficit irrigation) on mandarin trees

	Ψ_s	NIR	NDVI
Mann-Whitney U	2.500	37.000	40.000
Asymp. Sig. (2-tailed)	0.001	0.757	0.965

Using the Kruskal-Wallis test, it was observed that the NDVI showed significant variations depending on the quality of water used in the different treatments. This test was supplemented later by a new one (NPar test; Field, 2009), which allowed us to find pair relationships. As a result of this analysis, no significant differences were observed in the NDVI between trees irrigated with water of good quality (Tajo-Segura Aqueduct) and water of intermediate quality (Irrigation Community) (Table 2). However, significant differences in NDVI were found between trees irrigated with water from the aqueduct and from the WWTP (Table 3). Finally, there were also significant differences in the NDVI between trees irrigated with low-quality water (WWTP) and those irrigated with water of intermediate quality (Irrigation community) (Table 4).

Table 2. Mann-Whitney U test for different water sources (Tajo-Segura Aqueduct and Irrigation Community) on mandarin trees

	Ψ_s	NIR	NDVI
Mann-Whitney U	10.000	5.500	13.000
Asymp. Sig. (2-tailed)	0.195	0.045	0.423

Table 3. Mann-Whitney U test for different water sources (Tajo-Segura Aqueduct and WWTP) on mandarin trees

	ψ_s	NIR	NDVI
Mann-Whitney U	12.500	10.000	4.000
Asymp. Sig. (2-tailed)	0.375	0.200	0.025

Table 4. Mann-Whitney U test for different water sources (Irrigation Community and WWTP) on mandarin trees

	ψ_s	NIR	NDVI
Mann-Whitney U	15.000	9.000	5.000
Asymp. Sig. (2-tailed)	0.626	0.150	0.037

2. Grapefruit trees

Deficit irrigation treatments on grapefruit trees generated, as was the case in mandarin trees, significant differences in stem water potential, Ψs values in control treatments being higher compared to deficit treatments. Also, just like it was observed on mandarin trees, grapefruit trees irrigated with water of different quality showed significant differences in one of the studied variables, near-infrared (NIR) in this case.

To validate this information, we used the Shapiro-Wilk and Levene test, which showed that different quantities and qualities of water affected the dependent variables Ψs, NIR and NDVI (Table 5).

Table 5. Mann-Whitney U test for different water treatments (control and deficit irrigation) and water sources (Tajo-Segura Aqueduct, Irrigation Community and WWTP) on grapefruit trees

	Variable	Sum of Squares	df	Mean Square	F	Sig.
Quantity of water	ψ_s	35.042	1	35.042	34.800	0.000
	NIR	21420.375	1	21420.375	0.333	0.571
	NDVI	1137663630.042	1	1137663630.042	2.392	0.139
Quality of water	ψ_s	5.396	2	2.698	2.679	0.096
	NIR	457534.750	2	228767.375	3.559	0.050
	NDVI	1776264131.396	2	888132065.698	1.867	0.183

The results in Table 5 clearly show that the quantitative treatments had a significant impact on Ψs ($F=34.800$; $p<0.00$), while qualitative treatments significantly affected the NIR variable ($F=3559$; $p=0.05$). Finally, the interaction effect, i.e. the combined effect of quantity and quality of water was not significant for any of the variables considered.

As it was done in mandarin trees, the effect of water quality was analysed statistically considering differences between pairs, and thus it was observed that the NIR was significantly different between grapefruit trees irrigated with water from the Tajo-Segura Aqueduct (good quality) and those irrigated with water from the WWTP and the Irrigation Community (intermediate and low quality respectively), but did not differ between trees irrigated with community or WWTP water (Fig. 1).

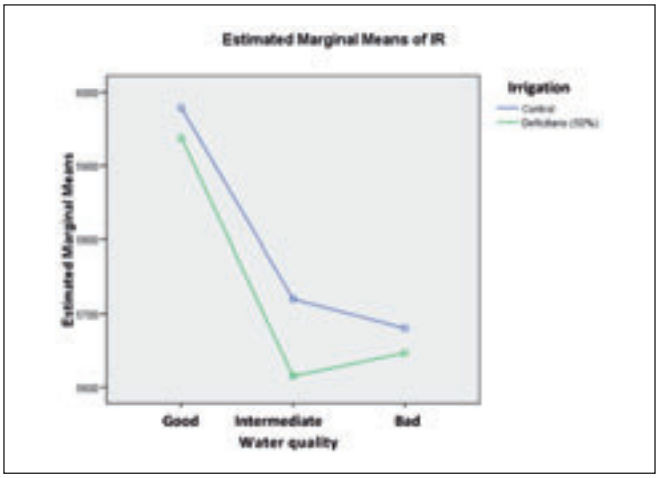

Fig. 1. Degree of discrimination between NIR values, considering the quantity of water and its quality, on grapefruit trees.

3. Peach trees

In the trial carried out on peach trees it could be observed, as shown by the Mann-Whitney test, that there were significant differences between different irrigation treatments for values of stem water potential (Ψs), near-infrared (NIR) and normalized difference index (NDVI) (Table 6).

Table 6. Results of Mann-Whitney test

	ψ_s	NIR	NDVI
Mann-Whitney U	0.0	12.0	13.0
Wilcoxon W	66.0	67.0	68.0
Z	3.87	3.02	0.95
Asymp. Sig. (2-tailed)	0.000	0.002	0.003
Exact Sig. (2-tailed)	0.000	0.002	0.002
Exact Sig. (1-tailed)	0.000	0.001	0.001
Point probability	0.000	0.000	0.000

Table 7. Table of correlations between various parameters

	ψ_s	NIR	NDVI	
ψs	Pearson Corr.	1	0.610††	0.746†
	Signif.		0.003	0.000
	N	21	21	21
NIR	Pearson Corr.	0.610†	1	0.752†
	Signif.	0.003		0.000
	N	21	21	21
NDVI	Pearson Corr.	0.746†	0.752††	1
	Signif.	0.000	0.000	
	N	21	21	21

† Correlation is significant at 0.01 (bilateral).

An average (r=0.61) significant correlation was found between Ψs and NIR, and a strong one (r=0.74) between Ψs and NVDI. There was also a high correlation between NIR and NDVI (r=0.75), but this was expected, since both variables are based on near-infrared data.

IV – Conclusions

It should be noted that both the values of stem water potential and the remote sensing parameters used in our study on citrus trees give us complementary information about the behaviour of trees under different irrigation treatments. Deficit irrigation led to temporary and limited changes in the water status of the trees that were shown by the decrease of stem water potential at the time of sampling. However, using water of different quality over a long period of time produced significant changes in multispectral data (NIR) recorded in trees.

As for the peach study, we conclude that the three considered indices (Ψs, NIR, NDVI) were sensitive to the degree of water deficit generated in the trees. These indices showed significant correlation values when compared two-by-two. The best correlation was found between the two parameters obtained from multispectral data analysis (NIR and NDVI), whereas stem water potential (Ψs) presented a better correlation with NVDI than with NIR.

References

Field A., 2009. *Discovering Statistics Using SPSS (Introducing Statistical Methods S.).* Sage Publications Ltd.

Crippen R.E., 1990. Calculating the Vegetation Index Faster. In: *Remote Sensing of Environment,* vol. 34, p. 71-73.

Lychak O. and Jaremy M., 2000. Influence of possible ways of remote sensing data and digital data nonlinear transformation on the results of unsupervised classification. In: *Conference on Applications of Digital Image Processing XXIII.* San Diego, EE.UU.

Hsiao T.C., 1990. Measurements of plants water status. In: Irrigation of Agricultural Crops (Stewart, B.A., Nielsen, D.R., eds.). In: *Agronomy Monograph* no. 30, pp: 243-279. Published by ASA, CSSA and SSSA, Madison, Wisconsin, USA.

Use of remote sensing and geographic information tools for irrigation management of citrus trees

M.Á. Jiménez-Bello*, L.Á. Ruiz, T. Hermosilla**, J. Recio** and D.S. Intrigliolo***

*Instituto Valenciano Investigaciones Agrarias, Ctra Moncada-Náquera km 4.500,
P.O. Box 46113 Moncada, Valencia (Spain)
**geo-Environmental Cartography and Remote Sensing Group. Universitat Politècnica de València,
Camino de vera s/n 46022 Valencia (Spain)

Abstract. The most widely used method for estimating crops water requirements is the FAO approach, which takes into account: (i) climatic variables included in the reference evapotranspiration and (ii) the crop type, characterized by the crop coefficient (Kc). In citrus trees, Kc is mostly function of the tree ground covers (GC). In large areas tree ground covers (GC) can be estimated by means of remote sensing tools, and once tree water needs are calculated, this information can be implemented in geographic information systems. The present article summarizes some of the research conducted in order to estimate citrus water needs in large irrigated areas. It describes first how tree ground covers (GC) can be obtained by using image analysis tools applied to multispectral images. Tree water needs are obtained and they are compared with the real water applications for a case study of citrus water use associations. The results obtained allowed to conclude that the tools developed might be useful for improving irrigation efficiency showing some of the deficiencies currently found in irrigation management of collective water networks.

Keywords. Crop coefficient – Ground cover – Image analysis – High-resolution remote sensing.

Utilisation des outils de télédétection et d'information géographique pour la gestion de l'irrigation en vergers d'agrumes

Résumé. *La méthode la plus largement utilisée pour estimer les besoins en eau des cultures est l'approche de la FAO, qui tient compte : (i) des variables climatiques incluses dans l'évapotranspiration de référence et (ii) du type de culture, caractérisé par le coefficient de la culture (Kc). Chez les agrumes, Kc est principalement fonction de la couverture végétale au sol (GC). Sur de vastes étendues, la couverture végétale au sol (GC) peut être estimée par des outils de télédétection, et après avoir calculé les besoins en eau des arbres, cette information peut être mise en place dans des systèmes d'information géographique. Le présent article résume certains des travaux de recherche menés afin d'estimer les besoins en eau des agrumes dans de vastes zones irriguées. D'abord il est décrit comment calculer la couverture végétale du sol (GC) en appliquant des outils d'analyse d'image aux images multispectrales. Les besoins en eau des arbres sont obtenus et comparés aux irrigations réelles pour une étude de cas concernant l'utilisation de l'eau par les associations de cultivateurs d'agrumes. Les résultats obtenus ont permis de conclure que les outils développés pourraient être d'utilité pour améliorer l'efficience d'irrigation car ils montrent certaines des lacunes rencontrées actuellement en matière de gestion de l'irrigation dans les réseaux d'eau collectifs.*

Mots-clés. *Coefficient de culture – Couvert du sol – Analyse d'images – Télédétection à haute résolution.*

I – Introduction

Irrigated agriculture has a noticeable importance with more than 45% of the total agriculture production in the world (Molden, 2007). Water demand has been steadily increasing during the last years and future forecasts indicate that water scarcity will become a major problem in many areas of the world (Fereres and González-Dugo, 2009). It is then very important to achieve optimum effi-

ciency in irrigation applications both on and off farm. It is striking that despite much effort has been done in order to improve efficiency of water distribution along the whole chain, less attention has been paid in terms of irrigation efficiency at the farm level. In this sense, the first crucial step is to perform irrigation application in order to match as much as possible the plant water needs.

The most widely used method for estimating crops water requirement is the FAO approach (Allen *et al.*, 1998), which takes into account: (i) climatic variables included in the reference evapotranspiration (ETo), and (ii) the crop type, characterized by the crop coefficient (Kc). The crop evapotranspiration (ETc), which is the sum of the plant transpiration (T) and soil evaporation (E), is then calculated as ETo by the Kc. The ETo is an estimation of atmosphere evaporation defined as the evapotranspiration rate from a reference surface. Owing to the difficulty of obtaining accurate field measurements, ETo is commonly computed from weather data. The principal weather parameters affecting ETo are radiation, air temperature and humidity and wind speed. Nowadays the FAO Penman-Monteith equation is the standard method for the definition and computation ETo (Allen *et al.*, 1998). With this model the ETo (mm/day) is obtained as

$$ETo(mm/day) = (0.408\Delta(R_n\text{-}G)+\gamma(900/T+273)U_2(e_s\text{-}e_a))/(\Delta+\gamma(1+0.34U_2))$$

where ET_o reference evapotranspiration [mm day^{-1}], R_n net radiation at the crop surface (MJ m^{-2} day^{-1}), G soil heat flux density (MJ m^{-2} day^{-1}), T mean daily air temperature at 2 m height (°C), u_2 wind speed at 2 m height (m s^{-1}), e_s saturation vapour pressure (kPa), e_a actual vapour pressure (kPa), e_s - e_a saturation vapour pressure deficit (kPa), Δ slope vapour pressure curve (kPa $°C^{-1}$), γ psychrometric constant (kPa $°C^{-1}$).

The other variable used for computing the ETc, the Kc takes into account those characteristics that differentiate each crop from the reference crop (Allen *et al.,*1998). Differences in resistance to transpiration, crop height, crop roughness, reflection, ground cover and crop rooting characteristics result in different ETc levels in different types of crops under identical environmental conditions. Most of these parameters depend on the plant ground cover (GC). In the case of citrus, Castel (2000) obtained an average yearly Kc based on the GC (Table 1).

Table 1. Crop Coefficient (Kc) according ground cover (GC,%) for citrus and fruit trees

GC(%)	Citrus
20 > GC	$K_c = 0.021 + GC * 0.0174$
20 < GC < 70	$K_c = 0.274 + GC * 0.005$
70 < GC	$K_c = K_{c70}$

Citrus trees crop coefficient also vary along the season with minima in spring and maxima in autumn (Table 2) reflecting mainly changes in ground cover produced by pruning and by growth of new leaves in spring and autumn, but also changes in soil evaporation produced by rainfall.

Table 2. Monthly citrus crop coefficient as reported in Castel (2000)

Average	Jan	Feb	Marc	Apr	May	Jun	Jul	Aug	Sep	Oct	Nov	Dec
0.68	0.66	0.65	0.66	0.62	0.55	0.62	0.68	0.79	0.74	0.76	0.73	0.63

For computing irrigation water requirements rainfall contributions to the orchard water balance should be also taken into account. Since, the total amount of rainfall is often not entirely available for tree transpiration the effective rainfall (P_{ef}) should be estimated. This is because some rainfall water might not be stored in the orchard due to runoff or drainage (FAO, 1978). In addi-

tion, in modern drip irrigated orchards, it is considered that the entire soil allotted per tree is not colonized by roots that should be more localized within the dripper zone. In order to consider P_{Ef} is estimated by means of a factor (Fpe) that relates the effective rainfall with the GC (Table 3).

Table 3. Effective rainfall for citrus and fruit trees according to season

Season	Fpe factor
Winter	Fpe = 1.25 * GC / 100
Summer	Fpe = 1.25 * GC / 100 (as maximum Fpe = 0.8)

It is then clear that for optimum irrigation management is crucial to precisely estimate tree ground covers that will be then used to both computing tree water requirements and rainfall contributions to the net water orchard balances. Plants ground cover can be directly measured with a sampling mesh as Wünsche *et al.,* (1995) proposed. On another hand, Castel (2000) used a ruler to measure canopy dimensions and GC was estimated as the horizontal projection of the canopy and it was expressed as ratio to the planting spacing. GC can also be estimated by indirect methods which are based mainly in the light interception measured by sensors (Giuliani *et al.,* 2000) and its representation in three dimension models (López-Lozano *et al.,* 2011). For the determination of a stand's LAI (Leaf Area Index), there are direct techniques like harvesting of the whole canopy or some samples of the vegetation, which are destructive and laborious. Taking samples of litter is non-destructive but also very time-consuming (Holst *et al.,* 2004). Due to the difficulties of the direct techniques, indirect techniques are preferred. Tools such as hemispherical photography and cover photography (Macfarlane *et al.,* 2007), the LAI 2000 and LAI 2200 (LI-COR Biosciences), LAI ceptometer (Decagon Devices) and Tracing Radiation and Architecture of Canopies (TRAC; Chen, 1996) allow measuring LAI in a non-destructive way.

However, for the determination of GC and LAI for large extensions, like irrigation areas, the use of these techniques entails a large amount of samples and long processing time. For this reason, remote sensing techniques become valuable tools in order to estimate these parameters. Due to the physiologic features of tree crops, high resolution images are required to estimate with accuracy these parameters.

High spatial resolution images have been available since the beginning of aerial photography, but their application to agriculture and forestry dramatically increased with the first near-infrared (NIR) photographs, and even more with the use of digital cameras that reduced acquisition costs and provided more homogeneity in terms of radiometric calibration of the scenes. Additionally, at the end of the 20th century and the very beginning of the 21st a new generation of high resolution satellites brought availability of data with a high frequency of acquisition. Among these satellites with onboard high resolution sensors, the series of Ikonos (2000), EROS-A and B (2000, 2006), QuickBird (2001), OrbView-3 (2003), WorldView-1 and 2 (2007 and 2009), GeoEye (2008) or RapidEye (2008) are very representative, typically having panchromatic and/or multispectral sensors, the former with spatial resolutions ranging from 0.5 to 1 m/pixel and the latter from 2 to 4 m/pixel. Panchromatic images have one band with spectral sensitivity in the visible and very near infrared, while the multispectral images from these high resolution sensors usually have four bands centred on the visible and NIR regions of the electromagnetic spectrum. Furthermore, the image fusion techniques allow for the combination of both types of images, obtaining a new image with the spatial detail of the panchromatic and the spectral bands of the multispectral, while preserving most of the information contained in the original images. These techniques are continuously improving and provide an excellent alternative and complement to the digital aerial colour-infrared imagery, several of them being reported in Wald *et al.,* (1997), Nuñez *et al.,* (1999), Ranchin and Wald (2000) and many other authors. Regarding new remote sensing sensors that

can be used in ground cover determination, it seems appropriate to mention the new Aerial Laser Scanning (ALS) or Light Detection and Ranging (LiDAR) systems, thoroughly described by Baltsavias (1999). LIDAR technology works by continuously sending energy pulses to the ground, that impact on Earth's surface and return to the sensor. The return time allows registering the position and coordinates of the recorded points and, therefore, measures terrain, vegetation, and other elements in 3D. The final point cloud data can be processed and analyzed for ground cover estimation, as well as many other applications. However, current unavailability of these data on a regular basis, as well as their high cost, make it out of the scope of this chapter.

II – Remote sensing tools for estimation of citrus tree ground cover

Automated detection of trees and ground cover from multispectral imagery has been mainly focused on forest applications (Wulder *et al.,* 2000; Culvenor, 2002; Pouliot *et al.,* 2002; Wang *et al.*, 2004), but some image processing methods have also been reported for olive tree detection, both semi-automated (Kay *et al.*, 2000) and automated (Karantzalos and Argialas, 2004; García-Torres *et al.*, 2008), and for Citrus and fruit tree identification (Recio *et al.,* 2009). In general, methods for ground cover estimation from images are based on classification techniques, supervised or unsupervised, on tree identification algorithms using local maxima approaches from vegetation indices or other band combinations and filtering approaches, or on hybrid methods combining segmentation, classification and the application of a variety of filters. In this section, a review and brief description of these techniques is made, focusing on the case of agricultural tree plots.

1. Overall methodology

Independently of the efficiency or performance of the method used, an important and practical aspect to consider in ground cover estimation is the fact that it is very sensitive to the binomial ground *tree size* and image *spatial resolution*. In small trees, the relative error due to the tree perimeter uncertainty becomes higher. Analogous effect occurs when the spatial resolution of the image is smaller (pixel size larger), that is, the tree border error quantifying the ground cover increases (Fig. 1a). Therefore, in the selection of the appropriate spatial resolution of the images, the average size of the trees to be processed is an important factor to be considered.

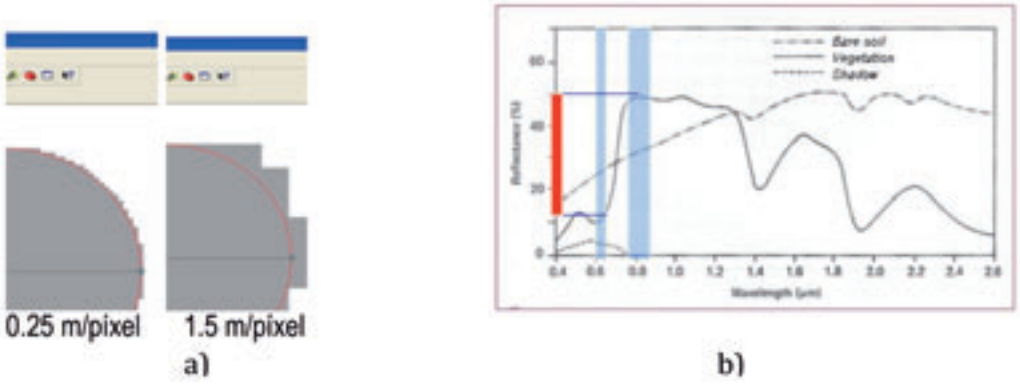

Fig. 1. (a) Effect of the image spatial resolution on the accuracy of the estimation of the ground cover area on the border of the tree; and (b) average spectral response curve of bare soil, vegetation and shadow, showing in blue the sensitivity of red and NIR bands, and in red their sharp difference in reflectance for vegetation.

Another important factor is the spectral information provided by the image. Since the spectral reflectance of the vegetation increases sharply in the infrared, due to the scattering of this radiation caused by the random arrangement of the cells and the intercellular air spaces in the spongy mesophyll layer of the leaves, the availability of visible and NIR bands is very important to accurately differentiate soil or shadow from a tree, and subsequently to obtain good ground cover estimations. Figure 1b illustrates this effect.

After the selection of the most appropriate images, and depending on the source and distribution institution or agency, a set of pre-processing operations must be done before applying any algorithm to the analysis of the data:

– The radiometric adjustment of the different scenes to be used, consisting of the reduction of the differences between scenes in terms of illumination or calibration of the sensors. This is usually more noticeable in aerial images, where images from different strips present distinct observation angles. The adjustment can be carried out by means of histogram matching, histogram specification, regression of radiometric values or similar techniques.

– Geometric corrections are needed to eliminate geometric distortions generated on the image due to the acquisition process. They are variable depending on the platform (satellite or aerial), and on the topography of the terrain.

– Fusion techniques refer to the combination of panchromatic and multispectral images to obtain a new image with the spatial resolution of the first and the spectral information of the second. They may be applied if these two types of images are available.

– Finally, some smoothing filtering processes may be applied to remove noise from the images and to enhance the differences between the trees and the background, facilitating the performance of the tree detection algorithms. These filters are variable depending on the authors and the characteristics of the agricultural plots.

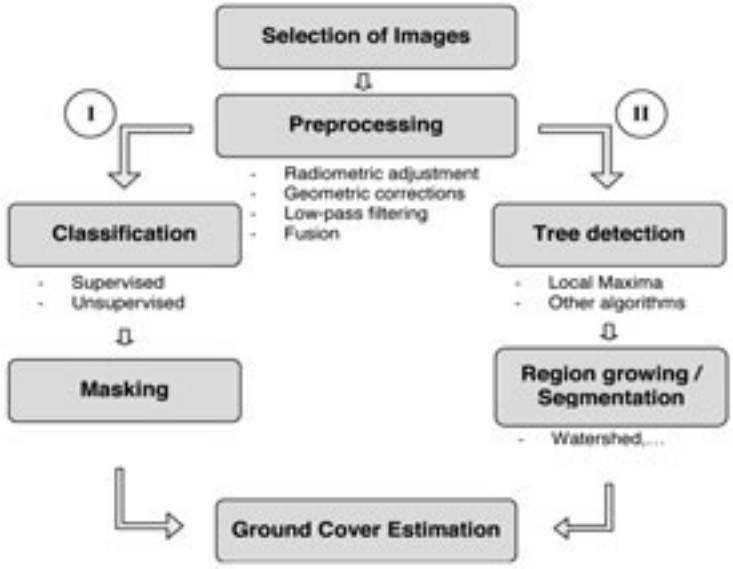

Fig. 2. Overall methodology for tree ground cover estimation from satellite and aerial images. (I) Procedures based on classification; (II) Procedures based on tree detection algorithms and segmentation.

Figure 2 shows a generic procedure for ground cover estimation, where two different types of approaches are distinguished (branches "I" and "II") after the pre-processing steps. The next two sections describe these general alternatives, one of them based on the multispectral classification of the images, and the other based on the detection of the trees followed by region growing procedures or analogous segmentation techniques.

2. Methods based on image classification

Image classification is the process used to produce thematic maps from imagery, and consists of the extraction of descriptive features from the pixels or objects in the image, and their assignation to a class or category according to that quantitative information. Two main types of image classification techniques can be considered: *supervised* and *unsupervised*. In supervised classification, the analyst selects representative sample sites of known cover type, called training areas, compiling a numerical description of each class. Each pixel or object in the data set is then compared to them and is labelled with the most similar class. Many different algorithms or classification methods can be used to measure this similarity and generate decision rules, such as minimum distance, maximum likelihood, other based on decision trees, neural networks, etc. The maximum likelihood classifier, a statistical standard method, quantitatively evaluates both the variance and covariance of the category spectral response patterns when classifying an unknown pixel, assuming that the distribution of the cloud points forming the category training data is Gaussian. Given the mean vector and the covariance matrix of each category pattern, the probability of a given pixel or object being a member of a particular land cover class can be computed (Lillesand and Kiefer, 2000). Figure 3b shows the result of classifying a citrus plot in three classes: tree, shadow and soil.

Unsupervised classifiers do not utilize training data as the basis for classification. Rather, they involve algorithms that examine the pixels in an image and aggregate them into a number of unknown classes based on the natural groupings or clusters present in the image values. In these approaches, spectrally separable classes are automatically determined and then their informational category is defined by the analyst. There are numerous clustering algorithms, one of the most common is the K-means, an iterative method that arbitrarily creates K clusters and each pixel is assigned to the class whose mean vector is closest to the pixel vector. This step is iterated until there is not significant change in pixel assignments. A common modification is known as the ISODATA algorithm, which includes merging the clusters if their separation is below a threshold, and splitting of a single cluster into two clusters if it becomes too large. These algorithms present the advantage, compared to the supervised, that they work in an automatic manner, since no previous information is needed to classify the images. However, several parameters must be initially set by the user, such as number of classes, number of iterations, or some thresholds used to stop the iterations. Figure 3c shows the result after classifying a plot in tree, shadow and soil.

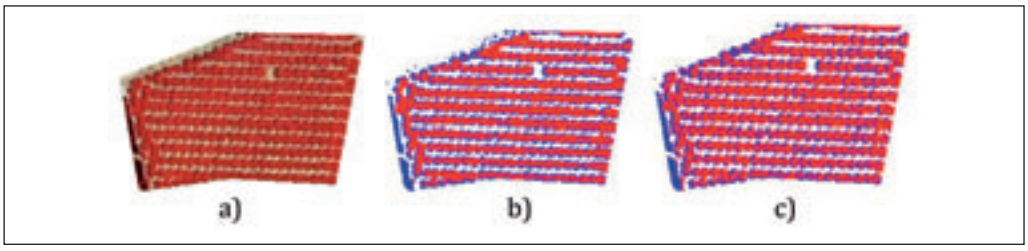

Fig. 3. Example of the classification of a citrus plot in 3 classes: tree (red), shadow (blue), soil and background (white). (a) Original colour-infrared image; (b) supervised classification using *maximum likelihood* algorithm; and (c) unsupervised (*ISODATA*) classification using the following parameters: 3 classes, 5 maximum iterations, 5% change threshold.

Classification methods for ground cover estimation are not considered as fully automated, since they require selection of training samples (supervised methods) or definition of parameters (unsupervised methods). However, the main handicap of supervised classification is the large variability of tree and soil response in different plots even from the same area, which makes the extrapolation of the training samples and the decision functions very difficult, making this technique by itself limited to small areas with homogeneous plantations. On the other side, the definition of parameters required by unsupervised approaches is difficult and involves uncertainty, yielding results that are only approximate. Finally, other limitation is that since they are usually based on the spectral response of the vegetation, weeds may be often misclassified as trees, with the subsequent commission error in tree coverage determination.

3. Methods based on tree detection and segmentation

These methods prioritize the identification and localisation of the trees that are present in a plot, and then use these locations as seeds for the definition of the tree crowns. Although there is a variety of methods that are used for tree detection, especially in forest applications, the most used are those based on the *local maximum filtering* (LMF) algorithm (Gougeon, 1995). This algorithm assumes that NIR reflectance has a peak at the tree apex and decreases towards the crown edge. Thus, after computing the *Normalised Difference Vegetation Index* (NDVI), that enhances the different reflectances of vegetation canopy in the NIR and red (NIR-Red/NIR+Red), a moving window can be applied over the NDVI image (Fig. 4a), considering a tree when the central value in the window is higher than the other values. The size of the filtering window can be either determined as a function of the average size of the trees, or automatically defined for each plot by the position of the first maximum on the semivariogram curve (Ruiz *et al.,* 2011). Figure 4b shows the result of the application of the LMF over a citrus plot.

After tree detection, region growing or segmentation algorithms are applied to define the crown surrounding each tree. Region growing is an iterative process which starts at "seed" pixels from the set generated using the LMF algorithm. Pixels from the neighbourhood of each seed are progressively classified as belonging or not to the same crown as the seed (Hirschmugl *et al.,* 2007). Classification criteria are typically based on absolute distance from the seed, brightness gradient thresholds, spectral coherence, etc. Figure 4c shows the ground cover mask resultant after the application of the region growing process.

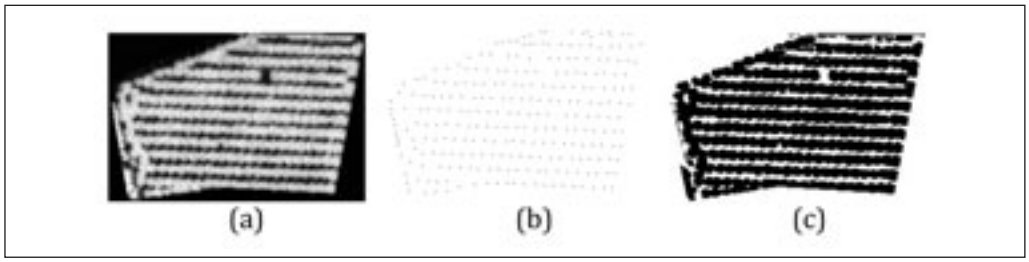

Fig. 4. Extraction of ground cover area on the image example of Fig. 3a using a tree detection approach. (a) NDVI image; (b) application of the local maxima on the NDVI image; (c) cover area after region growing.

Finally, other approaches are based on the application of hybrid methods, such as the combination of unsupervised classification, local maxima filtering, region growing, etc. An example of these combined techniques for ground cover estimation in citrus orchards is described in detail

in other chapter of this book. In addition, new sensors like airborne LiDAR allow for the integration of these data with multispectral images to provide a better accuracy in tree detection and crown cover. This will very likely be the trend during the next several years to increase the reliability of these methodologies. The methodology involves the preprocessing of LiDAR data to create a digital surface model (DSM), digital terrain model (DTM), and normalised digital surface model (nDSM). Then, the integration of spectral information from the images and height data from LiDAR, allows for a better estimation of ground cover (Fig. 5).

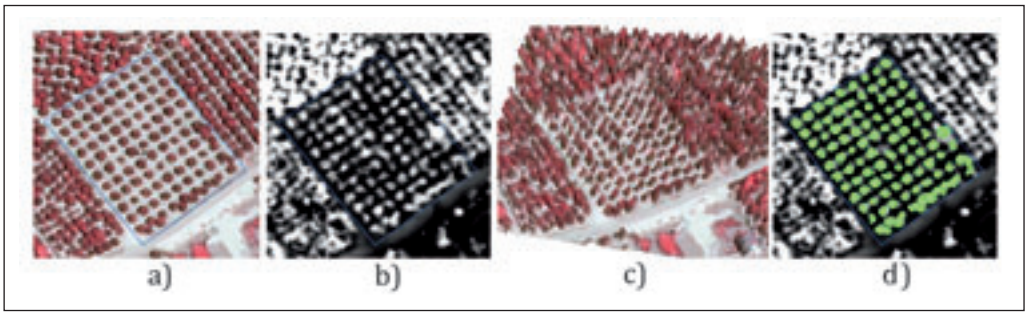

Fig. 5. Example of the combination of aerial images and LiDAR data for ground cover estimation. (a) Colour-infrared image; (b) nDSM directly computed from low density LiDAR data (source: PNOA 2009); (c) 3D perspective with the image draped over the DSM; and (d) tree crowns (in green) automatically delineated after region growing.

III – Integral irrigation water management at farm and district level

1. Implementation in Decision Support Systems

To optimize the use of all inputs involved in irrigation (water, energy and fertilizers) it is necessary to keep track of all the processes that are involved, with the aim of detecting weaknesses in management and try to improve them. Given the large amount of information required to do so, it is advisable to use a Decision Support System (DSS), which feeds the processes with different alternatives assessing the results in each case. Since most of the information used is spatial, Geographic Information Systems (GIS) are shown as the best working tool for this purpose.

The required data to be implemented in a DSS comes from different sources. Data can be grouped in two categories, according if they are used for agronomic or hydraulic purposes.

The agronomic processes deal with crop water requirements, irrigation scheduling and fertilization. To simulate these processes the needed data are:

– Cadastral information. This data let to know plot features as area and location. It can be obtained from public databases in standard formats.

– Soils. This information supplies soil characteristics like texture to calculate water crop requirements.

– Crops. In the case of citrus trees, planting spacing, ground cover, and root depth are required to estimate water crop requirements.

– Irrigation subunits. These data are useful to calculate irrigation time for scheduling. For example, in drip irrigation, emitter flow is required to calculate theoretical irrigation time. Moreover depending of the subunit and its management, net water crop requirements are increased to supply a minimum water amount to all plants (Arviza, 1996).

– Agroclimatic information. ETo ad Pe are required to compute net water crop requirements. Irrigation Advisory Services from local governments make available agroclimatic information obtained from station networks with daily frequency. Figure 6 shows the network of agroclimatic stations of the Valencia region (Spain).

This information can be incorporated to the DSS to calculate daily water crop requirements.

Fig. 6. Net of meteorological weather stations belonging to the Irrigation Technology service of the Instituto Valenciano Investigaciones Agrarias.

The hydraulic processes give information about how water is delivered and if it is done with the required guarantees of pressure, amount and quality. Also by means of performance indicators the system can be assessed (Córcoles *et al.,* 2010).

The required data about are the network layout, pumps, control devices (control systems, valves), hydrants, intakes, flow meters and irrigation scheduling. Figure 7 summarizes the data required for the agronomic and hydraulic management.

Focussing on the agronomic management, a DSS can calculate the crop water requirements and the irrigation time of all plots for irrigation scheduling.

In order to assess irrigation performing a DSS can give information about how water has been delivered to plots to meet crop water requirements. An indicator used for this purpose is the Seasonal Irrigation Performing Index (SIPI) that relates the crop water requirements with the water supplied (Faci *et al.,* 2002). Values lower than 100 mean that a crop it is being irrigated more than required. Values higher than 100 means that a crop is being irrigated less than required.

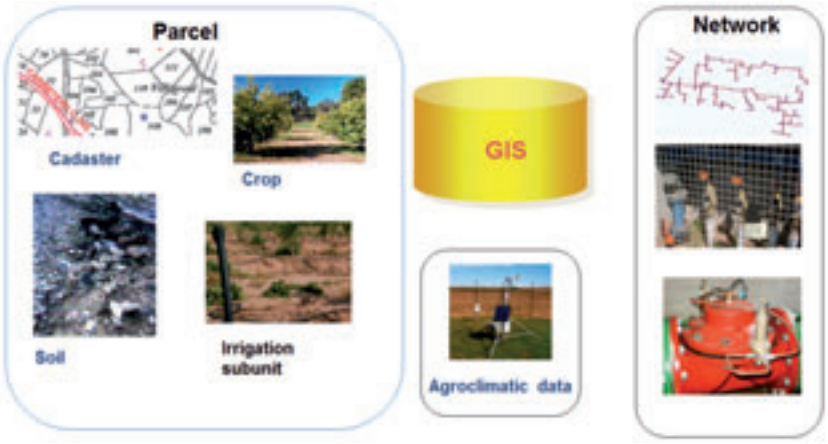

Fig. 7. Data required to be implemented in a DSS for the agronomic and the hydraulic management.

2. Application to a case study

Next it is showed the implementation of a case study of a DSS called HuraGIS (Jiménez-Bello, 2010) in the Water User Association (WUA) of Senyera in Valencia (Spain) a region with Mediterranean climate. The total irrigated area was 104 ha, cropped entirely with citrus. Water was allocated by a pressurised irrigation network. There were 280 operating intakes that irrigated 356 plots. The average plot size was 3093 m^2. Crops were dripping irrigated.

GC was calculated using techniques depicted in above with the 2006 and 2008 ortophotos from the Spanish National Plan of Aerial Photography. Water crop requirements were calculated using agroclimatic data from the nearest station of the network of Valencia region.

Figure 8 shows the monthly SIPI (%) for four irrigation seasons (2006, 2007, 2008, 2009) for all parcels of the WUA. The annual SIPI (%) for these years were 117, 80, 81, and 67, respectively.

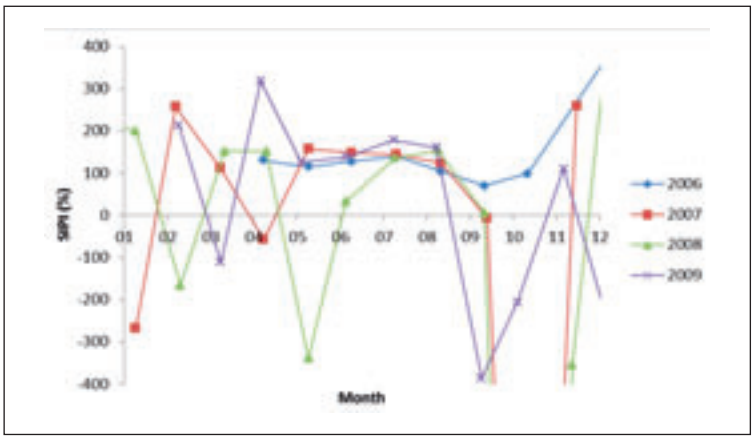

Fig. 8. Seasonal Irrigation Performing Index (SIPI) for the study case of Senyera for four seasons (2006, 2007, 2008, 2009).

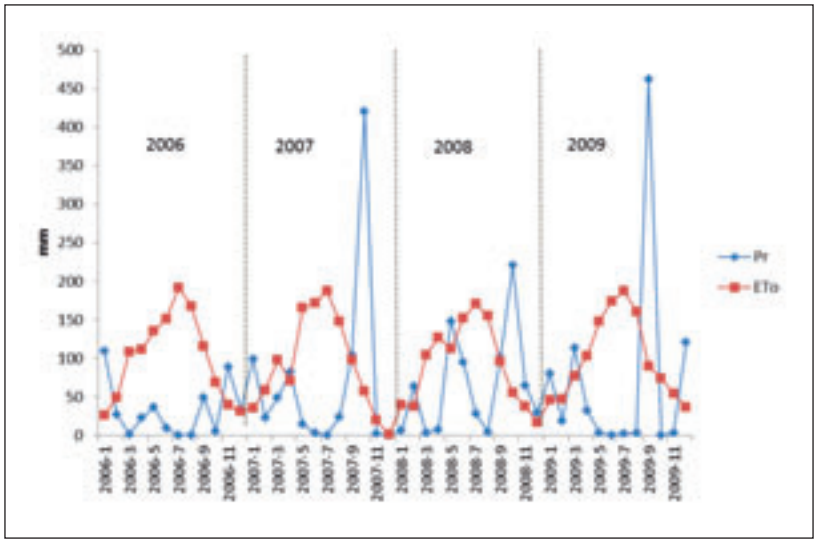

Fig. 9. Monthly ETo (mm) and Pr (mm) for the study case of Senyera.

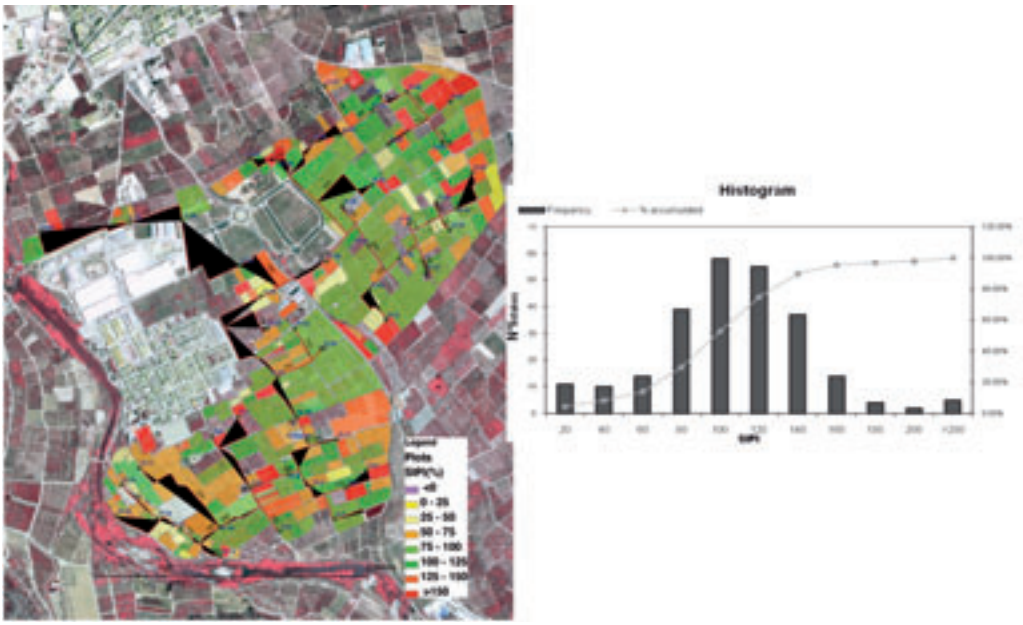

Fig. 10. (A) Map of Seasonal Irrigation Performance Index (%) for the 2010 of the study case of Senyera. (B) Histogram of SIPI(%) for the irrigation intakes of the study case.

Those values close to 100% mean that crops were properly irrigated. As it can been seen these values are around 100% in summer, the months with higher demand. Values below 0 are due to rainfall, which was not properly taken into account for irrigation scheduling as it can be seen in Figure 9. The lower values of monthly SIPI(%) correspond to the months of rains.

The map of Fig. 10 shows the annual SIPI(%) for each irrigated parcel in 2010 of the study case. The histogram shows the existing variability at WUA level. Most of plots irrigated by the network intakes have SIPI values that range from 80% to 120% which means that are properly irrigated. But 20% of plots are overirrigated. On the other side 20% of plots are underirrigated.

With this information obtained via performance analysis, recommendations can be given to users to improve their irrigation efficiency. For example, in plots which are under-irrigated, users can modify either their irrigation time or increase the emitter number with the aim of increasing the received water amount.

References

Allen R.G., Pereira L.S. and Raes D., 1998. Crop evapotranspiration. Guidelines for computing crop water requirements. *FAO Irrigation and Drainage Paper 56*. Food and Agriculture Organization of the United Nations, Rome.

Arviza J., 1996. *Riego localizado*. Universidad Politécnica de Valencia. Departamento de Ingeniería Rural y Agroalimentaria. Valencia. Spain.

Baltsavias E.P., 1999. Airborne laser scanning: basic relations and formulas. In: *ISPRS Journal of Photogrammetry and Remote Sensing*, 54, p. 199-214.

Castel J.R., 2000. Water use of developing citrus canopies in Valencia, Spain. In: *Proc Int. Soc. Citriculture, IX Congr.*, p. 223-226.

CGCtel J.R. 2000. Water use of Developing Citrus Canopies in Valencia, Spain. In: *Proceedings of the international Society of Citriculture. IX Congress.* 2000, p. 223-226

Chen J.M. and Blanken T.A, 1992. Defining leaf area index for non flat leaves. In: *Plant Cell Environ.*, vol. 15, p. 421-429

Chen J.M., 1996. Optically-bGCed methods for meGCuring seGConal variation in leaf area index of boreal conifer forests. In: *Agricultural and Forest Meteorology*, 80, p. 135-163

Corcoles J.I., de Juan J.A., Ortega J.F., Tarjuelo J.M. and Moreno M.A., 2010. Management evaluation of Water Users Associations using benchmarking techniques. In: *Agricultural Water Management*., 98, p. 1-11.

Culvenor D. S., 2002. TIDA: an algorithm for the delineation of tree crowns in high spatial resolution remotely sensed imagery. In: *Computers & Geosciences* 28 (1), p. 33-44.

Faci J.M., Bensaci A., Saltni A. and Playán E., 2000. A case study for irrigation modernisation. I. Characterisation of the district and analysis of water delivery records. In: *Agric. Water Manage*., 42, p. 315-334.

FAO, 1978. *Effective rainfall in irrigated agriculture*. FAO irrigation and drainage paper. N.G. Dastane

Fereres E. and Goldhamer D.A. 1990. Deciduous fruit and nut trees. In: Stewart BA, Nielsen DR, eds. *Irrigation of agricultural crops*, Agronomy 30. Madison, WI: ASA, CSSA, SSSA, p. 987-1017.

Fereres E. and Gonzalez-Dugo V., 2009. Improving productivity to face water scarcity in irrigated agriculture. In: Sadras VO, Calderini DF (eds) *Crop physiology: applications for genetic improvement and agronomy*. Academic Press, San Diego, p. 123-143.

García-Torres L., Peña-Barragán J.M., López-Granados F., Jurado-Expósito M. and López-Escobar R., 2008. Automatic assessment of agro-environmental indicators from remotely sensed images of tree orchards and its evaluation using olive groves. In: *Computers and Electronics in Agriculture*, 61 p. 179-191.

Giuliani R., Magnanini E., Fragassa C. and Nerozzi F., 2000. Ground monitoring the light-shadow windows of a tree canopy to yield canopy light interception and morphological traits. In: *Plant Cell Environ.* 23, p. 783-796.

Gougeon F.A. 1995. A crown-following approach to the automatic delineation of individual tree crowns in high spatial resolution aerial images. In: *Canadian Journal of Remote Sensing*, 21, p. 274-284.

Hirschmugl M., Ofner M., Raggam J. and Schardt M., 2007. Single tree detection in very high resolution remote sensing data. In: *Remote Sensing of Environment*, 110, p. 533-544.

Holst T., Hauser S., Kirchgäßner A., Matzarakis A., Mayer H., Schindler D. and Spiecker H., 2003. Measuring and modelling Plant Area Index in beech stands. In: *International Journal of Biometeorology*, 48 (4), p. 192-201.

Jiménez-Bello M. A., Martínez Alzamora F., Bou Soler V. and Bartoli Ayala H.J., 2010. Methodology for grouping intakes of pressurised irrigation networks into sectors to minimize energy consumption. In: *Biosystems Engineering*, 105, p. 429-438.

Karantzalos K. and Argialas D., 2004. Towards the automatic olive trees extraction from aerial and satellite imagery. In: *International Archives of the Photogrammetry, Remote Sensing & Spatial Information Sciences*, 35(5), p. 360-365., p. 1173-1177, Istanbul, Turkey.

Kay S., Léo O., Peedell S. and Giardino G., 2000. Computer assisted recognition of olive tree in digital imagery, Space Applications Institute, JRC of the European Commission, Ispra, Italy.

Lillesand T.M. and Kiefer R.W., 2000. *Remote Sensing and Image Interpretation*. John Wiley & Sons, Inc. New York.

López-Lozano R., Baret F., García de Cortázar Atauri I., Lebon E. and Tisseyre B. 2011. 2D approximation of realistic 3D vineyard row canopy representation for light interception (fIPAR) and light intensity distribution on leaves (LIDIL). In: *European Journal of Agronomy*, 35-3, p. 171-183.

Macfarlane C., Grigg A. and Evangelista C., 2007a. Estimating forest leaf area using cover and fullframe fisheye photography: thinking inside the circle. In: Agricultural and Forest Meteorology 146 (1-2), p. 1-12.

Molden D., 2007. *Water for Food, Water for Life: A Comprehensive Assessment of Water Management in Agriculture.* Earthscan, London.

Nuñez J., Otazu X., Fors O., Prades A., Palá V. and Arbiol R. 1999. Multiresolution-based image fusion with additive wavelet decomposition. In: *Transactions on Geoscience and Remote Sensing.* IEEE. 37(3), p. 1204-1211.

Pouliot D. A., King D.J., Bell F.W. and Pitt D.G., 2002. Automated tree crown detection and delineation in high-resolution digital camera imagery of coniferous forest regeneration. In: *Remote Sensing of Environment*, 82 (2-3), p. 322-334.

Ranchin T. and Wald L., 2000. Fusion of high spatial and spectral resolution images: the ARSIS concept and its implementation. In: *Photogrammetric Engineering and Remote Sensing,* 66(1), p. 49-61.

Recio J.A., Ruiz L.A., Fernández A. and Hermosilla T., 2009. Extracción de características estructurales en un sistema de clasificación de imágenes basado en parcelas. In: *XIII Congreso Nacional de la Asociación Española de Teledetección*, 23-26 septiembre 2009, Calatayud, p. 577-580.

Ruiz L.A., Recio J.A., Fernández-Sarría A. and Hermosilla T., 2011. A feature extraction software tool for agricultural object-based image analysis. In: *Computers and Electronics in Agriculture*, 76 (2), p. 284-296.

Wald L., Ranchin T. and Mangolini M., 1997. Fusion of satellite images of different spatial resolutions: assessing the quality of resulting images. In: *Photogrammetric Engineering and Remote Sensing*, 63 (6), p. 691-699.

Wang L., Gong P. and Biging G.S., 2004. Individual Tree-Crown Delineation and Treetop Detection in High-Spatial-Resolution Aerial Imagery. In: *Photogrammetric Engineering and Remote Sensing*, 70 (3), p. 351-357.

Wulder M., Niemann K.O. and Goodenough D.G., 2000. Local Maximum Filtering for the Extraction of Tree Locations and Basal Area from High Spatial Resolution Imagery. In: *Remote Sensing of Environment*, 73 (1), p. 103-114.

Wünsche J.N., Lakso A.N. and Robinson T.L., 1995. Comparison of four methods for estimating total light interception by apple trees of varying forms. In: *HortScience*, 30, p. 272-276.

Automated extraction of agronomic parameters in orchard plots from high-resolution imagery

J. Recio, T. Hermosilla and L.Á. Ruiz

Geo-Environmental Cartography and Remote Sensing Group - Universitat Politècnica de València, Camino de vera s/n 46022 Valencia, (Spain)

Abstract. The availability of high spatial resolution images obtained from aerial and satellite sensors together with the development of new image analysis methods are providing an important impulse to precision agriculture techniques and applications. We describe an automated methodology for the extraction of agronomic parameters from tree orchard plots based on the use of high-resolution remotely sensed imagery, which can be further used to increase the efficiency of irrigation and agricultural plot management in the SUDOE area. These methods are based on parcel-based image analysis, and a variety of parameters are obtained including tree detection, location and counting, planting patterns, tree crown, vegetation cover and others. Since common data and image processing techniques are used, they can be easily implemented in production processes and cover large agricultural areas. The methods are tested on citrus orchard plots located in Valencia (Spain), showing a good performance in particular for adult trees. In addition to the particular use of the ground cover for the estimation of water requirement, these parameters can also be used as support tools for agricultural inventories or database updating, allowing for the reduction of field work and manual interpretation tasks.

Keywords. Irrigation efficiency – Remote sensing – Parcel-based image analysis – Tree detection – High-resolution images.

Extraction automatique de paramètres agronomiques pour les parcelles de vergers à l'aide d'imagerie à haute résolution

Résumé. *La disponibilité d'images à haute résolution spatiale obtenues par des capteurs aériens et satellitaires, parallèlement au développement de nouvelles méthodes d'analyse d'images, ont donné un important élan aux techniques et applications de l'agriculture de précision. Nous décrivons une méthodologie automatique pour l'extraction de paramètres agronomiques concernant les parcelles de vergers, basée sur l'emploi d'imagerie à haute résolution obtenue par télédétection, qui peut être d'utilité pour accroître l'efficience de l'irrigation et de la gestion des parcelles agricoles dans la région SUDOE. Ces méthodes sont basées sur l'analyse d'images au niveau de la parcelle, obtenant une série de paramètres dont la détection, la localisation et le dénombrement des arbres, la configuration de la plantation, la couronne des arbres, le couvert de végétation et autres. Puisque l'on utilise des données et techniques courantes de traitement d'images, elles sont facilement applicables aux processus de production et peuvent concerner de vastes zones agricoles. Les méthodes sont testées dans des vergers d'agrumes situés à Valencia (Espagne), et montrent de bons résultats en particulier pour les arbres adultes. En plus de leur utilisation particulière pour le couvert végétal afin d'estimer les besoins en eau, ces paramètres peuvent aussi être utilisés comme outils d'appui pour l'actualisation des inventaires agricoles ou des bases de données, permettant ainsi de réduire le travail de terrain et les tâches d'interprétation manuelle.*

Mots-clés. *Efficience de l'irrigation – Télédétection – Analyse d'images basée sur la parcelle – Détection des arbres – Images à haute résolution.*

I – Introduction

The availability of high-spatial resolution aerial and satellite digital images opened new outlooks for the automatic extraction of information in the domains of agriculture and forestry. Traditionally, agricultural parameters such as the number of trees, spatial distribution and crown size or tree

canopy cover have been estimated by photointerpretation, relating the image-derived information with supporting field data. As stated in a previous chapter, algorithms for the automatic extraction of these parameters in large irrigation areas, in particular the tree canopy cover, would provide valuable information for a better estimation of crop coefficient (K_c) and its application to calculate crop water requirements.

Remote sensing technology has been used to obtain information about crop condition in precision agriculture (Viau *et al.*, 2005). Also, spectral data collected by multi-spectral optical sensors has been widely used to obtain different types of vegetation indices, which can be related to biophysical parameters that provide information about plant status or vegetation density (Mazzetto *et al.*, 2010). When remote sensing is used in conjunction with *variable rate technology*, water and chemicals can be selectively applied in the soil, enabling a cost-effective and environmental-friendly management (Du *et al.*, 2005). The detection and location of individual trees from images enables to improve the classification of different species through the analysis of within-crown spectral data, spatial distribution and crown shape (Pouliot *et al.*, 2002; Erikson, 2004). Further description of trees in an agricultural plot can be applied as well for the management and updating of agricultural inventories and land use databases by means of parcel-based image classification (Recio, 2009). Wang *et al.* (2007) related K_c of pecan orchards with the tree size and spacing (effective canopy cover, ECC) using image analysis techniques from images obtained from a balloon and satellite, rendering a model and concluding that this equation can help to get more accurate estimates of irrigation requirements for pecan open-canopy orchards.

In this chapter, we describe a methodology developed in the frame of the TELERIEG project (Interreg IVb Sudoe, project no. SOE1/P2/E082) for the automated extraction of agronomic parameters from high-resolution aerial and satellite images. These parameters may be used in large irrigation areas to improve crop requirement estimation, but also in other applications such as crop classification and change monitoring at plot level, agricultural inventories or detection of crop abandonment.

II – Data and study area

Digital orthoimages acquired in June 2006 using a Vexcel Ultracam-D with a mean flight height of 4,500 meters over the mean terrain height were used as basic data. Spatial resolution of images was 0.5 m/pixel, 8 bits quantization, and three spectral bands: near-infrared (NIR), red and green. The images were provided in the framework of the *Plan Nacional de Ortofotografía Aérea* (PNOA), and they were provided orthorectified, geo-referenced, panchromatic and multispectral band fused, and radiometrically adjusted. The limits of the plots were obtained from cadastral cartography at a scale of 1:2000 in *shapefile* format, produced by the Spanish General Directorate for Cadastre.

The study area is located in the municipality of Llíria in the province of Valencia, Spain. The area is mainly covered by citrus orchards, followed by horticulture crops, fruit orchards and carob trees. The methodology was tested over citrus crops. A total of 300 plots were selected to perform the study, occupying an area of 265 ha.

III – Tree detection and delineation

Several approaches have been reported in the literature regarding the automated location of individual trees and crown delineation, i.e. radiance peak filtering (Dralle and Rudemo, 1997; Wulder *et al.*, 2000), valley following (Gougeon, 1995), template matching (Pollock, 1996), and clustering (Culvenor, 2002).

Local maximum filtering methods are based on the assumption that reflectance is highest at the tree apex and decreases towards the crown edge. These approaches identify the peaks in image intensity representing the location of each tree crown but not its outline. A kernel is moved over the image and trees are located where the central digital value in the window is higher than all other values. The size of the kernel can be fixed according to the mean size of trees or it can be variable depending on the size of each tree (Wulder *et al.*, 2000). Ruiz *et al.* (2007) apply this method over NDVI images using a circular kernel with variable diameter size, ranging from 9 pixels to 23 pixels, and it is determined as the position of the first maximum value of the semivariogram curve computed for each tree crop parcel analyzed.

Contouring or boundary following methods delimit the objects from the background employing the similarity in data values. Valleys of shade or lower intensity areas between tree crowns are identified and remaining tree material is outlined (Gougeon, 1995; Leckie *et al.*, 2003). Template matching approaches are based on mathematical renderings of typologies of crowns for matching with the image brightness to locate trees and determine their crown size (Pollock, 1996). This methodology requires a library of three dimensional model trees, producing omission errors when tree crowns are smaller than the smallest radius in the template library or have irregular crowns (Erikson and Olofsson, 2005). Culvenor (2002) clusters around each local maximum those pixels with digital values greater than a threshold and not belonging to the boundary of the crown obtained as local minima. García Torres *et al.*, (2008) extract the trees by clustering pixels with values within a range defined using a supervised classification. Most of these methods require a certain degree of human intervention providing training samples to the system or defining different thresholds to de used in the tree extraction process.

The methodology used in this project is based on common image processing tools, using image analysis techniques to obtain the information and thresholds needed to perform the tree extraction in an effective way. The procedure is based on clustering and local maxima filtering and is applied in Citrus tree orchards.

1. Tree segmentation methodology

The working unit in the methodology used is the parcel contained in a geospatial database. Each parcel contained in the cartography is analyzed separately, reducing the factors that make difficult the tree extraction in wide areas, such as differences in illumination, calibration of the sensor or in tree canopy spectral response. Besides, the parcel is a spatial unit commonly used in agricultural management being easier to relate the agronomic parameters extracted from the trees and their spatial distribution derived from the imagery to the information contained in agricultural geospatial databases (Ruiz *et al.*, 2011).

Descriptive features derived from the representation of the parcels in the images are obtained in two levels of detail: at parcel level and at tree level.

The extraction of the trees is composed of four steps (Fig. 1):

(i) Pre-processing of the image.

(ii) Unsupervised image classification.

(iii) Identification of classes corresponding to trees in the unsupervised classified image.

(iv) Post-processing of the tree segmentation.

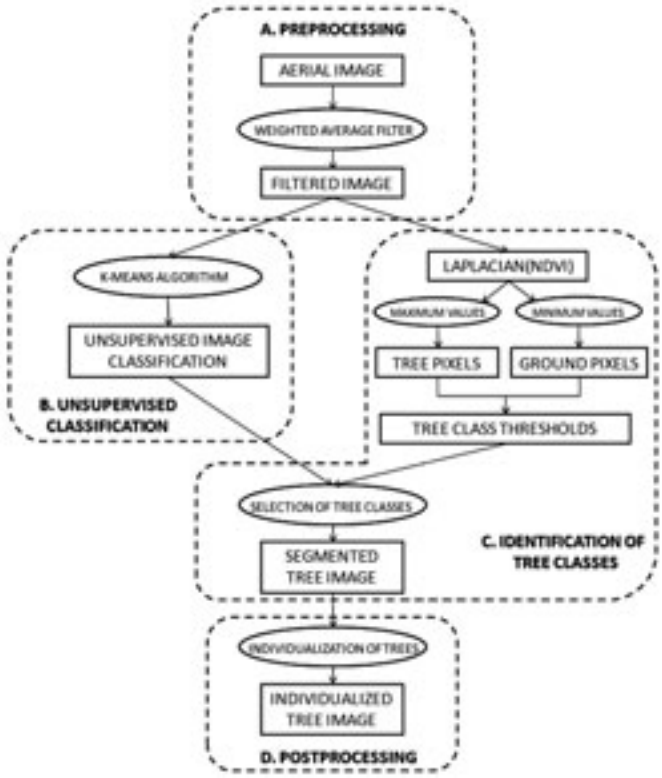

Fig. 1. Overall methodology workflow for tree detection.

A. Pre-processing

Basic geometric correction of the images is essential in order to superimpose the cartography to the images, and the same geographic reference system is required. Radiometric corrections are based on adjustments between different images, usually acquired in different strips in the case of aerial sensors. These techniques can be based on histogram matching, histogram normalisation based on the mean and standard deviation values from different images, regression techniques, etc.

Additionally, tree segmentation in high resolution images is hindered by different factors, such as the internal variability of trees and background, the reduced size of young trees with respect to the spatial resolution of the images, or the transition tree-soil pixels with mixed reflectance values. In order to reduce the effect of these factors in the segmentation process, preprocessing of the images is required. A practical method to reduce the mixed reflectance effect is based on the iterative application of a weighted average filter where the weight of each pixel in the kernel is inversely proportional to the spectral distance to the central pixel (Recio, 2009). The final value for each pixel in the filtered image is obtained using Equation 1.

$$DN'_{i,j} = \frac{\sum_{p=-1}^{1}\sum_{q=-1}^{1} DN_{i+p,j+q} FC_{i+p,j+q}}{\sum_{p=-1}^{1}\sum_{q=-1}^{1} FC_{i+p,j+q}} \quad (1)$$

where $DN_{i,j}$ is the original digital number of pixel *i,j*; $DN'_{i,j}$ is the output digital number for this pixel and *FC* is the filtering coefficient obtained from Equation 2.

$$FC_{i-1,j-1} = 1 - a \cdot \left| DN_{i-1,j-1} - DN_{i,j} \right| \quad (2)$$

where *a* is a weighted coefficient of the difference between the digital numbers of the central pixel and the neighbouring pixels. The higher the value of *a*, the smaller is the influence of neighbouring pixels in the output value of the central pixel. When the filtering coefficient is negative, its value is replaced by 0. If *a* is greater than 1, then an effect of independent homogenization of objects and background is produced, as well as the enhancement of the borders without blurring the smaller trees. Transition pixels are the most influenced, and their values trend to become similar to those of the object or the background, depending on their similarity in the original image. Figure 2 shows the effect of iteratively applying a filter over an image containing adult citrus trees. Transition pixels disappear and the trees and the background become more homogeneous, facilitating tree segmentation.

Original image **Image filtered (3 iterations)** **Image filtered (6 iterations)**

Fig. 2. Detail of the application of the weighted average filter.

B. Unsupervised image classification

The K-means unsupervised classification algorithm is applied to obtain spectrally homogeneous groups of pixels in the image. This algorithm classifies the image pixels into k classes using the criteria that each pixel is assigned to the class with the nearest mean, from an initial set of class prototypes. As the number of classes in each parcel is *a priori* unknown, looking for clusters with a high rate of fragmentation rather than heterogeneous, the number of clusters is initially fixed as ten, even considering that this value is usually greater than the actual number of cover types inside a parcel. Figure 3 shows the results of the unsupervised classification of colour-infrared images applied on two different parcels of the working area.

C. Identification of clusters corresponding to trees

Automated identification of clusters corresponding to trees is achieved by combining the information extracted of the unsupervised classified image and from the original image. In order to parameterise the spectral characteristics of trees and soil, first a 3×3 convolution with a Laplacian filter is applied over the NVDI image, then a set of pixels representing these two classes is automatically selected as the maximum and minimum values in the resulting image of the convolved image. Additionally, pixels with maximum and minimum values in the NDVI image are added to the tree and soil sample sets, respectively. Both sample sets are examined to remove

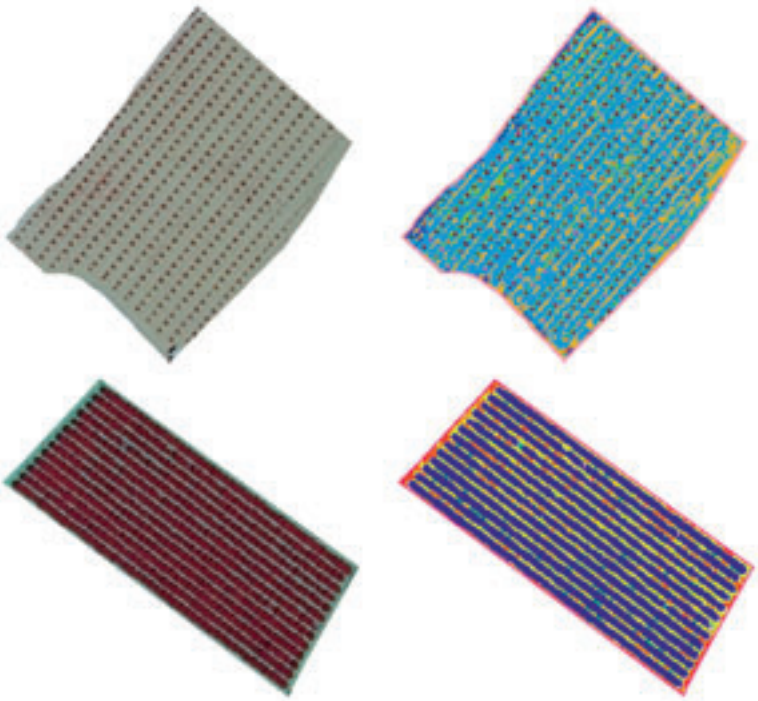

Original image **Unsupervised classification**

Fig. 3. Example of the unsupervised classification of two citrus orchard plots.

anomalous pixels. Tree pixels with NDVI values lower than the soil pixels mean value are removed from the sample set. Analogously, soil pixels with NDVI values higher than the tree pixels mean value are also removed.

The Normalized Difference Vegetation Index (NDVI) is frequently used to measure and monitor plant growth vegetation cover from multispectral aerial or satellite images and it is calculated with the Equation 3:

$$NDVI = \frac{NIR - R}{NIR + R} \quad (3)$$

where *NIR* and *R* represent the value of a pixel in the near infra-red and the red channel, respectively. In the red-light region of the electromagnetic spectrum, chlorophyll causes considerable absorption of incoming sunlight, whereas in the near-infrared region, leaf structure creates considerable reflectance. As a result, vigorously growing healthy vegetation has low red-light reflectance and high near-infrared reflectance and hence, high NDVI values. This index ranges from -1.0 to 1.0. Positive NDVI values indicate increasing amounts of green vegetation and negative values indicate non-vegetated areas.

The Laplacian filter is a measure of the second spatial derivative of an image and highlights regions of rapid intensity change and is therefore often used for edge detection. It normally takes a single gray level image as input and produces another gray level image as output (Fig. 4).

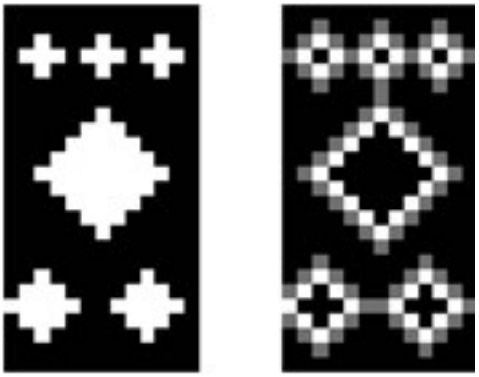

a) Original image **b) Filtered image**

Fig. 4. Example of the convolution of a binary image with a 3x3 Laplacian filter.

The Laplacian filter applied over the NDVI image generates the highest values for the pixels located inside the trees near their boundaries, and the lowest values in the external part of tree boundaries (Fig. 5).

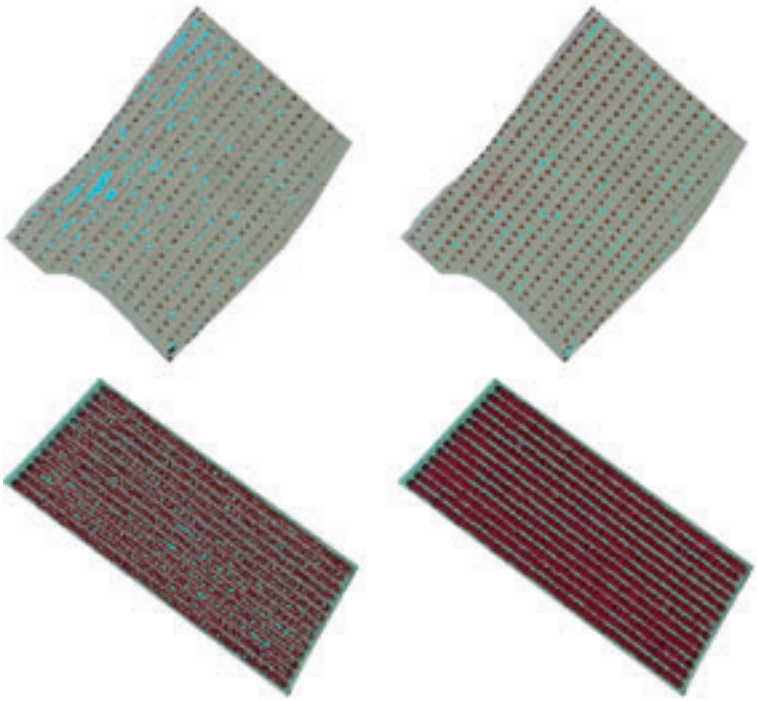

***Tree* pixels** ***Soil* pixels**

Fig. 5. Automatic selection of representative pixels from trees and soil.

Later, the parameters mean and standard deviation of tree and soil pixel values in all bands of the image are computed. In each band, the intersection of the adjusted Gaussian curves defined by tree and soil statistical parameters is determined.

The selection of clusters representing trees in the unsupervised classified image is done by defining two thresholds. Thus, a cluster of pixels is selected as a tree cluster when the mean value of every band is included in the interval limited by two thresholds (Fig. 6). The lower threshold is determined as the mean value of pixels belonging to class tree minus 2.5 times the standard deviation, and the upper threshold is the value obtained in the previous step as the intersection of the modelled Gaussian distribution curves. As a result of this, a binary image is obtained representing a mask of the plot area covered by trees. The Fraction of Vegetation Cover, that is, the proportion of vegetation cover per unit area, is computed as the amount of pixels masked as trees in the binary image divided by the total number of pixels in the parcel.

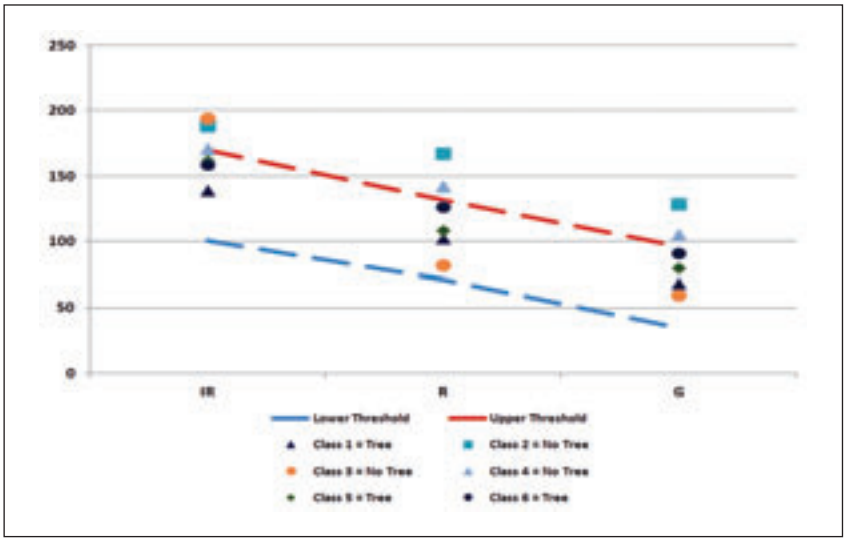

Fig. 6. Identification of classes corresponding to trees.

D. Post-processing

After obtaining image mask representing the area covered by trees by means of image classification or clustering, a post-processing is required in order to isolate the trees and to determine the individual tree cover area. In the case of contiguous trees with overlapping crowns, they are initially detected together in the same cluster, making difficult the tree counting process. The following steps are proposed to individualize the trees (Fig. 7):

1. The minimum distance from every pixel corresponding to a cluster of trees in the binary mask (Fig. 7b) to the background of the image is computed, obtaining a map of distances (Fig. 7c).
2. Over the distances image, an iterative local maxima search is applied using search windows of variable size. The sizes of the search windows range from the minimum to the maximum size of the trees in the area of study. As a result of this, a map of maxima is obtained (Fig. 7d).

3. Around every maximum a circle is drawn centered on it (Fig. 7e). The radius of this circle is the value of the distance from the maximum to the background. Pixels inside this circle will not be selected as maxima in the following steps. The location of the maxima obtained is assumed to correspond to the tree apex. In this process, the maximum size of the search windows should be greater than the biggest tree in the area of study, since an excessive size does not produce errors in the location of trees. However, the minimum size of the search windows should be accurately fixed, otherwise over-detection of trees can occur.
4. When all the maxima are selected, every pixel in the binary mask is assigned to the closest maximum in the same group of pixels. In this way, the groups of pixels in the binary mask are divided in smaller groups corresponding to the actual trees in the parcel (Fig. 7f).

This methodology enables to detect trees with different sizes and to obtain information about their location, quantity and size.

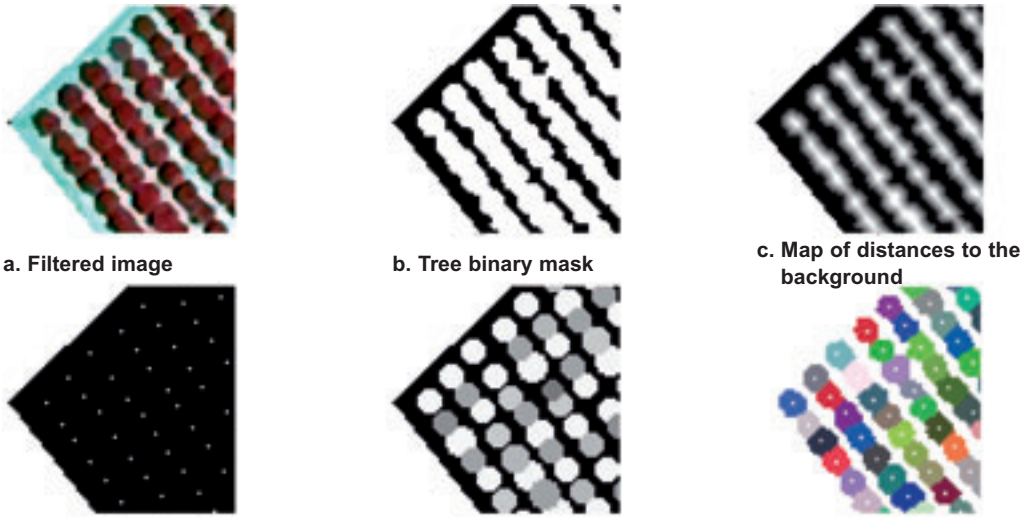

Fig. 7. Process of tree individualization.

IV – Extraction of agronomic parameters

Once finished the methodological procedure for tree detection and individual definition of tree crown cover, a set of agronomic parameters can be derived at tree and parcel levels. In this section we list and describe how they are extracted.

1. Per-tree parameters

Different descriptive parameters or attributes related to the tree location, size, shape and spectral properties can be computed from each cluster of pixels that represent a tree. Table 1 shows some of these parameters that can be directly derived from each segmented tree.

Table 1. Parameters extracted at tree level

Parameter	Abbreviation	Meaning	Units
Identifier	ID	Identifying numeric tag	–
Area of the tree	AT	Number of pixels assigned to the tree cluster	pixels
Coordinates of the centroid of the tree	X, Y	Coordinates of the maximum pixel	column, row
Estimated radius	R	Minimum distance from the maximum pixel to the background	pixels
Accumulated digital number or pixel values	ADN	Summatory of the pixel values inside a tree cluster	DN (pixel value)
Average digital number	MDN		DN (pixel value)

Parameters ADN and MDN can be extracted from all the layers or bands, or any combination or ratio derived from a multispectral image.

2. Per-parcel parameters

A variety of indices or parameters can be derived at parcel level, some of them as a result of generalizing the tree level parameters, and others related to global information (fraction of vegetation cover), or to the arrangement and distribution of trees in the parcel (tree planting pattern). In this sense, particular techniques such as the Hough transform can be used to accurately obtain this type of information.

The Hough transform (Hough, 1962) is a technique commonly used in digital image processing to detect lines or curves. It is based on the transformation of the coordinates of the centroids of trees from a Cartesian image space (X, Y) to a polar coordinate space (ρ, u), where ρ represents the minimum distance from the origin of coordinates to a line, and υ is the angle of the vector from the origin to the closest point of the line with the X axis (Fig. 8). Each point in the Cartesian space is transformed in a sinusoid in the polar space. This sinusoid represents the parameters of the lines passing through that point. The intersection of two sinusoids in the polar space represents the parameters of the particular line passing through these points.

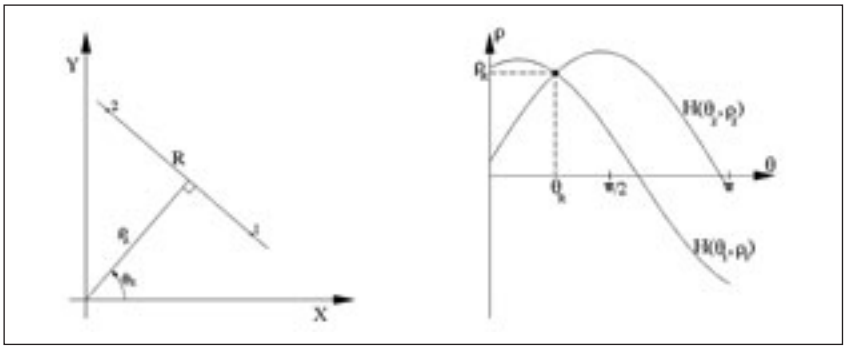

Fig. 8. Representation of a line in Cartesian and in the Hough space.

This transform is applied to the locations of the detected trees in the parcel (Fig. 9b). The results of this transformation are shown in the graph of Fig. 9c, where each intersection represents a line

in the image. From this graph, the parameters of the lines passing through a number of points can be obtained. Representing the frequency of the lines in the range of directions from 0º to 179º, the two most frequent directions, corresponding to the two main alignments of trees in the parcel, can be extracted (Fig. 9d). Once the two main directions are known, the median value of the distance between the lines in both directions gives us a measure of the separation of trees in the parcel or planting pattern (Figs 9e and 9f). The final parameters extracted from this methodology are the distance between the tree alignments in the two main directions, and the angular difference between these directions. If this angular difference is close to 90º means that the planting pattern follows a typical rectangular arrangement.

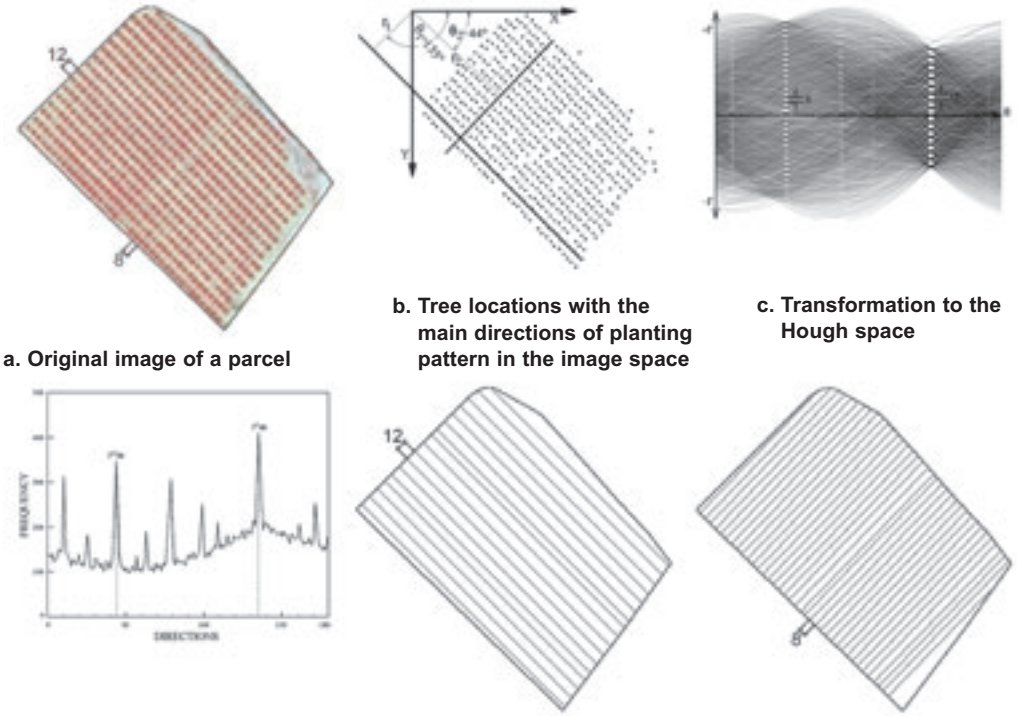

a. Original image of a parcel

b. Tree locations with the main directions of planting pattern in the image space

c. Transformation to the Hough space

d. Histogram of intersections of lines

e. Alignments in the first direction

f. Alignments in the second direction

Fig. 9. Procedure followed to determine the planting pattern from the Hough transform.

Based on this methodology, the set of parameters extracted after generalization of tree level parameters and those related to the geometric arrangements of trees in the parcel are described in Table 2.

Parameters related to pixel values can be extracted from all the layers or bands, or any combination or ratio derived from a multispectral image.

Table 2. Parameters extracted at parcel level

Parameter	Abbreviation	Meaning	Units
Area of the parcel	AP	Number of pixels in the parcel	Pixels
Number of trees	NT	Number of trees in the parcel	Trees
Area covered by trees	ACT	$\sum_{i=1}^{NT} AT_i$	Pixels
Average area of trees	MAT	ACT/NT	Pixels
Fraction of vegetation cover	FVC	ACT/AP	–
Average radius of trees	MR	$\sum_{i=1}^{NT} R_i / NT$	Pixels
Coefficient of variation of radius	CVR	$\frac{\sqrt{\sum_{i=1}^{NT} (R - MR)^2 / NT}}{MR}$	–
Density of trees per hectare	DT	$(10000 \cdot NT)/(AP \cdot pixel\ size)$	Trees / ha
Accumulated digital number of the trees	ADNT	$\sum_{i=1}^{NT} ADN_i$	DN (pixel value)
Accumulated digital number of the parcel	ADNP	Summatory of the DN of the pixels in the parcel	DN (pixel value)
Average digital number of the trees	MDNT	$ADNT/ACT$	DN (pixel value)
Average digital number of the parcel	MDNP	$ADNP/AP$	DN (pixel value)
Size of the planting pattern	SPP1, SPP2	Median of the distances between the lines in the two main directions	Meters
Angular difference between the directions of the planting pattern	ADPP	Difference between the two main directions	Degrees

V – Tree segmentation assessment

In order to evaluate the quality of the tree segmentation, the automatically obtained area covered by trees must be compared with reference data obtained with field measurements or manual digitization over the aerial orthoimages. Comparison results are commonly expressed by means of the branching factor, the miss factor and the quality percentage. The branching factor (Equation 4) is a measure of the over-detection of tree cover areas. The more accurate the detection, the closer the value is to zero. The miss factor (Equation 5) indicates the omission error in the detection of tree cover areas. These quality metrics are closely related to the boundary delineation performance of the tree extraction methodology. The quality percentage (Equation 6) measures the absolute quality of the detection model by combining aspects of boundary delineation accuracy and tree detection rate to summarize the system performance (Hermosilla *et al.*, 2011).

$$BF = \frac{100 \cdot FP}{TP + FN} \tag{4}$$

$$MF = \frac{100 \cdot FN}{TP + FN} \tag{5}$$

$$QP = \frac{100 \cdot TP}{TP + FP + FN} \tag{6}$$

These metrics are derived from the True Positive (TP), False Positive (FP) and False Negative (FN) values. TP represents those pixels corresponding to trees that are correctly detected, FP are those pixels not corresponding to trees but erroneously selected as trees, and FN represent the pixels corresponding to trees that are not detected (Fig. 10). The quality percentages of the area covered by trees in our study area range from 70% to 90%, obtaining the best results in the case of adult citrus trees.

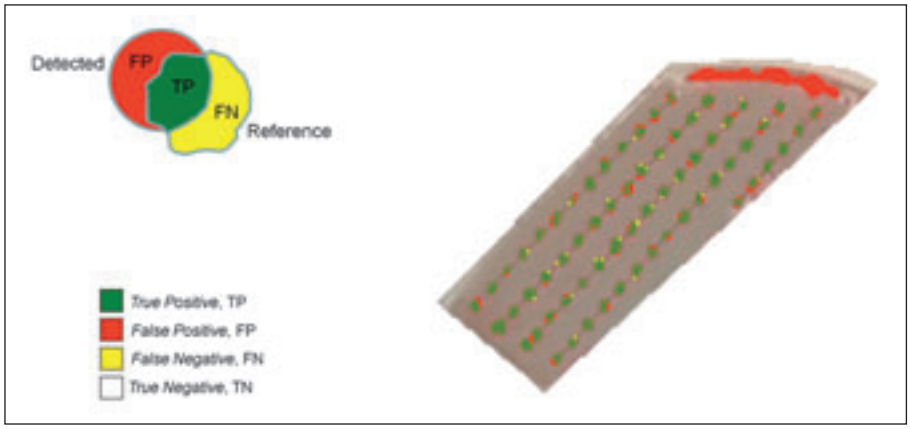

Fig. 10. Representation of the metrics used for evaluation (left) and example of their application to a citrus plot.

Planting pattern extraction assessment can be expressed by means of the root-mean-square error (Equation 7):

$$RMSE = \sqrt{\frac{\sum_{i=1}^{n} (d_i - d_{iobs})^2}{n}} \tag{7}$$

where n is the number of parcels, d_{iobs} is the observed dimension of the planting pattern and d_i is the predicted dimension automatically obtained. The overall performance of the method shows that trees are located with a mean error of 40 cm, and plantation patterns determined with a root-mean-square error of 22 cm.

VI – Conclusions

This work presents an automated methodology based on digital image processing of high spatial resolution multispectral imagery for computing a set of per-tree and per-parcel agronomic parameters that exhaustively characterize tree crops. This methodology is based on common image processing tools and it has been tested over citrus orchards in the province of Valencia (Spain). High spatial resolution multispectral aerial images (0.5 m/pixel) have been used in the tests, obtaining accurate results in the estimation of agronomic parameters. The quality percentages of the area covered by trees range from 70% to 90%, obtaining the best results in adult citrus trees, being more discrete in the case of young trees. The same methodology could be applied using high-resolution satellite imagery, expecting to obtain similar results.

These techniques can be massively applied to large agricultural databases in order to extract information regarding tree location, tree counting, crown size, canopy cover or tree spatial arrangement. This information, combined with precision agriculture techniques, can be used to improve the efficiency of irrigation and fertilization processes, detection of crop diseases, assessment of crop weather damages, harvest estimation, etc. Additionally, these methods may support the updating processes of agricultural inventories, and the parameters presented can be used as input information for semi-automatic parcel-based classification of agricultural databases, reducing field work or manual interpretation of the images, which are time consuming and expensive.

Acknowledgments

The authors appreciate the financial support provided by the SUDOE program (TELERIEG Project SOE1/P2/E082), and the Spanish Ministry of Science and Innovation and FEDER in the framework of the project CGL2010-19591/BTE.

References

Culvenor D.S., 2002. TIDA: an algorithm for the delineation of tree crowns in high spatial resolution remotely sensed imagery. In: *Computers & Geosciences*, 28, p. 33-44.

Dralle K. and Rudemo M., 1997. Stem number estimation by kernel smoothing of aerial photos. In: *Canadian Journal of Forest Research,* 26, p.1228-1236.

Du Q., Orduyilmaz A., Yang C. and Everitt J.H., 2005. Detecting citrus tree size, centroid, and health conditions from airborne high-spatial-resolution multispectral imagery. In: *Proceedings of ASPRS 2005 Annual Conference "Geospatial Goes Global: From Your Neighborhood to the Whole Planet",* March 7-11, Baltimore, Maryland.

Erikson M., 2004. Species classification of individually segmented tree crowns in high-resolution aerial images using radiometric and morphologic image measures. In: *Remote Sensing of Environment*, 91, p. 469-477.

Erikson M. and Olofsson K., 2005. Comparison of three individual tree crown detection methods. In: *Machine Vision and Applications*, 16 (4), p. 258-265.

García Torres L., Peña-Barragán J.M., López-Granados F., Jurado-Expósito M. and Fernández-Escobar R., 2008. Automatic assessment of agro-environmental indicators from remotely sensed images of tree orchards and its evaluation using olive plantations. In: *Computers and Electronics in Agriculture*, 61, p. 179-191.

Gougeon F.A., 1995. A crown-following approach to the automatic delineation of individual tree crowns in high spatial resolution aerial images. In: *Canadian Journal of Remote Sensing*, 21(3), p. 274-284.

Hermosilla T., Ruiz L.A., Recio J.A. and Estornell J., 2011. Evaluation of Automatic Building Detection Approaches Combining High Resolution Images and LiDAR Data. In: *Remote Sensing*, 3(6), p.1188-1210.

Hough P.V.C., 1962. Methods and means for recognizing complex patterns. U.S. Patent No. 3069654.

Leckie D.G., Gougeon F.A., Walsworth N. and Paradine D., 2003. Stand delineation and composition estimation using semi-automated individual tree crown analysis. In: *Remote Sensing of Environment*, 85, p. 355-369.

Mazzetto F., Calcante A., Mena A. and Vercesi A., 2010. Integration of optical and analogue sensors for monitoring canopy health and vigour in precision viticulture. In: *Precision Agriculture*, 11, p. 636-649.

Pollock R., 1996. The automatic recognition of individual trees in aerial images of forests based on a synthetic tree crown model. PhD Thesis, Dept. Computer Science, University of British Columbia, Vancouver, Canada.

Pouliot D.A., King D.J., Bell F.W. and Pitt D.G., 2002. Automated tree crown detection and delineation in high-resolution digital camera imagery of coniferous forest regeneration. In: *Remote Sensing of Environment*, 82, p. 322-334.

Recio J.A., 2009. Técnicas de extracción de características y clasificación de imágenes orientada a objetos aplicadas a la actualización de bases de datos de ocupación del suelo. PhD Thesis. Universitat Politecnica de Valencia, Valencia, Spain.

Ruiz L.A., Recio J.A. and Hermosilla T., 2007. Methods for automatic extraction of regularity patterns and its application to object-oriented image classification. In: *International Archives of Photogrammetry, Remote Sensing and Spatial Information Sciences*, Volume 36, 3/W49A, p. 117-121.

Ruiz L.A., Recio J.A., Fernández-Sarría A. and Hermosilla T., 2011. A feature extraction software tool for agricultural object-based image analysis. In: *Computers and Electronics in Agriculture*, 76, p. 284-296.

Viau A.A, Jang J.D, Payan V. and Devost A., 2005. The use of airborne Lidar and multispectral sensors for orchard trees inventory and characterization. In: *Proceedings of Information and Technology for Sustainable Fruit and Vegetable Production FRUTIC05*, 12-16 September, Montpellier France, p. 689-698.

Wang J., Sammis T.W., Andales A.A., Simmons L.J., Gutschick V.P. and Miller D.R., 2007. Crop coefficients of open-canopy pecan orchards. In: *Agricultural Water Management*, 88, p. 253-262.

Wulder M., Niemann K.O. and Goodenough D.G., 2000. Local maximum filtering for the extraction of tree locations and basal area from high spatial resolution imagery. In: *Remote Sensing of Environment*, 73, p. 103-114.

Thermal infra-red remote sensing for water stress estimation in agriculture

S. Labbé*, V. Lebourgeois, A. Jolivot** and R. Marti***

*Cemagref, 500 rue JF Breton, 34093 Montpellier (France)
**Cirad, UMR TETIS, Remote Sensing Center, 500 rue JF Breton, 34093 Montpellier (France)

Abstract. Thermal infrared images can be used to estimate vegetation water content of the plant and thus to locally adapt (precision agriculture) and globally adjust (sustainable management of water resources) irrigation water quantities. Thermal imaging cameras using micro-bolometer sensors loaded on light aerial vehicles are suitable to produce thermal images. These images are helpful for irrigation monitoring if they are: (i) coupled with simultaneous acquisition of images in the visible and near infrared bands; (ii) geometrically corrected to be superimposed with other images; and (iii) radiometrically corrected to take into account the drift of the thermal sensors and the effects of the atmosphere on the measured temperature.

Keywords. Thermal infrared images – Irrigation monitoring – Water stress – Remote sensing – Airborne images – Surface temperature – Vegetation.

Télédétection infrarouge thermique: application à la mesure du stress hydrique en agriculture

Résumé. *La thermographie infrarouge appliquée à la végétation permet d'estimer le contenu en eau de la plante et ainsi d'adapter des conduites d'irrigation différenciées (agriculture de précision) et précises (gestion raisonnée de la ressource en eau). Les caméras thermiques utilisant des détecteurs de type microbolomètre embarqués à bord d'aéronefs légers peuvent être utilisés pour réaliser des images thermiques. Ces images sont utilisables à des fins de conduite d'irrigation sous réserve : (i) d'être couplées à des acquisitions d'images dans le domaine du visible et du proche infrarouge ; (ii) d'être corrigées géométriquement pour être superposables aux autres données ; et (iii) d'être corrigées radiométriquement pour prendre en compte les dérives liées au capteur et les effets de l'atmosphère sur la température mesurée.*

Mots-clés. *Image thermique – Gestion de l'irrigation – Stress hydrique – Télédétection – Imagerie aérienne – Température de surface – Végétation.*

I – Introduction

Irrigation uses 70% of the water used worldwide. In a context of increasing food demand and scarcity of water resources, development of strategies to optimize water use in agriculture is a major challenge for sustainable development.

The rational management of water resources assumes a space and time optimization of water inputs across each plot. To achieve this objective the water needs of the crop must be determined. There are many methods to characterize, *in situ*, the water status of crops, however, they are often destructive and expensive.

Remote sensing data can provide a number of information on water status and health of crop and could assist in decision-making on irrigation. Recent developments (miniaturization) on light cameras in the visible and infrared bands and on vectors (satellites with high temporal repetitiveness, aerial light vectors) provide new ways of regular, non-destructive, monitoring of crops.

However, the use of remote sensing in agriculture is limited because of inadequacy of spatial, temporal and thematic products tailored to the needs of farmers.

To overcome these obstacles, Cemagref and CIRAD conduct applied research to develop technical solutions for original acquisition and processing of remotely sensed data. At the plot level, the solutions are based on ultra light aerial vehicles, equipped with low cost light sensors.

This paper shows geometric and radiometric preprocessing of data from uncooled thermal cameras to enable the integration of these data in spatial irrigation models.

II – Vegetation hydric stress

Producing one ton of crop needs about 100 tons of water. About 1% of the absorbed water is incorporated in the crop tissues, the rest is lost through transpiration (99%). This water is essential for the functioning of the plant and allows the regulation of leaf temperature and facilitates the absorption of nutrients through the roots.

Water requirements vary with the stage of plant growth and weather conditions (temperature and humidity, wind, etc.). The plant takes needed water from the ground. If there is a water deficit, in order to reduce water loss the plant closes its stomata. This will result in physiological changes (Fig. 1): (i) a decreased transpiration; (ii) a reduction in photosynthesis; (iii) an increase in leaf temperature.

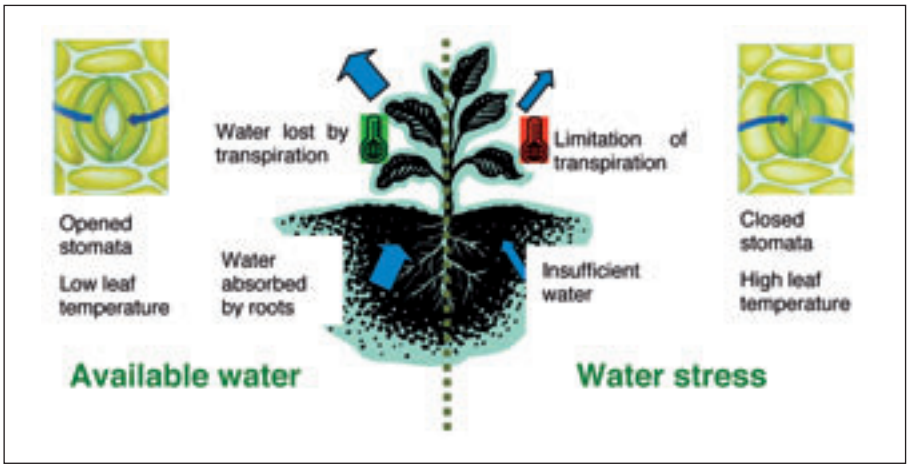

Fig. 1. Plant response to water stress.

According to its intensity, water stress can result in loss of quality. Significant water deficits can lead to irreversible changes leading to a significant drop in yield.

III – Remote sensing images of vegetation

1. Visible, near and middle infrared bands

When sunlight comes into contact with an object, it can be reflected by the surface of the object, absorbed or transmitted to lower levels. The spectral signature of an object is the expression of the reflectance (ratio of the radiance reflected by the object from the incident radiation, expressed in %) as a function of wavelength.

The common characteristic of all vegetation is to have a low reflectance curve in the visible (due to strong absorption by leaf pigments), high in the near infrared (spectral region sensitive to the amount of biomass) and through the medium infrared (mainly influenced by the water content of the canopy) (Fig. 2). Mineral surfaces (rocks, bare soil ...) have a spectral signature which increases from blue to near infrared. Water absorbs all infrared radiations.

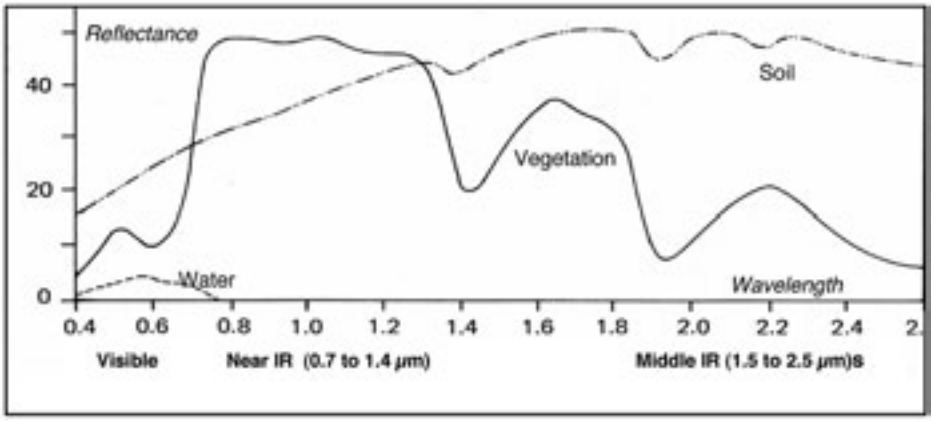

Fig. 2. Typical spectral signature of soil, vegetation and water (Lilliesand and Kieffer, 1987).

On a plot, the reflectance is a combination of spectral signatures of soil and vegetation, which depends on the amount of leaves. Vegetation indices based on combinations of spectral bands in the visible and near infrared, are useful to estimate the amount of vegetation from the images. One of the most common indices :NDVI (Normalized Difference Vegetation Index) is calculated from reflectance in the red and near infrared bands : NDVI = (R-NIR)/(R+NIR) (Fig. 3).

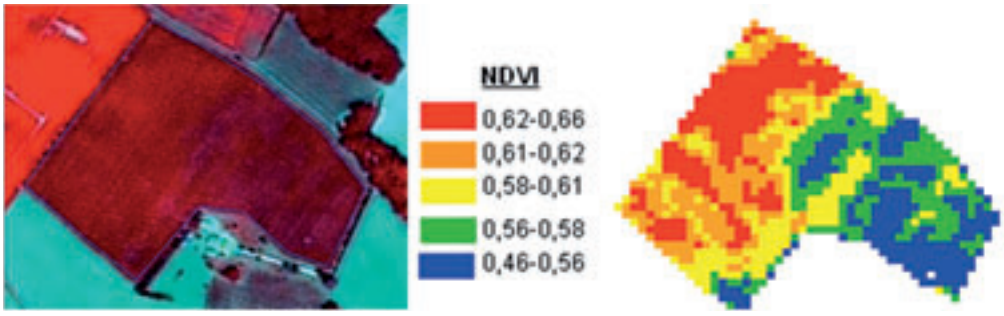

Fig. 3. Example of a 2009 SPOT image and NDVI values (Telerieg project - ANPN plot - Gers, France).

2. Thermal infrared band

Every object emits energy proportionally to the fourth power of its surface temperature (Stefan-Boltzmann law). The amount of energy emitted depends on the wavelength, the wavelength where the emission is maximum is greater as the temperature decreases. For most of the land surface-vegetation (between –20 and 50°C), this maximum corresponds to a wavelength near 10 microns (Fig. 4).

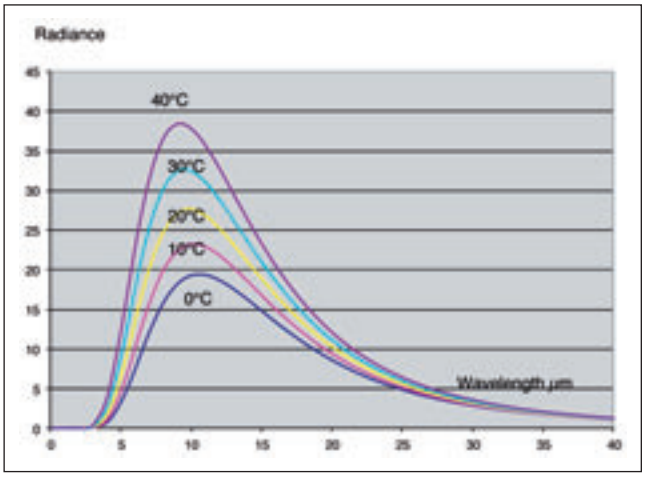

Fig. 4. Black body radiance – Plank Law.

For an ideal black body, it is possible, by measuring the emitted energy in a range of wavelength, to find the surface temperature of the body. However, natural surfaces behave like a gray body with emissivity that varies with the nature of the object. Vegetation cover have an emissivity between 0.95 and 0.99, higher when they are rich in chlorophyll and water (with an average of 0.98, meaning that the surface emits 98% of the energy emitted by blackbody at the same temperature).

Between 8 and 12 microns, solar radiation is negligible and the atmosphere is quite transparent. The measurement of radiation emitted by the Earth's surface in this spectral range and the knowledge of the emissivity of objects allows to estimate the surface temperature of vegetation.

If in addition if the air temperature is known (e.g. a weather station nearby), then the difference between surface temperature of the canopy and air temperature provides a good indicator of the water status of the plant (Fig. 5):

(i) If there is available water, due to transpiration, the plant temperature decreases and the difference between air temperature and canopy temperature increases;

(ii) During periods of water stress, the crop limits its transpiration using stomata regulation and the temperature of the plant increases.

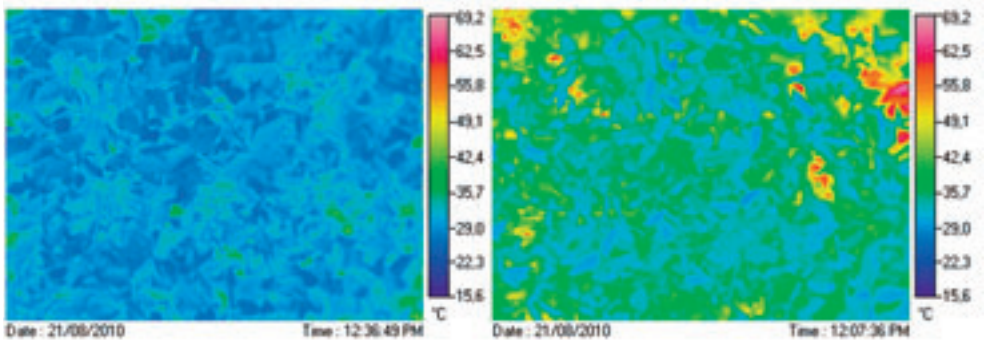

Fig. 5. Example of thermal images on soya bean plot - irrigated (left) and rainfed (right) part of the plot Telerieg project 2010- Experimental plot of Cemagref - Montpellier – France.

To approximate water stress with thermal data, one of the most widely used index is the Crop Water Stress Index (CWSI) (Idso *et al.* 1981) which takes into consideration the temperature of the plant, air temperature and relative humidity. CSWI is convenient for fully coverage crops. For crops like orchards, surface temperature measurement is a composite of soil temperature and canopy temperature. To find the temperature of the plant, the culture coverage must be computed, usually derived from a vegetation index (Lebourgeois 2009). The measure will be especially significant if the air temperature is high (i.e. hot weather at noon or early afternoon) and without strong wind.

Current satellites carrying sensors in the thermal infrared band, as ASTER (Advanced Spaceborne Thermal Emission Terra and Reflection Radiometer) or Landsat ETM + (Landsat Enhanced Thematic Mapper Plus) are of limited use for precise irrigation control because:

(i) Spatial resolution is insufficient (ASTER 90m, Landsat 60m);

(ii) The image acquisition is early in the morning (9 to 10 am in solar time) and water stress on crops does not result in significant differences in temperature;

(iii) The temporal resolution is low (one image every 16 days for Landsat) and should be synchronous with a clear sky.

Due to these limitations thermal satellite images are not useful at plot scale for precise irrigation monitoring. Aerial images are today more convenient, waiting for more efficient future satellites.

IV – Image acquisition devices

Many aircrafts can be used for low altitude image acquisition: small helicopter, ultralight aircraft (ULA), or unmanned aerial vehicles (UAV) (Fig. 6).

Fig. 6. Examples of aircrafts - UAV (hexacopter, Telerieg project) and ULA.

Onboard sensors include commercial visible and near infrared cameras (NIR cameras are modified commercial visible cameras) and thermal cameras (Figs 7 and 8).

During Telerieg project visible cameras (like Sony A 850 with 50 mm lens) and 320*240 pixels (like FLIR B20) thermal cameras were used.

The flight altitude was determined by the spatial resolution required. this resolution varies according to the sensors (Table 1). In the case of orchard a spatial resolution of 30 cm in the thermal band is necessary so that individual trees are visible on the images. For continuous crops, like durum wheat, a lower resolution can be used.

Fig. 7. Examples of visible and modified near infrared cameras on an ULA.

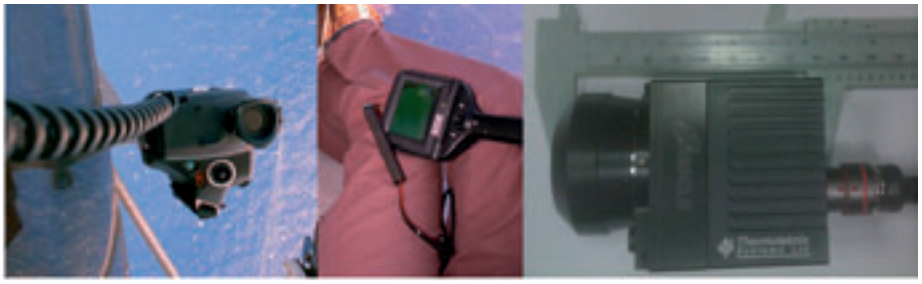

Fig. 8. Examples of thermal camera with remote screen control on ULA - small thermal camera for UAV.

Table 1. Resolution of images

Flight altitude over canopy	900 m (durum wheat)	300 m (apple orchard)
Visible and NIR resolution	10 cm	3 cm
Thermal resolution	1 m	30 cm
Swath	340 m	100 m

V – Thermal images preprocessing

1. Geometric correction

Images acquired using thermal cameras could have large geometric distorsions. In order to use these images for the calculation of indices of water stress it is necessary to correct the images geometrically (Fig. 9). Several approaches are detailed in Pierrot Desseligny *et al.* (2008).

In order to reference the thermal, visible and NIR images in a geographic information system (using an appropriate projection system) identifiable points whose coordinates are well known in the field are needed (The navigation systems used on ULA or UAV do not allow a very precise positioning of the images).

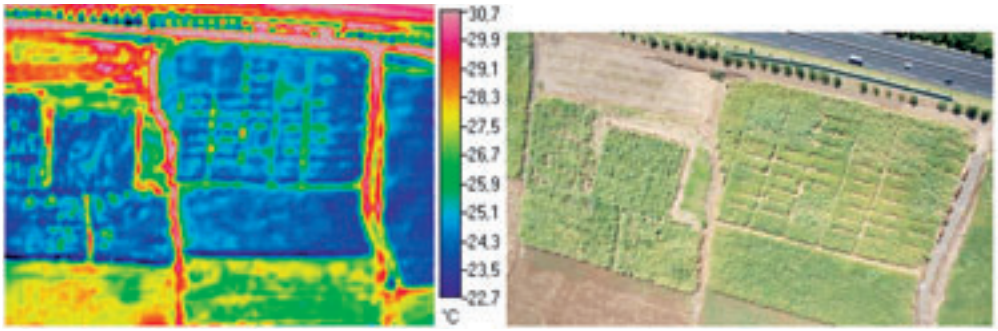

Fig. 9. Examples of thermal and visible images before geometric correction.

In order to have points visible in thermal images as in visible images, specific targets were used: a composition of an aluminium plate (noticeable in thermal image due to a very low emissivity) with a fine reflective cross sign (for visible and NIR images. Targets were positioned with a centimetre precision using a differential GPS system (Joliveau 2011) (Fig. 10).

Fig. 10. Aluminium targets – Position measurement – Targets seen as cold points on thermal image.

2. Radiometric correction

The thermal image is obtained through a matrix of uncooled microbolometers. Each individual microbolometer has a signal-noise ratio of about one celcius degree. This uncertainty is (just) consistent with the objectives of accuracy desired for use in agronomy (Pinter *et al.*, 1990).

Moreover the thermal radiance emitted by the crop is modified by the atmosphere between the crop and the sensor. The atmosphere: (i) reduces the original signal (by absorption and diffusion); and (ii) add its own signal (linked to the atmosphere temperature and contents)

In order to evaluate the atmosphere effects several images were taken of the same plot at several altitude. The next figure shows how the atmosphere (cooler than the soil) reduces the apparent measured temperature (Fig. 11).

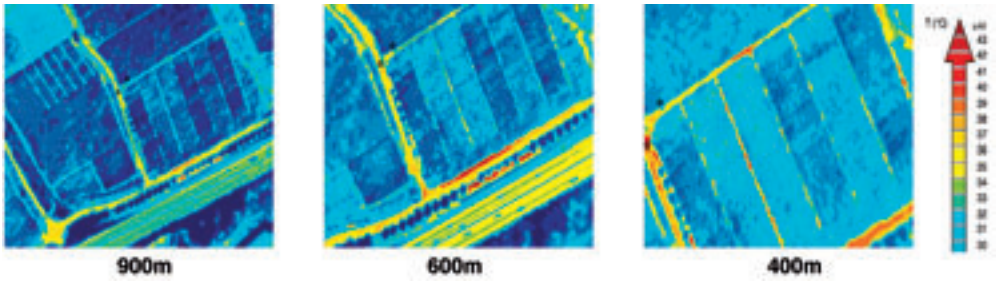

Fig. 11. Same plot at different altitudes.

As the hydric stress of vegetation is computed using a difference between air temperature and crop temperature the atmosphere effect needs to be corrected so that the crop temperature could be retrieved.

The correction of these effects can be made from measurements of *in situ* targets located in the studied area (e.g. using cold and hot targets to interpolate a range of temperature) and large enough to cover several pixels of the image. Targets' temperature are measured from the ground during the aircraft acquisition and used to correct images for atmospheric effects.

Several targets were tested during the Telerieg project. Due to a low emissivity EPS (polystyrene) is appropriate to simulate a cold surface, hot surfaces are generally existing (bare soils, roads, etc.) or can be simulated using dark materials (like black plastic sheeting) (Fig. 12).

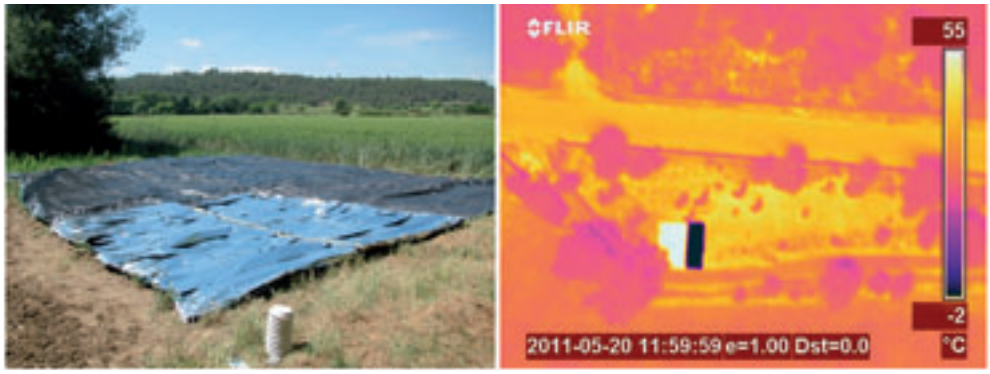

Fig. 12. Example of cold and hot targets on the field and in the thermal image.

This approach with hot and cold targets is efficient but costly, imposing a field operator with a thermal sensor during the aerial acquisition.

As an alternative, the use of radiative transfer models is interesting but requires the use of detailed atmospheric profiles (temperature, humidity, pressure, aerosols and gas molecules) (Jacob *et al.*, 2004). These data are often unavailable or do not coincide in time or space for local use.

To overcome this lack of data, a temperature and humidity sensors, connected to a data logger, was installed on the aircraft. This system allows to log a simplified profile atmospheric temperature / humidity during the phases of ascent and descent of the aircraft. This approach is convenient if the aerial data uses a UAV taking off from the plot.

These data were then used in a radiative transfer model developed by ONERA (MATISSE Advanced Earth Modeling for Imaging and Simulation of the Scenes and their Environment) (Simoneau *et al.*, 2001).

Using atmospheric profile and MATISSE software a first correction could be applied to overcome the atmosphere effect in the image according to the flight altitude (Marti, 2011) (Fig. 13).

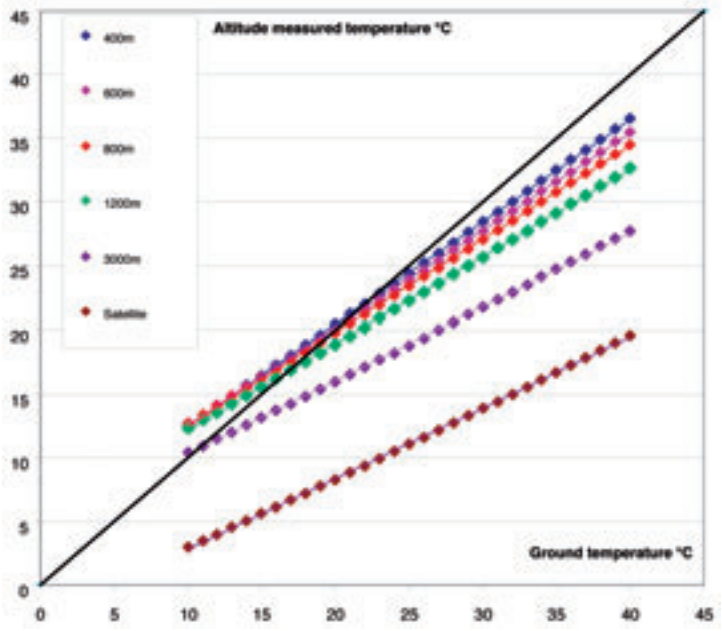

Fig. 13. Example of temperature correction using MATISSE.

VI – Conclusion

The development of uncooled thermal cameras can be considered as useful in airborne precision agriculture for irrigation monitoring and therefore for better management and conservation of water resources. Data preprocessing is still complicated and the results are at the limit of accuracy desired for operational use. Progress needs to be done (and are expected) on:

(i) Sensors such as improved thermal resolution.

(ii) Easier usability in radiative transfer models.

(iii) Physical / agronomic better determination of the relationship between the behavior of the vegetation and the signal measured in the thermal infrared.

In this objective, Cemagref and CIRAD continues this research today, with several scientific and operational partners in the South-western Europe (southern France, Spain, Portugal) thanks to the Telerieg project (Interreg IV-B SUDOE Programme).

References

Idso S.B., Jackson R.D., Pinter P.J., Reginato R.J. and Hatfield J.L., 1981. Normalizing the stressdegree-day parameter for environmental variability. In: *Agricultural Meteorology*, 24, p. 45-55.

Jacob F., Petitcolin F., Schmugge T., Vermote E., French A. and Ogawa K., 2004. Comparison of land surface emissivity and radiometric temperature derived from MODIS and ASTER sensors. In: *Remote Sensing of Envi ronment,* 90, p. 137-152.

Joliveau A., 2011. Usage de la télédétection pour le suivi de l'état hydrique des cultures. Mémoire de Master SILAT Agroparistech. 50 p.

Labbé S., Roux B., Lebourgeois V. and Bégué A., 2007. An operational solution to acquire multispectral images with standard light cameras: spectral characterization and acquisition guidelines. In: *ISPRS worshop - Airborne Digital Photogrammetric Sensor Systems,* Newcastle, England, 11-14 Sept.

Lebourgeois V., Bégué A., Labbé S., Mallavan B., Prévot L. and Roux B., 2008. Can Commercial Digital Cameras Be Used as Multispectral Sensors? A Crop Monitoring Test. In: *Sensors*, 8, p. 7300-7322.

Lebourgeois V., Labbé S., Bégué A. and Jacob, F., 2008. Atmospheric corrections of low altitude thermal airborne images acquired over a tropical cropped area. In: *IEEE International Geoscience and Remote Sensing Symposium, Boston, Massachusetts,* USA, 6-11 July 2008.

Lebourgeois V., 2009. Utilisation d'un système léger d'acquisitions aéroportées dans les domaines optiques réflectif et thermique pour la caractérisation de l'état hydrique et nutritionnel des cultures. Thèse de doctorat – Université de la Réunion, 21/04/2009, 174 p.

Marti R., 2011. Corrections atmosphériques d'images infrarouges thermiques acquises par système léger aéroporté à basses altitudes. Mémoire MsC SIIG3T - Université Montpellier III, 44 p.

Pierrot-Desseligny M. Labbé S., 2008. Relative geometric calibration of a thermal camera using a calibrated RGB camera. In: *ISPRS 2008 – WG I/4 – Airborne Digital Photogrammetric Sensor Systems.*

Pinter Jr P.J., Jackson R.D. and Moran M.S., 1990. Bidirectional reflectance factors of agricultural targets: A comparison of ground-, aircraft- and satellite-based observations. In: *Remote Sensing of Environment*, 32, p. 215-228.

Simoneau P., Berton R., Caillault K., Durand G., Huet L., Labarre C., Malherbe C., Miesh C., Roblin A. and Rosier B., 2001. MATISSE, Advanced Earth Modeling for Imaging and Scene Simulation. In: *ESO/SPIE Europto European Symposium on Remote Sensing,* Toulouse, FR, 17-21 September 2001.

Contribution of airborne remote sensing to high-throughput phenotyping of a hybrid apple population in response to soil water constraints

N. Virlet*, S. Martínez*, V. Lebourgeois, S. Labbé** and J.L. Regnard***

*INRA Cirad, UMR AGAP,TA A-108/03, Avenue Agropolis, 34398 Montpellier Cedex 5 (France)
**Cemagref, Cirad, UMR TETIS, Remote Sensing Center, 500 rue JF Breton, 34093 Montpellier (France)

Abstract. In this study, we developed a remote sensing approach, normally applied to management of crop irrigation, with the purpose of phenotyping a plant population in the field. The experiment was performed on 'Starkrimson' x 'Granny Smith' apple progeny (122 hybrids, 4 replicates) at adult stage, cultivated in field on Diaphen platform (INRA Montpellier, France). Airborne images acquisition in RGB and NIR bands permit to compute the Normalized Difference Vegetation Index (NDVI), while differences between tree canopy surface measured by thermal IR imaging (T_s) and air temperature (T_a) made it possible to calculate water stress indices. The Water Deficit Index (WDI), derived from the Crop Water Stress Index (CWSI), was considered for its applicability to discontinuous plant cover. WDI was computed on each individual tree, and focused on its central zone (60 cm diameter buffer). The first results showed significant genotypic effects and drought effects for indices during imposed summer water shortage, without interaction between them. Moreover, this first experiment permits to determine field measurements that are necessary to validate the method, linking image interpretation and tree water status variables.

Keywords. *Malus domestica* Borkh – Genetic variability – Water stress – Thermal imaging – Airborne images acquisition.

Contribution de la télédétection aérienne au phénotypage à haut débit pour une population de pommiers hybrides en réponse aux contraintes hydriques du sol

Résumé. *Dans le cadre de cette étude, nous avons développé une approche de télédétection, normalement appliquée à la gestion de l'irrigation des cultures, afin de phénotyper une population végétale aux champs. L'expérience a été effectuée sur une descendance de pommiers 'Starkrimson' x 'Granny Smith' (122 hybrides, 4 répétitions) au stade adulte, cultivés aux champs sur plate-forme Diaphen (INRA Montpellier, France). L'acquisition d'images aériennes dans les bandes RGB et NIR a permis de calculer l'Indice de Végétation Normalisé (NDVI), tandis que les différences entre la surface de la canopée des arbres mesurée par images thermiques IR (Ts) et la température de l'air (Ta) ont permis de calculer les indices de stress hydrique. L'Indice de Déficit Hydrique (WDI), dérivé de l'Indice de Stress Hydrique des Cultures (CWSI), a été considéré en raison de son applicabilité à un couvert végétal discontinu. Le WDI a été calculé pour chaque arbre individuel, en se focalisant sur sa zone centrale (avec une zone-tampon de 60 cm de diamètre). Les premiers résultats montrent des effets génotypiques significatifs et des effets de la sécheresse pour les indices pendant la pénurie d'eau imposée en été, sans interaction entre eux. De plus, cette première expérience permet de déterminer les mesures de terrain qui sont nécessaires pour valider la méthode, mettant en rapport l'interprétation des images et les variables liées à l'état hydrique des arbres.*

Mots-clés. Malus domestica *Borkh – Variabilité génétique – Stress hydrique – Imagerie thermique – Acquisition d'images aériennes.*

I – Introduction

Thermal imaging is generally used for water status monitoring and irrigation scheduling on annual crops. Leaf temperature is an indicator of water status and permits an estimation of stomatal conductance (Jones *et al.,* 1999). Water stress indices like CWSI have been developed since

some years (Idso *et al.,* 1981; Jackson *et al.,* 1981). They were designed for application to continuous cover, and revealed a particular interest in semi-arid and arid conditions, where active transpiration increases leaf to air temperature differences. Moran *et al.* (1994) proposed and developed an extension of CWSI to the partially covering crops, with the Water Deficit Index (WDI).

Taking into account the current high-throughput genotyping possibilities, it appears necessary to develop tools and approaches which could permit in parallel high-throughput phenotyping of plant traits (Berger *et al.,* 2010). For perennial crops such as fruit trees, measurements performed in controlled conditions at juvenile stage do not permit a straightforward prediction of mature tree behavior in field. Some leaf traits like stomatal conductance can be positively affected by the fruit acting as a sink, or be negatively affected by higher vapor pressure deficits which generally prevail. Moreover in the context of global change, the current breeding traits adopted in fruit trees such as fruit quality, pest and disease resistances, or regularity of yield, are not fully satisfying sustainable production objectives (Laurens *et al.,* 2000). New breeding traits could be proposed and implemented, consisting in better adaptation to water stress and/or better water use efficiency (Condon *et al.*, 2004; Regnard *et al.*, 2008).

On these bases, our study consisted in applying multispectral imaging to phenotyping plant responses to water stress. It was performed on an apple hybrid population where ecophysiological measurements are time consuming and produce variable results, along with the atmospheric variations affecting the crop (e.g. air temperature, wind speed, solar irradiance). Our work hypotheses were (i) that use of very high resolution imaging at tree scale (airborne image acquisition in RGB, NIR and TIR) will be a relevant method for phenotyping leaf traits at plant canopy scale – the whole population being considered at the same time; and (ii) that high resolution imaging and use of water stress indices will constitute a relevant and sensible method for discriminating plant stomatal response to water stress.

II – Material and methods

1. Location, field set-up and environmental measurements

The study was performed on an apple orchard located at Melgueil experimental farm and belonging to INRA Diaphen platform (Mauguio, 43°36'35N, 3°58'52 E). The plant material consisted in an apple progeny of 122 hybrids ('Starkrimson' x 'Granny Smith') repeated 4 times. Trees were grafted on M9 rootstock, and distributed along 10 rows within the plot, with 5 rows supporting a summer drought treatment: stressed trees (no irrigation, S), while 5 rows were well watered (not stressed trees, NS). The S and NS rows were alternated within the experimental set-up (Fig. 1). For normally watered trees, irrigation was scheduled according to soil water potential, with a microsprayer system located in the row, in line with professional practice. Environmental conditions were monitored by meteorological sensors. Global and photosynthetically active solar radiation, soil and air temperatures, air humidity, wind speed and precipitations were measured, averaged and stored by a CR10X data logger. Soil water status was monitored with capacitive and tensiometric probes.

2. Airborne image acquisition, field measurement

Image acquisition system was composed of two digital cameras Canon EOS 400D (10.1 Megapixel CMOS sensor) each equipped with an objective focal length of 35mm, and one thermal camera FLIR B20HS (320x240 matrix) for the acquisition of TIR images (8.5 to 14.0 µm). One digital camera acquired visible images in Red, Green and Blue bands (RGB) while the second was modified according to Lebourgeois *et al.* (2008) to acquire pictures in the Near Infrared (NIR). The 2010 airborne campaign comprised four ultra-light aircraft flights planned during summer 2010. One flight

(July 16) was scheduled before the application of water stress, two flights during the mid-summer soil water stress (August 3 and 17), and the last one after normal irrigation retrieval, on September 14. Images were taken between 9:00 and 11:00 (solar time) at 300 to 680 m elevation. Pictures taken at 300 m elevation showed a 5cm resolution in RGB and NIR, and 30 cm in TIR.

Nine aluminum targets were distributed within the experimental field for image geolocation (Fig. 1). Moreover, temperature measurement of cold and hot reference surfaces were performed with a thermal infrared thermoradiometer KT19 (Heitronics®) during each airborne acquisition.

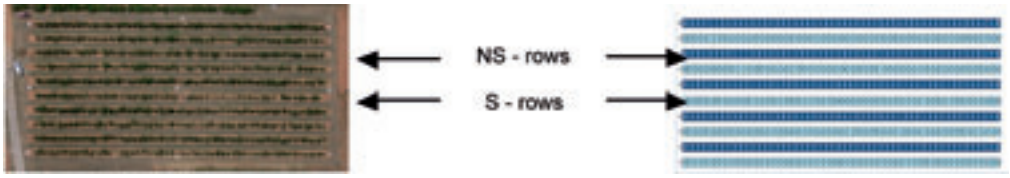

Fig. 1. RGB image of experimental field (ca. 6000 m², left), and field plan (right). Aluminium targets (9 white points) placed at field periphery and middle were DGPS localised for accurate image geolocation. On plan, NS rows are colored in dark blue and S rows colored in clear blue.

3. Determination of WDI with vegetation index (NDVI) and temperature differences between leaf surface (T_s) and air (T_a)

For image transformation we used Erdas Imagine® software.

The Normalized Difference Vegetation Index (NDVI) was computed according to Rouse *et al.* (1973) from red (R, extracted from RGB matrix) and near infrared (NIR) bands:

$$NDVI = (NIR-R) / (NIR+R)$$

T_s-T_a value was obtained by difference between the surface temperature of vegetal cover (T_s) and the air temperature (T_a) acquired by meteorological data logger. T_s at tree level was estimated from thermal values measured at aircraft level (TIR images) corrected by the atmospheric interference, which was itself measured by the temperature difference between soil reference surfaces (KT19 measurements) and corresponding temperatures measured at aircraft level.

Within each tree a central buffer zone of 60 cm diameter was delimited to compute average values of NDVI and T_s-T_a values.

WDI is relative to the Vegetation Index/Temperature (VIT) concept (Moran *et al.*, 1994), which is based on the trapezoidal shape formed by the relationship between (T_s-T_a) and vegetation cover (Fig. 2). Theoretical equations for computation of the trapezoid vertices are given these authors. The ratio between actual evapotranspiration (ET_{actual}) and maximal evapotranspiration (ET_{max}) reflects the water stress intensity, and can be calculated using the following equation:

$$WDI = 1 - [ET_{actual} / ET_{max}] = [(T_s-T_a)_{min} - (T_s-T_a)] / [(T_s-T_a)_{min} - (T_s-T_a)_{max}] = AC / AB$$

Where $(T_s-T_a)_{min}$, $(T_s-T_a)_{max}$, (T_s-T_a) correspond respectively to points A, B and C (Fig. 2).

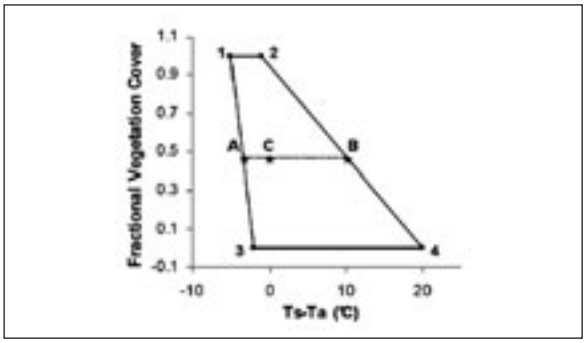

Fig. 2. Illustration of Moran VIT concept and WDI computation. 1: well watered and fully covering vegetation; 2: water stress and fully covering vegetation; 3: saturated bare soil; 4: dry bare soil.

III – Results and discussion

1. Monitoring of soil water stress

Water stress intensity during summer was measured by a series of tensiometric probes located in the middle of the experimental field. For each treatment and at each soil depth, median values of soil water potential (SWP) were considered. Before the summer stress period, we can observe (Fig. 3) a transient decrease of SWP due to irrigation deficit. From May 1, a continuous decrease of SWP was observed for S rows at 60 cm depth (red curve), and the soil drought situation was maintained until end of October, 2 months after irrigation restoring. Considering the tensiometric probe located at tree root depth (30 cm) the soil stress period (pink curve, SWP<0.08 MPa) began concomitantly with the first flight (July-16), and was sharply interrupted by the resumption of irrigation at the end of August. Contrastingly, the SWP values shown by blue curves (NS rows, 30 and 60 cm) were almost always higher than -0.08 MPa (stress threshold) indicating a situation of tree hydric comfort.

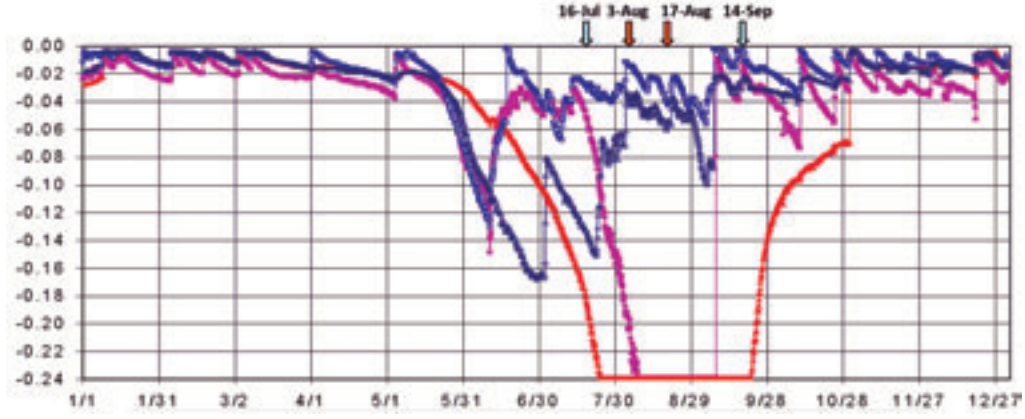

Fig. 3. Monitoring of soil water potential (MPa) in 2010 with tensiometric probes located at two depths (30 cm and 60 cm). The NS treatment is represented by the clear and dark blue curves, for 30 cm and 60 cm respectively, and the S treatment is represented in pink and red, for 30cm and 60cm respectively. Dates of airborne flight image acquisition are indicated by vertical arrows.

2. Water Deficit Index and G, E and GxE effects

The Fig. 4 represents the WDI values computed for each pixel of the experimental plot (dark points), and a series of superimposed blue and red points corresponding to average values of WDI within each individual tree buffer zone, for NS and S trees respectively. Differences between S and NS tree groups, materialised by the distance between blue and red scattered points, were clear except at the last date. From July 16 until August 17, particularly, WDI differences between S and NS trees increased with increasing stress (see F values, ANOVA results, Table 1). After irrigation restoring (September 14), WDI values of S trees did not present any differences with those of NS trees. The transient decrease of SWP, due to a temporary irrigation deficit at the beginning of summer period (Fig. 2) can explain slight but significant differences between WDI values on July 16 (Fig. 4, onset of blue and red point differentiation), before the real stress period after this date.

Table 1 presents the results of a two-way ANOVA on WDI values, testing the effects of genotype, soil, and their possible interaction. This analysis reveals significant drought and genotype effects at the three first dates, while no difference was observed on September 14 (not shown). Drought effect was globally prevailing, as shown by *p*-values. On August 17 the genotype effect was less significant than at the two first date, as indicated by a higher *p*-value. This results could result from a lower resolution thermal images, because the airborne acquisition was performed at 680 m instead of 300 m. No interaction was revealed between genotype and drought factors, suggesting either that their effects were purely additive, or that a severe drought situation could mask differential responses of genotype to intermediate soil drought.

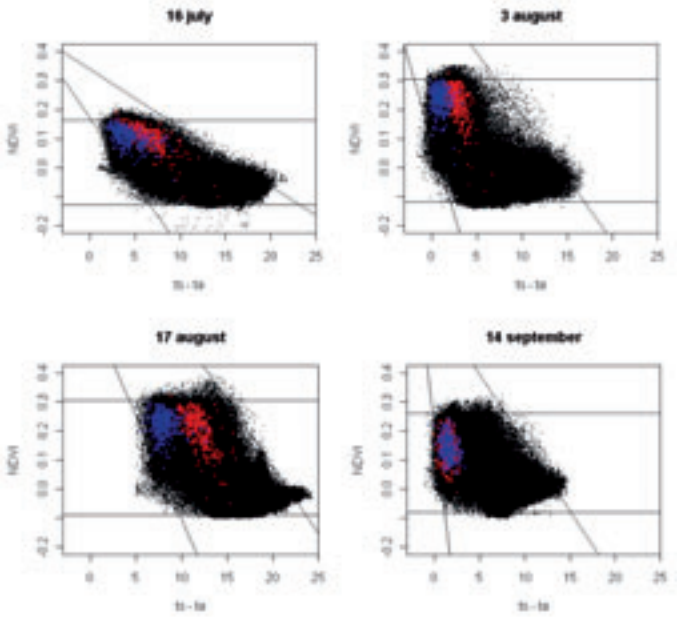

Fig. 4. Graphic representation to WDI values of all field pixels (dark points) and of the apple trees central one. Blue points represent NS trees and red ones S trees. Ts-Ta are expressed in °C.

Table 1. Two-way ANOVA applied to WDI (2010 campaign). *p*-values less than 0.05 show significant effects. No values are presented for Sept.14 because there were no significant effects of both factors

Effect		07-16	08-03	08-17
Genotype	F	1.8	1.9	1.5
	p-value	$<10^{-4}$	$<10^{-4}$	$<10^{-2}$
Drought	F	501	772	1661
	p-value	$<10^{-6}$	$<10^{-6}$	$<10^{-6}$
G * D	F	0.5	0.5	0.6
	p-value	p# 1.0	p# 1.0	p# 1.0

IV – Conclusions

These first results showed that it is possible to reveal the effects of tree genotype and drought by the use of remote sensing tools, thanks to high spatial resolution of airborne images. This result present a "snapshot" dataset, image acquisition are made just at one moment. But for 2010 some supplementary measurements will be necessary to validate the results. We don't have knowledge of each plant water status. Moreover the vegetation index (NDVI) that was used for WDI calculation requires to be assessed in respect to its intrinsic parameters, the leaf area index (LAI) and leaf chlorophyll content (Bégué *et al.*, 2010). These measurements have been taken into account during the 2011 campaign (results currently analyzed). During this 2011 campaign (three airborne imaging flights) water status of some trees was periodically assessed by stem water potential measurements at airborne acquisition dates. In comparison to WDI, our project will be to test and compare the relevancy and the sensitivity of S-SEBI (Simplified Surface Energy Balance Index, Roerink *et al.*, 2000), another water stress index applicable to heterogeneous cover.

On the basis of a study of Möller *et al.* (2007), who used visible and thermal imaging to estimate crop water status, we also plan to acquire more proximal ortho-images of trees and try to assess to which extent airborne acquired images and the resulting vegetation indices are affected by the resolution of TIR images.

Genetic analysis of the hybrid apple population will be realized on the basis of WDI and S-SEBI results, over 2010 and 2011 campaigns, and also through to the analysis of another plant traits, more time-integrative, like fruit carbon isotope discrimination ($\Delta^{13}C$), which is a proxy for water use efficiency (Brendel *et al.*, 2002). Further heritability analysis on functional traits, QTL detection and refined genetics studies related to QTL zones are planned.

References

Bégué A., Lebourgeois V., Bappel E., Todoroff P., Pellegrino A., Baillarin F. and Siegmund B., 2010. Spatio-temporal variability of sugarcane fields and recommendations for yield forecast using NDVI. In: *International Journal of Remote Sensing*, 31, p. 5391-5407.

Brendel O., Handley L. and Griffiths H., 2002. Differences in delta C-13 and diameter growth among remnant Scots pine populations in Scotland. In: *Tree Physiology*, 22, p. 983-992.

Berger B., Parent B. and Tester M., 2010. High-throughput shoot imaging to study drought responses. In: *Journal of Experimental Botany*, 61, p. 3519-3528.

Condon A.G., Richards R.A., Rebetzke G.J. and Farquhar G.D., 2004. Breeding for high water-use efficiency. In: *Journal of Experimental Botany*, 55, p. 2447-2460.

Idso S.B., Jackson R.D., Pinter P.J., Reginato R.J. and Hatfield J.L., 1981. Normalizing the stress-degree-day parameter for environmental variability. In: *Agricultural Meteorology*, 24, p. 45-55.

Jackson R.D., Idso S.B., Reginato R.J. and Pinter P.J., 1981. Canopy temperature as a crop water-stress indicator. In: *Water Resources Research*, 17, p. 1133-1138.

Jones H.G., 1999. Use of thermography for quantitative studies of spatial and temporal variation of stomatal conductance over leaf surfaces. In: *Plant, Cell & Environment*, 22, p. 1043-1055.

Laurens F., Audergon J.M., Claverie J., Duval H., Germain E., Kervella J., Lezec M.I., Lauri P.E. and Lespinasse J.M., 2000. Integration of architectural types in French programmes of ligneous fruit species genetic improvement. In: *Fruits* (Paris), 55, p. 141-152.

Lebourgeois V., Bégué A., Labbé S., Mallavan B., Prevot L. and Roux B., 2008. Can Commercial Digital Cameras Be Used as Multispectral Sensors? A crop monitoring test. In: *Sensors*, 8, p. 7300-7322.

Möller M., Alchanatis V., Cohen Y., Meron M., Tsipris J., Naor A., Ostrovsky V., Sprintsin M. and Cohen S., 2007. Use of thermal and visible imagery for estimating crop water status of irrigated grapevine. In: *Journal of Experimental Botany*, 58, p. 827-838.

Moran M.S., Clarke T.R., Inoue Y. and Vidal A., 1994. Estimating crop water deficit using the relation between surface-air temperature and spectral vegetation index. In: *Remote Sensing of Environment*, 49, p. 246-263.

Regnard J.L., Ducrey M., Porteix E., Segura V. and Costes E., 2008. Phenotyping apple progeny for eco-physiological traits: how and what for? In: *Acta Horticulturae*, 772, p. 151-158.

Roerink G.J., Su Z. and Meneti M., 2000. S-SEBI: A simple remote sensing algorithm to estimate the surface energy balance. In: *Physics and Chemistry of the Earth, Part B: Hydrology, Oceans and Atmosphere*, 25, p. 147-157.

Rouse J.W., Hass R.H., Schell J.A., and Deering D.W., 1973. Monitoring vegetation systems in the great plains with ERTS. In: *3rd ERTS Symposium*, p. 309-317.

Case studies

Irrigation Decision Support System assisted by satellite. Alqueva irrigation scheme case study

J. Maia*, L. Boteta*, M. Fabião*, M. Santos*, A. Calera and I. Campos****

*Irrigation Technology Centre – COTR, Quinta da Saúde, apartado 354, 7801-904 Beja (Portugal)
**Sección de Teledetección y SIG. Instituto de Desarrollo Regional, Universidad de Castilla-La Mancha Campus Universitario s/n, 02071, Albacete (Spain)

Abstract. In irrigated farming systems is important to increase the processes for the rational use of water improvement, to achieve water maximum productivity, respecting the environment. For that, the Irrigation Advisory Services (IAS), included in the Irrigation Extension Services (IES) must be considered a regular instrument for the best irrigation management. To increase the IES efficiency, COTR proposed, firstly, with the development of the AQUASTAR–Alqueva project, and now within the TELERIEG project, to apply the irrigation scheduling methodology developed in the DEMETER project (Calera *et al*., 2005) to the Alqueva irrigation area (EFMA, Portugal), and based on that, develop the IES, based on Earth observation technologies and other information and communication technologies, which allows near real time to estimates the real crop water use at a large scale. In this work we intend to show the results and the operational side of the irrigation decision support system developed for the Alqueva irrigation scheme.

Keywords. Earth observation – Water management – NDVI.

Système d'aide à la décision d'irrigation assisté par satellite. Cas d'étude du périmètre irrigué d'Alqueva

Résumé. *Dans une exploitation avec un système d'irrigation, il est important d'augmenter les processus pour l'amélioration de l'utilisation rationnelle de l'eau, pour atteindre un maximum de productivité de l'eau, tout en respectant l'environnement. Pour ça, le service personnalisé de recommandation d'irrigation, contenu dans un service de recommandation agricole, doit être considéré comme un instrument régulier pour une meilleure gestion de l'irrigation. A fin de pouvoir améliorer le service de recommandation extensive d'irrigation, le Centre Opératif et de Technologie d'Irrigation (COTR) a proposé premièrement, avec le développement du projet AQUASTAR–Alqueva, et maintenant avec le projet TELERIEG, d'appliquer le calendrier d'irrigation développé par les méthodologies du projet DEMETER (Calera* et al*., 2005) pour la zone de irrigation du Alqueva (EFMA, Portugal). Basé sur les technologies d'observation de la Terre et sur d'autres technologies de l'information et de la communication, le système permet d'obtenir en temps réel des estimations des besoins d'eau pour les cultures à grande échelle. Dans ce travail nous montrons les résultats et le fonctionnement du système d'aide à la décision pour l'irrigation dans le périmètre d'irrigation de Alqueva.*

Mots-clés. *Observation de la Terre – Gestion de l'eau – NDVI.*

I – Introduction

The irrigation farming is now a days full of challenges and pressures. If it is the main responsible for the food needs fulfil, it also the main responsible for the fresh water use. Based on that, the irrigated agriculture is under a tremendous pressure and in direct competition with other users.

In these conditions, to increase the irrigation farming protection, it is very important that the rational water use, requesting for it, the restricted volume of water need, in the right moment, must become a common reality. This way it is supposed to achieve the maximum water productivity, in economical and environmental terms.

To respond to these needs, the Irrigation Extension Services (IES) must use the Irrigation Advisory Services (IAS), based on technical tools, as a natural water management resource, that allow a more rational water use by the farmers, reducing the water use based on the real water needs, in a way to maximize the production and the cost benefit relation (Allen *et al*., 1998).

These IAS must be structured based on the end users needs, as technical reports deliverables, sent in real time, or near real time, using as much as possible the information and communication technologies facilities. The crop water use models must use field data, like soils and crops information, fitted to the region.

This strategy has not been considered in the south of Portugal, which leads during the end of the last century to the lack of technical support to help farmers to use these concepts in their farms, using water as a valuable input.

The implementation of the Irrigation Technology Centre (COTR), with the target to transfer the knowledge and the technology to the farmers, gave the opportunity to reduce the lack of technical support in this field. This was possible with the establishment of the IES near the farmers, in their own professional associations, adapted to each local reality.

This IES use, as base resource, the information obtained from the IAS. The IAS follow the FAO (Allen *et. al*., 1998) methodology, known as the K_c-ETo methodology, where K_c is crop coefficient and the ETo is the reference evapotranspiration.

To increase the efficiency of the IAS an ultimate effort has been made by COTR with the development of the AQUASTAR-Alqueva Project, whose results achieved were improved during the TELERIEG project with the use of Earth observation and communication technologies, to estimate, in near real time, the real crop water demands over large areas, with a spatial distribution, that allows to analyze the different crop behaviours or even in the same field the differences due to different grow conditions, for example, due to the lack of uniformity in water distribution. Consequently, this allows acting during the field campaign to reduce the negative impact in the crop.

All the work results in an adaptation, to the Alqueva irrigated area, of the methodology developed during the DEMETER project (Cuesta *et al.*, 2002).

II – Materials and methods

1. Location

All the work was developed in the Alentejo region, in the South of Portugal, in the Alqueva Irrigation Scheme (www.edia.pt) (Fig. 1) and in some others plots near the influence area, as a way of use as much as possible, the spatial distribution and differences from the region, which will allow, to validate the system at the farmer level, irrigation scheme level or at the river basin level.

Fig. 1. 2011 farmers location.

2. Automatic weather stations network

The decision support system uses, as main information, the weather data obtained from the regional automatic weather stations network SAGRA (www.cotr.pt/sagra.asp), implemented for regional irrigation water demand decision. The SAGRA system is based in fourteen automatic weather stations (Fig. 2) with a single data base of different atmospheric parameters which allow the reference evapotranspiration determination following the FAO Penman-Monteith methodology (Allen *et al*., 1998).

Fig. 2. Automatic Weather Station location.

3. Satellite imagery and processing

The pre-processing of remotely sensed image consists on geometric and radiometric characteristics analysis. By realizing these features, it is possible to correct image distortion and improve the image quality and readability. Radiometric analysis refers to mainly the atmosphere effect and its corresponding ground feature's reflection, while geometric analysis refers to the image geometry with respect to sensor system.

DEMETER's multi-temporal approach requires images of different dates. The use of a temporal images sequence is very demanding over a precise geometric correction because it needs overlay products from different dates and different sensors.

A. Geometric correction

Geometric correction of satellite images involves establishing a mathematical relationship between the image and ground coordinate systems. The rectification method used consist on second order polynomials that model the positional relationship between points on a satellite image and ground control points (GCP) obtained from a georeferenced image (source: EDIA and "Associação de Municipios do Alentejo"). The output images are resampled to the standard pixel size of products (30 m).

Also, as these polynomials only correct locally at GCPs, a high number of GCPs is required to adequately model the distortions in an image. For this reason, about 100 GCPs are used, which are accepted as a valid one if the root mean square error (RMSE) of the polynomial residuals is less than 0.5 pixels (i.e. 15 m).

The adjustment is made interactively using standard image processing software Erdas™.

B. Reflectivity and NDVI determination

The Normalized Difference Vegetation Index (NDVI) is a numerical indicator that uses the visible and near-infrared bands of the electromagnetic spectrum (NDVI = (NIR-red)/(NIR+red)), and is adopted to analyze remote sensing measurements and assess whether the target under observation contains live green vegetation or not. NDVI has found a wide application in vegetative studies as it has been used to estimate crop yields, pasture performance, and rangeland carrying capacities among others. It is often directly related to other ground parameters such as percent of ground cover, plant photosynthetic activity, surface water, leaf area index and the amount of biomass. NDVI was first used by Rouse *et al*. (1973) and nowadays is the one most often used.

The determination of the NDVI is done with DEMETER (2002) Atmospheric Correction Module 1.0. This module has been designed for the atmospheric correction of the LANDSAT images. The algorithm works retrieving the atmospheric parameters from the multispectral data provided by LANDSAT in the six bands covering the solar spectrum, 1^{st}-5^{th} and 7^{th}, by means of a multiparameter inversion of the Top-of-Atmosphere (TOA) radiances of five reference pixels Once the atmospheric reflectance and transmission functions are calculated, the algorithm decouples the surface and atmospheric radiative effects and calculate de Bottom-of-Atmosfere (BOA) NDVI.

C. KC-NDVI determination

The similarity between the temporal evolution of NDVI and crop coefficient during the crop growth cycle has been repeatedly observed. The crop coefficients obtained from the spectral response of vegetation cover represent a real crop coefficient obtained in real time. It doesn't require the planting date for calculation procedure and but it detect the beginning and end of the different stages that express the evolution of Kc.

Experiences in this direction were carried out in Spain, Italy and Portugal in the DEMETER project (Calera *et al*., 2003) and Aquastar-ALQUEVA (COTR).

For Landsat sensors, the following expression is used:

$$Kc\text{-}NDVI = 1.15\ NDVI(BOA) + 0.17 \qquad \text{(Equation 1)}$$

Kc-NDVI: crop coefficients obtained from the spectral response of vegetation cover;

NDVI(BOA): Normalized Difference Vegetation Index at the Bottom-of-Atmosphere.

D. Web service information system

All the information obtained is available on SPIDER platform, developed by the PLEIADES project (www.pleiades.es). This information is the result of the methodology described previously and includes not only the charts, but also the tabular results obtained through the Earth observation platforms, using the algorithms that allow the crop coefficients determination.

III – Results

1. Web service platform

The web service platform (Fig. 3) allows the end user to access, in a personalized session, to all the information from his influence area, with the information of the crop water needs (Fig. 4). The system DB allows the access to files from previous years or different crops, and also allows the access to different information sources, like other spatial data. Such flexibility turns it into a powerful service to the end user with much more information access.

Fig. 3. Web service access.

After the upload of the information required, it becomes to be possible the access, by the user, to the evolution of Kc, NDVI and ETc, and with base on that make the best irrigation scheduling.

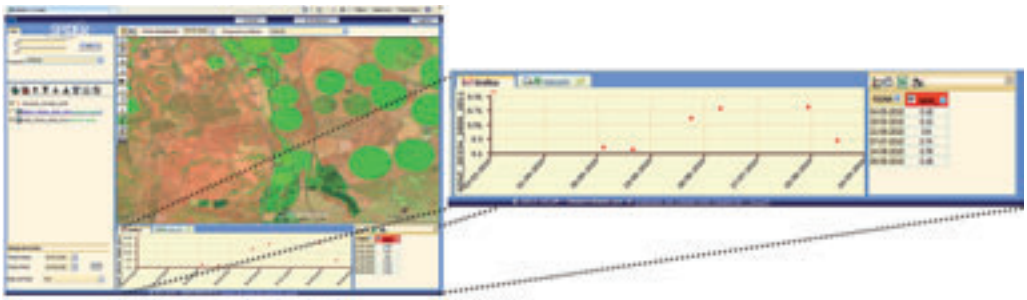

Fig. 4. Tomato water needs evolution.

On Fig. 4, it's possible to see the picture with the green areas that reflect the green vegetation, actively growing, mainly, center-pivots with maize and smaller plots with tomato. Below the picture, it is possible to identify the NDVI evolution of the selected plot of tomato that by equation 1 application, gives the Kc evolution.

With the information obtained, and based on the evapotranspiration determined by the SAGRA network, produces at the time, the real crop water need.

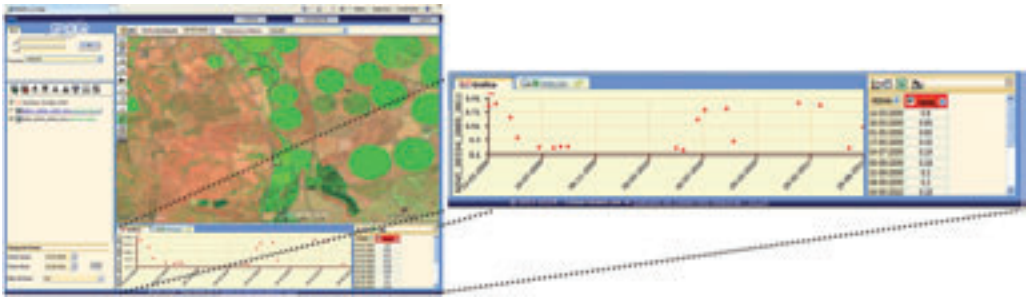

Fig. 5. Water needs evolution over large period of time.

As shown on Fig. 5, the system has the potential to store data from several years, in this case between 2009 and 2011, and also over large areas. Such potential will allow a quick analysis over a large area, as a river basin, for a long period of time, important for water needs planning.

2. e-IAS development

The IES development is a high consumer of human resources, which makes it an expensive activity, because of the intensive field data uptake and analysis, and the timely information deliver to the user.

To increase the efficiency of such services, based on the referred tools to uptake and analyse the data and deliver the information, it was developed the IAS based on the Earth observation techniques and information and communication technologies (e-IAS), that in real or near real time allows the uptake, process and deliver the results to the end user.

The information delivery process usually includes the web service, but nowadays it is possible to supply through the last generation of cellular phones all the information to the user, even if it is pictures, maps or graphic analysis (Fig. 6).

Fig. 6. Information access through last cellular phones generation.

IV – Conclusions and remarks

The Earth observation technologies are a very important jump on the level of information that is possible to collect and deliver to the farmer as an information end user. With it is possible to get step ahead on the irrigation scheduling and the rational water use, as it is possible to correct immediately any decision on the water use, for example, the lack of uniformity in water distribution due to clogging of the sprayers.

The decision support system based on the e-IAS, allow the irrigation manager to access real information about his crops water demands, in a particular period. It is usually referred that the farmers are not a frequent web services users, mainly, in the south of Portugal, but they are a very frequent use of mobile communications. In that sense, the e-IAS allows the cellular phone as way to deliver the information, and allows a quick decision.

The main challenge of the e-IAS is to give the step ahead of include all the irrigation farms of a specific region and, based on that, decide the water distribution from a water source in a particular year or situation.

Acknowledgments

This work was supported by the project "Telerieg" from the Interreg IV B Sudoe Programme (project no. SOE1/P2/E082). The authors are particularly grateful to the Alensado tomato growers association (www.alensado.pt) for its help and collaboration during the data collection.

References

Allen R.G., Pereira L.S., Raes D. and Smith M., 1998. Crop evapotranspiration. Guidelines for computing crop water requeriments. *FAO Irrigation and Drainage* 56. FAO, Rome 300 pp.

Calera A., 2003. Space-assisted irrigation management: Towards user-friendly products. In: *Use of remote sensing of crop evapotranspiration for large regions*, R.G. Allen and W.G. Bastiaansen, (eds). Montpellier, France: ICID-CIID.

Calera A. and Martín de Santa Olalla F., 2005. Uso de la Teledetección em el Seguimiento de los Cultivos de Regadío. In: *Agua y Agronomía*, Cap. XIV, Santa Olalla, López and Calera (eds). Madrid: Ed. Mundiprensa.

Cuesta A., Montoro A., Jochum A.M., López P. and Calera A., 2002. Metodología operativa para la obtención del coeficiente de cultivo desde imágenes de satélite. In: *ITEA,* 101 (2), p. 91-100.

DEMETER, 2002. Demonstration of Earth observation Technologies in Routine irrigation advisory services. VI Framework Program, European Commission. www.demeter-ec.net

Moreno-Rivera J.M., Osann A. and Calera A., 2009. SPIDER - An Open GIS application use case. In: First Open Source GIS UK Conference, Nottingham.

Rouse J.W., Hass R.H., Schell J.A. and Deering D.W., 1973. Monitoring Vegetation Systems in the Great Plains with ETRS. In: Proceedings of the third ERTS Symposium, p. 309-317.

Transpiration and water stress effects on water use, in relation to estimations from NDVI: Application in a vineyard in SE Portugal

M.I. Ferreira*[1], N. Conceição*, J. Silvestre and M. Fabião*****

*CEER, Instituto Superior de Agronomia (ISA), Univ. Técnica de Lisboa, (Portugal)
**INRB, I.P., INIA – Dois Portos, Quinta da Almoínha, 2565-191 Dois Portosm(Portugal)
***COTR, Quinta da Saúde, Apartado 354, 7801-904 Beja (Portugal)
[1]E-mail: isabelferreira@isa.utl.pt

Abstract. Remote sensing can give contributions to answer the classical questions in irrigation management: when to irrigate and how much (irrigation depth). In order to compare with estimations partially derived from remote sensing, evapotranspiration (ET) and its components (transpiration, T and soil evaporation, Es) as well as selected water stress indicators were measured in a commercial vineyard with deficit irrigation, in SE Portugal. A combination of micrometeorological, sapflow and microlysimeter methods were used to measure water flux densities. The seasonal results reported (2009) are explored in relation to T obtained from practical models based on meteorological data (reference ET, ETo), crop basal coefficients (Kcb) and stress coefficients (Ks) where the use of the normalized difference vegetation index (NDVI) is included. Results from stress cycles (2010) confirm the selection of predawn leaf water potential (PLWP) as water tress indicator for the purpose of the analysis. A preliminary conclusion, confirmed later, on the meaning of NDVI in the conditions of this study (-0.2 MPa>PLWP>-0.7 MPa), suggested that it is not affected by short term but by long term water stress. Kcb measured and estimated from NDVI agreed generally well, with exceptions. The comparison between T measured and estimated from ETo.Kcb.Ks (being Ks obtained from PLWP) highlights the importance of Ks on T estimation. For practical uses, alternative tools to obtain Ks are proposed.

Keywords. Basal crop coefficient – NDVI – *Vitis vinifera,* L. – Water stress.

Transpiration et effets du stress hydrique en relation avec des estimations à partir de télédétection : application sur une vigne dans le SE du Portugal

Résumé. *La télédétection peut contribuer à répondre aux questions classiques de la gestion de l'irrigation : quand irriguer et quelle quantité apporter. L'évapotranspiration (ET) et ses composantes (transpiration, T et l'évaporation du sol, Es), ainsi que certains indicateurs de stress hydrique ont été mesurés dans un vignoble commercial soumis à une irrigation déficitaire, dans le sud-est du Portugal, afin de les comparer avec des estimations partiellement obtenues par télédétection. Une combinaison de méthodes de mesures micrométéorologiques, de flux de sève et par microlysimètres a été utilisée pour mesurer les densités de flux d'eau. Les résultats saisonniers (2009) sont analysés par rapport à T obtenu à partir de modèles pratiques basés sur les données météorologiques (ET de référence, ETo), les coefficients culturaux de base (Kcb) et les coefficients de stress (Ks) incluant l'utilisation de NDVI. Les résultats obtenus à partir de cycles de stress (2010) confirment la pertinence du potentiel des feuilles avant l'aube (PLWP) comme indicateur du stress hydrique pour cette analyse. Une conclusion préliminaire, confirmée ultérieurement, sur la signification de NDVI dans les conditions de cette étude (-0,2 MPa> PLWP> -0,7 MPa), suggère qu'il est affecté par un stress hydrique de long terme et non de court terme. La concordance entre Kcb mesuré et Kcb estimé à partir de NDVI est généralement bonne, avec des exceptions. La comparaison entre T mesurée et T estimée à partir de ETo.Kcb.Ks (Ks étant obtenu de PLWP) souligne l'importance de Ks dans l'estimation de T. Pour des utilisations pratiques, des outils alternatifs pour obtenir Ks sont proposés.*

Mots-clés. *Coefficient de stress basal – NDVI –* Vitis vinifera, *L. – Stress hydrique.*

I – Introduction

The need for adequate water management increases with water scarcity and the impacts of excessive use of water and agrochemicals in soil and underground water. In order to manage irrigation, there are three questions to solve: when, how much and how to apply water, the last being related to equipment and efficiency of irrigation. The answer to the two first questions can be related to each other or not, depending on irrigation frequency and irrigation scheduling method.

In the following, the nomenclature used is approximately the one used in FAO Irrigation and Drainage paper 56 (Allen *et al*. 1998):

ET: evapotranspiration or actual ET

ETo: reference ET

T: transpiration (in general or actual T)

Es_ water evaporated directly from soil surface

Kc: crop coefficient (=ET_m/ETo)

ET_c or ET_m: ET for a certain well irrigated crop

Kcb: basal crop coefficient (=T_m/ETo)

T_m: T of a well irrigated crop (=ETo.Kcb)

Ks: stress coefficient (=T/T_m)

With daily irrigation, the main question is to calculate irrigation depth. In case of a so-called well watered crop, the user refills the water reservoir (for the layers where roots are found). Therefore, irrigation depth corresponds to the water consumption or actual evapotranspiration (ET≈ ETo. Kcb+Es) of last day, adding an extra to account for the application losses. In deficit irrigation, the user may want to keep a lower soil water status and the irrigation depth will reflect that choice. In this case, a stress coefficient is applied (ET≈ ETo.Kcb.Ks+Es).

If irrigation is applied at intervals of several days, it is necessary to identify when to apply water, to prevent critical water stress implications on yield. Usually, a water status indicator (soil, plant or atmosphere) is selected, using a certain pre-determined threshold value. If using water balance to estimate soil water depletion, a certain percentage of soil water content or a percentage of readily accessible water can be used, for instance. There is a remarkable cumulated experience on indicators and their threshold values, which includes tables of critical percentages of readily accessible water (for the last, e.g. the FAO Irrigation and Drainage papers 24 and 56). Irrigation opportunity and depth are linked: the more irrigation is delayed, the higher is irrigation depth. Traditional irrigation science and practice provide the means for such determinations which work satisfactorily for well irrigated low crops that fully cover the soil.

There are stands and conditions where irrigation is more difficult to manage, even if they are homogeneous. This includes (i) stands submitted to deficit irrigation, where T is reduced as a consequence of water stress, and Ks has to be included in T estimation, (ii) woody crops, for which not only (due to methodological reasons) there is less information on crop coefficients (Kc and Kcb) but also, in Mediterranean areas, soil water balance is difficult to estimate due to deep root systems, (iii) anisotropic stands, where crop coefficients are highly dependent on plant density and architecture or (iv) the combination of 1 to 3.

Further difficulties are related to soil and water application heterogeneities at plot scale. In land use planning and water management in large areas, there are other limitations related to unknowns in mixed or less controlled areas, i.e., heterogeneities at larger space scales. Remote sensing tools have been studied aiming to access water use, support irrigation scheduling and stress diagnosis, with lower costs and higher efficiency in all these situations.

When using remote sensing tools for ET estimation, a common approach is to calculate NDVI (normalized difference vegetation index) to obtain Kcb. When the crop is under water stress, the same approach can be used, if considering a stress coefficient (Ks), T being estimated from Kcb×Ks×ETo. We intend to verify the reliability of this approach using ground truth seasonal data and assuming a linear relationship between Kcb and NDVI (Calera *et al*., 2001). A first step is to

answer the following: to which extent is NDVI affected by short term and/or long term water stress, in the conditions of our study? If the ratio between T measured and ETo×Kcb (being Kcb estimated from NDVI) can be identified with Ks, this means that NDVI is not affected by short term water stress. In that case, will NDVI be influenced by long term stress impacting Kcb? In order to analyze these preliminary aspects, the ratio between T measured and ETo×Kcb was first related to a selected water stress indicator. In a second step, Kcb measured was compared to Kcb estimated from NDVI. In a third step, T measured (2009) is compared to T estimated using an equation for Ks (from a water status indicator) derived during a stress cycle experiment performed in 2010.

II – Materials and methods

1. Experimental site

The experimental plot is located in a commercial irrigated vineyard (*Vitis vinifera* L. Aragonez 'syn. Tempranillo', grafted on '1103P') with 6.0 ha, situated within a continuous area of a 30 ha vineyard, with fetch above 300 m, near Beja (38º 02' 59'' N, 7º 55' 15''W, 200 m above sea level), in the warmest and driest region of Portugal (Alentejo): 606 mm precipitation and 1775 mm ETo (average 30 yrs). Plants were spaced 2.8 m x 1.1 m. The training system was vertical shoot positioning. The grapevines were spur pruned on a bilateral Royat cordon with 16 buds per vine. The mean grapevines height and canopy width were about 1.8 m and 1.0 m, respectively. The row orientation was approximately N-S. Beneath the canopy and between the rows the soil was bare, not mobilized and mobilized respectively. The soil is a shallow clay vertisol with abundant gravels and few stones, profile type Ap-Bw-C-R derived from basic rocks. Main root zone depth is about 0.6 m; some fine roots explored rock fissures up to 1.5 m depth. The vineyard was drip irrigated, with emitters for each 1.0 m (flow 2.4 l/h), suspended above the ground in the vine row. The nominal flow was 2.4 l/h.

The experimental work took place between flowering and the end of the vegetative cycle (May to October) from 2008 to 2010. During summer 2010, several sub-plots were temporarily irrigated with different strategies, being a well irrigated sub-plot used as a reference (Tm), in order to study the relationship between Ks and plant water status.

2. Evapotranspiration measurements

The eddy covariance technique (EC) was used to measure convection heat flux densities: sensible (H) and latent heat flux (LE) or evapotranspiration (ET_{EC}). The sensors were a CSAT 3-D sonic anemometer and a KH20 krypton hygrometer (Campbell Scientific, Inc. Logan, UT, USA), placed on a metallic tower at a height of 3.2 m, oriented into the dominant wind direction (NW, N). The data were stored (30 min averages) in a CR23X data logger (Campbell Scientific, Inc. Logan, UT, USA). LE was corrected using WPL correction and for oxygen absorption. A wind vane (W200P, Vector Instruments, Rhyl, United Kingdom) as well as a capacitive sensor (air temperature and humidity) were installed at the tower and used for EC corrections and footprint analysis. Net radiation (Rn) was measured with a net radiometer (model NR2, Kipp & Zonen, Delft, Netherlands) 3.2 m above the ground. Seven soil heat flux plates (HFT-3.1, Rebs, Seattle, USA) were placed in a transept at a depth of 0.05 m. Soil heat storage above plates was calculated from soil temperature (0.025 m deep) and water content dependent soil parameters. Soil heat flux (G), was calculated using the soil heat flux densities and the variation in heat storage. Data were stored in a CR10X data logger (Campbell Scientific, Inc. Logan, UT, USA). G, H and Rn were measured to verify the energy balance closure contributing to the evaluation of the EC data quality. Other details and references on corrections can be found in Conceição *et al*. (2011).

EC data could not be obtained with rain, dew or when the wind turned from dominant direction The EC data served to transform the seasonal SF data into reliable absolute T values.

3. Sap flow measurement and transpiration calculation

Sap flow (SF) was monitored with 1.0 and 0.5 cm long radial sap flow sensors (heat dissipation method, Granier 1985), (UP, Germany) installed at 0.30 to 0.45 m from soil. The temperature difference between the heated (downstream) and non-heated (upstream) probes was measured every 60 s and averaged every 30 min (CR10X with an AM416 relay multiplexer, Campbell Scientific, Inc. Logan, UT, USA). Transpiration during the whole season was obtained from SF data after calibration from EC using periods of negligible Es (when ET≈T) or from the relationship ET_{EC}-Es versus SF data, when Es was obtained from a model adjusted from lysimeter measurements (data not shown).

4. Measured and estimated basal crop coefficient

Measured basal crop coefficients (Kcb) were obtained from the relationship T/(ETo.Ks) for the periods were it could be assumed that Ks=1. The data to support this assumption were obtained during the 2010 experiments with stress cycles (not shown).

Estimated basal crop coefficient (Kcb_{NDVI}) was derived from NDVI as Kcb=1.36×NDVI-0.066, according to Calera *et al*. (2001), Project DEMETER. NDVI maps were obtained from LANDSAT 5 TM images (geometrical and atmospheric corrections). NDVI was calculated as NDVI = (IRC - R) / (IRC + R) as described in Conceição *et al*. (2011).

5. Other measurements

Leaf water potential at pre-dawn (PLWP) was measured in at least 9 leaves with a pressure chamber (PMS Instruments, Corvallis, Oregon, USA). Ks was obtained from T/(Kcb.ETo). Meteorological data from a nearby station belonging to COTR [*Centro Operativo e de Tecnologia de Regadio* (www.cotr.pt)], located at Beja (38º 02' 15'' N, 07º 53' 06'' W, ca. 206 m height above sea level) were used to calculate ETo with Penman-Monteith equation using the crop parameters of a well irrigated healthy grass (0.12 m height, 70 $s.m^{-1}$ surface resistance and 0.23 of albedo, according to Allen *et al*. 1998).

III – Results and discussion

1. Impact of short or long term stress on NDVI

By short term stress effect, we mean a stress effect that can be rapidly recovered with irrigation; it is related to Ks. Conversely, long term stress means that it cannot be resumed by a few irrigation events: the long term stress affects leaf area and therefore the capacity to transpire even if enough water was suddenly provided. It can be assumed that it affects Kcb.

Ks was first estimated as T/(ETo×Kcb_{NDVI}) and related with PLWP. The results (Conceição *et al*. 2011) are similar to the relationship between Ks and PLWP obtained from independent Ks measurements (not shown). This fact suggests that the assumption that NDVI was not affected by short term stress was correct, for -0.2 MPa >PLWP> -0.7 MPa. Otherwise, the value estimated for Kcb_{NDVI} would have been underestimated and thus Ks overestimated in relation to the correspondent output from the relationship obtained in 2010 (from direct measurements).

As a consequence of this first result, values of Kcb and Kcb_{NDVI} could be compared using the 2009 Kcb seasonal course (Fig. 1). The values compare well, except for the two last points. This fact can be explained by the loss of basal leaves (documented by photos) due to long term stress (impacting on leaf area but not significantly on ground cover or NDVI).

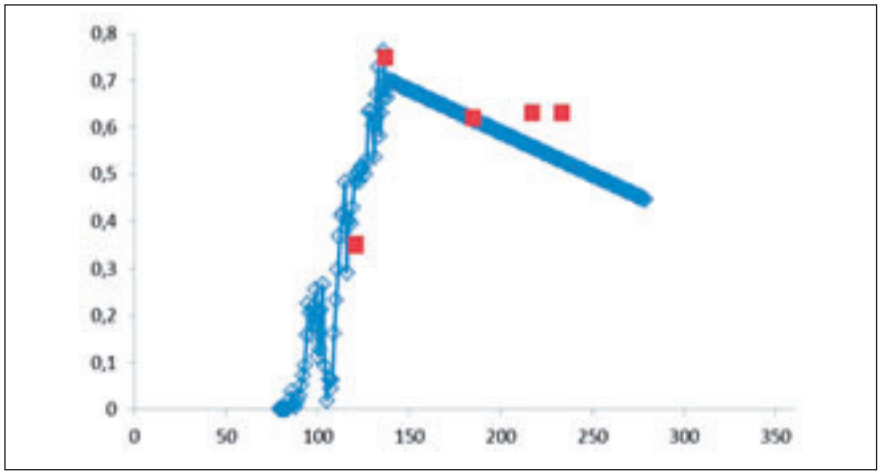

Fig. 1. Seasonal course (DOY 2009) of Kcb (adimensional) measured (blue line) and estimated from NDVI (red quares) Beja, Portugal.

2. Transpiration estimated and importance of the stress coefficient

T estimated from ETo.Kcb.Ks (where Ks was not measured but calculated from PLWP measurements, using the independent relationship obtained in 2010) was compared to T measured. Kcb was either estimated from NDVI or measured.

Fig. 2 shows the seasonal course of ETo, T measured and T estimated using the relationship between Ks and PLWP obtained during the 2010 stress cycles experiments. These results show

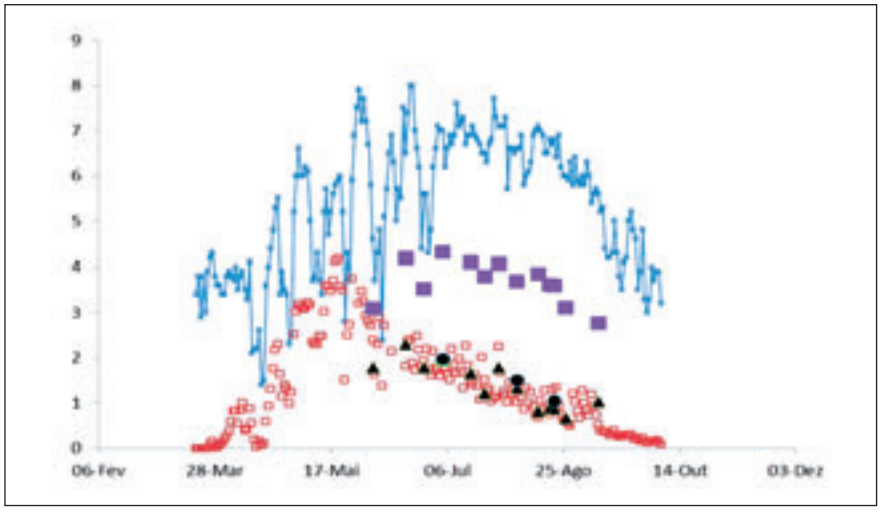

Fig. 2. Seasonal course during 2009 of daily ETo (line), Tm (filled squares), T measured (open squares), T estimated from ETo.Kcb.Ks and ETo.Kcb_{NVDI}.Ks (respectively black triangles and circles) with Ks always estimated from the Ks vs PLWP relationship obtained in 2010 (mm/day). Beja, Portugal.

that (i) the T values calculated as ETo.Kcb.Ks with Kcb from direct measurements or calculated from NDVI are remarkably similar, (ii) after late spring, T measured was much lower than Tm obtained from ETo.Kcb (1 to 3, at the end of dry summer) emphasising the importance of Ks estimation in this irrigated vineyard. The relationship between Ks and automated water status indicators (e.g. stem diameter variations, differences in surface temperature from remote sensing) was not successful. Further data analysis will follow on alternatives, such as soil water depletion estimated from cumulated ET since last irrigation (Ferreira *et al*., 1989, 2008) or others derived from on-going field studies in the frame of a Ph D thesis (2nd author).

IV – Conclusions

Reliable values of T during the seasonal course obtained using a combination of methods served as reference to evaluate the meaning and validity of Kcb estimations from NDVI.

The results suggest that Kcb was not affected by short term stress. Kcb from direct measurements or Kcb calculated from NDVI were remarkably similar, except for the late season. T measured was much lower than Tm obtained from ETo.Kcb, emphasising the importance of Ks estimation in stands submitted to deficit irrigation. After late spring, T values calculated as ETo.Kcb.Ks (with Ks estimated from PLWP) compared very well with T measured.

Acknowledgments

The projects PTDC/AGR-AAM/69848/2006 "Estratégias de rega deficitária em vinha - indicadores de carência hídrica e qualidade" (FCT, Portugal) and "Uso da teledetección para a recomendaccion e seguimiento de las practicas de riego en el espacio SUDOE" (SOE1/P2/E082) provided financial support. We thank *Sociedade Agrícola do Monte Novo e Figueirinha* for the vineyard's facilities.

References

Allen R.G., Pereira L.S., Raes D. and Smith M., 1998. Crop Evapotranspiration Guidelines for Computing Crop Water Requirements. *FAO Irrigation and Drainage Paper 56*. FAO, Rome, Italy.

Calera A., Martínez C. and González-Piqueras J., 2001. Integration from multiscale satellites, DAIS and Landsat, applying a linear model to the NDVI values in La Mancha (Spain). In: *Proceedings ESA Workshop*, 15-16th March 2001.

Conceição N., Ferreira M.I., Fabião M., Boteta L., Silvestre J. and Pacheco C.A., 2011. Transpiration measured and estimated from ETo, NDVI and predawn leaf water potential for a vineyard in South Portugal. In: *Acta Hort.* (in press).

Ferreira M.I., Itier B. and Katerji N., 1989. In: *Modelação Matemática em Hidr. e Rec. Hídricos (Proc. 4º Simp. Luso-Brasileiro em Hidráulica e Recursos Hídricos)*, APRH, Lisboa.

Ferreira M.I., Paço T.A., Silvestre J. and Silva R.M., 2008. Evapotranspiration estimates and water stress indicators for irrigation scheduling in woody plants. In: ML Sorensen (ed.) *Agricultural Water Management Research Trends*. Nova Science Publishers, Inc., New York. p. 129-170.

Granier, A., 1985. Une nouvelle méthode pour la mesure du flux de sève brute dans le tronc des arbres. In: *Annales des Sciences Forestières*, 42, p. 193-200.

Contribution of remote sensing in analysis of crop water stress. Case study on durum wheat

A. Jolivot, S. Labbé and V. Lebourgeois

UMR TETIS, Maison de la télédétection, 500 rue J-F. Breton, 34093 Montpellier Cedex 5 (France)

Abstract. Precision irrigation requires frequent information on crop conditions spatial and temporal variability. Image-based remote sensing is one promising techniques for precision irrigation management. In this study, we investigated the use of broad band multispectral (visible, near infrared and thermal infrared bands) and thermal airborne imagery for the characterization of water status of durum wheat crop through two indices: the Water Deficit Index (WDI) and the Simplified Surface Energy Balance Index (S-SEBI). Comparisons between these two indices and the ratio between actual and potential evapotranspiration (AET/PET) show that such techniques are promising for precision irrigation management.

Keywords. Irrigation – Water stress – Remote sensing – Thermal infrared – Airborne images – Surface temperature – WDI – S-SEBI – Evapotranspiration.

Contribution de la télédétection à l'analyse du stress hydrique des cultures. Etude de cas du blé dur

Résumé. *L'irrigation de précision requiert des informations fréquentes sur la variabilité spatiale et temporelle de l'état des cultures. L'imagerie acquise par télédétection constitue une technique prometteuse pour la gestion de l'irrigation de précision. Dans cette étude, nous avons étudié l'utilisation de l'imagerie multispectrale large bande (bandes visible, proche infrarouge et infrarouge thermique) acquise par voie aéroportée pour la caractérisation de l'état hydrique des cultures de blé dur à travers deux indices: le Water Deficit Index (WDI) et le Simplified Surface Energy Balance Index (S-SEBI). Les comparaisons entre ces deux indices et l'indice de satisfaction des besoins en eau de la plante (ETR / ETM) montrent que ces techniques sont prometteuses pour la gestion de l'irrigation de précision.*

Mots-clés. *Irrigation – Stress hydrique – Télédétection – Infrarouge thermique – Images aéroportées – Température de surface – WDI – S-SEBI – Évapotranspiration.*

I – Introduction

In the present context of global warming, crops are increasingly faced with non-optimal growing conditions. Thereby, researches on crop tolerance to water stress or a better use of irrigation are the major challenges of tomorrow's agriculture (Hamdy *et al*. 2003). Agriculture is the most important water-consuming activity in the world but would consume two times more water than necessary (Fernandez and Verdier, 2004). In the past few decades, new approaches for plant water status sensing have been proposed using infrared thermometry. Canopy temperature has been known for a long time to be linked to the water status of crops . Based on this statement, many crop water stress indices derived from thermal infrared (TIR) measurements were developed, and some of these have been suggested for use in irrigation management. The most successful index is the crop water stress index (CWSI) that has been empirically developed by Idso *et al*. (1981) and theoretically defined by Jackson *et al*. (1981). CWSI is restricted to full-canopy conditions, to avoid the influence of viewed soil on the canopy temperature measurements. However, when thermal infrared spectra are remotely sensed at the vertical mode using an aircraft platform, the difficulty in interpreting these data as an index of crop water stress is linked to the proportion of soil that can be viewed by the sensor over partial crop cover. To overcome these limitations, Moran *et al*. (1994) developed the Vegetation Index / Temperature (VIT) concept, which

allows for the application of the Crop Water Stress Index (CWSI) to partially covered canopies. It is based on the relationship between surface minus air temperature and a spectral vegetation index, such as the Normalized Difference Vegetation Index (NDVI) (Rouse *et al*., 1973), representing the crop cover fraction. From this concept, Moran *et al*. (1994) developed the Water Deficit Index (WDI), which is related to the ratio of actual (AET) and potential (PET) evapotranspiration (WDI = 1 – AET / PET) and which is adapted to partially covered and fully vegetated canopies. Roerink *et al.* (1999) also proposed a Simplified Surface Energy Balance Index (S-SEBI), based on the use of the (temperature, albedo) space to estimate the evaporative fraction from visible, infrared and thermal remote sensing measurements.

The general objective of this study is to test the ability of an ultra-light airborne system equipped with multispectral sensors (visible, near infrared and thermal) to characterize the water status of durum wheat crop through WDI and S-SEBI indices at field scale.

II – Material and methods

In order to validate the use of broad band multispectral (visible and infrared bands) and thermal airborne imagery for the characterization of water status of durum wheat crop, we compared WDI and S-SEBI derived from the aerial acquisition with AET/PET derived from a crop model («PILOT», Maihol *et al*., 1997 and Maihol *et al*., 2004) and in situ measurements.

The study was conducted in two farms (in Prades and Castries cities) located near Montpellier. In each farm, two durum wheat fields having the same characteristics and agricultural practices (cultivar, soil, nitrogen supply…) were chosen. In one field per farm, the irrigation was stopped during the experiment in order to obtain contrasted water statuses between the fields.

Two flights were performed above each field during summer 2011.

1. Data acquisition

A. Aerial acquisitions

a] Spectral image acquisition

The acquisition system used in this study consisted of an ultra-light aircraft or and helicopter equipped with sensors that measured the sunlight reflected in four different spectral bands, as well as the radiation emitted by the Earth's surface. To measure the radiometric signal in the visible RGB spectral bands (Red, Green and Blue), a commercial camera (Sony A850) was used. The same type of camera was adapted and equipped with a 715 nm band pass filter (XNiteBPG, LDP LLC) to measure the radiation in the Near Infrared (NIR) spectral band. The settings of the two cameras (aperture, shutter speed, and sensitivity) were kept unchanged throughout the duration of the experiment. Images were recorded in raw format, allowing us to work on unprocessed CMOS data files.

The radiation emitted by the canopy was also measured using a microbolometer thermal infrared (TIR) camera (B20 HSV, FLIR). The radiance detected over the 7.5-13 μm spectral band is equivalent to the temperature, assuming a target emissivity equal to unity. The system provided 240 x 320-pixel images with a radiometric resolution of 0.1°C and an absolute precision of 2°C.

b] Pre-processing

The signal measured by a numeric camera is not linearly proportional to the radiance of the target. Factors affecting the signal are related to features of the camera (colour processing algorithms, camera settings and vignetting) and environment (sun geometry, atmosphere and flight altitude). The correction steps that were applied to the images (decoding the digital photo format and vignetting correction) are described in Lebourgeois *et al*. (2008a).

When remotely sensed from airborne sensors, the thermal infrared signal emitted by crops must be corrected for atmospheric effects (Jiménez-Muñoz and Sobrino, 2006). To correct for these effects, we used linear regressions established between ground and airborne surface temperature measurements for each acquisition date [see details in (Lebourgeois *et al*., 2008b)].

Blue, green, near infrared and thermal infrared images were co-registered using the red band as a reference.

B. In situ *measurements*

In situ measurements of soil water status and crop parameters (leaf area index, leaf humidity, foliar potential) were performed weekly on one point in each field.

2. Evapotranspiration indices

A. WDI and S-SEBI indices

The Vegetation Index / Temperature concept is based on the trapezoidal shape formed by the relationship between (Ts – Ta; Ts: leaf surface temperature; Ta: air temperature) and vegetation cover (Fig. 1), which can be represented by a spectral vegetation index such as NDVI. Theoretical equations for computation of the trapezoid vertices are given in (Moran *et al*., 1994). WDI has been defined from this concept (Moran *et al*., 1994). It is related to the ratio between actual (AET) and potential evapotranspiration (PET) and can be calculated using the following equation:

$$WDI = 1 - (AET/PET) = CA / BA$$

On the below graph of Fig.1: for a given fractionnal vegetation cover, A represents the surface temperature for a PET situation, B the surface temperature for the maximum stressed situation, if C represents the measured surface temperature then CA / BA represents the difference between C and A divided by the difference between B and A).

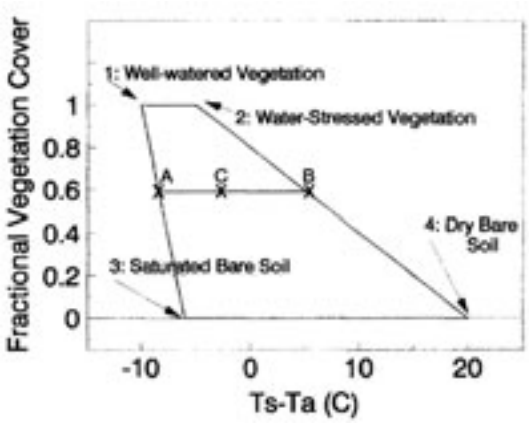

Fig. 1. Illustration of Moran's VIT concept and WDI calculation.

The analytical calculation of WDI requires many meteorological on-site measurements. When these inputs are missing, WDI can be defined empirically (Clarke, 1997) by calculation of the trapezoid based on the image data. However, defining empirical WDI boundaries is not easy when the scenes viewed by the airborne optical and thermal infrared sensors do not contain the

dry and wet bare soil and vegetated states corresponding to the vertices of the trapezoid. Therefore, we chose to define the WDI boundaries using a statistical method by calculating the 1% and 99% quantiles of NDVI for the upper and lower limits. Lines (1-3) and (2-4) (Fig. 1) were defined by calculating the 1% and 99% quantile regressions of (Ts – Ta) as a function of NDVI. The calculations were carried out using the R software, according to Koenker (2008).

The Simplified Surface Energy Balance Index (S-SEBI) has been developed by Roerink *et al.*(1999) to solve the surface energy balance with remote sensing techniques on a pixel-by-pixel basis. S-SEBI requires scanned spectral radiances under cloudfree conditions in the visible, near-infrared and thermal infrared range to determine its constitutive parameters: surface reflectance or albedo, surface temperature. With this input the energy budget at the surface can be determined. The upper and lower limits of the (albedo, surface temperature) scatter plot represent dry (Hmax) and well-watered conditions (λEmax). S-SEBI is then computed as follow (see also Fig. 2):

$$S\text{-}SEBI = T_H - T_S / T_H - T_{\lambda E}$$

Where T_s is the surface temperature, and T_H and $T_{\lambda E}$ are the maximal and minimal temperatures for a given range of albedo.

For more information concerning the upper and lower limits calculation, see Roerink *et al*. (1999).

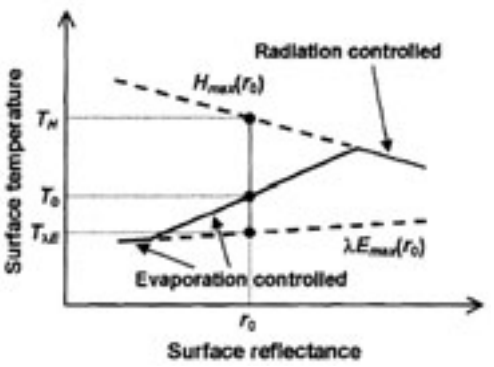

Fig. 2. Illustration of Roerink's S-SEBI concept.

WDI and S-SEBI ranges from 0 to 1:

– for WDI: 0 is a well-watered crop transpiring at the maximum rate and 1 is stressed;

– in contrast for the S-SEBI 1 is a well-watered crop and 0 is stressed.

These two indices were calculated for each acquisition date.

B. AET / PET

AET/PET was simulated using «PILOT» crop model (Maihol *et al*., 1997 and Maihol *et al*., 2004) and from *in situ* measurements. This model allows the simulation of water balance from an actual conduct or a defined irrigation strategy (dates and amount of water). The model outputs are validated through the comparison between observed and simulated water stock. It provides a daily estimation of crop water stress. For a best simulation, PET is corrected by a crop coefficient (Kc) to obtain the maximal evapotranspiration (MET).

III – Results and discussion

1. Water stress indices

A. Indices derived from airborne acquisitions

Maps of water stress indices derived from airborne images correctly reflect the situation observed in the field as seen on Fig. 3 example: high WDI on non-irrigated plot, very low WDI on parts of the field where irrigation is in progress.

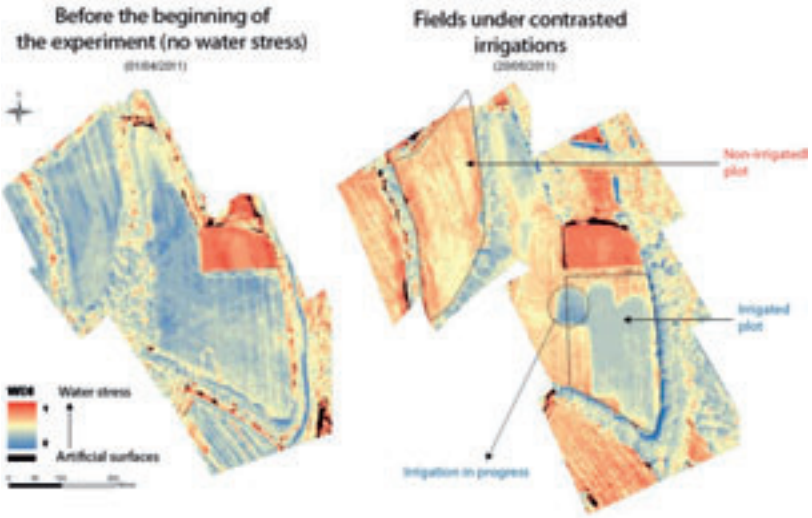

Fig. 3. Maps of WDI (Castries fields).

The dispersion of WDI values (data from the second flight) shows a good discrimination between irrigated plots and non-irrigated plots (Fig. 4).

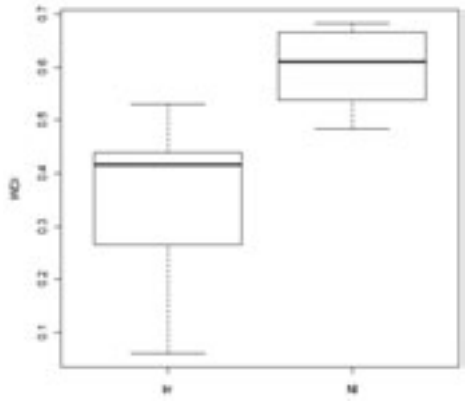

Fig. 4. Dispersion of WDI of irrigated (irr) and non-irrigated (NI) plots (flight no. 2).

B. AET / MET

The temporal evolution of AET / MET obtained from «PILOT» simulations seems consistent with water supply (Fig. 5). However, some parameters (drainage, runoff, root depth) could not be measured during the study. Consequently, they have been estimated and adjusted until the simulated data better approximate the measured data.

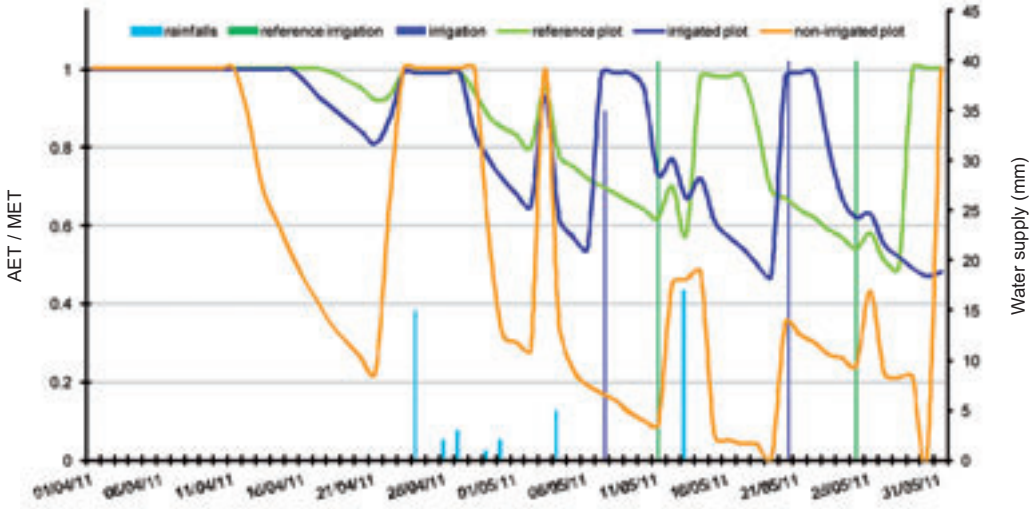

Fig. 5. Evolution of simulated AET / MET and water supply (irrigations and rainfalls) on Prades fields.

2. Relationships between AET / MET and indices derived from airborne acquisitions

A. Evapotranspiration: AET / MET

Linear regressions show a good correlation between indices derived from airborne acquisitions and AET / MET ($R^2 = 0.64$ and $R^2 = 0.61$ for WDI and S-SEBI respectively). An example of linear regression between WDI and AET MET is given on Fig. 6 (left). In this graph, we can see that the correlation between WDI and AET / MET is weaker for the points corresponding to the non irrigated plots. This is due to "PILOT" model that is not initially designed to simulate AET / MET in conditions of strongly limited water supply. Therefore, the points corresponding to non irrigated plots were removed, improving the relationships between AET / MET and the water stress indices derived from airborne acquisitions ($R^2 = 0.8$ and $R^2 = 0.75$ for WDI and S-SEBI respectively) (see Fig. 6, right).

B. Plant humidity

Relationships between the water stress indices derived from airborne acquisitions and the other measurements of plant water status (like leaf humidity or leaf potential) are weak as seen in Table 1.

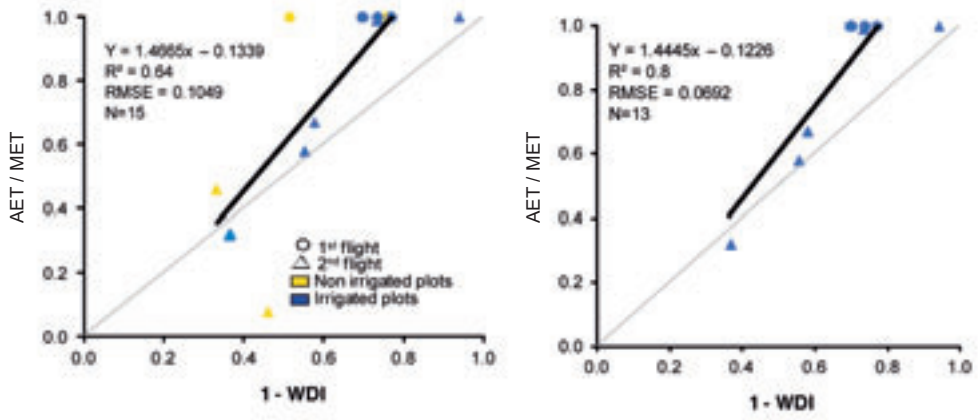

Fig. 6. Linear regressions between WDI and AET / MET (left: all values, right: without values of non irrigated plots).

Table 1. Relationships between the water stress indices derived from airborne acquisitions (WDI, S-SEBI) and the other measurements of plant water status

R^2	WDI	S-SEB	INb points
AET/MET (all points)	0.64	0.61	15A
ET/MET (without non-irrigated fields)	0.8	0.75	11
Leaf humidity	0.06	0.01	8
Leaf potential	0.06	0.23	4
Available soil water	0.32	0.5	13

IV – Conclusion

In this study, we show that the calculation of WDI and S-SEBI using multispectral airborne imagery in visible, near infrared and thermal infrared bands allowed the estimation of the water status of durum wheat through a good estimation of AET / MET. These first results are promising regarding the use of remote sensing techniques for precision irrigation management.

References

Clarke T.R., 1997. An empirical approach for detecting crop water stress using multispectral airborne sensors. In: *Horticulture Technology*, 7, p. 9-16.

Erlher W.L., 1973. Cotton leaf temperatures as related to soil water depletion and meteorological factors. In: *Agronomy Journal*, 65, p. 404-409.

Hamdy A., Ragab R. and Scarascia-Mugnozza E. (2003). Coping with water scarcity: Water saving and increasing water productivity. In: *Irrigation and Drainage*, 52, p. 3-20.

Idso S.B., Jackson R.D., Pinter P.J., Reginato R.J. and Hatfield J.L., 1981. Normalizing the stress-degree-day parameter for environmental variability. In: *Agricultural Meteorology*, 24, p. 45-55.

Jackson R.D., Idso S.B., Reginato R.J. and Pinter P.J., 1981. Canopy temperature as a crop water stress indicator. In: *Water Resource Research*, 17, p. 1133-1138.

Jiménez-Muñoz J.C. and Sobrino J.A., 2006. Error sources on the land surface temperature retrieved from thermal infrared single channel remote sensing data. In: *International Journal of Remote Sensing*, 27, p. 999-1014.

Koenker R., 2008. Quantreg: Quantile Regression. R package version 4.17.
Lebourgeois V., Bégué A., Labbé S., Prévot L. and Roux B., 2008a. Can commercial digital cameras be used as multispectral sensor? A crop monitoring test. In: *Sensors*, 8 (11), p. 7300-7322. (Not cited).
Lebourgeois V., Labbé S., Bégué A. and Jacob F., 2008b. Atmospheric corrections of low altitude thermal airborne images acquired over a tropical cropped area. In: *IEEE International Geoscience and Remote Sensing Symposium*, Boston, Massachusetts (USA), 6-11 July, 4 p.
Maihol J.C., Olufayo O. and Ruelle P., 1997. AET and yields assessments based on the LAI simulation. Application to sorghum and sunflower crops. In: *Agricultural Water Management*, 35, p. 167-182.
Mailhol J.C., Zaïri A., Ben Nouma B. and El Amami H., 2004. Analysis of irrigation systems and irrigation strategis for durum wheat in Tunisia. In: *Agricultural Water Management*, 70 (1) p. 19-37.
Moran M.S., Ckarke T.R., Inoue Y. and Vidal A., 1994. Estimating crop water deficit between surface-air temperature and spectral vegetation index. In: *Remote Sensing of Environment*, 46, p. 246-263.
Roerink G.J., Su Z. and Menenti M., 1999. S-SEBI : A simple remote sensing algorithm to estimate the surface energy balance. In: *Physics and Chemistry of the Earth*, 25(2), p. 147-157.
Taner C.B., 1963. Plant Temperature. In: *Agronomy Journal*, 55, p. 210-211.

Application of INSPIRE directive to water management on large irrigation areas

M. Erena*, P. García*, J.A. López*, M. Caro*, J.F. Atenza*, D. Sánchez*, Z. Hernández*, R.M. García and R.P. García*****

*IMIDA (Instituto Murciano de Investigación y Desarrollo Agrario y Alimentario), C/ Mayor, s/n, 30150 La Alberca, Murcia (Spain)
**Irrigation General Direction of the Regional Department of Agriculture and Water of Murcia, Plaza Juan XXIII s/n, 30071 Murcia (Spain)
***Mapping Service of the Regional Department of Public Works of Murcia, Plaza de Santoña, 6, 30071 Murcia (Spain)

Abstract. The goal of this paper is to illustrate how INSPIRE can facilitate orientation and advice to calculate the water requirements of crops. These technologies can provide information adapted to specific conditions, updated daily and in an interactive way. These tools permit the integration and management of georeferenced agroclimatic data, soil maps, quality of waters, crop information and technical parameters of a farm. The final objective is to develop a decision support system to facilitate decision-taking processes in a comfortable and generic access on-line, incorporating different techniques and access into GIS data. The information technologies and in a more precise way, the new technologies, applied in different agriculture environments, can introduce important improvements in optimization of the agricultural production factors. Directive 2007/2/EC1 of the European Parliament and of the Council of 14 March 2007 establishing an Infrastructure for Spatial Information in the European Community (INSPIRE) entered into force on the 15th May 2011. INSPIRE lays down general rules to establish an infrastructure for spatial information in Europe for the purposes of Community environmental policies, and policies or activities which may have an impact on the environment. One of the aspects that INSPIRE regulates is the interoperability and harmonization of spatial data sets and services for 34 so-called data themes that are laid down in the three Annexes to the INSPIRE directive. These include land-cover, land-use and weather data.

Keywords. INSPIRE – GIS – OGC – Remote sensing.

Application de la directive INSPIRE à la gestion de l'eau sur de grandes zones irriguées

Résumé. *Le but de cet article est d'illustrer comment les nouvelles technologies peuvent faciliter l'orientation et le conseil pour calculer les besoins en eau des cultures. Ces technologies peuvent fournir des informations adaptées aux conditions spécifiques, mises à jour quotidiennement et de manière interactive. Ces outils permettent l'intégration et la gestion de données agroclimatiques géoréférencées, de cartes des sols, de la qualité des eaux et de l'information concernant les cultures et les paramètres techniques des exploitations. L'objectif final est de développer un système d'aide facilitant les processus de prise de décision, par le biais d'une application en ligne aisément accessible, incorporant des techniques différentes et permettant la consultation de données SIG. Les technologies de l'information et, plus précisément, les nouvelles technologies, appliquées à différents environnements agricoles, peuvent apporter des améliorations importantes dans l'optimisation des facteurs de production agricole. La Directive 2007/2/EC1 du Parlement européen et du Conseil du 14 mars 2007 établissant une infrastructure d'information géographique dans la Communauté européenne (INSPIRE) est entrée en vigueur le 15 mai 2007. INSPIRE établit les règles générales destinées à établir une infrastructure d'information géographique en Europe aux fins de la politique communautaire de l'environnement, et les politiques ou les activités susceptibles d'avoir une incidence sur l'environnement. Un des aspects qui réglemente INSPIRE est l'interopérabilité et l'harmonisation des ensembles de données et des services géographiques, pour 34 thèmes précisés dans les trois annexes de la directive. Parmi eux, on trouve notamment l'occupation des terres, leur usage et les données météorologiques.*

Mots-clés. *INSPIRE – SIG – OGC – Télédétection.*

I – Introduction

TELERIEG project, "Remote sensing use for irrigation practice recommendation and monitoring in the SUDOE space" (www.telerieg.net), aims to achieve a more efficient and rational management of water resources in agriculture. One of its objectives is to improve irrigation advice on the main crops in the area of the Tajo-Segura Aqueduct (ATS), which covers 150,000 ha between the provinces of Murcia and Alicante (South-East Spain) (Fig. 1).

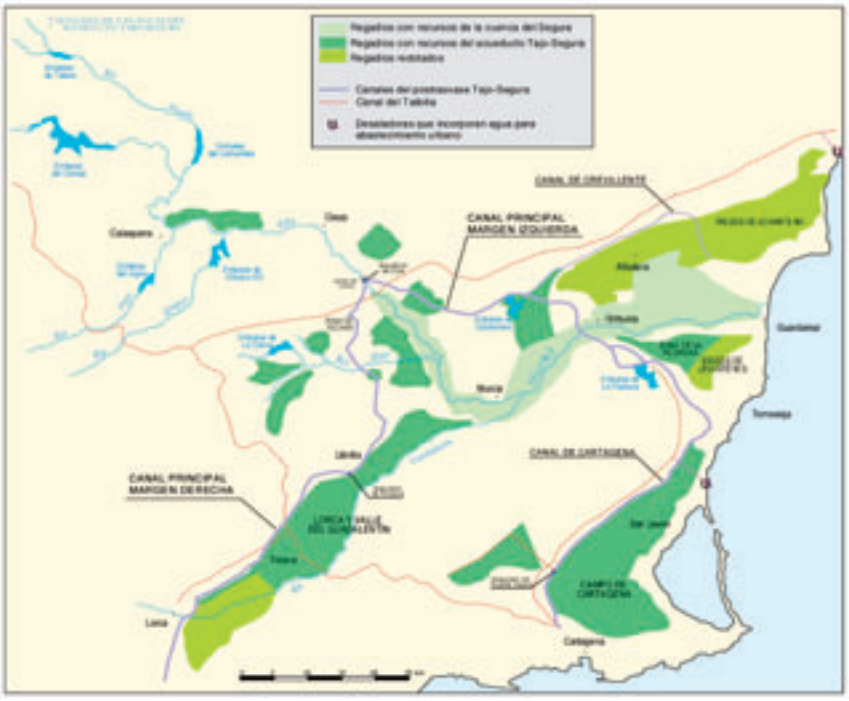

Fig. 1. Pilot zone: Irrigation areas of Aqueduct Tajo-Segura.

TELERIEG sought to integrate information from different European, national and regional governments by using standards recommended by the INSPIRE directive, in order to provide added value for agriculture and climate risk management in the pilot project areas covered by the project. The EU has already developed very advanced initiatives which implement this directive, especially related to soil at European level, such as those described in the publications of the Joint Research Centre Institute for Environment and Sustainability (JRC, 2011).

II – Material and methods

When trying to improve water management, one of the main issues we face is that we need a lot of agroclimatic data from various government and agencies, which generally store their data in different formats that greatly complicate their use. To solve this problem, global standards have been defined that tend to make data more accessible and open regardless of its origin. Therefore, the OGC (Open Geospatial Consortium) created, among other services, a series of standards for search, access and distribution, applicable to any spatially-referenced data. In this sen-

se the EU developed the INSPIRE Directive, aiming to solve many issues related to accessibility and interoperability of spatial data (INSPIRE, 2007).

The equipment used to improve the irrigation advisory service in the ATS area, as defined in Rincón and Erena (1998), consists of (Fig. 2):

Hardware:

- WA database server for weather data.
- Two servers for NOAA satellite images.
- A server to connect stations with GSM modem.
- 48 weather stations (3 different types of stations: Campbell, Thies, Geonica): 11 with a GPRS modem (data capture in real time) and 37 with a GSM modem.

Software:

- PC208W: a commercial application to manage Campbell stations.
- SADECA: an application developed in Visual Basic to manage Thies and Geonica stations.
- Oracle Database 11g Release 1 (11.1.0.6.0) for Oracle Linux.
- The Dartcom HRPT/CHRPT Grabber software.
- The Dartcom SIAMIV (Satellite Image and Meteorological Information Viewer) software.
- Adobe® Flash® Builder™ 4.5.
- Cartographic Viewer done with FLEX language using API's from ESRI.
- ArcGIS Server 9.3.1.

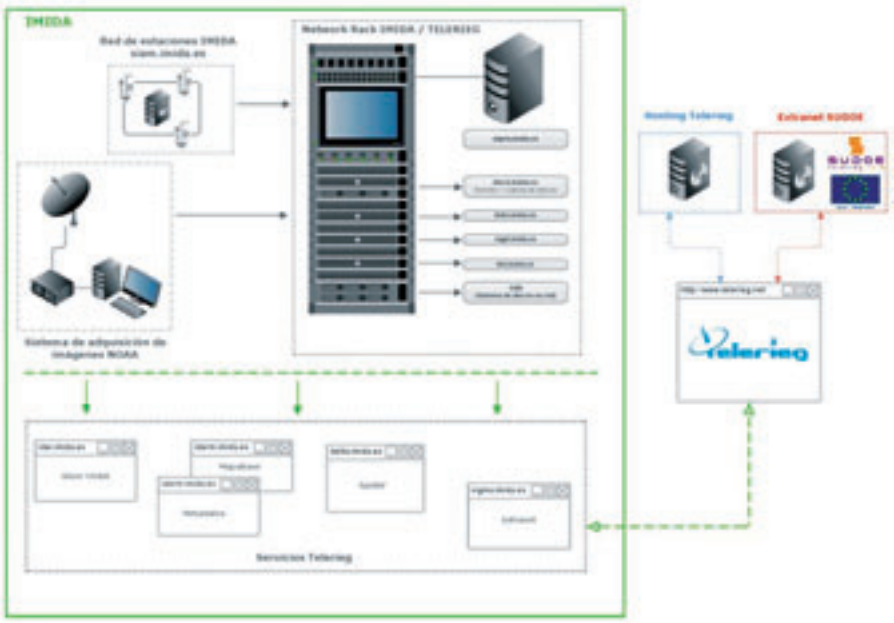

Fig. 2. System architecture of the TELERIEG project (http://www.telerieg.net).

The Fig. 3 below shows the functionality of the software used to develop the geoportal, following the standards of the INSPIRE directive (ESRI, 2007).

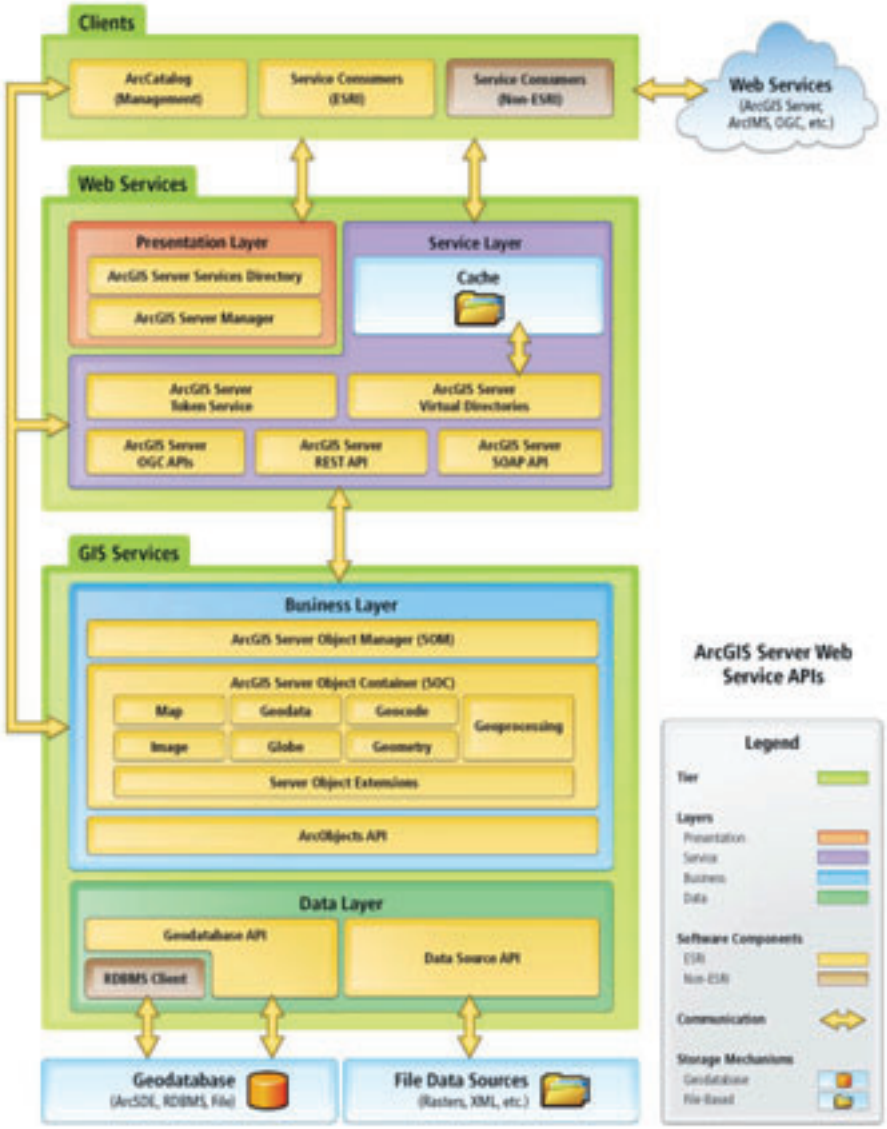

Fig. 3. System description of GIS component.

The INSPIRE directive (INSPIRE, 2007), aiming at the establishment of an Infrastructure for Spatial Information in the European Community, entered into force in May 2007. This directive recognizes that the general situation on spatial information for environmental purposes in Europe is one of fragmentation of datasets and sources, gaps in availability, lack of harmonization between datasets at different geographical scales and duplication of information collection. The

initiative intends to trigger the creation of a European spatial information infrastructure that delivers to the users integrated spatial information services. These services should allow the users to identify and access spatial or geographical information from a wide range of sources, from the local level to the global level, in an inter-operable way for a variety of uses. Policy-makers at European and national level are among the main targeted users who would need access to a number of services that include the visualization of information layers, overlay of information from different sources, spatial and temporal analysis, etc.

III – Results and discussion

The geo-portal developed within the project Telerieg integrates datasets from various government bodies which have in common a spatial component that allows its location in the territory. In this sense, the INSPIRE directive has been applied as a framework. Furthermore, a spatial data infrastructure based on OGC services (OGC, 2004; IDEE, 2007) has been built to query and manage useful information, especially for irrigation communities, becoming a support tool in decision-making for efficient water management in ATS irrigation areas.

For this purpose, a highly functional map viewer that integrates the information obtained by the SIAM (Agricultural Information System of Murcia) from the agro-climatic stations network of the Region of Murcia has been created in the Oracle® APEX environment on an Oracle® 11g database. The viewer uses the application programming interface (API) of ArcGIS for Adobe Flex, providing the basis of a web application that includes the following services: map viewer, geocoding, metadata access and geoprocessing based on ESRI ArcGIS Server. The abovementioned ArcGIS API for Adobe Flex allows us to develop high-performance applications that deliver GIS content and functionality for geo-portal users (Fig. 4).

Fig. 4. Flex viewer on the TELERIEG website (http://iderm.imida.es/telerieg/).

IV – Conclusions

In order to provide a service rich and adapted to the new technologies that make the Web 2.0, we have used those technologies along with GIS, remote sensing, agro-climatic data and recommendations of the INSPIRE directive for improving the irrigation advisory systems in the pilot area. Irrigators and other particular users easily get a great deal of information that will be useful to improve the efficiency of water use in agriculture, as this information is essential for proper irrigation scheduling based on climatic evolution and crop development.

We believe that these technologies are well suited for the implementation of systems which support the definition of irrigation programs on farms, thus improving crop development, as well as some water savings, which is especially important in areas with limited resources such as the south-eastern Spain.

Acknowledgments

This work has been done through the project TELERIEG "Remote sensing use for irrigation practice recommendation and monitoring in the SUDOE space" (SOE1/P2/E082) financed by the South West Europe Territorial Cooperation Programme (SUDOE-Interreg IVb), which supports regional development through European Regional Development Fund (ERDF) co-financing of transnational projects.

References

Erena M., Navarro E., Rincón L. and Garrido R., 1998. Los sistemas de información geográfica en la caracterización agroclimática. In. *Riegos y Drenajes,* XXI, 103/98, p. 20-24.

ESRI, 2007. Support for ISO and OGC Standards [online]. ESRI. [Last accessed on December 2007]. <http://www.esri.com/software/standards/support-iso-ogc.html>

IDEE. 2007. Información IDE [online]. In: Infraestructura de Datos Espaciales de España. [Last accessed on December 2007]. <http://www.idee.es/>

INSPIRE, 2007. Directive 2007/2/EC of the European Parliament and of the Council of 14 March 2007 establishing an Infrastructure for Spatial Information in the European Community (INSPIRE), published in the Official Journal on the 25th April 2007, entering into force on the 15th May 2007. *Official Journal of the European Union,* ISSN 1725-2555, L 108, Volume 50, 25 April 2007. <http://www.ec-gis.org/inspire/>

JRC, 2011. Land Quality and Land Use Information in the European Union. Catalogue Number LB-NA-24590-EN-C ISBN 978-92-79-17601-2 ISSN 1018-5593 doi: 10.2788/40725.

OGC, 2004. The Spatial Web. An Open GIS Consortium (OGC) White Paper. [online]. Open GIS Consortium, 2004. <http://www.opengeospatial.org/>

Rincón L., Erena M., Caro M., García F. and García A., 1998. The agrarian information service of Murcia Region-SIAM. In: 1st Inter-regional conference on enviroment-water: innovative issues in irrigation and drainage. Lisbon, Portugal.

Soil salinity prospects based on the quality of irrigation water used in the Segura Basin

F. Alcón*, J.F. Atenza, M. Erena** and J.J. Alarcón*****

*Universidad Politécnica de Cartagena, Paseo Alfonso XIII, 48, 30203 Cartagena, Murcia (Spain)
**Instituto Murciano de Investigación y Desarrollo Agrario y Alimentario (IMIDA)
C/ Mayor s/n, 30150 La Alberca, Murcia (Spain)
***Centro de Edafología y Biología Aplicada del Segura (CEBAS-CSIC)
Campus Universitario de Espinardo, 30100 Espinardo, Murcia (Spain)

Abstract. The main objective of this study was to determine the effect of the quality of irrigation water currently used in various agricultural demand units (ADU) on the soil-water salinity, assessing the effects of its use on crop yields and soils agronomic properties. The current state of the water quality used in all ADUs of the Segura Basin (Spain) was identified through sampling points located in surface and groundwater bodies. The geographical relationship established between water quality and crops in each ADU allowed a prospective analysis of the major agronomic risks of salinity, infiltration, toxicity by undesirable ions and the resulting environmental risks of soil degradation. WATSUIT software was used for each existing relationship between water bodies and ADUs. The results of this study provide geo-referenced knowledge of the current status of water quality and of the problems that its use may cause on the crops and the environment. It is also the starting point in establishing actions to increase the quality of irrigation water improving environmental conservation.

Keywords. GIS – WATSUIT – Agricultural Demand Unit – Segura River Basin – Spain.

Prospective de la salinité des sols en fonction de la qualité de l'eau d'irrigation dans le bassin du Segura

Résumé. *L'objectif principal de l'étude était de déterminer l'effet de la qualité de l'eau d'irrigation utilisée actuellement dans les diverses unités de demande agricole (UDA) sur la salinité de l'eau dans le sol, en évaluant ses effets sur les rendements agricoles et les propriétés agronomiques des sols. Pour atteindre cet objectif, nous avons identifié l'état actuel de la qualité de l'eau utilisée dans toutes les UDA du bassin versant du Segura (Espagne) grâce à des points d'échantillonnage dans les eaux de surface et souterraines. Le lien géographique établi entre la qualité de l'eau utilisée et les cultures de chaque UDA a permis de mener une analyse prospective de la situation concernant la qualité de l'eau d'irrigation basée sur une série de risques agronomiques majeurs : la salinité, l'infiltration, la toxicité due à des ions indésirables et les risques environnementaux de dégradation des sols qui en résultent. Pour ce faire, le logiciel WATSUIT a été utilisé pour étudier chacun des rapports existant entre masses d'eau et UDA. Les résultats de cette étude permettent de connaître de façon géo-référencée l'état actuel de la qualité de l'eau d'irrigation et les problèmes que son utilisation peut entraîner sur les cultures et l'environnement. Elle nous permet également d'établir un point de départ pour la mise en place de mesures visant à augmenter la qualité de l'eau d'irrigation et préserver l'environnement.*

Mots-clés. *SIG – WATSUIT – Unité agricole de demande en eau – Bassin du Segura.*

I – Introduction

The Segura River Basin is located in southeast Spain and has an area of 18,870 km² occupied by 1,944,690 inhabitants. It covers territories from 4 regions: Andalusia, Castile-La Mancha, Murcia and Valencia, with a total of six provinces and 132 municipalities. The Murcia region is fully integrated in this basin encompassing most of its surface (59.3%) and population (73.3%) (CHS, 2008).

The climatic characteristics that define the Segura Basin are a semi-arid Mediterranean climate, with mild winters (11ºC on average in December and January) and hot summers (with highs of

45ºC). The average annual temperature is 10-18ºC, rainfall is low, around 365 mm per year, although there is a high variation range (200-1,000 mm). April and October are the wettest months, with frequent torrential rains. The distance from the sea and the features of the terrain means that there are differences in temperature between the coast and inland. The low rainfall contrasts with the high average potential evapotranspiration (827 mm) (CHS, 2008; AEM, 2010).

Agriculture of this basin is among the most profitable in Spain. However, the predominantly intensive agriculture may present a risk of soil salinization due to overuse of fertilizers or irrigation mismanagement. In the Region of Murcia, which accounts for most irrigated crops, irrigated agriculture contributes 75% to the final production of the agriculture product, with vegetables (38%) and fruits (21%) being the major contributors (Arcas *et al*., 2010).

The irrigation water demands in the Segura Basin are recorded, for 74 Agriculture Demand Units (ADU), in the Segura Basin Water Plan (SBWP). The ADU is defined as a separate unit of agricultural management, either by origin of resources, administrative conditions, hydrological similarity or strictly territorial considerations. Based on the information contained in the National Hydrological Plan (NHP), the water irrigation demand for all the ADUs of the basin is 1,662 hm³/year. The provision of irrigation water per ADU is highly variable and, although on average the net allocation is 3,628 m³/ha, the variation range is between 938 and 7,483 m³/ha (MMA, 2001).

The origin of the water used for irrigation in each ADU is very variable, with six different sources. Water comes mostly from surface resources (495 hm³/year) followed by underground resources (412 hm³year) and water from the Tagus-Segura Aqueduct (385 hm³/year). To a lesser extent, ADUs are supplied by water from *azarbes* (trenches or drains for irrigation waters), wastewater treatment plants and other sources, complementing an allocation of 1 432 hm³/year. Considering the total agriculture demand for water (1.662 hm³/year), the deficit in the whole basin is around 229 hm³/year, which together with the overexploitation of groundwater resources (174 hm³/year) would amount up to 403 hm³/year (MMA, 2001).

This paper identifies the current status of the water quality in all ADUs in the Segura basin, aiming a prospective analysis of the major agronomic risks induced by the use of poor water quality in the irrigation: salinity, infiltration and ions toxicity. The results of this study will provide geo-referenced knowledge of the current status of water quality and of problems that its use may cause on the crops and the environment. It will also represent the starting point in establishing actions to increase the quality of irrigation water and improve environmental conservation.

II – Material and methods

Demands for irrigation water have been linked with the quality of different water sources through a model based on a geographic information system (GIS) which has allowed relating the quality sampling points with ADUs. Through this process all the variables generated in the study have been represented in maps.

The analysis unit used is the ADU. Both the agronomic characteristics of the ADUs and the source of irrigation water used in them have been obtained from the Segura Basin Water Plan, and the data on quality of irrigation water in 2007 have been provided by the Hydrographical Confederation of the Segura River.

Subsequently, for each sources of water and unit of demand, we used the software WATSUIT (USDA) which predicts soil salinity, sodicity and toxic solute concentration resulting from the use of irrigation water with specific characteristics. The lower quality water has been selected when different water sources are used in one ADU, therefore the simulation results derive from the most unfavourable scenario.

The main outputs of WATSUIT are: electrical conductivity (EC), sodium absorption ratio (SAR) and chlorides content in the root zone (Cl). These parameters allow estimating the risk of salinity, infiltration and toxicity of irrigation water on the crops.

Subsequently, for each ADU, we analysed several risks related to the water quality use: loss of crop yield, following the criteria of Maas and Hoffman (1977) adapted by Ayers and Westcot (1985); compaction and loss of top-soil infiltration, using the criterion of Rhoades (1977) adapted by Ayers and Westcot (1985); and chloride toxicity, determined from the threshold defined by Ayers and Westcot (1985).

III – Results and discussion

There are 74 ADUs in the Segura River Basin which can be divided into 9 macro-ADUs (Fig. 1). The mean values of EC, Cl and SAR for each macro-ADU are shown in Table 1 and Table 2 for surface water bodies and groundwater bodies respectively. Furthermore, after feeding the parameters of irrigation water into WATSUIT, we obtained the values of EC, Cl and SAR in the soil as average values for the entire root area (Tables 1 and 2).

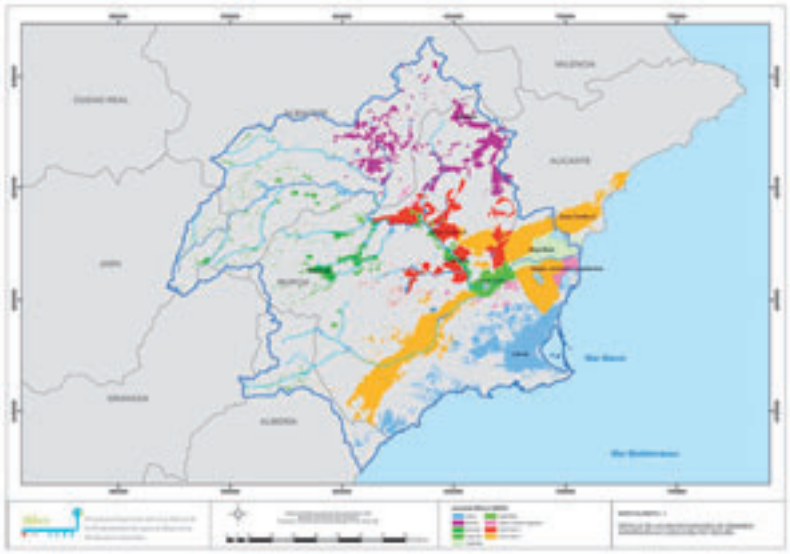

Fig. 1. Location of the nine macro-ADUs in the Segura Basin.

Table 1. Surface water characteristics and soil prospective induced by its use for each macro-ADU

Macro-ADU	Surface water			Soil prospective		
	EC dS/m	Cl meq/l	SAR mmol/l	EC dS/m	Cl meq/l	SAR mmol/l
Litoral	5.70	41.64	8.05	9.59	72.86	16.40
Noreste	2.56	9.48	2.19	3.77	20.83	5.10
Noroeste	1.58	5.16	1.49	2.40	12.36	3.21
Vega Alta	1.51	5.63	2.03	2.39	12.08	4.22
Vega Baja	3.99	19.76	5.65	6.38	39.34	11.86
Vega Media	5.33	10.00	10.61	9.91	76.54	21.22
Vegas, excl. regulat.	3.29	15.57	4.95	5.21	26.83	10.10
Zona Centro 1	3.88	21.62	4.61	5.86	40.95	9.82
Zona Centro 2	5.52	44.45	13.54	10.66	83.11	26.34
Average	3.70	19.26	5.90	6.24	42.77	12.03

Table 2. Groundwater characteristics and soil prospective induced by its use for each macro-ADU

Macro-ADU	Surface water			Soil prospective		
	EC dS/m	Cl meq/l	SAR mmol/l	EC dS/m	Cl meq/l	SAR mmol/l
Litoral	3.97	33.58	6.44	8.12	63.64	13.37
Noreste	1.43	5.11	1.83	2.11	9.99	3.64
Noroeste	0.60	1.73	0.73	0.90	3.67	1.58
Vega Alta	0.73	6.34	2.66	1.83	12.33	4.84
Vega Baja	2.28	15.99	3.65	4.79	29.40	7.62
Vega Media						
Vegas, excl. regulat.	6.44	41.26	7.08	9.65	79.36	15.50
Zona Centro 1	2.08	14.44	6.11	3.98	25.43	12.68
Zona Centro 2	3.55	21.07	5.84	5.56	42.66	9.71
Average	2.64	17.44	4.29	4.62	33.31	8.62

Considering the EC of irrigation water for each macro-ADU, it is possible to appreciate that groundwater quality is higher than surface water for the entire basin. The Coastal Zone *(Zona Litoral)* presents a very high level of EC, 5.7 and 3.97 dS/m for surface water and groundwater respectively. The average quality of surface waters in the 2nd Central Zone *(Zona Centro 2)* is also very high (5.52). In groundwater, the highest EC values are in the fertile valleys *(Vegas)* excluded from hydraulic regulation (6.44). By contrast, the highest-quality sources of irrigation water, both from surface and underground, are found in the north of the basin, with values below 2.56 dS/m for surface water and 1.43 dS/m for groundwater.

Analysing the values obtained for the different ADUs, and considering the quality of irrigation water according to SAR and EC, severe use restrictions according to the infiltration criteria established by Rhoades (1977) and Oster and Schroer (1979) have not been found. However, a slight reduction in infiltration is found in the Northeast *(Noreste)* and Northwest *(Noroeste)* ADUs for both sources of water, while in the 1st Central Zone the risk only exists in some ADUs being supplied with groundwater (Fig. 2).

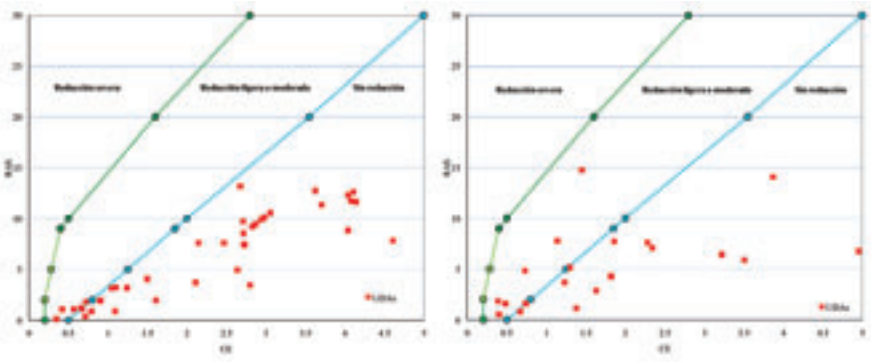

Fig. 2. Relative reduction of infiltration caused by salinity and sodium adsorption ratio in ADUs of the Segura Basin, for surface water (left) and groundwater (right).

Under the criteria described above, we also analysed the potential risk of surface crusting from the use of irrigation water. As occurred with the degree of infiltration, crusting risk is greater in ADUs of the northern region, due to the use of very hard water with low salinity (Fig. 3).

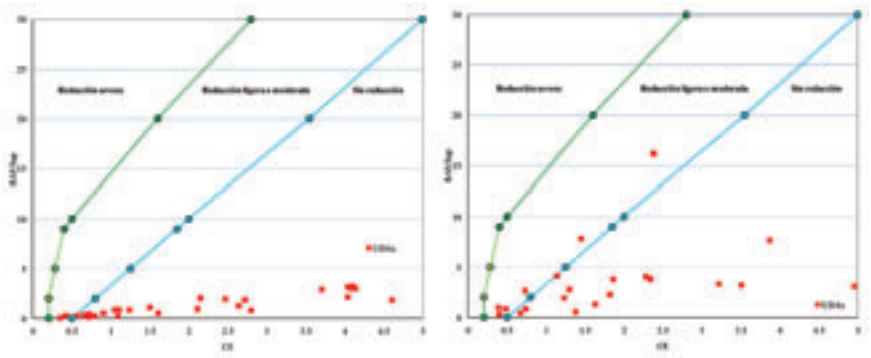

Fig. 3. Risk of surface crusting caused by salinity and sodium adsorption ratio in ADUs of the Segura Basin, for surface water (left) and groundwater (right).

Regarding irrigation water toxicity due to high chloride concentration, it is clear that most of the water used for irrigation in Murcia exceeds the threshold set by Ayers and Westcot (1985), which consider values greater than 10 meq/l as a significant problem. These levels are exceeded in all macro-ADUs except northern ones (Northwest, Northeast and *Vega Alta*). In general, the chloride concentration is higher in surface waters (Fig. 4).

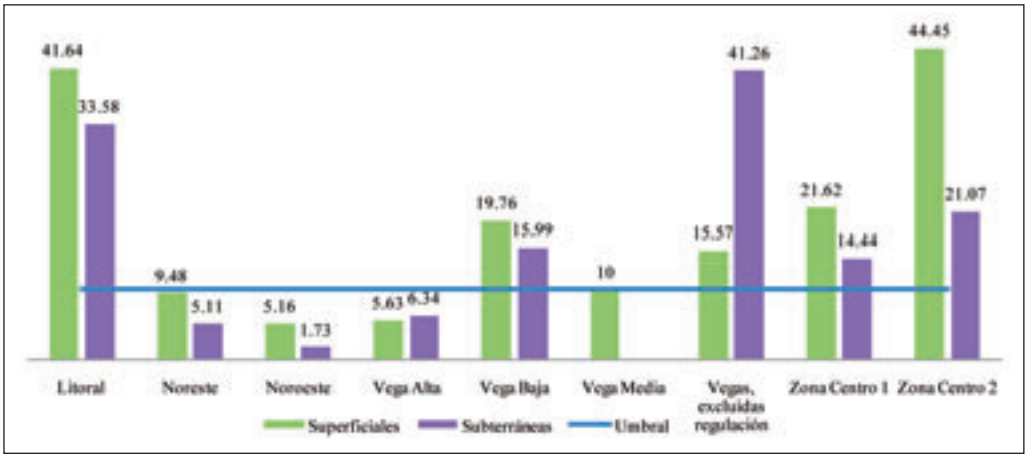

Fig. 4. Concentration of chlorides in irrigation water.

The most important predictive parameter related to the quality of irrigation water has been the estimated crops yield loss. The potential risk of yield loss per ADU was estimated by the ratio between surface water and groundwater used. This overall yield parameter is shown on Fig. 5, where significant risks of reduced yield production are observed for the Coastal Zone and Middle and Lower *Vegas* of the Segura Basin.

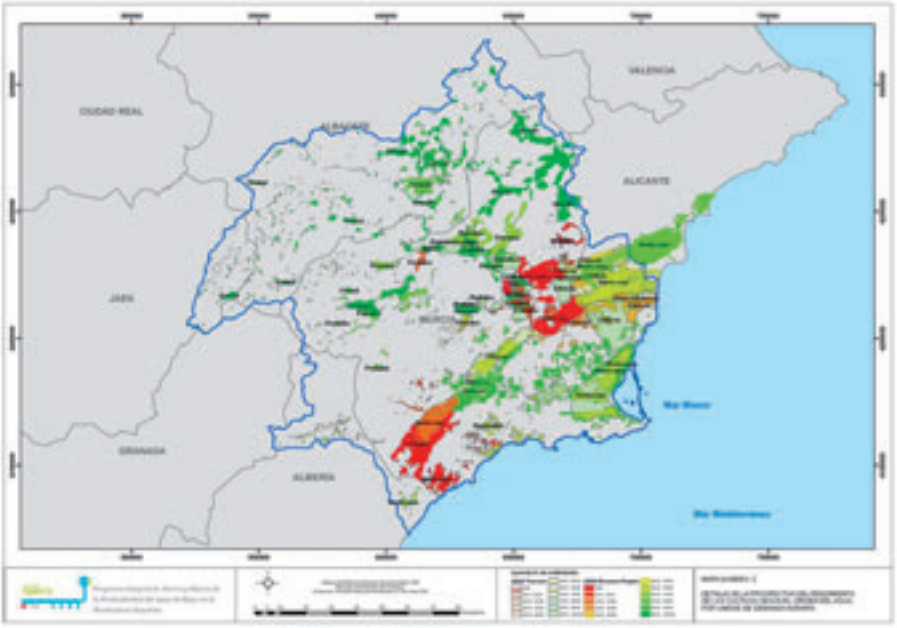

Fig. 5. Estimated percentage of yield reduction for each ADU of the Segura Basin, depending on the quality of water used and the main crop.

IV – Conclusions

The quality of irrigation water in the basin is, in general, moderately acceptable given the arid conditions in south-eastern Spain. In general, the quality of surface water is lower than groundwater. While in the upper watershed resources are of better quality, water salinity increases as we descend through the valleys of the different rivers, both for surface water and groundwater, with the quality of water in coastal zones being the lowest.

Surface waters in the high valley of the Segura, as well as those from the Tajo-Segura Aqueduct, have an acceptable quality which decreases as the distance between the source of water and the point where it is applied increases. The good-quality waters channelled through the post-aqueduct infrastructure represent an essential contribution for irrigation in the Guadalentín Valley, the *Campo de Cartagena* and the Segura Lower Valley.

As for groundwater, permanent withdrawals and overexploitation of many aquifers in the basin have resulted in a widespread loss of quality that gets stronger in the lower areas of valleys and in the Coastal Zone. The continued use of these water resources for irrigation will probably put crops and the environment at risk from salinization, soil compaction and undesirable ions toxicity. This situation will result in a loss of crop yield and therefore will impact the welfare of farmers.

In the coastal area, significant yield reductions are expected. In the *Campo de Cartagena* (yield=72%) and especially in the west coast (yield=40%) these reduction could be alleviated with the use of alternative water resources (reclaimed water, desalinized water, Tajo-Segura transfer, etc.). In these areas, it is necessary a reduction in withdrawals to allow recovery of aquifers, highly saline. There are no problems of loss of soil structure, but chloride toxicity risks are found.

Irrigated crops in the Northeast and Northwest areas, both with surface and groundwater resources, will not suffer from reduced yields in the future, although the low conductivity of irrigation water may generate a slight problem of infiltration. Toxicity problems are not foreseen.

The waters flowing through the Segura River require special attention as river flow decreases. In the upper part *(Vega Alta),* serious loss of crop yields is not expected neither infiltration nor surface crusting. In the middle part *(Vega Media),* problems begin to be most prominent, as yields could fall to 35% of the agronomic potential due to toxicity risk, and in the lower part *(Vega Baja)* yields could fall to 15% as the risk of toxicity from chlorides increase. The levels of water salinity will prevent infiltration and surface crusting problems.

In the Central Zone, irrigated areas mainly use water from the Aqueduct and although in the Mula River Basin some water bodies are of reduced quality, overall performance in the region exceeds 70%, being in most ADUs close to 100%. Again, the contributions of the Aqueduct are able to compensate for the low quality of the rare surface waters of the inland basins and the medium quality of groundwater. The risks of soil compaction are practically inexistent and those related to chlorides toxicity will depend on the use of groundwater and intermittent streams. Given the current situation of irrigation in the Segura Basin and the potential risk of degradation of irrigation water and agricultural soils, it will be necessary to take action on water bodies, both surface and groundwater, in order to support the continuation of efficient and profitable farming system in the basin. These actions should be aimed at increasing the quality of irrigation water, especially in the middle and lower parts of the watersheds and in coastal areas. The waters of the Tajo-Segura Aqueduct have proved to be a source of vitality for irrigation, without which crop yields in the basin would be seriously compromised, and the problems of soil salinity and toxicity should be further aggravated. Thus, the new Segura Basin Water Management Plan must consider not only the quality aspects of water bodies, but also the impact of these waters on the crops and the risk of soil salinization.

Acknowledgments

This work was carried out under the national project RIDECO (Consolider-Ingenio 2010 - CSD2006-0067) and the European Project "Sustainable use of irrigation water in the Mediterranean Region" (SIRRIMED - FP7-FOOD-CT-2009-245159).

References

AEM, 2010. Agencia Estatal de Meteorología. Disponible en: http://www.aemet.es

Arcas N., Alcón F., López E., García R. and Cabrera A., 2010. *Análisis del sector agrícola de la Región de Murcia. Año 2009*. Informes y Monografías nº 24. Fundación Cajamar, Almería.

Ayers R. and Westcot D., 1985. Water quality for agriculture. *FAO Irrigation and Drainage Paper 29 rev. 1*. FAO Rome.

CHS, 2005. *Informe de los artículos 5, 6 y 7 de la Directiva Marco del Agua*. Confederación Hidrográfica del Segura. Available in: http://www.chsegura.es

CHS, 2007. *Estudio General Sobre la Demarcación Hidrográfica del Segura. Confederación Hidrográfica del Segura*. Confederación Hidrográfica del Segura. Available in: http://www.chsegura.es

CHS, 2008. *Memoria 2008*. Confederación Hidrográfica del Segura. Available in: http://www.chsegura.es

Maas E.V. and Hoffman G.J., 1977. Crop salt tolerance – Current assessment. In: *J. Irrigation and Drainage Division,* ASCE 103(IRZ), p. 115-134. Proceeding Paper 12993.

MMA, 2001. *Plan Hidrológico Nacional*. Ministerio de Medio Ambiente. Madrid.

Oster J.D. and Schroer F.W., 1979. Infiltration as influenced by irrigation water quality. In: *Soil Sci. Soc. Amer. J.*, 43, p. 444-447.

Rhoades J.D., (1977). Potential for using saline agricultural drainage waters for irrigation. In: *Proc. Water Management for Irrigation and Drainage*. ASCE, Reno, Nevada. 20-22 July 1977. p. 85-11.

Radar-aided understanding of semiarid areas: Maximum depression storage and storm motion

J. García-Pintado*, G.G. Barberá, M. Erena***, J.A. Lopez***, V.M. Castillo** and F. Cabezas***

*Euromediterranean Water Institute, Campus de Espinardo, E-30100 Murcia (Spain)
**CSIC-CEBAS, Soil and Water Conservation Department
Campus de Espinardo, PO BOX 164, E-30100 Murcia (Spain)
***Institute of Environmental and Agricultural Development (IMIDA)
C/ Mayor s/n, E-30150 La Alberca, Murcia (Spain)

Abstract. Weather radar supports the estimation of accurate spatiotemporal rainfall inputs. These may be of great help to hone water management strategies, as those involving irrigation plans or flood risk analyses. If these strategies are supported by simulation models, the radar-based estimates should lead in turn to lower biases in estimates of model parameters and to improved model structures. E.g., flash floods pose a danger for life and property and, in semiarid agricultural areas, have a strong relationship with soil loss processes. Unfortunately, in arid and semiarid environment the runoff generation shows a complex nonlinear behavior with a strong spatiotemporal non-uniformity. Predictions by forecasting models are subject to great uncertainty and better descriptions of physical processes at the watershed scale need to be included into the operational modelling tools. We analyze a convective storm, in a 556 km^2 semiarid Mediterranean watershed, with a complex multi-peak response. Radar was instrumental in the understanding and analysis of runoff generation. In the central area, a significant time-variability in the maximum depression storage resulted in the *a posteriori* model structure, pointing to failures in agricultural terraces and/or protection structures. Sensitivity analysis to storm motion indicates that a partial coverage upstream-moving storm on the infiltrating plane results in greater responses.

Keywords. Agricultural land – Semiarid zones – Floods – Hydrological model – Model structure.

Compréhension des zones semi-arides à l'aide de radars : capacité maximale de stockage d'eau dans le micro-relief et mouvement des tempêtes

Résumé. *Les radars utilisés à des fins météorologiques contribuent à estimer avec plus d'exactitude l'apport spatiotemporel des précipitations. Ceci peut être d'une grande utilité pour améliorer les stratégies de gestion de l'eau, notamment celles qui font appel à la planification de l'irrigation ou à l'analyse des risques d'inondation. Lorsque ces stratégies s'appuient sur des modèles de simulation, les estimations faites à l'aide de radars devraient permettre à leur tour de réduire les biais que présentent les estimations des paramètres du modèle et d'améliorer les structures du modèle. Par exemple, les crues subites posent un danger pour la vie et la propriété et, dans les milieux agricoles semi-arides, elles sont fortement corrélées aux processus de perte de sol. Malheureusement, dans les environnements arides et semi-arides, le ruissellement provoqué montre un comportement non linéraire complexe et fortement non uniforme spatiotemporellement. Les prédictions des modèles de prévision sont soumises à une grande incertitude et il est donc nécessaire d'incorporer de meilleures descriptions des processus physiques à l'échelle du bassin dans les outils opérationnels de modélisation. Nous analysons une tempête convective, dans un bassin hydrographique méditerranéen semi-aride de 556 km2, présentant une réponse complexe multi-pics. Le radar a fortement contribué à la compréhension et à l'analyse du ruissellement provoqué. Dans la zone centrale, il y a eu une variabilité temporelle significative de la capacité maximale de stockage dans le micro-relief, ce qui a permis de structurer le modèle a posteriori et a révélé les faiblesses des terrasses agricoles et/ou des structures de protection. Une analyse de sensibilité par rapport au mouvement de la tempête a montré que l'on pouvait obtenir de meilleures réponses en se focalisant partiellement en amont du mouvement de la tempête sur le plan d'infiltration.*

Mots-clés. *Terres agricoles – Zones semi-arides – Inondations – Modèle hydrologique – Structure du modèle.*

I – Introduction

The past several decades have seen increasing interest in the river systems that drain the world's extensive hyper-arid, arid, semiarid and dry sub-humid regions. These *drylands* cover nearly 50% of the world and support ~20% of its population (Middleton and Thomas, 1997). The spatial generation of runoff is strongly non-uniform in semiarid areas, and is mainly controlled by the rainfall characteristics and the surface physical and chemical properties (Yair and Klein, 1973). Combined effects of tillage patterns with topographic relief in agricultural areas involve a wide range of surface depression storage (Guzha, 2004). At larger scales than the micro-topography, small earth dams in agricultural plots and terraces are generally built in or near drainage lines with the primary purpose for impounding water for storage. These retention structures can intercept important amounts of water in areas greater than thousands of square meters, and, after an uncertain retention time, they may eventually fail with hardly foreseeable effects on downstream flows. Although these micro-dams have a high influence on the hillslope hydrology, literature about their behavior is scarce (Bellin *et al.*, 2009).

Uncertainty in model structure is attracting increasing attention in hydrology (Refsgaard *et al.*, 2006), and the presence of time-varying parameters (TVPs) indicates model's structural inadequacies (e.g. Lin and Beck, 2007). Maximum depression storage (*D*) is commonly assumed to remain constant along time in flash flood modelling. Here we allow it to evolve. Its state-dependence is formulated by a simple parsimonious model. The *a priori* model structure (constant *D*) is evaluated versus an *a posteriori* structure with TVP *D* formulation. We adhere to Knighton and Nanson (2001), who advocate an event-based approach to dryland river hydrology to account for the specific characteristics of diverse floods. Thus we analyze in detail one convective storm, in October 2003, in the *Rambla del Albujón* watershed; a semiarid Mediterranean coastal watershed in SE Spain with some urbanized areas and high agricultural pressures. We show how the model is able to locate areas where failures in agricultural protection structures is more likely to have occurred.

We also analyze the sensitivity of the watershed response to storm motion. While this has been the subject of a number of investigations, there is a general lack of analyses conducted on real storms at operational scales, mostly in semiarid environments.

II – Rainfall-runoff modelling framework and analytic techniques

1. Quantitative precipitation estimates (QPE)

QPE errors can dominate the uncertainty in the modeled semiarid runoff, and weather radar has become highly useful for flood forecasting (e.g. Moore, 2002; Carpenter and Georgakakos, 2004). However, radar QPE are prone to inaccuracies, with systematic and random errors often exceeding 100% (Baeck and Smith, 1998). So, adjustment of systematic biases in radar-rainfall using rain gauge measurements has been widely recognized as one of the most important steps in rainfall estimation. Here we used the Concurrent Multiplicative-Additive Objective Analysis Scheme (CMA-OAS) for multi-sensor QPE (García-Pintado *et al.*, 2009a). We used the national radar mosaic, ENS-R-N, from the Spanish Meteorological Agency (AEMET), which includes physically-based processing (with Vertical Profile Reflectivity correction) to estimate reflectivity at the ground level. Ground rainfall data were obtained from 91 tipping-bucket gauges (0.2 mm resolution), operated by the Agro-climatic Information Service of Murcia region (SIAM), and the Automatic Hydrological Information System (SAIH) of the Segura Basin Hydrological Confederation (CHS). Integration time was 1 h.

2. Modelling framework

We used the MARIAM (Mediterranean and Arid areas Redistribution Input Analysis Model); an event-oriented, distributed, and physically-based forecasting model (García-Pintado *et al.*, 2009b). Inner time step was 1 min, and spatial resolution 50 x 50 m. The *a priori* model structure considers terrain relief as static. Two relief properties were identified as likely time-varying in the observed rainfall-runoff event: maximum depression storage (*D*) in land, and roughness in channels. Here we focus on the former. The following subsection shows how we modeled the observations through a dynamic formulation of *D*. The innovated model structure is such that the physical/conceptual meaning of *D* remains the same as in the *a priori* structure.

3. Dynamic maximum depression storage

The maximum depression storage *D* is a relief-dependent property that indicates the maximum water that could be stored on surface. Available watershed models consider *D* as a constant parameter, either lumped or spatially distributed. Then, either *D* is applied at the beginning of the storm and only water in excess of *D* is allowed to runoff, or the rate of filling of the deposit *D* is inversely proportional to the available remaining space in *D*. Several formulations have been proposed for the latter option; which allows for a proportion of the effective rainfall to be released as runoff, even for small rainfall rates, before *D* is completely full.

Mitchell and Jones (1978) demonstrated the value of a dynamic description of the maximum depression storage at the plot scale. Our focus is, however, on processes occurring at the catchment scale. Values of *D* may remain fairly constant in totally natural, commonly more vegetated, areas. However, our field observations in storm events indicate (i) that anthropogenic "soft structures", mostly for agricultural tasks (such as tilling patterns, terraces, small earth dams around agricultural plots...), may lead to high *D*, and (ii) that intense energy storms and floods weaken the retention capability of these structures, whose eventual failure and possible cascading effect, speeding up downstream flows, is difficult to predict. Sandercock *et al.* (2007) comment that small earth dams around agricultural plots have a big influence on the connectivity of the hill slope; however, during large rainfall events the runoff might cause them to collapse, and at that moment the runoff flow might damage all lower lying earth dams as well. Our view of this process indicates that the global retention capability of agricultural semiarid watersheds fails by structural breaching (gradual failure), with increased hydraulic pressures implying more abrupt breaching.

We suggest a model in which the time history of water stage *h(t)* produces a gradual damage accumulation in the initial *D* (D_0), which may fall up to a final operation mode (D_s), after all the "soft" spatially distributed retention capability of the watershed has failed. Here we propose a time-varying maximum depression storage *D(t)* to be simulated by a logistic decay:

$$D(t) = Ds + \frac{(D_0 - D_s)\,(1 + \alpha_D)}{1 + e^{\beta_D \int_0^t h(\tau)d\tau}} \qquad (1)$$

where the parameters α_D (–) and β_D ($m^{-1}\ s^{-1}$) control the shape of this S-type decay model, and τ is a dummy variable of time. For a specific (α_D; β_D), relatively low *h(t)* values may never be able to significantly modify the initial *D(t)* value, D_0. However, relatively high *h(t)* values may cause structures to collapse in a very short time. Equation (1) may be combined with the formulations that allow some water stored in *D(t)* to be released as a function of the level *h(t)* (e.g. see Bras, 1990). However, this would require extra parameters. Thus taking into account the principle of parsimony, just water in excess of *D(t)* is allowed here to be routed. In addition, while the possible combinations of the four parameters in equation (1) (D_0, D_s, α_D, β_D) allow a wide spectrum of decaying depression storage evolutions, the constraint $\alpha_D = \beta_D$ was added in this study to further

reduce the analyzed parametric space. Also, this constraint facilitates evaluation of feasible parameter ranges through mapping α_D and β_D onto a parameter with temporal meaning. That is, we can solve equation (1) for a parameter I_D (which equals both α_D and β_D) as a function of a desired *D(t)* evolution under the hydraulic pressure given by a constant water column *h* applied a specific time span Δt. So, if for a constant *h* we consider the half-life $\Delta t_{0.5}$ as that time in which $D(t)=(D_0+D_s)/2$, we can make the corresponding substitutions in equation (1) to obtain:

$$f(\lambda_D) = 1 + \lambda_D (2 - e^{\lambda_D h \Delta t_{0.5}}) = 0 \quad (2)$$

whose solution will yield the parameter I_D. Then, I_D is used for substituting both α_D and β_D in the theoretical curve, given by equation (1), which will be used in the model with time-varying *h(t)* conditions. The function $f(I_D)$ in equation (2) has a well defined maximum and only one real root I_D over [0, ∞), and its solution may be found by Newton's method. If, in addition, *h* is set to $h=(D_0+D_s)/2$ in equation (2), the values of $\Delta t_{0.5}$ represent the half-life of the structures when these are constantly subjected to a hydraulic head equal to the half of the decaying range allowed for maximum depression storage. This approach still allows a wide variety of *D(t)* behaviors as a function of the free parameters (D_0; D_s, and $\Delta t_{0.5}$) input into the model.

4. Watershed and gauge points

Mean annual precipitation in the *Rambla del Albujón* watershed (556 km^2) is 300 mm, generally concentrated short episodic stormy events. Potential evapotranspiration is 890 mm year^{-1}. Figure 1 shows Hydrological response Unit (HRU; area assumed as responding homogeneously) subdivision and flow gauge points.

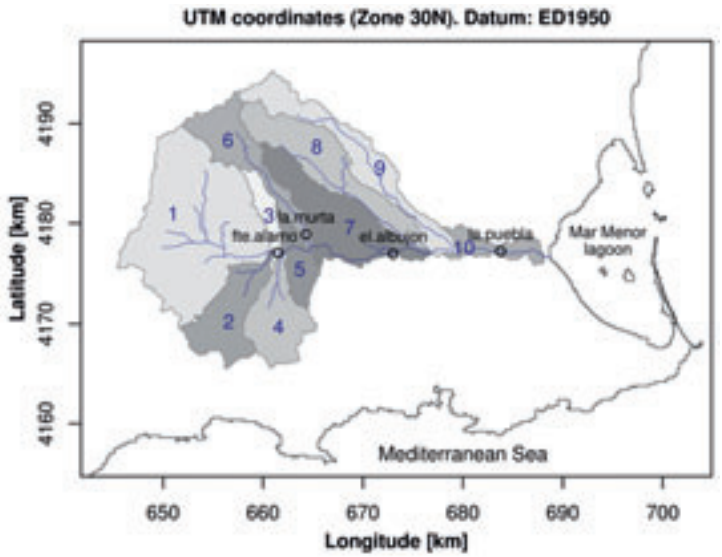

Fig. 1. Location of the Rambla del Albujón watershed and the Mar Menor coastal lagoon at the Southeast of Spain. HRUs are numbered in flow aggregation order. Circles indicate gauge locations.

5. Calibration approach and a priori parameter distribution

We evaluated model and parameter uncertainty with the Generalized Likelihood Uncertainty Estimation (GLUE) methodology (Beven and Binley, 1992). The problem was posed so that the model with constant D is a subset structure of that with time-varying D, in which specific additional parameters in the improved structures take specific values. Evaluation of behavioral runs (those with adequate likelihood) allows making inferences to update our *a priori* beliefs. Evaluation of time-decaying D considers three parameters: D_0; D_s, and $\Delta t_{0.5}$. For every HRU_j, in which maximum depression storage was evaluated as time-decaying, $D_i(t)$, half-life $\Delta t_{0.5}$ was always evaluated with a priori uniform distribution with $\Delta t_{0.5}$ h. On the other hand, we considered that both the initial and the final values of maximum depression storage (D_{0i}, D_{si}) had *a priori* uniform density ranging between the same bounds [$D_{i,\min}$, $D_{i,\max}$]. The sampled were drawn from these uniform priors. Then, for each j random sample, if $D_{si,j} > D_{0i,j}$, the former was set to the latter value as $D_i(t)$ was just considered to decay. We are interested in the parameter defined by the random variable $\Delta D_i = D_{0i} - D_{si}$, and this experimental design gives equal a priori probability $f = 0.5$ to the hypothesis that $\Delta D_i = 0$, and to the alternative hypothesis that $D_i(t)$ decays. In effect, being $\Delta D_{i,r} = D_{i,\max} - D_{i,\min}$, the resulting prior right-continuous cumulative distribution function ($F(x)=P(X\leq x)$) of ΔD_i, is shown in Figure 3.

Objective functions used for multicriteria analysis are shown in Table 1, where $O = \{o_1,\ldots,o_n\}$ is the vector of streamflow observation data at time steps 1,…, n, and $S(\xi, \Theta) = \{s_1(\xi, \Theta),\ldots,s_n(\xi, \Theta)\}$ is the vector of simulated flows for a specific structure ξ with a specific parameter set Θ.

Considering the objective functions and gauge points, we refer to a behavioral simulation under a specific OF and considering the observed hydrograph at point X as OF-X-behavioral. If all OF criteria are fulfilled at X, the simulation is denoted as total-X-behavioral, and if all available nested hydrographs fulfill a specific OF criterion, it is a OF-global-behavioral.

Table 1. Objective functions and behavioral bounds considered in this study

OF	Formula	Behavioral
PDIFF††	$\lvert max_{1\leq t\leq n}\{o_t\} - max_{1\leq t\leq n}\{s_t(\xi,\Theta)\}\rvert / max_{1\leq t\leq n}\{o_t\}$	[0.4-0]
PTLAG††,†††	$\lvert time\{max_{1\leq t\leq n}\{o_t\}\} - time\{max_{1\leq t\leq n}\{s_t(\xi,\Theta)\}\}\rvert$	[3600-0]
FV	$\left\lvert \sum_{t=1}^{n}(o_t - s_t(\xi,\Theta)) \right\rvert \Big/ \sum_{t=1}^{n} o_t$	[0.2-0]
NS	$1 - \sum_{t=1}^{n}(o_t - s_t(\xi,\Theta))^2 \Big/ \sum_{t=1}^{n} (o_t - \bar{o})^2$	[0.4-1.0]

† PDIFF: absolute normalized peak difference; PTLAG: absolute time lag for peaks; FV: absolute normalized volume difference; NS: Nash-Sutcliffe efficiency; see text for definition of terms in formulae.

†† Just the global peak is considered for these statistics.

††† (s); remaining OF are dimensionless.

III – Calibration results and discussion

Calibration was conducted in three stages: Stages I and II have a lumped and a distributed parameterization, respectively, for the a priori model; and Stage III analyzes the posterior model structure (dynamic D). Here we focus on D. Remaining parameters (e.g. hydraulic conductivity or friction coefficients) were sampled, for all stages, from common *a priori* distribution and ranges.

Stage I, with lumped parametrizations, completely failed in simulated the watershed hydrology and obtaining the multi-peak observed response. Stage II, with spatially distributed parameter, beha-

ved much better in simulating the different behaviour of the various parts of the watershed. However, still a systematic bias evidenced that a certain amount of water should be first retained in the central parts of the watershed, and it should be later released, in a relatively abrupt way, to contribute to the second flow wave coming from the upper parts of the watershed. This problem was resolved in Stage III, with specific accounting of this process through the time-varying maximum surface depression storage. Figure 2 shows some simulation results from Stage III.

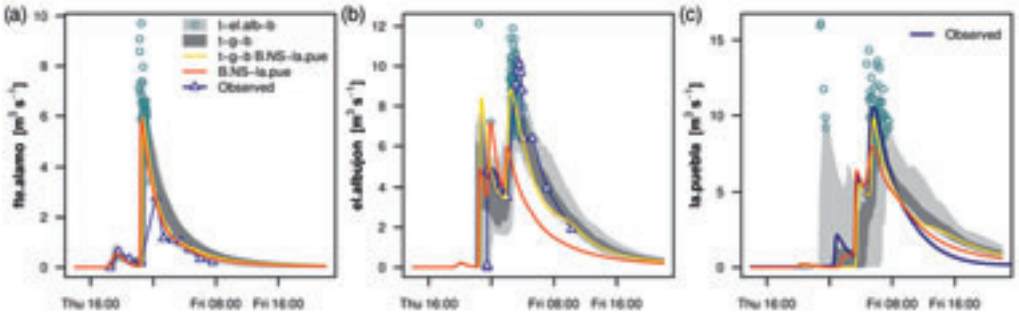

Fig. 2. Stage III. Step 2. MC simulation (21 000 runs). Light grey areas cover the GLUE-sense 95% confidence intervals (c.i.) of total-el.albujon-behavioral simulated hydrographs (t-el.alb-b, n = 94) at (a) fte.alamo, (b) el.albujon, and (c) la.puebla. Dark grey areas cover the 95% c.i. of total-global-behavioral simulations (t-g-b, n = 37). The t-g-b simulation with the highest NS at la.puebla (NS = 0:84) is in yellow, and the best NS-la.puebla simulation (NS = 0:90, but not in the t-el.alb-b subset) is in red.

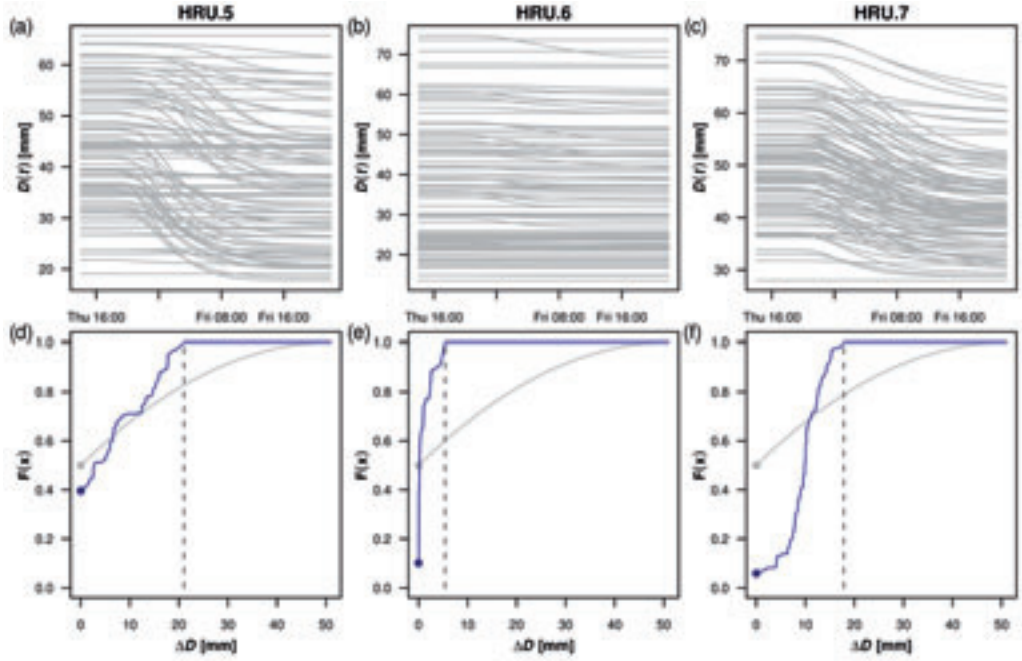

Fig. 3. Stage III. Simulations that were simultaneously total-fte.alamo-behavioral and total-el.albujon-behavioral, showing areal mean *D*(*t*) evolution in the HRUs contributing to runoff between these two measurement points and evaluated for time-varying maximum depression storage. The bottom row show corresponding a priori (grey) and a posteriori (blue) cumulative distribution functions of Δ*D*.

GLUE-based inference supported the hypothesis that the structural breaching was into effect, leading to dynamic maximum depression storage. The magnitude of the time-variability of the maximum depression storage had a high spatial variability. Figure 3 indicates that the posterior distribution of ΔD in HRU.7 gave a very small probability mass ($P(X = 0) = 0.07$) to the hypothesis that $\Delta D = 0$, and most of the probability concentrated around $\Delta DHRU.7 = 10$ mm. In HRU.5 there was no clear support to the alternative hypothesis, but the behavioral range was limited up to $\Delta DHRU.5 = 22$ mm. In HRU.6, was relatively disproved ($P(X = 0) = 0.2$); however, the behavioral probability range, $\Delta DHRU.6$ [0, 5] mm, indicated more stable retention structures with respect to HRU.7. As a comparison, Bellin *et al*. (2009) found in a nearby catchment that a storm with a return period of 8 years produced structural damages in 16% of walls and other soil conservation structures.

IV – Sensitivity of simulated response to storm motion

The importance of storm motion on the hydrograph shape has been acknowledged, but related literature is scarce. The October 2003 storm was aligned with the main channel. Thus the radar-based QPE is an opportunity to conduct a concise simulation analysis about the hypothetical scenario of an identical storm with reversed upstream motion. We simulated the watershed response to the upstream storm motion with the ensemble of parameter sets within NS-el.albujon-behavioral or NS-la.puebla-behavioral simulations in the posterior model (3415 sets). Figure 4 shows three dimensionless descriptors of the integrated hydrograph at la.puebla. These are (a) relative flow volume (RFV [–]), i.e., ratio between total simulated flow and total observed flow with the downstream motion; (b) relative peak flow (RPF [–]), i.e., ratio between peak simulated flow and peak observed flow; and (c) relative Shannon entropy (RSE [–]) as a descriptor of the general compression or dispersion of the hydrograph regardless of the net flow amounts. To calculate RSE, first the hydrographs were scaled to integrate to one (as a PDF); then, RSE was obtained as the ratio of the Shannon entropy (Shannon, 1948) obtained for the scaled hydrograph to that obtained for a uniform distribution function. Thus RSE [0, 1], where higher values indicate higher dispersion.

Hydrographs were significantly affected by the storm movement, and global behavior may be summarized in three features. First, the storm moving upstream had a trend to decouple the successive peaks of the hydrograph obtained in the downstream-moving storm. Thus the runoff wave generated in HRU.1 arrived generally later than that generated in the middle areas as to form a more independent second flow wave at the outlet with respect to that resulting from the downstream-moving storm. So, the flow tended to be more distributed in time resulting in higher RSE values (Fig. 4). Second, despite this partial decoupling, the individual runoff amounts and peaks of the upstream-moving storm hydrograph pertaining to either water generated in the middle areas or water coming from HRU.1 tended to be greater than those for the downstream-moving storm. As a result, the total runoff at la.puebla was quasi-systematically higher for the former (RFV in Fig. 4). Some past studies, considering impervious surfaces, concluded that downstream-moving storms tend to create higher peaks (e.g. Ogden *et al.*, 1995; Singh, 2002). However, Singh (2005), with a kinematic analytical solution for runoff resulting from storms with partial coverage moving on an infiltrating plane, drew the conclusion that "for the same areal coverage and the same duration of storm, the peak is greater for the storm moving upstream than that for the storm moving downstream". This is supported by our results, and the most likely reason being that infiltration has higher opportunity time to occur for storms moving downstream. Third, despite the individual peaks of the upper and middle areas of the watershed increased for the upstream-moving storm, its decoupling implied that these peaks did not overlap as much as they did in the downstream-moving storm. As a result, the absolute peaks were approximately similar in both scenarios, with just slight increases for the upstream-moving storm (RPF in Fig. 4).

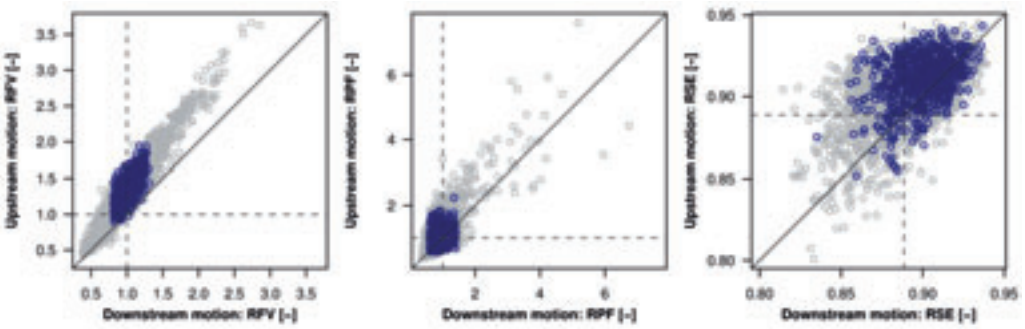

Fig. 4. Effect of storm motion on the watershed response. Dark blue indicates total-la.puebla-behavioral simulations. Dashed lines refer to the observed hydrograph.

V – Conclusions

We show a time-varying formulation for maximum depression storage, whose evolution was significant in the central areas of a semiarid watershed during a flash flood driven by a convective storm. Radar information was instrumental in understanding the runoff generation mechanisms and in the estimation of the *a posteriori* model structure. Radar data also supported the evaluation of storm motion, for which our results show that, in the evaluated case, a storm with partial coverage moving upstream on the infiltrating plane tends to create greater responses. A relationship with failures in agricultural terraces and other soil protection structures was identified.

Acknowledgments

We would like to thank the support of the REDSIM project (REmote-sensing based DSS for Sustainable Drought-adapted Irrigation Magagement), funded by the European Commission, DGE, as a "Pilot project on development of prevention activities to halt desertification in Europe".

References

Baeck M.L. and Smith J.A., 1998. Rainfall estimation by the WSR-88D for heavy rainfall events. In: *Weather Forecast*, 13, p. 416-436.

Beven K.J. and Binley A.M., 1992. The future of distributed models: model calibration and uncertainty prediction. In: *Hydrol. Proc.*, 6, p. 279-298.

Bellin N., van Wesemael B., Meerkek, A., Vanacker, V. and Barberá, G.G., 2009. The decay of soil and water conservation structures. A case study from Southeast Spain. In: *Catena*, 76, p. 114-121.

Carpenter T.M. and Georgakakos, K.P., 2004. Impacts of parametric and radar rainfall uncertainty on the ensemble streamflow simulations of a distributed hydrologic model. In: *J. Hydrol.*, 298, p. 202-221.

García-Pintado J., Barberá G.G., Erena M. and Castillo, V.M., 2009a. Rainfall estimation by raingauge-radar combination: a concurrent multiplicative-additive approach. In: *Water Resour. Res.*, 45, W01415. doi:10.1029/2008WR007011.

García-Pintado J., Barberá G.G., Erena M. and Castillo, V.M., 2009b. Calibration of structure in a distributed forecasting model for a semiarid flash flood: dynamic surface storage and channel roughness. In: *J Hydrol,* 377, p. 165-184.

Guzha A.C., 2004. Effects of tillage on soil microrelief, surface depression storage and soil water storage. In: *Soil Tillage Res.*, 76(2), p. 105-114.

Knighton A.D. and Nanson G.C., 2001. An event based approach to the hydrology of arid zone rivers in the Channel Country of Australia. In: *J. Hydrol.*, 254(1-4), p. 102-123.

Lin, Z. and Beck, M.B., 2007. On the identification of model structure in hydrological and environmental systems. In: *Water Resour. Res.* 43, W02402. doi:10.1029/2005WR004796.

Middleton N.J. and Thomas D.S.G., 1997. *World Atlas of Desertification*, second ed. UNEP/Edward Arnold, London.

Mitchell J.K. and Jones Jr. B.A., 1978. Micro-relief surface depression storage: changes during rainfall events and their application to rainfall–runoff models. In: *J. Am. Water Resour. Assoc.*, 14(4), p. 777-802.

Moore R.J., 2002. Aspects of uncertainty, reliability and risk in flood forecasting systems incorporating weather radar. In: *Risk, Reliability, Uncertainty and Robustness of Water Resources Systems* (ed. By J. J. Bogardi and Z. W. Kundzewicz). Cambridge University Press, pp. 30-40.

Ogden F.L., Richardson J.R. and Julien P.Y., 1995. Similarity in catchment response: 2. Moving rainstorms. In: *Water Resour. Res.*, 31(6), p. 1543-1547.

Refsgaard J.C., van der Sluijs J.P., Brown J. and van der Keur P., 2006. A framework for dealing with uncertainty due to model structure error. In: *Adv. Water Resour.*, 29, p. 1586-1597. doi:10.1016/j.advwatres.2005.11.013.

Sandercock P.J., Hooke J.M., Lesschen J.P. and Cammeraat L.H., 2007. Sediment connectivity. In: *Conditions for Restoration and Mitigation of Desertified Areas Using Vegetation (RECONDES): Review of Literature and Present Knowledge* (ed. by European Commission, Directorate-General for research Information and Communication Unit). ISBN: 92-79-03072-8.

Shannon C.E., 1948. A mathematical theory of communication. In: *Bell Syst. Tech. J.*, 27, p. 379-423, 623-656.

Singh V.P., 2002. Effect of the duration and direction of storm movement on planar flow with full and partial areal coverage. In: *Hydrol. Proc.*, 16, p. 3437-3466.

Singh V.P., 2005. Effects of storm direction and duration on infiltrating planar flow with partial coverage. In: *Hydrol. Proc.*, 19, p. 969-992.

Yair A. and Klein M., 1973. The influence of surface properties on flow and erosion processes on debris covered slopes in an arid area. In: *Catena*, 1, p. 1-18.